THE UNIVERSITY
of EDINBURGH

Design and engineering genetic tools for *Desulfovibrio alaskensis*

Miguel E. Cueva

Thesis submitted for the degree of Doctor of Philosophy to The University of Edinburgh

2019

Abstract

Microorganisms, such as the anaerobic bacterium *Desulfovibrio alaskensis*, have evolved various mechanisms to resist high concentrations of toxic heavy metals; one of these mechanisms involves the synthesis of nanoparticles (NPs). It may be possible to utilise this ability to both reclaim heavy metals from contaminated effluents and to convert them into industrially useful NPs. By engineering a genetically modified *D. alaskensis*, through synthetic biology, cell surface engineering and by designing a modular cloning (MoClo) toolkit, there is a further opportunity to tailor nanoparticle synthesis.

DNA assembly techniques have revolutionised biotechnology research and innovation. However, despite many advances in molecular biology, the assembly of DNA parts into new constructs remains cumbersome and unpredictable. The innovation of cloning toolkits and standards such as MoClo have standardised the process of DNA assembly, making it easier, faster, modular and cost-effective. The *D. alaskensis* MoClo toolkit developed in this work consists of characterised oxygen-independent reporters, synthetic promoters and ribosome binding site (RBS) libraries.

The *D. alaskensis* MoClo toolkit was utilised to assemble a combinatorial library of transcriptional units (TUs) expressing the NiFe hydrogenase small subunit. Platinum NPs were synthesised by the combinatorial library, and examined for their oxidative and reduction catalytic activities were tested.

To enhance *D. alaskensis* resistance to Cu, Pt and Pd, cell surface engineering was used to express synthetic phytochelatin EC20 on the outer membrane. Tests of *Escherichia coli* expressing EC20/IgA to Cu, Pt and Pd concluded that EC20 confers a higher resistance to all metals.

Lay Summary

Desulfovibrio alaskensis is a microorganism that survives unfavourable environments highly enriched with metals; it survives such environments because it possess qualities to resist toxic concentrations of metals. One of these qualities is their ability to turn toxic metal concentrations into a non-toxic form, called nanoparticles. These qualities can be utilised to help us capture metals from contaminated land, water, and industry waste, to make nanoparticles, which are of value in industry. Genetic engineering tools that enable the fast and cost-effective modification of *D. alaskensis* qualities were developed, for the ultimate goal of better nanoparticles.

Declaration

I hereby declare that this thesis was composed by me and that the research presented herein is my own work unless otherwise stated. This work has not been submitted for any other degree or professional qualification.

Miguel E. Cueva

2019

Acknowledgements

Firstly, I would like to express my sincere gratitude to my supervisor Dr Louise Horsfall, for the continuous support throughout my PhD project and related research, for her patience, motivation and immense knowledge. Her guidance helped me throughout my research and the writing of this thesis.

Besides my supervisor, I would like to thank the rest of my thesis committee: Prof Chris French, Dr David Clarke and Dr Andrew Free, for their insightful comments and encouragements, but also for the hard questions and guidance, which propelled me to widen my research.

My sincere thanks also goes to Dr Mike Capeness, Dr Matt Edmundson, Dr Virginia Echavarri-Bravo and Dr Nick Pantidos for their advice, conceptual and technical support throughout my PhD project, and of course the countless stimulating discussions. In addition, I am grateful to all my lab colleagues at the Horsfall Lab, because every single member contributed to my PhD and without them the lab would be a dull place.

Most importantly, I would like thank my friends and family who kept me sane and grounded throughout my PhD. That during the hard and stressful times, they encouraged me, supported me, and were that nagging voice of wisdom that told me not to quit.

Finally, I would like to thank CONACyT, BBSRC and The University of Edinburgh for financial support.

Abbreviations

2,6-DMP	2,6-Dimethoxyphenol
bp	Base-pair
CDS	Coding sequence
cm	Centimetres
CuNP	Copper nanoparticle
DIC	Differential interference contrast
DNA	Deoxyribonucleic acid
dsDNA	Double stranded deoxyribonucleic acidEDTA Ethylenediaminetetraacetic acid
Ep-PCR	Error-prone polymerase chain reaction
FbFP	Flavin-based fluorescent protein
fmol	Femtomol
g	Gram
GFP	Green fluorescent protein
hrs	Hours
ICP-OES	Inductively coupled plasma – Optical emission spectroscopy
Kb	Kilobase-pair
kV	Kilovolts
L	Litre
M	Molar
MB	Methylene blue
mg	Milligram

min	Minutes
mL	Millilitre
mM	Millimolar
MoClo	Modular Cloning Assembly Standard
MOPS	3-[N-Morpholino]propanesulphonic acid
ng	Nanogram
nm	Nanometre
OD_{600}	Optical density at 600 nm
OE-PCR	Overlap extension polymerase chain reaction
ORF	Open reading frame
PBS	Phosphate Buffered Saline
PCR	Polymerase chain reaction
PdNP	Palladium nanoparticle
PGM	Platinum group metals
pH	Power of hydrogen
PtNP	Platinum nanoparticle
RBS	Ribosome binding site
rpm	Rotations per minute
RT-PCR	Real-time polymerase chain reaction
SOC	Super Optimal Broth
SRB	Sulphate-reducing bacterium
ssDNA	Single stranded deoxyribonucleic acid
TAE	Tris-acetate-EDTA

TEM	Transmission Electron Microscopy
TIR	Translation initiation rate
TU	Transcriptional Unit

Table of Contents

List of Figures and Tables

Chapter 1

Chapter 2

Chapter 3

Chapter 4

Chapter 5

Chapter 6

Chapter 7

Appendix – Additional Data

Chapter 1: Introduction

1.1. *Desulfovibrio alaskensis* Nanoparticle synthesis and its role in sustainability

Nanoparticles (NPs) are particles having one or more dimensions below 100 nm [1]. Heavy metal NPs possess unique physical, chemical, photo electrochemical, mechanical, electrical, magnetic, optical and biological properties [1]. The NPs size plays a critical role in those properties, particularly their catalytic activity. Decreasing the NP's size to a smaller nano-scale, increases the physical surface interaction of atoms, increasing its surface energy and decreases its imperfections [1]. Potential applications of biogenic metal NPs range from biomedical purposes (e.g. antiviral, antibacterial, antiparasitic, medical imaging, drug delivery, cancer treatments and medical diagnostics), through environmental remediation purposes (e.g. pollutant degradation and catalytic treatments), to industrial purposes (e.g. catalytic organic chemistry and nanoelectrochemistry) [2].

Metals play an integral role in the life processes of microorganisms. Some metals such as Cr, Ca, Mg, Mn, Cu, Na, Ni and Zn are essential micronutrients for various metabolic activities and for redox processes [3]. Microorganisms have the ability to discern between these essential metals and those that are toxic, and have the ability to tightly regulate their transport in and out of the cell [3]. Microorganisms have evolved various mechanisms to resist higher concentrations of toxic heavy metals, such as exclusion by permeability barrier, active transport of metals out of the cell, intracellular sequestration (protein binding), extracellular sequestration, enzymatic detoxification, reduction in metal sensitivity [4] and the ability to convert heavy metals into less toxic nanoparticles (NPs) [5]. Examples of microorganism capable of synthesising NPs include: *Desulfovibrio desulfuricans*, *Bacillus subtilis*, *Cupriavidus metallidurans*, *Escherichia coli*, *Candida glabrata*, *Thermomonospora* sp., *Rhodopseudomonas capsulate*, *Pseudomonas aeruginosa*, *Shewanella* sp., *Rhodococcus* sp., and *Verticilliium* sp. [6, 7]. While, currently the range of metal NPs (in its elemental state) that are able to be synthesised by microorganisms include (but is not limited to) As, Ag, Al, Au, Cd, Cr, Cu, As, Pb, Pd and Pt [7-10].

Biogenic metal nanoparticles are produced by the microorganisms' natural metal resistance and metabolic pathways, through either an intracellular or an extracellular

mechanism [11]. The intracellular mechanism occurs in the cytoplasm of the cell and involves the reduction of metals to their elemental form through electrostatic and enzymatic interactions, forming NPs that are held within the cell [11]. The extracellular mechanism is mediated either through enzymatic reduction at the cell surface or by secreted molecules that reduce metals ions into their elemental form [12].

The focus of this thesis is dedicated to *Desulfovibrio alaskensis* a Gram-negative anaerobic sulphate-reducing bacterium (SRB) that is exceptionally well adapted to survive environments with high concentrations of heavy metals, converting them to NPs [4]. *Desulfovibrio* sp. have been shown to be able to reduce Cr, Mg, Fe, Te and even U to nanoparticle forms [13-17]. *Desulfovibrio* sp. such as *D. alaskensis* G20 have been most studied because they are able to reduce Pt and Pd to zero-valent NP [5], as they are highly tolerant to Pt and Pd ions, able to survive up to 2 mM and 5 mM, respectively [5]. *D. alaskensis* G20 is a spontaneously nalidixic acid-resistant derivative of *Desulfovibrio desulfuricans* G100A [18], a deltaproteobacterium that was isolated from a producing oil well in Ventura County, California [19]. Its complete genome has been sequenced [18], and it provided great insight into its energy conversion through sulphate respiration, fermentation of organic acids and living in microbial syntrophy. Moreover, recent proteomic analysis of *D. alaskensis* G20 in response to platinum and palladium highlighted those proteins involved in both the reductive pathways and the wider stress-response system to this metals [20]. Both accomplishments will help elucidate *D. alaskensis* sp. metal NP synthesis, and the future possibility to tailor NPs' size to acquire a desirable catalytic activity.

Biogenic platinum and palladium NPs have been found to be useful in a number of cases; for example biogenic palladium NPs synthesised by *Desulfovibrio* sp. have been shown to be an effective catalyst in hydrogen fuel cells [21], while *Desulfovibrio* sp. cells synthesise palladium NPs which are bound to the cell surface which have been used in chromium (IV) decontamination [22]. These palladium NPs proved to be considerably stable, and lasting over eleven times longer that it's industrially produced counterpart [22]. The reduction of platinum group metals (PGMs, Rh, Ir, Ru, and more importantly Pt and Pd) by *Desulfovibrio* sp is hypothesised to occur due to the bacteria incorporating the metals into their electron transfer pathways [5]. Pt and Pd in the presence of hydrogen act as terminal electron acceptors, in *Desulfovibrio* sp

respiration, causing those metal ions to be reduced to a zero valence state [23, 24]. The reduction of such metals occurs in the periplasm, where hydrogenases and cytochromes, such as NiFe hydrogenase are able to reduce them. NPs are exported outside of the cell and subsequently attached to the cell surface [5]. The newly cell-attached NPs act as a catalyst for further metal reduction [25]. An illustration of the reduction of Pd ions to NPs is in Figure 1.1. Platinum group metals ions have been observed to cause DNA lesions and inhibit growth in other bacteria such as *E. coli* and *Pseudomonas* sp. [26, 27]. *Desulfovibrio* sp. experience DNA lesions when exposed to higher concentrations of platinum group metals in comparison to *E. coli* and *Pseudomonas* sp. [5], since the attachment of metal NP to the cell surface and the further reduction of metals could form part of a bacterial survival mechanism [5].

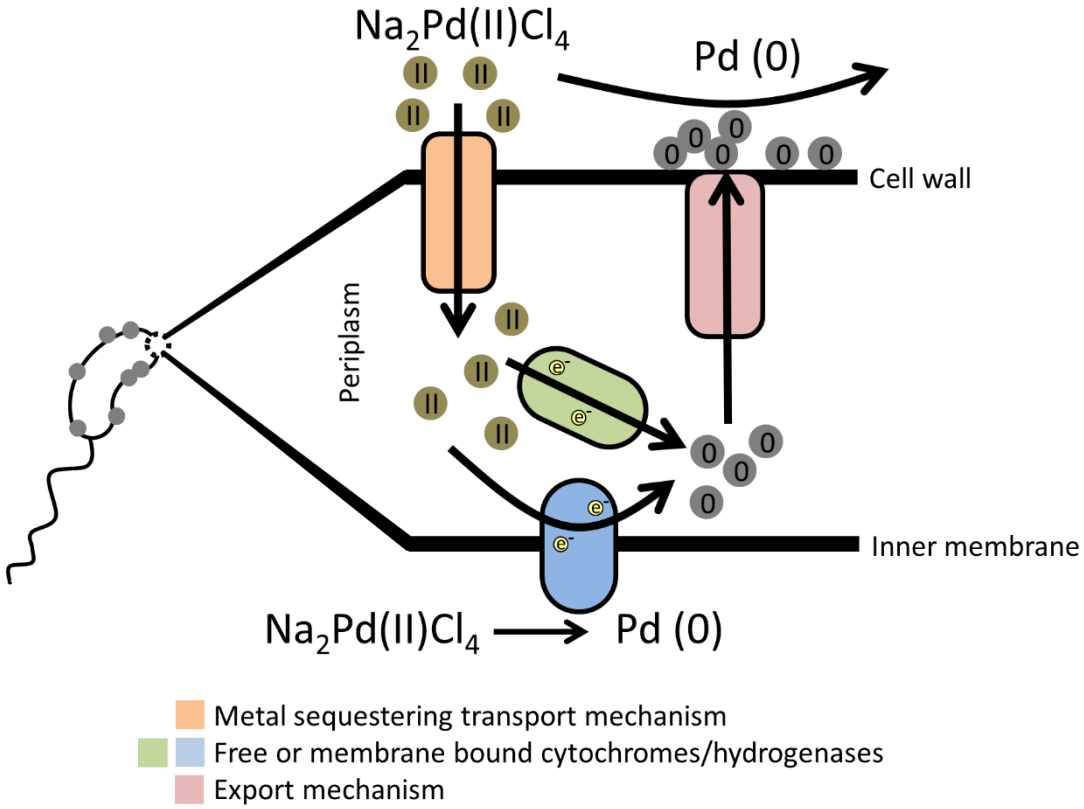

Figure 1. 1. Proposed mechanism of palladium reduction to nanoparticle in the periplasm of *Desulfovibrio.* Pd^{2+} ions are taken up by *Desulfovibrio* across the outer membrane into the periplasm, where they are hypothesised to be reduced by cytochromes and/or hydrogenases to form NPs. The NP is exported outside the cell, where they are attached to the cell surface, to act as a catalytic site for increased Pd reduction. Schematic taken from 'Nickel and platinum group metal nanoparticle production by *Desulfovibrio alaskensis* G20', by M.J. Capeness *et al* [5].

The use of *D. alaskensis* for the reclaiming of PGMs is of great importance as they play a key role in modern society, as PGMs possess a range of unique chemical and physical properties and are of specific importance for clean technologies and other high tech equipment [28]. PGMs have applications as chemical processes catalysis, catalytic converters, consumer electronics, and fuel cells [28]. Metals including PGMs are not consumed, instead they become dispersed into the environment in many ways, e.g. mines' run-offs, waste from metal processing, and automobiles' catalytic converters [29]. Heavy metal pollution degrades the quality of soil and water, rendering them unsustainable and of little or no use, while also negatively affecting the biological health of ecosystems. It is imperative to develop technologies that will enable a more sustainable reclamation of metals, and enable to clean polluted land and water. Such sustainable technologies are imperative because a growing world population crucially drives the scarcity of metals, and has caused the global supply and demand of metals to be of importance in the developed world [28, 29].

Attempts to develop technology and research to achieve sustainability through the means of recovering metals have been devised using physical, chemical and biological approaches. Physical and chemical approaches are proven to remove a broad spectrum of contaminants, but these methods rely on high consumption of energy and the use of additional chemicals [30], therefore proving not to be sustainable. Unlike such methods, bioremediation (biological approach) uses microorganisms to reclaim, immobilize and detoxify metal pollutants without the use of excessive energy and additional chemicals [11, 29, 31].

Genetic and molecular biology technologies are available for *D. alaskensis* sp. Genetic tools to engineer *Desulfovibrio* sp have been developed [32], transposon mutant libraries have been generated [33] and systems biology tools have been applied [34], but all available tools and technologies were developed to study *D. alaskensis* sp, energy metabolism and not their NP synthesis. No synthetic biology or genetic tools are available to specifically engineer genetically modified strains of *D. alaskensis* for bioremediation purposes. However, synthetic and genetic tools abound for the model organisms *E. coli*, a gammaproteobacterium closely related to *D. alaskensis* sp, a deltaproteobacterium. Proteobacteria compromise of the largest and phenotypically most diverse division among prokaryotes [35]. Sequence alignments of proteins have

led to the identification of numerous conserved inserts and deletions that are shared among proteobacterial species. These findings provide the molecular means to understand their evolutionary relationships between proteobacterial species. Species belonging to the deltaproteobacteria subdivision are more closely related to the alpha, beta and gammaproteobacteria, in view of the paucity of sequence data on these subdivisions in comparison to other proteobacteria [35]. The close relationship between *E. coli* and *D. alaskensis* sp, can be indicative that the tools available for *E.coli* can potentially be used to engineer *D. alaskensis* for bioremediation purposes.

One of the objectives of this project is to engineer genetically modified strains of *D. alaskensis* as a bioremediation technology, to reclaim metals such as Pt and Pd, in the form of NPs. Not only is this practice sustainable, it also adds value to Pt and Pd recovery [36], as they are recovered as industrially useful NP [11].

1.2. Synthetic Biology Tools

1.2.1. Broad Overview of Synthetic Biology and its Applications

Synthetic biology is an exciting and rapidly evolving scientific field that merges engineering principles and practices with modern molecular biology and biotechnology techniques. This focus on engineering principles is what distinguishes synthetic biology from more traditional biological techniques, emphasising the design and construction of core biological parts, that can be modelled, understood and engineered to meet a specific outcome [37].

One of the driving forces in synthetic biology is the desire to make biological design and implementation easier and more predictable for biotechnology applications [38]. Conceptual engineering frameworks underpin the research basis of synthetic biology. Modularisation, standardisation and characterisation are key engineering principles used within synthetic biology for the systematic design of biologically-based devices and systems. The modularity concept is when a device, pathway or system is reduced to a number of components parts, where each component part is characterised in detail, to underpin how it operates under different conditions. Component parts are

standardised in order that, in principle, a combination of standard parts can be assembled to create a pathway. This approach, thoroughly used within engineering, is an important enabler because an entire biological device then does not have to be created from scratch, rather it can be assembled from existing standard parts [38]. This synthetic biology design approach is known as parts, devices (genes) and systems (pathways) [38]. Parts or bioparts (most notably synthetically designed DNA) encode biological functions. Devices are made from a collection of bioparts. Systems perform tasks to control or obtain a desired biological function or output. In principle, to construct the most simple device, comprised of a promoter, ribosome binding site (RBS), protein coding sequence (CDS), which contains the open reading frame (ORF) necessary for translation, and terminator, it will consist of joining four different bioparts to assemble a device (gene or transcriptional unit, TU). Multiple devices assembled together work as a system (pathway), designed for a desired outcome. See Figure 1.2 for an illustration of terms used in synthetic biology.

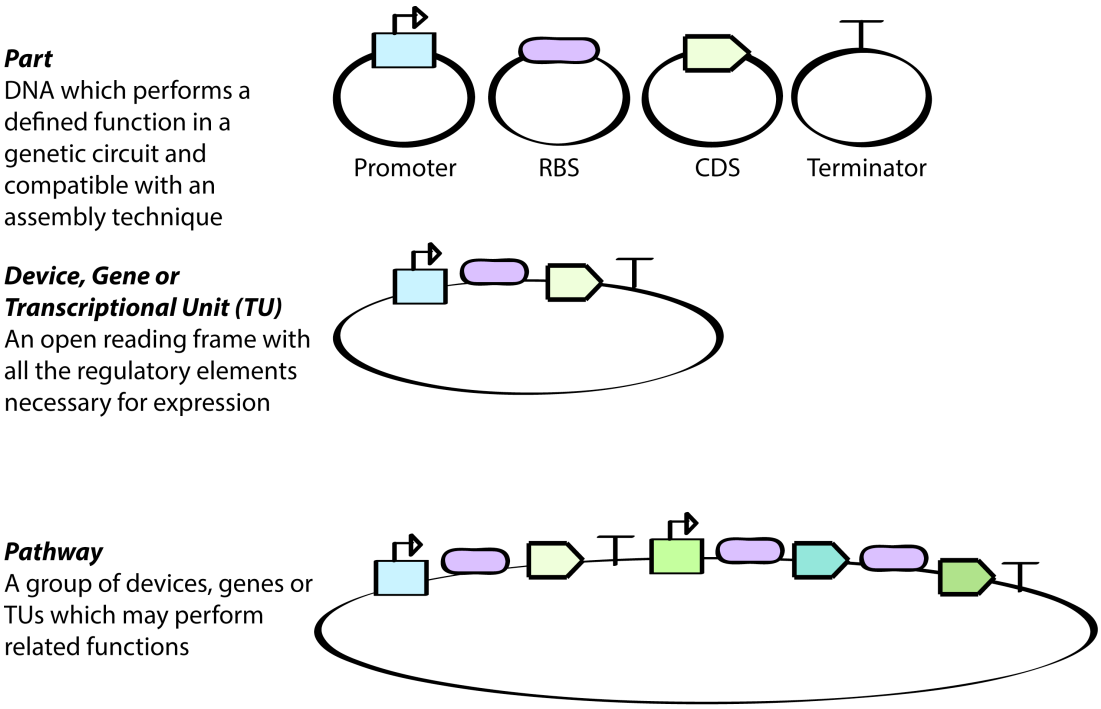

Figure 1. 2. Illustration of the terms used in synthetic biology. Adapted from 'DNA Assembly for synthetic biology: from parts to pathways and beyond', by T. Ellis et al [39].

Synthetic biology strategies and tools are being applied to facilitate the engineering of tailor-made microorganisms capable of tackling some of society's toughest challenges. Synthetic biology relies on the gathering of bioinformatics data, coupled with engineering principles where the assembly of devices and systems is streamlined, and has broadened the possible applications of this new scientific field. Within industrial biotechnology, synthetic biology has enabled the development of new biosynthetic pathways for the production of renewable fuels and chemicals, programmable logic controls to regulate and optimize cellular functions, and robust microorganisms for the accumulation and removal of harmful environmental contaminants [40]. Synthetic biology has expanded the diversity of chemical products that can be synthesised biologically. These molecules serve important industrial roles as monomers for producing bioplastics (potential replacements to many conventional plastic materials)[41], bulk and fine chemicals, as well as long-chain alcohols (usually not efficiently synthesised by microorganisms) [42], and other biofuels with improved compatibility (increasing the yield of biofuel production) [43].

Within a biomedical setting, synthetic biology has tackled key challenges, like the need for drug-target specificity, precise drug-dosing regimens, minimising side effects, better diagnostics, and the avoidance of drug-resistance pathogens [44]. Synthetic biology has enabled scientists to research and understand a disease by synthetically emulating a pathogen mechanism, for example the H1N1 virus was first sequenced and then synthesised to provide information of its enhanced viral replication [45]. Synthetic biology has recently provided new insights into immune disorders, for example, the functional reconstitution and analysis of the human B cell antigen receptor signalling cascade in insects revealed that human B cell antigen receptors are not activated by antigen-specific crosslinking [46]. Synthetic biology has also been applied to the suppression of insect vector transmission of infectious diseases, such as malaria and dengue virus, where transgenic mosquitoes prevent the propagation and proliferation of vectors [47]. Notably synthetic biology has also propelled drug discovery and development efforts; the novel use of mammalian synthetic biology has enabled scientists to identify new antimicrobial peptides like MSI-78 [48], and discover small molecules responsible for overcoming pathogenic drug resistance [49]. The large-scale economic production of high-valued drugs,

precursor compounds and secondary metabolites, has been advanced with the advent of synthetic biology; a notable examples of such is the production of the anti-malaria drug Artemisinin [50] and the anti-cancer drug Taxol [51]. Drug delivery systems developed using synthetic biology, for example the use of synthetic protein-polyacrylamide and DNA-polyacrylamide monomers that release a trigger dependent subcutaneous dosage have been developed[52]. Anti-cancer devices that provide precise timing, location and dosing of drug production by external cues have recently been designed using synthetic biology tools, an example of such are engineered bacteria that selectively invade and proliferate in tumour tissue and release cytotoxic compounds [53].

Within environmental biology, synthetic biology applications such as biosensors, bioaccumulation of metals, and bioremediation have been researched. The detection and quantification of pollutants in the environment is essential due to the threat they pose to the balance of the ecosystem and to human health [54]. The design of whole cell microbial biosensors to sense and quantify arsenic have been used [55], for example the design of an amplified arsenic biosensor that can quantify arsenic concentrations, by calculating the fluorescent emission expressed form a bacterial biosensor using a microfluidic device [56]. The use of microbial biomass as a platform for heavy metal ion accumulation and removal are being studied [57]. Nonetheless, the use of wild type microorganisms to accumulate heavy metals from wastewater effluent has its limitations. The uptake of metals into the cytoplasm of Gram-negative bacteria and their narrow tolerance to toxic metals are both limiting factors; therefore, it requires synthetic biology to optimise the heterologous expression of metal-binding proteins, or metal ion import systems [57]. Bioremediation may use microorganism to degrade toxic chemicals *via* complete mineralisation or co-metabolism [58], and synthetic biology has considerably helped advance efforts in this scientific field. For example, a co-culture of engineered *E. coli* SD2 and *Pseudomonas putida* KT2440 was used successfully to mineralize parathion (insecticide) [59].

This work utilises synthetic biology technologies to enable the modularisation, standardisation and characterisation of bioparts, for the facile engineering of *D. alaskensis* strains, and their use in bioremediation and metal reclamation as NPs.

1.2.2. DNA Assembly Techniques and the Modular Cloning (MoClo) Toolkit

The ability to reliably assemble and test DNA components in a high throughout manner is essential in the use of synthetic biology. This can be achieved through the standardisation and modularisation of the essential parts that make up a biological device or system. However, even with the simplicity of a standardised assembly, the DNA assembly process is still a limiting factor within research, hampering rapid prototyping of many devices [39], because the engineering design principles are too simplistic to efficiently create complex biological systems [60]. Nowadays, DNA assembly techniques abound, but in the advent of synthetic biology, the need for a universal connecting method to facilitate the construction of progressively complex parts was appeased with the development of the Biobricks ™ standard. This standard is based on the cloning of parts *via* restriction digestion and ligation, a digestion resultant with sticky ends that are accordingly ligated, re-forming the prefix sequence and leaving a 'scar' between parts. BioBricks™ relies on the XbaI, SpeI and PstI restriction enzymes where a sequential, ordered assembly of parts into a device is easily achieved. The BioBricks™ method has a downside, that it leaves the same 8 bp scar sequence between parts [39]. This scar can be problematic on certain locations, notably before the RBS and when assembling fusion proteins, because it encodes an in-frame stop codon [39]. Similar to BioBricks™, another DNA assembly technique standard is BglBricks, which replaced restriction enzymes used on BioBricks™ with BglII, BamHI and XhoI and has a smaller 6 bp scar in between parts [61]. Neither BioBricks™ nor BglBricks methods can assemble a scarless sequence from parts. However, scarless assembly can be achieved using another DNA assembly method called overlap extension polymerase chain reaction (OE-PCR). OE-PCR uses PCR primers to create homologous ends between different DNA molecules, homology then allows the extension of both parts in a second PCR, therefore allowing the scarless DNA assembly of devices without the use of restriction enzymes [62]. Another scarless assembly method is circular polymerase extension cloning (CPEC), utilises a primer-less single cycle of PCR to circularise a gene into a linearised plasmid [63]. However, these methods are limited in their ability to scale up, where plasmid assembly become less efficient at larger sizes and by the error rate of PCR, which to

date remains problematic for a reliable amplification of large constructs [39]. The aforementioned DNA assembly methods, particularly the BioBricks ™ and BgIBricks standards are becoming less relevant in light of new technology, specifically the Gibson and Golden Gate assembly methods [64]. Gibson assembly is an isothermal, single-reaction, ligation-independent assembly method that relies on the use of a high fidelity DNA polymerase, T5 exonuclease and *Taq* DNA ligase, were the assembly of multiple overlapping DNA molecules is achieved [65]. This method utilises a slow chew back mechanism resulting from the 3'-5' proofreading exonuclease activity, which generates long overhangs of overlapping DNA fragments, and instead of using a ligation enzyme to assemble parts, Gibson assembly relies on the *in vivo* DNA repair [65]. This method is particularly attractive due to its simplicity and use of common lab enzymes [39]. DNA assembly methods that rely on Type IIs restriction enzymes were developed to assemble DNA at larger scales. Type IIs restriction enzymes cut outside of their recognition site, leaving 4 bp overhangs, which can be customised and thus the assembly of devices can be scarless. The Golden Gate assembly method is one that uses this technique. It enables the sequential, combinatorial and scar-free assembly of parts into devices in a one-pot reaction [66-68]. Golden Gate assembly is a rapid DNA assembly technique, but it may require the removal of any internal Type IIs restriction sites, since it prevents the correct DNA assembly. Another scarless DNA assembly technique is PaperClip, which relies on the use of double stranded bridging oligonucleotides (clips). For each DNA part to be joined four short oligonucleotides (that can be reused) are designed and assembled to join parts *via* PCR [69]. Order of the parts in the assembly is controlled by the order of the oligonucleotides ligated to create the clips [69]. A comparative schematic of the DNA assembly techniques described is presented in Figure 1.3.

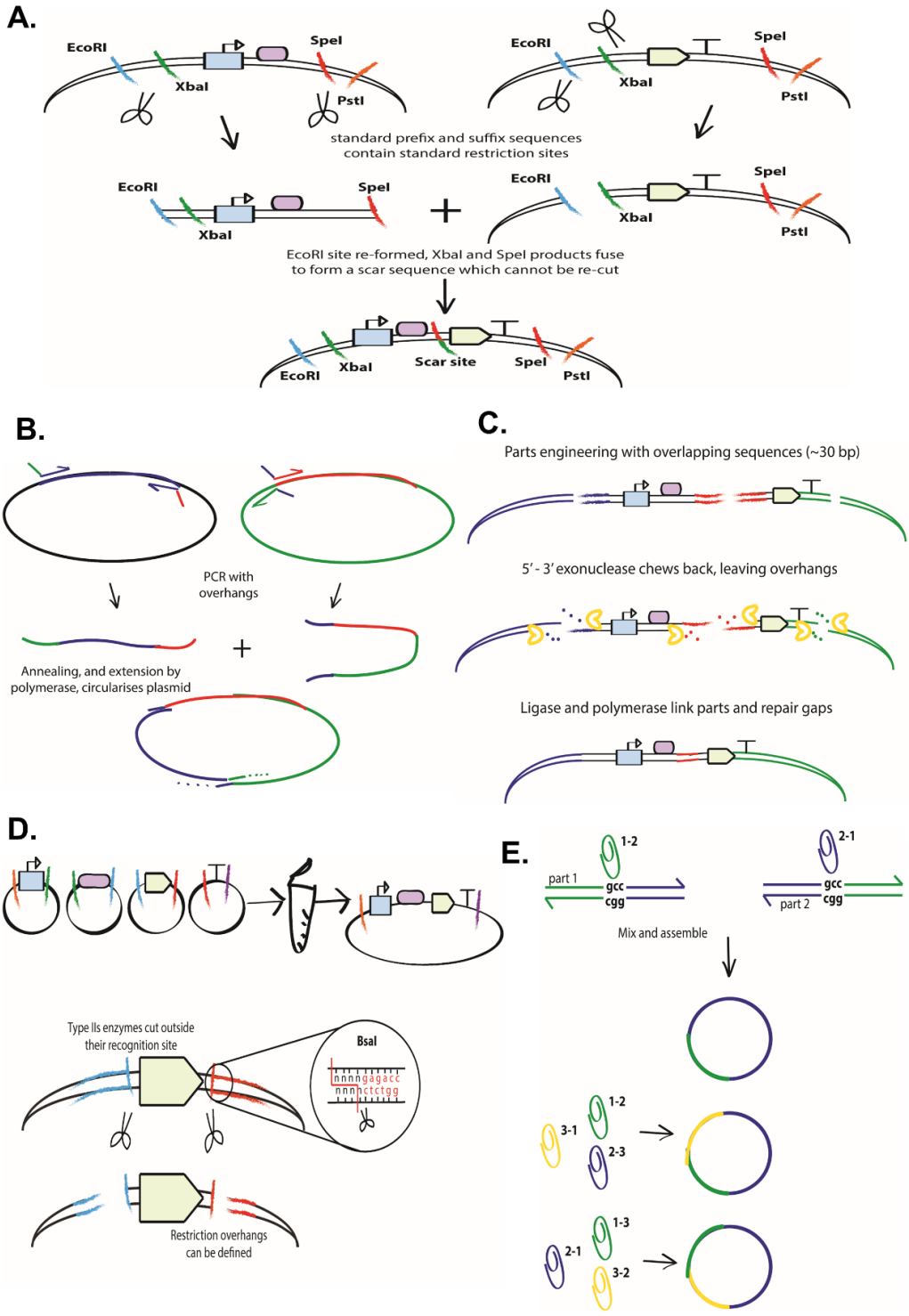

Figure 1. 3. Overview of DNA assembly techniques. A) BioBricks [TM], cloning parts via restriction digestion and ligation of resultant compatible sticky ends. B) OE-PCR, where complementary overhangs attached to DNA targets anneal during PCR. C) Gibson isothermal assembly technique, where parts have a 30 + bp overlap, and ends are processed and fused together using an exonuclease, a ligase and a polymerase. D) Golden Gate, a one-pot assembly reaction reliant on Type IIs restriction enzymes. E) PaperClip, with the use of double stranded bridging oligonucleotides (clips) constructs are assembled via PCR. Adapted from T. Ellis et al [39] and M. Trubitsyna et al [69].

The Golden Gate assembly method was chosen because this particular method, unlike BioBricks™, BglBricks, OE-PCR, CPEC, PaperClip and Gibson assembly, can assemble DNA in a single reaction. This method also allows a sequential and combinatorial assembly of parts, genes and pathways, in a cost effective and streamlined manner that better fits with synthetic biology's cycle of design, build and test (and learn) [70]. More specifically, a type of Golden Gate assembly method called Modular Cloning or MoClo was used throughout this research. MoClo tools were designed and engineered specifically for *D. alaskensis,* with an aim to assemble and test DNA components in a fast and facile manner. To date multipart modular assembly libraries have been developed for use in yeast [71, 72], *E. coli* [66, 73-75], plant [76], mammalian [77] and microalgae [78] based systems; however, to our knowledge, no such library has been reported for *D. alaskensis* or any other SRB.

From the MoClo toolkits available for *E. coli,* Table 1.1 summarises each MoClo toolkit. At the time of the conception of this project, only two MoClo toolkits were available, CIDAR MoClo and EcoFLEX. The CIDAR MoClo toolkit, was selected here because it had more parts available, the reported assembly method is very straightforward and shorter than EcoFLEX, and because most of the parts contained in the CIDAR toolkit are derived from the Biobricks Registry of Standard Biological Parts, which were selected for their functional reliability and utility in synthetic biology designs [66]. With CIDAR MoClo as our chosen toolkit, new CIDAR compliant bioparts were designed and engineered for *D. alaskensis.* Provision of these new tools to the research community and alongside those already available for *E. coli*, will enable the prompt assembly of genes and pathways tailored for *D. alaskensis.* These tools will therefore not only advance scientific research into the use of sulphate-reducing bacteria as a chassis for biotechnology, but also inform their use in heavy metal bioremediation and NP synthesis.

Table 1. 1. Comparison of MoClo toolkits available for *E. coli*

MoClo Toolkit	Time of protocol (mins)	Selection Method	Parts Available	Type IIs Enzymes	Ref.
CIDAR	Standard: 82.5 Rapid: 37.5 - 60	*LacZα* blue-white	93 parts	BsaI and BbsI	[66]
EcoFLEX	Standard: 230	*LacZα* blue-white and RFP markers	78 parts	BsaI, BsmBI and BpiI	[73]
Mobius Assembly	Standard: 85 16 TU construct: 212.5	amilCP (purple), spisPink and sfGFP (yellow) markers	16 parts	BsaI and AarI	[74]
Star-Stop Assembly	Standard: 320	*LacZα* blue-white	40 parts	SapI, BsaI and BbsI	[75]

1.2.3. Engineering and designing expression control elements

Expression control elements are required for a functional gene in prokaryotes, they form a device and consist of a promoter, a RBS, a CDS and lastly a terminator. Functional devices require all these expression control elements to be assembled in order; those with known functional characteristics are important as they allow the rational modification of metabolic pathways and the assembly of synthetic and heterologous pathways [79].

In synthetic biology, the expression control elements are DNA sequences characterised by precise functions in either transcription or translation. Promoters are DNA sequences where RNA polymerases recognise and bind at the -35 and -10 regions of an *E.coli* σ^{70} promoter and initiate the DNA transcription to mRNA. RBSs are the place where ribosomes recognise the Shine-Dalgarno sequence found on their sequence and bind to it to initiate translation. CDS encodes ORFs or small RNAs, which go through transcription until reaching a terminator. Terminators are sequences that terminate transcription, are placed at the end of a TU, and contain G-C rich motifs that during transcription they fold into a hairpin that slows down mRNA elongation by the RNA polymerase. Then a short U-A double stranded sequence is formed into the RNA polymerase active site to allow it to dissociate from the DNA [80]. All these expression control elements can be assembled into biological devices, such as important tools in research, like TUs that express reporter proteins.

This study will focus on the design and engineering of synthetic promoters and RBSs. There are two common types of promoters, constitutive and regulated. Constitutive promoters are not regulated by any DNA binding proteins, and are therefore always 'on' [38]. They are useful in synthetic biology because they provide a mostly constant level of expression. Regulated promoters frequently contain additional DNA sequences, known as operators, which allow other protein factors to bind to the DNA and modulate the transcription rate [38]. Therefore, in eukaryotic cells the transcription can be controlled by the addition of a small molecule that recruits transcription factors to the promoter regions, or utilising a second genetic circuit to produce the accessory proteins that activate the promoter. Regulated promoters can be either positively regulated (factors binding to DNA to increase transcription rate)

or negatively regulated (factors binding to DNA to decrease transcription rate) or both[38].

In prokaryotes, the RNA polymerase requires a specialised subunit, sigma factor (σ) to recognise promoter regions [81]. The prokaryote σ performs all initiation functions, and promotes transcription of thousands of genes, and many alternative sigma factors (σ^{70}, σ^{19}, σ^{24}, σ^{28}, σ^{32}, σ^{38} and σ^{54}) each promoting transcription of specialised genes necessary to cope with cellular stress or development [81].

In the gammaproteobacteria, *E. coli* the σ^{70} is the housekeeping σ factor, and performs two main functions: directs the RNA polymerase to the appropriate transcription sites, and initiates the strand separations of the double-helical DNA [81].

In deltaproteobacteria such as *D. alaskensis* spp*,* research has shown that the recognition of the promoter sequences is done primarily by a different sigma factor, σ^{54} [82]. In comparison with all other known sigma factors, σ^{54} differs that it recognizes and binds characteristic promoters with GG -24 and TGC -12 motifs, and it strictly requires ATP hydrolysis activity for the activation of the promoter complex [82, 83].

Due to the lack of a consensus σ^{54} promoter architecture, this study will focus on the design and engineering of *E. coli* σ^{70} promoters and test them in *D. alaskensis*. The *E. coli* σ^{70} core promoter structure and that of most prokaryotes, include a -35 motif and a -10 motif, which are separated and surrounded by nucleotide spacer regions in which little or no nucleotide homology has been deduced and has a consensus length of 17 bp [84-86]. The bacterial transcription initiation is a multistep process that is regulated by the σ^{70} core promoter structure [87, 88]. The first step is as previously mentioned, where the RNA polymerase recognises the -35 and -10 motifs. The sequence-specific recognition of these motifs within the dsDNA sequence contributes to the specificity of the promoter binding and orients the RNA polymerase with respect to the -10 motif, the most highly conserved and essential promoter motif [89, 90]. In the second step the promoter isomerisation generates an open complex in which the DNA between -11 and +4 is melted [91]. At the -10 motif, strand separation is triggered by the sequence-specific ssDNA binding activity, to continue the transcription [87, 91].

It is well established that the length of spacer region is critical [92]. Research suggests that alterations in the spacer region sequence can increase the promoter activity in *E.coli* [93]. However, it has a limited effect over the transcription initiation in comparison with the -35 and -10 motifs [89].

The core promoter region is considered a minimal promoter, since these are the minimal elements necessary to enable transcription initiation [85], (Figure 1.4). Promoter engineering is done by varying the sequence within the core promoter structure, particularly within the -35 and -10 motifs, making it possible to vary the strength of the promoter, either to increase or decrease the number of mRNA copies that are made from it per second. An upstream region called the up-element is present in some promoters, this region is typically adenine/thymine rich, and can boost transcription rate through interactions with the c-terminal domain of the RNA polymerase α-subunit [84].

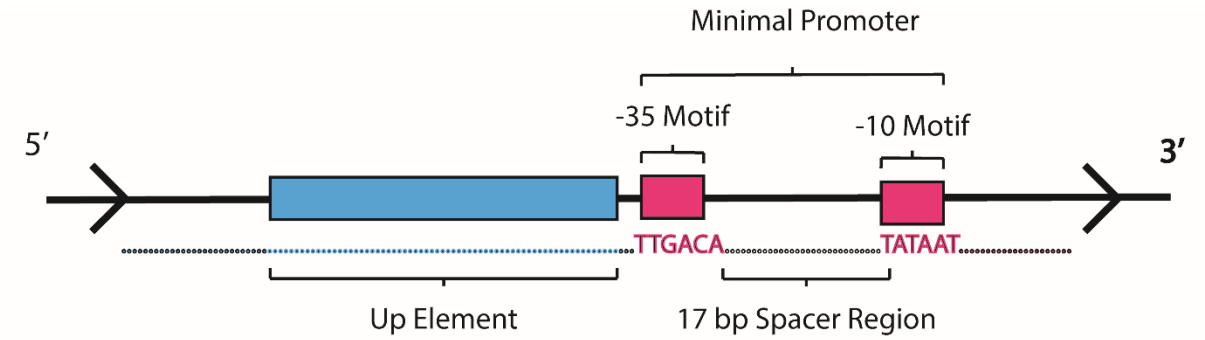

Figure 1.4. Consensus promoter motifs and architecture for prokaryotic promoters; based on *E.coli* σ^{70} promoter architecture. Adapted from 'Promoter engineering: Recent advances in controlling transcription at the most fundamental level', by J. Blazeck *et al* [85].

Promoter engineering is becoming an enabling technology that will facilitate the optimisation of metabolic pathways and fine-tune expression of heterologous proteins. The basis for promoter engineering is related to its architecture. By varying the DNA in these spacer regions, changing the motifs in already existing promoters, or designing new synthetic promoters (not found in nature) you can modulate the expression potential of such promoters. Many techniques exist to engineer the prokaryotic promoters. Error-prone-PCR (Ep-PCR) introduces random mutations into the DNA sequence of choice. An example of the use of Ep-PCR for promoter engineering is for the generation of an engineered promoter library of P_L-λ constitutive *E. coli* of varying strengths [94]. This technique led to the engineering of a promoter library with varied strength that were used to fine-tune the expression of heterologous proteins, such as GFP [94]. Another promoter engineering technique is through the saturation mutagenesis of nucleotide spacer regions, while maintaining the -35 and -10 motifs intact. A promoter library of *Lactococcus lactis* was engineered using saturation mutagenesis to modulate its strengths [95]. This finding is relevant because it highlights the importance of the spacer region's sequence to modulate a promoter strengths. Not only was this research able to generate a promoter library with varying strengths for *L. lactis*, but this library was also proven to work in *E. coli,* but with different strengths. An additional promoter engineering technique is through hybrid promoter engineering, which entails the assembly of enhancer element-core promoter fusions to rationally enhance basal core transcriptional capacity or enable novel promote regulation [85]. This technique led to the engineering of many commonly used promoters, including the *tac* promoter (hybrid of *trp* and *lac* promoters) [96] and the $rhaP_{BAD}$, (hybrid of arabinose and rhamnose regulated promoters) [97].

To predict a promoter's DNA sequences, or more importantly to predict the -35 and -10 motifs, many bioinformatics tools could be used, each with a specific algorithm tailored for a specific organism or sigma factor. A list of bioinformatics tools to predict bacterial promoters are: BPROM (Softberry) [98], finds potential promoters with significant features of conserved sequences of known promoters in *E. coli*. BacPP (Bacterial promoter prediction) [99] , predicts promoters from all know σ factors. Promoter Prediction by Neural Network [100], an eukaryotic core promoter

region predictor based on *Drosophila melanogaster*. PromoterHunter [101], a tool for promoter search in prokaryote genomes. PePPER [102], a mining and visualising software of prokaryote promoter elements. DOOR2 [103], an online operon prediction on user-provided genomic sequences. Virtual Footprint [104], a pattern-matching tool for the prediction of promoter regions. CNNPromoter[105], a prokaryote and eukaryote convolutional neural network promoter predictor. In this study, BPROM was used to predict the -35 and -10 motifs to design and engineer synthetic promoters, because at the time, this tool was cited on numerous publications of importance to this project [106, 107].

Modifying the RBS strength is an efficient approach to tune gene expression level in prokaryotic systems. Small changes in the RBS sequence can result in the up- or down- regulation of translation [108]. RBS engineering tools are geared to change the translation initiation rate (TIR), because the TIR can be calculated solely from the RBS nucleotide sequence [108]. The engineering of RBS nucleotide sequences relies on bioinformatics tools that predicts nucleotide sequence and their respective TIR, to generate libraries that can be characterised. Similarly, to the methods and technologies used to engineer promoters, engineering the RBS is mostly done by targeted mutagenesis and iteration of nucleotide sequences with a different predicted TIR [109].

To predict the RBS's nucleotide sequences and its respective TIR, many bioinformatics tools could be used, each with a specific algorithm tailored for a specific organism. A list of bioinformatics tools to predict bacterial RBS are: the RBS calculator [110], is a predictive design method for controlling translation initiation in bacteria. The 'MAGE Oligo Design Tool' (MODEST) [111], allows the identification of most regulatory coding regions. The 'Empiric Model and Oligos for Protein Expression Changes' (EMOPEC) [112], a free tool that modulates the expression level of any *E. coli* gene. 'Reduced Libraries' (RedLibs) [113], algorithm that identifies globally optimal degenerate RBS. RBSDesigner [114], an algorithm that predicts the translation efficiency of an existing mRNA sequence and designs RBSs. The UTR Designer, a quantitative prediction method that predicts the translation efficiency and designs RBS's sequences. In this study, the RBS calculator was used to predict nucleotides in order to design and engineer synthetic RBS. At the time, this

tool was cited on numerous publications of importance to this project [108, 110, 115, 116], it is also a proven reliable *E. coli* RBS predictor [110], and has the option to enter *D. alaskensis* G20 into the program as the organism of choice.

1.2.4. Characterising expression control elements

Synthetic biology aims to robustly characterise expression control elements, particularly promoters and RBSs, to aid the assembly of fine-tuned pathways and devices that give a predictable response [39]. The utility of expression control elements will increase if their behaviour, both in isolation and in combination, were more predictable. The prediction of behaviour depends on the initial designs and refinement of the expression control elements, the characterisation of each is imperative. The proper characterisation of expression control elements is embedded in synthetic biology, since the standardisation and characterisation of parts has been instrumental in the managing of complexity in engineering fields [117].

To ascertain a thorough characterisation of expression control elements, it is ideal to characterise them *via* quantitative methods. Not only it will enable to compare quantitative values but it can also establish their order within a synthetic library. Expression control elements such as promoters are characterised by the expression of a reporter gene that can be quantified, for example GFP (green fluorescent protein). Numerous promoter libraries from a variety of microorganisms have been characterised using fluorescent reporters, for example *E. coli* [112, 117-120] , *B. subtilis* [118], *Saccharomyces cerevisiae* [94, 118], and *Yarrowia lipolytica* [72]. An alternative quantitative method is through the measurement of a desired gene at the transcriptional level, by measuring its mRNA level relative to that of a gene expressed at a constant level using quantitative RT-PCR. Characterising expression control elements through RT-PCR has been undertaken with *E. coli* [112, 120] , and *S. cerevisiae* [94]. Parts can also be characterised by assaying their resistance to antibiotics, by measuring the minimum inhibitory concentration among the libraries, expressing an antibiotic resistance cassette under different expression controls [94]. Alternative measurement methods for the characterisation of parts are by using colorimetric reporters including glucuronidase [121], β-galactosidase [122], alkaline

phosphatase [123] and chloramphenicol acetyltransferase [124]. Additionally luminescent reporters such as luciferase, have been used to characterise expression control elements [122]. The choice of reporter used to characterise expression control elements, however, will depend on the cell line used, the nature of the experiment, and the adaptability of the assay to the appropriate detection method [125, 126].

Reporter genes are the most commonly used technology to characterise expression control elements. Reporter gene technology was first used as a method for analysing the activity of expression control elements such as enhancers and promoters in the upstream region of genes [127]. The popular use of reporter genes as a technology to characterise expression control elements is because they have the advantage of low background activity in cells and in many cases, the activity can be amplified to produce a highly sensitive, and often easy to detect response [127]. Table 1.2 summarises some of the advantages and disadvantages of the most common reporter genes used to characterise expression control elements. The reporter gene used to monitor transcriptional activity in cells was chloramphenicol acetyltransferase [128] ; is a bacterial enzyme that can detoxify chloramphenicol, an inhibitor of prokaryotic protein synthesis, by catalysing the transfer of acetyl groups from acetyl CoA to the 3-hydroxyl position of chloramphenicol [127]. However, this method relied on radioisotopes and ELISA, the linear range and sensitivity of the assay is not as broad as other methods. β-galactosidase is a well-characterised bacterial enzyme and has been used as a simple colorimetric assay of poor sensitivity and narrow dynamic range to monitor transcriptional activity in cells. It has an advantage over chloramphenicol acetyltransferase in that the assay is simpler and does not involve the use of radioisotopes [127]. Luciferase refers to a family of enzymes that catalyse the oxidation of various substrates (e.g. luciferin and coelenterazine), resulting in light emission, which can be quantified to monitor transcriptional activity in cells. The downside of using a luciferase reporter gene is that it requires a substrate and ATP and in most occasions, it requires oxygen. The secretable form of alkaline phosphatase (SEAP) is a reporter gene that quantifies transcriptional activity in cells through an inexpensive colorimetric assay. The protein is secreted from the cell and can be detected by sampling the culture medium, cells remain intact and viable. Aequorin and GFP are proteins that were isolated from the bioluminescent jellyfish

Aequorea victoria. GFP is autofluorescent and does not require the presence of any cofactors or substrates to generate light unlike Aequorin. The greatest advantage of GFP is that in the absence of cell lysis, noninvasive monitoring of living tissue is possible [127]. However, it requires the presence of oxygen to successfully mature and fluoresce.

Low oxygen environments are frequently a requirement in a broad range of biomedical and industrial bioprocesses, including bioremediation, fermentation of high-value biomolecules, and especially in biotechnology applications for obligate anaerobes [129]. Methods to characterise expression control elements abound, however to rapidly measure and characterise them under anaerobic conditions, the options are limited. Most reporter genes require molecular oxygen [127], an important limitation that needs to be addressed, to enable further research of the anaerobic bacterium, *D. alaskensis*. Recently flavin-based fluorescent proteins (FbFPs), such as iLOV, which are derived from Light-Oxygen-Voltage (LOV) photoreceptor proteins [130, 131], have become the staple oxygen-independent fluorescent reporters. FbFPs have many advantages over GFP and its related analogues, for example, FbFPs have been shown to be expressed and to fluoresce anaerobically in multiple organisms such as *Porphyromonas gingivalis*, *Saccharomyces cerevisiae* and *Candida albicans* [132-136], while they are also thermostable and fast-maturing probes with a broad operational pH range (4 – 11) [137]. CreiLOV, an FbFP with blue light LOV domains, found in *Chlamydomonas reinhardtii* has been demonstrated to be the brightest FbFP reporter to date [137]. CreiLOV has a reported quantum yield ~1.5-fold larger than iLOV [130, 137, 138].

In this study, designed oxygen-independent fluorescent reporters were engineered and screened for fluorescence emission, and ultimately used to characterise expression control elements in *D. alaskensis*.

Table 1. 2. Comparison of commonly used reporter genes. Adapted from 'Reporter Gene Technology: The Future Looks Bright', by L.H. Naylor [127]

Reporter Gene	Advantages	Disadvantages
Chloramphenicol acetyltransferase	No endogenous activity. Automated ELISA available. Does not require presence of O_2.	Narrow linear range; use of radioisotopes; stable. Enzymatic reaction.
β-galactosidase	Well characterised; stable; simple colorimetric readouts; sensitive bio- or chemiluminscent assays available. Does not require presence of O_2.	Endogenous activity (mammalian cells). Enzymatic reaction.
Luciferase (firefly)	High specific activity; no endogenous activity; broad dynamic range; convenient assays.	Requires substrate (luciferin) and presence of O_2 and ATP. Enzymatic reaction.
Luciferase (bacterial)	Good for measuring/analysing prokaryotic gene transcription. Does not require presence of O_2.	Less sensitive than firefly luciferase; not suitable for mammalian cells. Enzymatic reaction.
Alkaline phosphatase	Secreted protein; inexpensive colorimetric and highly sensitive luminescent assays available.	Endogenous activity in some cells, interference with compounds being screened. Enzymatic reaction.
Green fluorescent protein (GFP)	Autofluorescent (no substrate needed); no endogenous activity; mutants with altered spectral qualities available.	Requires post-translational modification and presence of O_2; low sensitivity (no signal amplification).
FBFPs LOV	Autofluorescent (no substrate needed); no endogenous activity; works under anaerobic and aerobic conditions [130, 131].	Requires post-translational modification; low sensitivity (no signal amplification); not well characterised.

1.3. Cell-Surface Engineering

1.3.1 Overview of Cell-Surface Engineering

Microorganisms, such as *D. alaskensis* cannot grow without metal ions; however, some of these metal ions are toxic at high concentrations but are essential at trace concentrations [139]. In addition, some metal ions have strong toxic activity at low concentrations. As previously mentioned, metal pollution has become an important environmental issue because of the non-degradable nature of metal ions [140]. Not only will the recovery of metal ions from wastewater, contaminated land and discarded technology products be an invaluable future resource of these metal ions, but it will also help reach sustainability goals. Conventional methods and approaches traditionally used for the recovery of metal ions, rely on physicochemical techniques that include precipitation, ion exchange, electrochemical methods, solvent extraction, membrane filtration and reverse osmosis [139]. However, these techniques lack specificity, are not environmentally friendly, not always cost-effective, and are inefficient when dealing with low concentrations [141]. Potentially, a more environmentally friendly approach is through bioadsorption, or the innate ability of microorganisms, fungi, algae and plants to absorb metal ions [142].

Microorganisms use two processes of metal ion adsorption. The first adsorption process is bioaccumulation, which is the active uptake of metal ions, where they are transported into the cytoplasm and then either sequestered into cellular compartments or detoxified by enzymatic reduction. However, it is hard to recover metal ions that have been bioaccumulated, because it requires a lysis step. The second adsorption process is a through the binding of metal ions to the cell surface by polysaccharides, adsorption associated proteins, and functional groups [139]. Cell surface adsorption occurs in living and dead cells, because it is the cell surface that interacts with the surrounding material, which enables an easy recovery of metal ions. Cell surface engineering enables outer membrane expression of proteins and peptides by fusing these to anchoring proteins (transmembrane proteins), which enable the tethering of proteins on the outer membrane. This technique was used in this study, as a potential way to enhance *D. alaskensis*' ability to thrive in environments highly enriched with heavy metals. The use of cell surface engineering for displaying proteins and peptides tethered to the microorganisms' outer membrane has been performed in

various bacteria [143-145]. Methallothioneins and phytochelatins are naturally occurring, cysteine-rich metal-binding peptides [145]. The expression of these metal-binding peptides on the outer membrane of microorganism may confer a higher tolerance to those metals and may improve heavy metal NP synthesis. Gram-negative bacteria such as *D. alaskensis* possess a complex cell envelope structure, meaning that the anchoring proteins require an efficient signal peptide, a strong anchoring structure, compatibility with the host cell, and be protease resistant [143]. Anchoring proteins such as IgA protease (subunit, no protease activity), Ice Nucleation Protein (INP), OmpA, Lpp-OmpA are anchoring motifs that are regularly used in cell surface engineering of Gram-negative bacteria [143, 146, 147]. An illustration of the depiction of cell surface engineering in *D. alaskensis* can be appreciated on Figure 1.5.

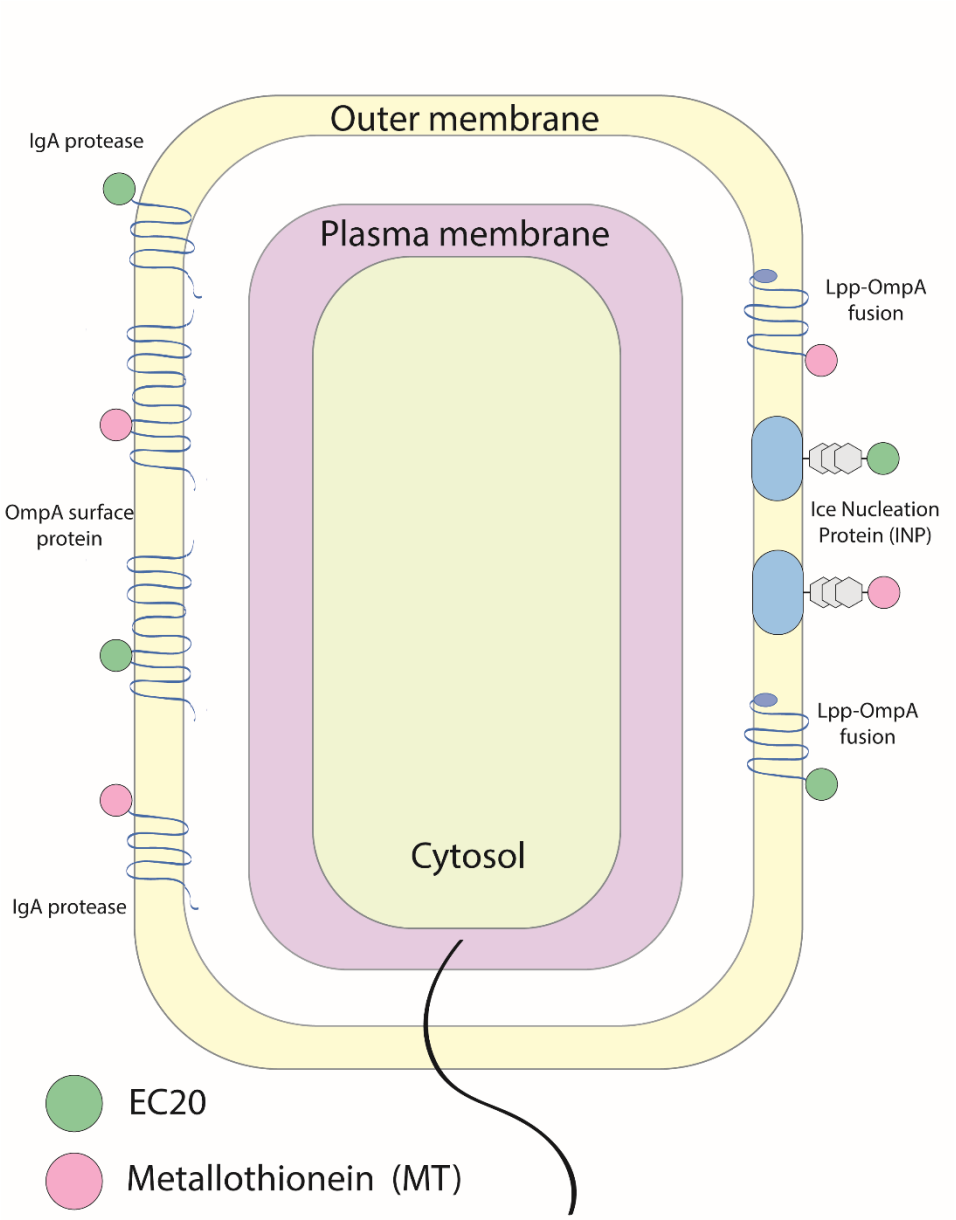

Figure 1. 5. Illustration of cell surface engineering in *D. alaskensis*. Metal binding proteins (EC20 and MT) are tethered to the cell membrane using anchoring proteins (IgA protease, OmpA surface protein, Ice Nucleation Protein, and Lpp-OmpA fusion protein).

The synthetic phytochelatin EC20 has previously been used to enhance the bioaccumulation of heavy metals in Gram-negative bacteria [148]. Moreover, it has been shownthat the expression of phytochelatin synthase and metallothionein conferred to *E. coli* the ability to synthesize different metal NPs such as Cd, Se, Zn, Te, Fe, Co, Ni, Mn, Cs, Sr, Au, Ag, Pr and Gd[6]. Recently, recombinant *E. coli* strains expressing either phytochelatoin synthase, phytochelatins or metallothionein, were reportedly able to synthesize EuSe NPs, which exhibited high fluorescence, magnetic and anticancer properties [149]. The successful expression of synthetic phytochelatin EC20 in other Gram-negative microorganisms such as *Moraxella sp* [145], *Pseudomonas putida* [150] and *Ralstonia eutropha* [151] sets precedent for the possibility to express EC20 on the outer membrane of the Gram-negative bacteria *D. alaskensis*. The expression on EC20 on the outer membrane of *D. alaskensis* to our knowledge has never been attempted, and since it has been shown that EC20 has metal-binding properties, it was hypothesised that if expressed by *D. alaskensis* it may increase its affinity to metals, confer better metal-binding capacity and/or specificity and selectivity [152].

1.4 Aims of Research in Presented Thesis

The interest in carrying out this project was led by the lack of synthetic biology tools available for non-model organism *D. alaskensis.* This research aims to adapt already existing tools to *D. alaskensis,* engineer new tools for it, and to design the necessary parts for a complete MoClo toolkit, which includes libraries of characterised oxygen-independent fluorescent reporters, and synthetic promoter and RBS libraries. With the ultimate aim to accelerate the research into heavy metal bioremediation and NP synthesis, the newly engineered *D. alakensis* MoClo toolkit will enable the easy, time and cost effective DNA assembly of genes and pathways involved in the synthesis of NPs. These tools will be applied to tailor *D. alaskensis* NP synthesis and its applications within the bioremediation studies.

As a proof of concept, the *D. alaskensis* MoClo toolkit was used to tailor NPs synthesis. Using a NiFe hydrogenase small subunit (KEGG, Dde_2137), a periplasmic enzyme proven to reduce metals such as Pt and Pd. A combinatorial

library was assembled using this toolkit; their Pt NP synthesis were assessed and compared to controls, and their oxidative and reducing catalytic activities were tested. This accomplishment showed that the application of these synthetic biological tools could be used to study NP synthesis in *D. alaskensis.*

Moreover, a cell-surface engineering study was undertaken for *D. alaskensis,* to test if the expression of the synthetic phytochelatin (EC20), affects its tolerance to Cu, Pt and Pd ions, and if it affects its NP synthesis capabilities.

Chapter 2: Materials & Methods

2.1. Materials and Reagents

Chemicals were purchased from Sigma-Aldrich (St. Louis, MO): ampicillin, chloramphenicol, spectinomycin, sodium chloride, isopropyl-β-D-thiogalactopyranoside (IPTG), 5-bromo-4-chloro-3-indolyl β-D-galactopyronaside (X-GAL), Methylene-blue and 2,6-Dimethoxyphenol (2,6-DMP). PCRs were performed using Phusion polymarease, New England Biolab (NEB Cat #M0530S). Restriction enzymes, polymerases, ligases, and 1 Kb DNA ladders were purchased from NEB. Transformations were performed with NEB 5-alpha competent cells (NEB). Agarose gel DNA Extraction, PCR Purification, Plasmid Isolation kits were purchased from QIAGEN. Primers were synthesised by Sigma-Aldrich. Plasmids with CreiLOV and *E.coli* CreiLOV genes were synthesised by Genewiz (South Plainfield, NJ). Gblocks were synthesised by Integrated DNA Technologies (IDT).

2.2. Molecular Biology Methods

2.2.1. Polymerase Chain Reaction (PCR)

All PCR reactions were carried out using commercially available reagents from New England Biolabs, following the manufacturer's protocol with the Phusion High-Fidelity DNA Polymerase(NEB). PCR conditions were tailored to the size of PCR product and the annealing temperatures of the primers used in each reaction as instructed by the provided kit. All PCR reactions were performed using a Bio-Rad T100 Thermal Cycler.

2.2.2. Restriction Digestion and Ligation

Restriction digestion reactions were carried out using commercially available reagents from NEB. Reaction volumes were adjusted accordingly to 50 µL or 25 µL, depending on their purpose, following the manufacturer's protocol.

Ligation reactions were performed in 20 µL total volume reactions, using T4 DNA Ligase, NEB Cat#M0202S. Following the manufacturer's protocol, the vector to insert ratio was 1:3.

2.2.3. DNA Sequencing

DNA sequencing was performed by DNA Sequencing & Services (MRC I PPU, School of Life Science, University of Dundee, Scotland, www.dnaseq.co.uk) using Applied Biosystems Big-Dye Ver 3.1 chemistry on Applied Biosystems model 3739 automated capillary DNA sequencer.

2.2.4. Site-Directed Mutagenesis

Mutations to plasmids were performed using QuikChange Lighting Site-Directed Mutagenesis Kit, Agilent Technologies, and Cat#210518. DNA primers were designed using Agilent's primer design program. Primers were synthesised by Sigma-Aldrich. Verification of the mutations was carried out by sequencing.

2.2.5. Agarose Gel Electrophoresis

Agarose gels were made to a concentration of 0.8% by adding agarose to 1X TAE buffer (Table 2.4). The solution was then heated to boiling temperature until the agarose was completely dissolved. A volume of 0.005% mL SYBR Safe DNA Gel Stain was added to the dissolved solution. The gel was poured onto the casting stand (Geneflow electrophoresis tank) and allowed to cool. The gel was submerged into a gel tank filled with 1X TAE buffer (Table 2.4). Electrophoresis was performed with a voltage ranging from 90 -110 V and for 40 – 60 min. Electrophoresis was performed using a Bio-Rad PowerPac HC. Visualisation of DNA in agarose gels was performed using a Syngene, G:Box with a SYBR Safe detection filter.

2.2.6. Plasmid isolation and sequence analysis

All plasmid extractions were carried out using a commercially available plasmid extraction kit (QIAGEN, QIAprep Spin Miniprep Kit, Cat#27104) following the manufacturer's protocols. Sequences were analysed using the Electronic Lab Notebook software Benchling (San Francisco, CA, USA).

2.2.7. Agarose gel DNA extraction

DNA extractions and purifications from agarose gels were carried out using the QIAGEN, QIAquick Gel Extraction Kit, Cat#28704.

2.2.8. PCR purification

PCR DNA amplified products were purified using the commercially available kit QIAGEN, QIAquick PCR purification Kit, Cat#28104.

2.2.9. MoClo Assembly Reaction

The MoClo assembly reaction was performed by adding equimolar amounts of 10-60 fmol of each DNA component and acceptor vector to a 0.2 mL tube (ΔpMOMoClo, DVA_AB, DVA_BC, DVA_CD and ΔpMOMoClo_AF). To the same tube, 10 U of BsaI (NEB), 20 U of Quick T4 DNA Ligase (NEB), 1x T4 DNA Ligase Buffer (NEB) and sterile deionized water to a total volume of 20 µL was added. Reactions were performed using the following parameters: 16 cycles at 37°C for 1.5 min, then 16°C for 3 min, followed by 50°C for 5 min and 80°C for 10 min and were then held at 4°C.

2.3. *E. coli* culturing

2.3.1. Growth and transformations of *E. coli*

E. coli strains were grown in LB broth (Table 2.4) at 37°C with rotary shaking at 250 rpm, or LB agar plates. All transformations were performed with 2-5 µL of the desired reaction into 50 µL of NEB 5- alpha Competent *E. coli* (NEB). For heterologous protein expression in *E. coli*, transformations were performed with 2-5 µL of the desired reaction into 50 µL of *E. coli* JM109 cells. Cells were plated on appropriate antibiotic selection LB agar (See Table 2.3). For blue-white screening, plates were supplemented with 20 mg/µL 5-bromo-4-chloro-3-indolyl β-D-galactopyronaside (X-GAL) and 0.1 M isopropyl-β-D-thiogalactopyranoside (IPTG), Sigma-Aldrich (St. Louis, MO). Blue-white screening was used to select colonies which were grown overnight at 37°C in LB supplemented with the appropriate antibiotic (See Table 2.3).

2.3.2. Frozen stock preparation

E. coli cultures were grown for 24 hours at optimum growth conditions. A volume of 0.5 mL of bacterial culture was transferred to a screw top microcentrifuge tube. A volume of 0.5 mL of 50% glycerol was added to each tube to obtain a 25% glycerol stock of each bacterial culture. Glycerol stocks were stored at -80°C.

2.4. *D. alaskensis* culturing

2.4.1. Growth of *D. alaskensis*

Growth of *D. alaskensis* G20 (purchased from DSMZ, DSM No. 17464) was conducted using Postgate Media C (PGMC, Table 2.4) using lactate as a source of

carbon. Growth and manipulations of *D. alaskensis* were carried out at 30°C in an anaerobic hood fed with 10% CO_2 and 10% H_2 in nitrogen.

2.4.2. Preparing electrocompentent cells and Electrotransformation of *D. alaskensis*

D. alaskensis competent cells were made by following a modified version of Li and Krumholz (2007) [153]. Cultures of *D. alaskensis* G20 were grown to early stationary phase (OD_{600}; 0.6 -0.8) under anaerobic conditions. Cells were centrifuged for 15 minutes at 4000 rpm and resuspended in 10 mL ice-cold sucrose solution (400 mM Sucrose, 1 mM $MgCl_2$, filtered and sterilized). The pellets were then resuspended and centrifuged twice more, with the final resuspension using 1 mL sucrose solution. To 100 µL, 1 µg of plasmid DNA was added and transferred into a 1mm electroporation cuvette (Eurogentec, Belgium). Cells were then shocked with 1.5 kV using a Micro-Pulser ™ (Bio-Rad, CA). Cell were recovered with 1 mL PGMC and transferred into microcentrifuge tubes, incubated anaerobically at 30°C and fed with 10% CO_2 and 10% H_2 in nitrogen for 4 hours. Cells were spun down and resuspended in 100 µL of PGMC, then plated onto PGMC plates supplemented with the appropriate antibiotic (See Table 2.3).

2.4.3. *D. alaskensis* frozen stocks preparation

Bacterial cultures were grown anaerobically until cultures reached an OD_{600} 0.6–0.8 at optimum growth conditions. A volume of 0.5 mL of bacterial culture was transferred to a screw top microcentrifuge tube. A volume of 0.5 mL of 50% glycerol was added to each tube to obtain a 25% glycerol stock of each bacterial culture. Glycerol stocks were snap-frozen using liquid nitrogen and stored at -80°C.

2.5. Tables of oligonucleotides, plasmids, reagents and strains used

No.	Oligonucleotide	Sequence
1.	DaP01_pMO9075-F	CGCAGTACTCCTTACGTAG
2.	DaP02_pMO9075-R	CAGATCGTGATCCCCTG
3.	DaP21_pMO9075-GGA-F	ATTCCGGGGTCTCCATCGCAGTACTCCTTACGTA
4.	DaP22_pMO9075-GGA-R	ATTCCGGGGTCTCGTCAGATCGTGATCCCCT
5.	DaP23_BsLOV-GGA-F	ATTCCGAGGTCTCCCTGATTCAACTATTCATTAAGGAGGGA
6.	DaP24_BsLOV-GGA-R	ATTCCGAGGTCTCCCGATAACGCGAAGTAATCTTTTCG
7.	DaP25_PpLOV-GGA-F	GCCTCTTGGTCTCGCTGCAAACAGTAATACATAAAAGAGGAGG
8.	DaP26_PpLOV-	GCCTCTTGGTCTCCCGATAACGCGAAGTAATCTTTTCG

	GGA-R	
9.	DaP15_pMO9075_ins-F	CCGCCAAGGATCTGATG
10.	DaP16_pMO9075_ins-R	GAATTCGCCCTTGCATG
11.	FWD Kan Prom	GTTCTAGAGGGTCTCAGGAGATCCGGAATTGCCAGCTGGGGC
12.	REV Kan Prom	CTGAATTCAGGTCTCTAGTAACCCCTGCGCCATCAGATCCTT
13.	FWD mBFP pMO9-10	GTTCTAGAGGGTCTCAAATGATATGCAGAACCTGAATGGTAA
14.	REV mBFP pMO9-10	CTGAATTCAGGTCTCTACCTACGGCCGCGAAGCCCCCGTCAA
15.	FWD GFP pMO8-7	GTTCTAGAGGGTCTCAAATGATATGGTGTCCAAAGGGGAAGA
16.	REV GFP pMO8-7	CTGAATTCAGGTCTCTACCTACTTTATAAAGCTCATCCATCC
17.	Vector Forward VF2	TGCCACCTGACGTCTAAGAA
18.	Vector Reverse VR	ATTACCGCCTTTGAGTGAGC
19.	Seq MoClo Fwd 2	GCGAAGTCGAGGCATTTCTGTC
20.	Seq MoClo Rev 2	AAGAGCGCACTTATACATCG
21.	AE_pMO9075 FWD	TTCTACTAGTAGCGGCCGCTAACATGTGAGCAAAAGGCCA
22.	AE_pMO9075 REV	GTGCAGGTCTCTAAGCATGTCTTTCCTGCGTTATCCCCTG
23.	DVK_AE FWD	CAGGGGATAACGCAGGAAAGACATGCTTAGAGACCTGCAC
24.	DVK_AE REV	TGGCCTTTTGCTCACATGTTAGCGGCCGCTACTAGTAGAA
25.	FWD_BbsIMutant pMO	GAAAGGCTCAGTCGGCTGGGCCTTTCGTTT
26.	REV_BbsIMutant pMO	AAACGAAAGGCCCAGCCGACTGAGCCTTTC
27.	FWD pMO8 BbsIMutant	AACTGAAAGGCATTGATTTCAAAGAGGACGGAAATATACTGGG
28.	REV pMO8 BbsIMutant	CCCAGTATATTTCCGTCCTCTTTGAAATCAATGCCTTTCAGTT
29.	FWD_2137	GTTCTAGAGGGTCTCAAATGAATGAAGTTTTCTGTGGGTCT
30.	REV_2137	CTGAATTCAGGTCTCTACCTACCTACATTTCGTAGAACGGGC
31.	FWD_SiteMut_2137	AAGTTTTCTGTGGGCCTCGGCAAAGAGGGC
32.	REV_SiteMut_2137	GCCCTCTTTGCCGAGGCCCACAGAAAACTT
33.	REV_phiLOV2	CTTCTAGAAGGTCTCTTACCTACGATCGTGATCACTAGTTTAC
34.	FWD_phiLOV2	GTTCTAGAGGGTCTCAAATGATGCTAGCTCAGTCCTAGGTAT
35.	FWD_DsLUC	GTTCTAGAGGGTCTCAAATGATATGATCGAAAAGTCCTTCGT
36.	REV_DsLUC	CTGAATTCAGGTCTCTACCTACTTACACGTGGTCGGAGCCCA
37.	FWD_BbsIMutant	GAAAGGCTCAGTCGGCTGGGCCTTTCGTTT
38.	REV_BbsIMutant	AAACGAAAGGCCCAGCCGACTGAGCCTTTC
39.	#EC20pHEB FWD	TCTGATGGCGCAGGGGATCAATGAAATACCTATTGCCTACGG
40.	#EC20pHEB REV	GGGGGCTTGAATTCGCCCTTTTAGAAACGAATCTGTATTTTAATTTGT
41.	#pMO9075 FWD	AAATACAGATTCGTTTCTAAAAGGGCGAATTCAAGCCCCC
42.	#pMO9075 REV	GTAGGCAATAGGTATTTCATTGATCCCCTGCGCCATCAGA
43.	Seq #pMO9075 FWD	TTTTGAGACACGGGCCAGAGCTGC
44.	Seq #pMO9075 REV	CCCGATTCTCGACGAGCTGAAAGC
45.	FWD PR-8	ACTAGGGGTCTCAGGAGATTTCAAAGGCATGCATAAGGCTCG CGTTACGAAATTACTAGAGACCATATCC
46.	REV PR-8	TGATCCCCAGAGTCCTCTAAAGTTTCCGTACGTATTCCG AGCGCAATGCTTTAATGATCTCTGGTATAGG
47.	FWD PR-10	ACTAGGGGTCTCAGGAGATTTCAGA GGCATGCATAAGGCTCG GGTTACCATATTACTAGAGACCATATCC
48.	REV PR-10	TGATCCCCAGAGTCCTCTAAAGTCTCCGTACGTATTCCG AGCCCAATGGTATAATGATCTCTGGTATAGG

Table 2. 1. List of oligonucleotides used in this work. Oligonucleotides designed for oxygen-independent reporter library cloning No. 1-10. Oligonucleotides to PCR-amplify pMO9075 backbone for Gibson assembly No. 1-2. Golden Gate assembly oligonucleotides No. 3-8. Sequencing oligonucleotides No. 9 and 10. Oligonucleotides designed for new MoClo basic parts No. 11- 16 and No. 33 -36.

Sequencing oligonucleotides No. 17-20; No 17-18 correspond to oligonucleotides used to sequence new basic parts, No. 19 and 20 correspond to oligonucleotides used to sequence transcriptional units (TUs). No. 21-24 correspond to oligonucleotides used to amplify the insert and vector to assemble the acceptor vector ΔpMOMoClo. No. 25 and 26 correspond to oligonucleotides used to remove the BbsI recognition sites in ΔpMOMoClo through Site-Directed Mutagenesis. No. 27 and 28 correspond to oligonucleotides used to remove the BbsI recognition sites in DVa_pMO8 through Site-Directed Mutagenesis. No. 29 and 30 are oligonucleotides used to adapt the NiFe hydrogenase to MoClo. No. 31 and 32 correspond to oligonucleotides used to remove the BsaI recognition sites in pMO2137. No. 37 and 38 correspond to oligonucleotides used to remove the BbsI recognition site from DVa_LUC. No. 39 - 42 correspond to oligonucleotides to PCR the backbone and insert for Gibson assembly of pMOEC20. No. 43 and 44 are oligonucleotides used for the sequencing of pMOEC20. No. 45–48 correspond to the set of complementary oligonucleotides of the synthetic promoter PR-8 and PR-10.

Table 2. 2. Strains used in the study.

Strain	**Characteristics**	**Reference/Source**
E. coli NEB 5- alpha	cloning strain	New England Biolabs
D. alaskensis G20	wild-type strain	[153]
E. coli JM109	cloning strain	New England Biolabs

Table 2. 3. Plasmids used in the study.

Plasmid	**Relevant details**	**Antibiotic Used**	**Reference**
pUC19	pMB1, *lacZα*	50 µg/mL Ampicillin	NEB
pMO9075	pBGI *D. alaskensis* plasmid backbone.	50 µg/mL Spectinomycin	[5]
DVA_AB	MoClo destination vector, based on PSB1A2 with fixed illegal site, and *lacZα*.	50 µg/mL Ampicillin	Addgene #66039
DVA_BC	MoClo destination vector, based on PSB1A2 with fixed illegal site, and *lacZα*.	50 µg/mL Ampicillin	Addgene #66044
DVA_CD	MoClo destination vector, based on PSB1A2 with fixed illegal site, and l *lacZα*.	50 µg/mL Ampicillin	Addgene #66045
DVK_AE	MoClo destination vector, based on pSB1K3, *lacZα*.	50 µg/mL Kanamycin	Addgene #66067
DVK_EF	MoClo destination vector, based on pSB1K3, *lacZα*.	50 µg/mL Kanamycin	Addgene #66069
DVA_AF	MoClo destination vector, based on pSB1K3, *lacZα*.	100 µg/mL Ampicillin	Addgene #66041
ΔpMOMoClo	pBGI *D. alaskensis* plasmid backbone, MoClo destination vector, *lacZα* and fixed illegal site.	50 µg/mL Spectinomycin	This study
ΔpMO9075	pBGI *D. alaskensis* plasmid backbone, and fixed illegal site.	50 µg/mL Spectinomycin	This Study
ΔpMOMoClo AF	pBGI *D. alaskensis* plasmid backbone, MoClo destination vector, *lacZα* and fixed illegal site.	40 µg/mL Chloramphenicol	This Study

	Fusion sites A and F		
pMOEC20	pBGI *D. alaskensis* plasmid backbone, EC20/IgA gene	50 µg/mL Spectinomycin	This Study
pMO1	pBGI *D. alaskensis* plasmid backbone, BfgV D8 gene	50 µg/mL Spectinomycin	This Study
pMO2	pBGI *D. alaskensis* plasmid backbone, Truncated BfgV D8 gene	50 µg/mL Spectinomycin	This Study
pMO3	pBGI *D. alaskensis* plasmid backbone, Truncated BfgV D8 WR198NK gene	50 µg/mL Spectinomycin	This Study
pMO4	pBGI *D. alaskensis* plasmid backbone, BsLOV gene	50 µg/mL Spectinomycin	This Study
pMO5	pBGI *D. alaskensis* plasmid backbone, Truncated BsLOV C62A gene	50 µg/mL Spectinomycin	This Study
pMO6	pBGI *D. alaskensis* plasmid backbone, PpLOV gene	50 µg/mL Spectinomycin	This Study
pMO7	pBGI *D. alaskensis* plasmid backbone, AvGFP R10-3 gene	50 µg/mL Spectinomycin	This Study
pMO8	pBGI *D. alaskensis* plasmid backbone, AvGFP R10-3 S66A gene	50 µg/mL Spectinomycin	This Study
pMO9	pBGI *D. alaskensis* plasmid backbone, mBFP gene	50 µg/mL Spectinomycin	This Study
pMO10	pBGI *D. alaskensis* plasmid backbone, mBFP G188S gene	50 µg/mL Spectinomycin	This Study
pMO11	pBGI *D. alaskensis* plasmid backbone, PpLOV C53A gene	50 µg/mL Spectinomycin	This Study
pMO12	pBGI *D. alaskensis* plasmid backbone, BsLOV C62A gene	50 µg/mL Spectinomycin	This Study

Table 2. 4. Stock Solutions, Media and Buffers

Solution/Media/Buffer	**Relevant details**
Agarose gel	0.8% Agarose, 0.005% SYBR Safe DNA Gel Stain
LB Medium	1% w/v Tryptone, 0.5% w/v Yeast Extract, NaCL, NaOH
LB Agar Medium	LB Medium supplemented with 1.5% agar
PGMC Medium	0.5 g KH_2PO_4, 1 g NH_4Cl, 4.5 g Na_2SO_4, 0.06 g $CaCl_2 \cdot 6H_2O$, 0.06 g $MgSO_4 \cdot 7H_2O$, 10 mL/L Sodium lactate, 1 g Yeast Extract, 0.004 g $FeSO_4 \cdot 7H_2O$, 0.3 g Sodium citrate, 1000 mL H_2O_{dd} – Adjust pH to 7.5
PGMC Agar Medium	PGMC Medium supplemented with 10g/L of agar
Sucrose solution	400 mM Sucrose, 1 mM $MgCl_2$
SOC (Super optimal broth)	0.5% w/v Yeast Extract, 2% Trytone, 10 mM NaCl, 2.5 mM KCl, 20 mM $MgSO_4$, 20 mM Glucose
TAE Buffer (20x Stock)	96.8 g Tris base, 22.8 mL glacial acetic acid, 7.4 g EDTA disodium salt, H_2O_{dd} to 1 L.
TE Buffer (10x Stock)	1 M Tris-HCl pH 7.5, 0.5 M EDTA pH 8.0, 880 mL H_2O_{dd}
TPM Buffer	30 mM $MgSO_4$, 10 mM KH_2PO_4, 10 mM Tris-HCl
PBS Buffer	137 mM NaCl, 2.7 mM KCl, 10 mM Na_2HpO_4, 800 mL H_2O_{dd}

Table 2. 5. List of gBlocks used for cloning and CreiLOV sequences. RED: Flanking sequence; BOLD: RBS Sequence; GOLD: Bidirectional *HisI* terminator; UNDERLINED: Substitutions

Nucleotides & gBlocks	Sequence
pMO1	TGATGGCGCAGGGGATCACGATCTG**GAAGGAGGAAAGAGATAAACA**ATGG CATCCATGACCGGAGGCCAGCAGATGGGCCGTGGCTCCATGAAGAAACTGG TCGTTATCACCGGTGCAAGCTCGGGTATTGGCGAGGCCATAGCACGCCGGTT CTCCGAAGAGGGCCATCCCCTGCTGCTCCTGGCCCGCCGTGTGGAACGGCTG AAGGCCCTGAATCTCCCGAACACCCTTTGCGCGCAGGTCGACGTGACAGACA AATACACGTTCGATACCGCCATCACGCGAGCGGAAAAAATCTATGGCCCTGC CGATGCGATTGTCAACAACGCCGGCATGATGCTGCTGGGGCAGATCGACAC ACAGGAAGCCAATGAATGGCAGCGCATGTTCGACGTGAACGTTCTGGGCCTT CTTAACGGTATGCAAGCCGTGCTGGCTCCGATGAAGGCCCGTAACTGCGGCA CCATAATTAACATTTCCTCTATAGCCGGAAAGAAAACCTTTCCCGACCATGC AGCGTATTGCGGCACCAAATTCGCGGTGCACGCCATTTCTGAGAATGTTCGC GAAGAAGTAGCCGCATCCAATGTGCGCGTCATGACCATCGCACCGAGTGCTG TAAAAACCGAATTGCTGAGCCATACGACGTCCCAGCAGATCAAAGACGGTT ATGATGCCTGGCGGGTGGACATGGGAGGTGTCCTGGCGGCCGATGACGTGG CCAGAGCCGTGCTGTTTGCGTACCAACAGCCCCAGAATGTATGCATTCGCGA AATAGCCCTGGCACCGACGAAGCAGCAGCCCAAGCTGGCGGCAGCCCTGGA ACACCACCACCACCACCATTAATGATCCGGCAAAAAAGGGCAAGGTGTCAC CACCCTGCCCTTTTTCTTTAAAACCGAAAAGATTACTTCGCGTTATCGCAGTA CTCCTTACGTAGTTTAA
pMO2	TGATGGCGCAGGGGATCACGATCTG**GAAGGAGGAAAGAGATAAACA**ATGA AGAAACTGGTCGTTATCACCGGTGCAAGCTCGGGTATTGGCGAGGCCATAGC ACGCCGGTTCTCCGAAGAGGGCCATCCCCTGCTGCTCCTGGCCCGCCGTGTG GAACGGCTGAAGGCCCTGAATCTCCCGAACACCCTTTGCGCGCAGGTCGACG TGACAGACAAATACACGTTCGATACCGCCATCACGCGAGCGGAAAAAATCT ATGGCCCTGCCGATGCGATTGTCAACAACGCCGGCATGATGCTGCTGGGGCA GATCGACACACAGGAAGCCAATGAATGGCAGCGCATGTTCGACGTGAACGT TCTGGGCCTTCTTAACGGTATGCAAGCCGTGCTGGCTCCGATGAAGGCCCGT AACTGCGGCACCATAATTAACATTTCCTCTATAGCCGGAAAGAAAACCTTTC CCGACCATGCAGCGTATTGCGGCACCAAATTCGCGGTGCACGCCATTTCTGA GAATGTTCGCGAAGAAGTAGCCGCATCCAATGTGCGCGTCATGACCATCGCA CCGAGTGCTGTAAAAACCGAATTGCTGAGCCATACGACGTCCCAGCAGATCA AAGACGGTTATGATGCCTGGCGGGTGGACATGGGAGGTGTCCTGGCGGCCG ATGACGTGGCCAGAGCCGTGCTGTTTGCGTACCAACAGCCCCAGAATGTATG CATTCGCGAAATAGCCCTGGCACCGACGAAGCAGCAGCCCTAATGATCCGG CAAAAAAGGGCAAGGTGTCACCACCCTGCCCTTTTTCTTTAAAACCGAAAAG ATTACTTCGCGTTATCGCAGTACTCCTTACGTAGTTTAAA
pMO3	TGATGGCGCAGGGGATCACGATCTG**GAAGGAGGAAAGAGATAAACA**ATGA AGAAACTGGTCGTTATCACCGGTGCAAGCTCGGGTATTGGCGAGGCCATAGC ACGCCGGTTCTCCGAAGAGGGCCATCCCCTGCTGCTCCTGGCCCGCCGTGTG GAACGGCTGAAGGCCCTGAATCTCCCGAACACCCTTTGCGCGCAGGTCGACG TGACAGACAAATACACGTTCGATACCGCCATCACGCGAGCGGAAAAAATCT ATGGCCCTGCCGATGCGATTGTCAACAACGCCGGCATGATGCTGCTGGGGCA GATCGACACACAGGAAGCCAATGAATGGCAGCGCATGTTCGACGTGAACGT TCTGGGCCTTCTTAACGGTATGCAAGCCGTGCTGGCTCCGATGAAGGCCCGT AACTGCGGCACCATAATTAACATTTCCTCTATAGCCGGAAAGAAAACCTTTC CCGACCATGCAGCGTATTGCGGCACCAAATTCGCGGTGCACGCCATTTCTGA GAATGTTCGCGAAGAAGTAGCCGCATCCAATGTGCGCGTCATGACCATCGCA CCGAGTGCTGTAAAAACCGAATTGCTGAGCCATACGACGTCCCAGCAGATCA AAGACGGTTATGATGCCAACAAAGTCGACATGGGAGGTGTCCTGGCGGCCG ATGACGTGGCCAGAGCCGTGCTGTTTGCGTACCAACAGCCCCAGAATGTATG CATTCGCGAAATAGCCCTGGCACCGACGAAGCAGCAGCCCTAATGATCCGG CAAAAAAGGGCAAGGTGTCACCACCCTGCCCTTTTTCTTTAAAACCGAAAAG ATTACTTCGCGTTATCGCAGTACTCCTTACGTAGTTTAAA

pMO4	TGATGGCGCAGGGGATCACGATCTG**ATTCAACTATTCATTAAGGAGGGAA** **AGT**ATGGCCTCGTTTCAGTCATTTGGTATTCCTGGGCAGCTCGAAGTCATCA AGAAAGCACTGGATCACGTCCGGGTAGGGGTGGTGATCACAGACCCCGCCC TCGAGGATAACCCGATTGTTTATGTCAACCAGGGCTTCGTGCAGATGACCGG CTACGAAACAGAAGAAATCCTTGGCAAAAACTGCCGCTTTCTGCAGGGCAA GCATACAGACCCTGCGGAAGTGGATAACATTCGTACCGCACTGCAGAACAA AGAACCCGTGACCGTTCAGATTCAGAACTATAAAAAAGACGGGACCATGTTT TGGAATGAACTTAATATCGATCCCATGGAGATAGAAGACAAAACGTATTTCG TTGGCATCCAGAACGATATCACCAAACAAAAAGAGTATGAAAAGCTGCTTG AGGACAGCCTTACGGAAATTACGGCCCTGAGCACTCCCATCGTTCCGATTCG CAACGGCATAAGCGCACTGCCTCTGGTCGGAAATCTGACTGAGGAACGGTTT AATTCCATTGTGTGCACCCTGACCAACATCCTGTCTACCAGCAAGGACGACT ACCTGATCATCGATCTGTCGGGCCTCGCCCAGGTGAATGAACAGACAGCCGA CCAGATCTTCAAGTTGAGCCATTTGCTGAAACTGACCGGGACCGAGCTGATA ATAACCGGCATTAAACCTGAACTTGCCATGAAGATGAATAAGCTTGACGCTA ACTTCAGCAGCCTGAAAACCTACTCGAATGTGAAAGACGCGGTTAAGGTCCT TCCCATTATGTAATGATCCGGCAAAAAAGGGCAAGGTGTCACCACCCTGCCC TTTTTCTTTAAAACCGAAAAGATTACTTCGCGTTATCGCAGTACTCCTTACGT AGTTTAAA
pMO5	TGATGGCGCAGGGGATCACGATCTG**ATTCAACTATTCATTAAGGAGGGAA** **AGT**ATGGCCTCGTTTCAGTCATTTGGTATTCCTGGGCAGCTCGAAGTCATCA AGAAAGCACTGGATCACGTCCGGGTAGGGGTGGTGATCACAGACCCCGCCC TCGAGGATAACCCGATTGTTTATGTCAACCAGGGCTTCGTGCAGATGACCGG CTACGAAACAGAAGAAATCCTTGGCAAAAACTGCCGCTTTCTGCAGGGCAA GCATACAGACCCTGCGGAAGTGGATAACATTCGTACCGCACTGCAGAACAA AGAACCCGTGACCGTTCAGATTCAGAACTATAAAAAAGACGGGACCATGTTT TGGAATGAACTTAATATCGATCCCATGGAGATAGAAGACAAAACGTATTTCG TTGGCATCCAGAACGATATCACCAAACAAAAAGAGTATGAAAAGCTGCTTG AGTAATGATCCGGCAAAAAAGGGCAAGGTGTCACCACCCTGCCCTTTTTCTT TAAAACCGAAAAGATTACTTCGCGTTATCGCAGTACTCCTTACGTAGTTTAA A
pMO6	TGATGGCGCAGGGGATCACGATCTG**CAAACAGTAATACATAAAAGAGGAG** **GTAAAAT**ATGATCAATGCCAAACTGCTGCAGCTGATGGTCGAGCACTCTAAC GATGGTATTGTGGTCGCCGAACAAGAAGGTAACGAAAGCATTCTGATCTACG TTAACCCGGCCTTTGAACGCCTCACGGGCTATTGCGCAGATGACATCCTTTAT CAGGATTGCAGGTTCCTGCAGGGTGAGGACCACGACCAACCAGGTATAGCT ATCATCCGCGAGGCCATACGCGAAGGCCGCCCGTGTTGCCAGGTTCTGAGAA ATTACCGGAAAGACGGCAGCCTTTTCTGGAACGAATTGAGCATAACCCCCGT GCACAATGAAGCGGACCAGCTGACGTACTACATAGGGATCCAACGCGACGT AACTGCGCAGGTCTTCGCCGAGAACGCGTGAGAGAGTTAGAAGCAGAAGTG GCCGAGCTTCGTCGCCAACAGGGCCAAGCAAAACATTAATGATCCGGCAAA AAAGGGCAAGGTGTCACCACCCTGCCCTTTTTCTTTAAAACCGAAAAGATTA CTTCGCGTTATCGCAGTACTCCTTACGTAGTTTAAA
pMO7	TGATGGCGCAGGGGATCACGATCTG**AACGGAGCAAGAAGGAGGTAAAC**AT GGTGTCCAAAGGGGAAGAGCTTTTCACGGGCGTGGTTCCGATCCTGGTCGAG CTGGATGGGGACGTTAACGGCCACAAATTTTCGGTTTCCGGCGAAGGCGAAG GCGACGCCACATATGGCAAGCTGACCCTGAAACTGATATGCACCACCGGCA AACTGCCTGTGCCTTGGCCGACCCTCGTTACGACGCTGTCCTATGGTAACCA ATGTTTCTCTCGCTATCCGGACCACATGAAGCAGCACGATTTTTTTAAAAGTG CTATGCCAGAAGGGTACGTACAGGAACGGACCATTTTTTTTAAAGATGATGG CAATTATAAAACGCGCGCTGAAGTCAAATTTGAAGGCGACACCCTTGTGAAT CGTATTGAACTGAAAGGCATTGATTTCAAAGAAGACGGAAATATACTGGGTC ACAAACTTGAGTACAACTACAATTCCCACAACGTATACATAATGGCAGACAA GCAGAAGAACGGGATCCAGGCCAACTTCAAAGTTAGACACAACCTCGAGGA CGGTTCAGTGCAGCTGGCCGATCATTACCAGCAGAACACCCCCATTGGCGAC GGCCCCGTTCTGCTGCCTGATAACCACTACCTGTCCACACAATCCGCGCTGTC GAAGGACCCGAACGAGAAGCGCGACCATATGGTGCTGCTAGAGTTCGTGAC CGCAGCAGGAATCACACTGGGGATGGATGAGCTTTATAAATGATGATCCGG CAAAAAAGGGCAAGGTGTCACCACCCTGCCCTTTTTCTTTAAAACCGAAAAG ATTACTTCGCGTTATCGCAGTACTCCTTACGTAGTTTAAA
pMO8	TGATGGCGCAGGGGATCACGATCTG**AACGGAGCAAGAAGGAGGTAAAC**AT GGTGTCCAAAGGGGAAGAGCTTTTCACGGGCGTGGTTCCGATCCTGGTCGAG CTGGATGGGGACGTTAACGGCCACAAATTTTCGGTTTCCGGCGAAGGCGAAG GCGACGCCACATATGGCAAGCTGACCCTGAAACTGATATGCACCACCGGCA

	AACTGCCTGTGCCTTGGCCGACCCTCGTTACGACGCTGGCCTATGGTAACCA ATGTTTCTCTCGCTATCCGGACCACATGAAGCAGCACGACTTCTTTAAAAGT GCTATGCCAGAAGGGTACGTACAGGAACGGACCATCTTCTTTAAAGATGATG GCAATTATAAAACGCGCGCTGAAGTCAAATTTGAAGGCGACACCCTTGTGAA TCGTATTGAACTGAAAGGCATTGATTTCAAAGAAGACGGAAATATACTGGGT CACAAACTTGAGTACAACTACAATTCCCACAACGTATACATAATGGCAGACA AGCAGAAGAACGGGATCCAGGCCAACTTCAAAGTTAGACACAACCTCGAGG ACGGTTCAGTGCAGCTGGCCGATCATTACCAGCAGAACACCCCCATTGGCGA CGGCCCCGTTCTGCTGCCTGATAACCACTACCTGTCCACACAATCCGCGCTGT CGAAGGACCCGAACGAGAAGCGCGACCATATGGTGCTGCTAGAGTTCGTGA CCGCAGCAGGAATCACACTGGGGATGGATGAGCTTTATAAATGATGATCCG GCAAAAAAGGGCAAGGTGTCACCACCCTGCCCTTTTTCTTTAAAACCGAAAA GATTACTTCGCGTTATCGCAGTACTCCTTACGTAGTTTAAA
pMO9	TGATGGCGCAGGGGATCACGATCTG**TCCAGTAAAATACCGAATAGAGGGG** **GGAATAA**ATGCAGAACCTGAATGGTAAGGTGGCCTTCGTGACAGGCGGGTC CCGCGGTATTGGCGCCGCGATAGTGCGCCGGCTTGCCGCCGATGGCGCTGAC ATCGCATTTACGTACGTCAGTGCGAGCTCCAAAAACGTCGCAACGGCCCTGG TCCAGGAATTGGAAGCGAAGGGACGCCGTGCCCGGGCTATACAGGCAGATT CCGCCGACCCGGCCCAGGTCCGGCAAGCAGTCGAGCAGGCTATTGTGCAGCT CGGCCCAGTTGATGTGCTTGTCAACAATGCCGGTATATTCCTGGCCGGTCCC CTGGGAGAAGTTACGCTTGACGACTATGAACGTACTATGAACATCAACGTGC GCGCCCCGTTCGTTGCGATTCAGGCAGCACAGGCGAGCATGCCCGACGGCG GCCGCATAATAAATATTGGCTCCTGTCTGGCAGAACGTGCCGGTCGAGCGGG GGTGACATTATACGCCGCATCGAAATCGGCCCTGTTGGGTATGACCAGAGGG CTGGCGCGCGACCTGGGAGCACGCGGGATAACCGCCAACGTCGTCCATCCC GGTCCCATTGACACAGACATGAACCCAGCTGACGGTGAGCGCAGTGGAGAA CTGGTGGCCGTCCTTTCCTTGCCCCACTACGGGGAGGTGCGCGATATTGCCG GCATGGTGGCATTTCTCGCAGGACCCGACGGTCGTTATGTGACAGGTGCTAG CCTTGCCGTTGACGGGGGCTTCGCGGCCTAATGATCCGGCAAAAAAGGGCA AGGTGTCACCACCCTGCCCTTTTTCTTTAAAACCGAAAAGATTACTTCGCGTT ATCGCAGTACTCCTTACGTAGTTTAAA
pMO10	TGATGGCGCAGGGGATCACGATCTG**TCCAGTAAAATACCGAATAGAGGGG** **GGAATAA**ATGCAGAACCTGAATGGTAAGGTGGCCTTCGTGACAGGCGGGTC CCGCGGTATTGGCGCCGCGATAGTGCGCCGGCTTGCCGCCGATGGCGCTGAC ATCGCATTTACGTACGTCAGTGCGAGCTCCAAAAACGTCGCAACGGCCCTGG TCCAGGAATTGGAAGCGAAGGGACGCCGTGCCCGGGCTATACAGGCAGATT CCGCCGACCCGGCCCAGGTCCGGCAAGCAGTCGAGCAGGCTATTGTGCAGCT CGGCCCAGTTGATGTGCTTGTCAACAATGCCGGTATATTCCTGGCCGGTCCC CTGGGAGAAGTTACGCTTGACGACTATGAACGTACTATGAACATCAACGTGC GCGCCCCGTTCGTTGCGATTCAGGCAGCACAGGCGAGCATGCCCGACGGCG GCCGCATAATAAATATTGGCTCCTGTCTGGCAGAACGTGCCGGTCGAGCGGG GGTGACATTATACGCCGCATCGAAATCGGCCCTGTTGGGTATGACCAGAGGG CTGGCGCGCGACCTGGGAGCACGCGGGATAACCGCCAACGTCGTCCATCCC AGCCCCATTGACACAGACATGAACCCAGCTGACGGTGAGCGCAGTGGAGAA CTGGTGGCCGTCCTTTCCTTGCCCCACTACGGGGAGGTGCGCGATATTGCCG GCATGGTGGCATTTCTCGCAGGACCCGACGGTCGTTATGTGACAGGTGCTAG CCTTGCCGTTGACGGGGGCTTCGCGGCCTAATGATCCGGCAAAAAAGGGCA AGGTGTCACCACCCTGCCCTTTTTCTTTAAAACCGAAAAGATTACTTCGCGTT ATCGCAGTACTCCTTACGTAGTTTAAA
LacZAF_CmR	GTGAGCCTTTCTCGAGTCGTAGACTCCTGTTGATAGATCCAGTAATGACCTC AGAACTCCATCTGGATTTGTTCAGAACGCTCGGTTGCCGCCGGGCGTTTTTTA TTGGTGAGAATCAAGCGAGCTCGATATCAAATTACGCCCCGCCCTGCCACTC ATCGCAGTACTGTTGTAATTCATTAAGCATTCTGCCGACATGGAAGCCATCA CAAACGGCATGATGAACCTGAATCGCCAGCGGCATCAGCACCTTGTCGCCTT GCGTATAATATTTGCCCATGGTGAAAACGGGGGCGAAGAAGTTGTCCATATT GGCCACGTTTAAATCAAAACTGGTGAAACTCACCCAGGGATTGGCTGACACG AAAAACATATTCTCAATAAACCCTTTAGGGAAATAGGCCAGGTTTTCACCGT AACACGCCACATCTTGCGAATATATGTGTAGAAACTGCCGGAAATCGTCGTG GTATTCACTCCAGAGCGATGAAAACGTTTCAGTTTGCTCATGGAAAACGGTG TAACAAGGGTGAACACTATCCCATATCACCAGCTCACCGTCTTTCATTGCCA TACGAAATTCCGGATGAGCATTCATCAGGCGGGCAAGAATGTGAATAAAGG CCGGATAAAACTTGTGCTTATTTTTCTTTACGGTCTTTAAAAAGGCCGTAATA TCCAGCTGAACGGTCTGGTTATAGGTACATTGAGCAACTGACTGAAATGCCT CAAAATGTTCTTTACGATGCCATTGGGATATATCAACGGTGGTATATCCAGT

	GATTTTTTTCTCCATGTTTGCTTTTCTCCTCTTTCTCCCCTATAGTGAGTCGTA TTAATTCGGTGTTTGCTCCCTCAGTGGGTCTCAGGAGATGTCTTCTGCACCAT ATGCGGTGTGAAATACCGCACAGATGCGTAAGGAGAAAATACCGCATCAGG CGCCATTCGCCATTCAGGCTGCGCAACTGTTGGGAAGGGCGATCGGTGCGGG CCTCTTCGCTATTACGCCAGCTGGCGAAAGGGGGATGTGCTGCAAGGCGATT AAGTTGGGTAACGCCAGGGTTTTCCCAGTCACGACGTTGTAAAACGACGGCC AGTGAATTCGAGCTCGGTACCCGGGGATCCTCCAGAGTCGACCTGCAGGCAT GCAAGCTTGGCGTAATCATGGTCATAGCTGTTTCCTGTGTGAAATTGTTATCC GCTCACAATTCCACACAACATACGAGCCGGAAGCATAAAGTGTAAAGCCTG GGGTGCCTAATGAGTGAGCTAACTCACATTAATTGCGTTGCGCTCACTGCCC GCTTTCCAGTCGGGAAACCTGTCGTGCCAGCTGCATTAATGAATCGGCCAAC GCGCGGGGAAGACGTCGCTAGAGACCTACTTCTAGAGACTTGTCCC
RBS Library	CTTAGAAATGAGGGTAGGGAACCCATAAGGTCTCATACTATATCCACACAAG TCGAACAATATAAGGAAGGAGGTAAACGATAATGAGAGACCATATCCACTA GGGGTCTCATACTATTCAATTTTTAAAAAATCACAAGGAAGGAGGTATTATA TAATGAGAGACCAATGCAATCGTAGTGGTCTCATACTATTACTGCTCGACAA TAAAAACTAATAACTGGAGGAGGTTTAACATAATGAGAGACCCCACCTGAT CGTACGGTCTCATACTATCTGGTTATCCGCGAGGAAATTAAAGGCATAGGTT TTTTTATAATGAGAGACCTATAGGTGATCCGGTCTCATACTATAACTGAGTTA GAGCTAAGAGGAACTATTTTATAATGAGAGACCTAGCGTGACAGCCGCCCCT TTTGCCCAC
MIN PROM LIRBARY	CACTAGCTCAGATTCAGTAGACCGCTGTTGCTTAGAAATGAGGGTAGGGAAC CCATAAGGTCTCAGGAGATTTGCCCGGCATGCATAAGGCTCGTCTTAATTTA TTACTAGAGACCATATCCACTAGGGGTCTCAGGAGATTTGACTGGCATGCAT AAGGCTCGTACTACATTATTACTAGAGACCCACAGAGCATAAAGGGTCTCAG GAGATTGGTCAGGCATGCATAAGGCTCGGGCTATCATATTACTAGAGACCGC ACCTGTGAACGGTCTCAGGAGATTTCACCGGCATGCATAAGGCTCGAGGTAG TCTATTACTAGAGACCGTCGTTTGCTTTTCGTGACAGCCGCCCCTTTTGCCCA CTAGTAATGCAGACACTTGCGGTCCATCTCGAGCTGTCAGCACTACTAACTT GCGGTCAGT
PROM Library 2	ACTAGCTCAGATTCAGTAGACCGCTGTTGCTTAGAAATGAGCGATAACCCAT AAACTAGGGGTCTCAGGAGATTTGCCCGTCTGAAAAACAGTCTTAATTTATT ACTAGAGACCATATCCTCCTCAGCAGGCAAACGGTCTCAGGAGATTTGAATA TAAAGGAGATTCTTCAAAAATATTACTAGAGACCATATCCCAAAAGTGGTCT CAGGAGATTTCACCGCGAGGCCAAGTAGGTAGTCTATTACTAGAGACCATAT CCGTGAACTTATGGTCTCAGGAGATTTCCTGGGCATGCATAAGGCTCGATGT ACAGTATTACTAGAGACCTAGCAGACACTTGCGGTCCATCTCGAGCTGTCAG CACTACTAA
CreiLOV	GCCGGCCTGCGCCACACCTTCGTGGTGGCCGACGCCACCCTGCCCGACTGCC CCCTGGTGTACGCCTCCGAAGGCTTCTACGCCATGACCGGCTACGGCCCCGA CGAAGTGCTGGGCCACAACGCCCGCTTCCTGCAGGGCGAAGGCACCGACCC CAAGGAAGTGCAGAAGATCCGCGACGCCATCAAGAAGGGCGAAGCCTGCTC CGTGCGCCTGCTGAACTACCGCAAGGACGGCACCCCCTTCTGGAACCTGCTG ACCGTGACCCCCATCAAGACCCCCGACGGCCGCGTGTCCAAGTTCGTGGGCG TGCAGGTGGACGTGACCTCCAAGACCGAAGGCAAGGCCCTGGCC
E. coli CreiLOV	GCTGGTCTGCGTCACACCTTCGTTGTTGCTGACGCTACCCTGCCGGA CTGCCCGCTGGTTTACGCTTCTGAAGGTTTCTACGCTATGACCGGTTA CGGTCCGGACGAAGTTCTGGGTCACAACGCTCGTTTCCTGCAGGGTG AAGGTACCGACCCGAAAGAAGTTCAGAAAATCCGTGACGCTATCAA AAAAGGTGAAGCTTGCTCTGTTCGTCTGCTGAACTACCGTAAAGACG GTACCCCGTTCTGGAACCTGCTGACCGTTACCCCGATCAAAACCCCG GACGGTCGTGTTTCTAAATTCGTTGGTGTTCAGGTTGACGTTACCTCT AAAACCGAAGGTAAAGCTCTGGCT

2.6. Adapting *D. alaskensis* to MoClo standards

2.6.1. PCR amplification of A:*LacZα*:E insert and pMO9075 vector

From the DVK_AE plasmid obtained from CIDAR MoClo Parts Kit (Cidar MoClo Parts Kit, Douglas Densmore, Addgene Kit # 1000000059) the LacZα gene fusion sites and BsaI and BbsI flanking recognition sites were PCR amplified. The pMO9075 backbone containing the pBGI and its multiple cloning site, was also PCR amplified. Primers were designed to uphold the Gibson Assembly standards (Table 2.1, No. 21-24). The resulting PCR products were confirmed by electrophoresis on a 0.8% agarose gel, then excised and purified.

2.6.2. Gibson Assembly

The DNA insert and backbone purified fragments were assembled by HiFi DNA Assembly® Reaction protocol, NEB, Cat#E2621S. Assembled plasmids were transformed into chemically competent *E. coli* NEB 5 - alpha.

2.6.3. Confirmation through Blue-White Screening

To confirm the successful cloning of *LacZα* from DVK_AE, the resulting colonies were restreaked onto a blue/white screening plate. Plates were supplemented with 1 µL per 1 mL of Media of 100 mM IPTG and 20 µg/µl X-Gal, and its respective antibiotic.

2.6.4. Insert specific PCR Confirmation

Each blue colony was cultured overnight and their plasmids isolated. An insert specific PCR was performed for each plasmid using the primers 19 and 20 shown in Table 2.1, with an anneal temperature of 62°C. The resulting PCR products were confirmed by electrophoresis on a 0.8% agarose gel.

2.6.5. Diagnostic Digest Reaction with BsaI

To further confirm, a BsaI diagnostic digest reaction (NEB protocol) was performed followed by electrophotesis on a 0.8% agarose gel was performed. The plasmid was then sequenced (see Table 2.2 for sequencing primers).

2.6.6. Site-directed mutagenesis of BbsI recognition site

The BbsI recognition site found in the pMO9075 backbone needed to be removed to be compliant with MoClo standards. Through site-directed mutagenesis, the BbsI

recognition site was deleted from the MoClo adapted pMO9075 plasmid (ΔpMOMoClo). Primers for the deletion of the BbsI recognition site were designed (Table 2.1, No. 25 and 26) to delete the BbsI recognition site. The QuikChange Lighting (Agilent) Site-Directed Mutagenesis kit protocol was followed. Mutant plasmids were transformed into chemically competent *E. coli* NEB 5- alpha cells.

2.6.7. Diagnostic digestion reaction with BbsI

To confirm the deletion of the BbsI recognition site a diagnostic digest reaction with BbsI (NEB protocol) was performed, followed by electrophoresis on a 0.8% agarose gel.

2.6.8. MoClo Cloning Assembly Test

To test the adapted MoClo construct ΔpMOMoClo the components J23100_AB, B0034m_BC, C0012m_CD, and B0015_DE from the CIDAR MoClo Parts Kit were cultured overnight and purified following previously mentioned *E. coli* methods. Using these components together with ΔpMOMoClo, a transcriptional unit (TU) was assembled through a MoClo assembly reaction. The resulting reaction was inserted into *E. coli* NEB 5-alpha competent cells and plated onto blue/white screening plates. pUC19 was used as a positive transformation control. Confirmation was done through a blue/white screening test on plates supplemented with 50 µg/mL Spectinomycin.

2.6.9. Assembly of multi-gene expression acceptor vector ΔpMoMoClo AF

To assemble ΔpMoMoClo AF, the Chloramphenicol resistance gene, with a T7 bacterial promoter, strong bacterial RBS and lambda T0 terminator were synthesized as a gBlock (Table 2.5; LacAF_CmR). The gBlock also contained the essential *lacZα* gene from the acceptor vector DVK_AF and was flanked by a XhoI and XbaI recognition sites listed and described on Table 5. The gBlock was resuspended in TE buffer. gBlock and plasmid ΔpMO9075 were digested with XbaI and XhoI. ΔpMO9075 was ran prior to gel electrophoresis in a 0.8% agarose gel. ΔpMoMoClo AF was assembled by ligating both digested parts. The resulting ligation reaction was inserted into *E. coli* NEB 5-alpha competent cells and plated onto blue/white screening plates supplemented with Chloramphenicol. Blue colonies were restreaked

onto fresh blue/white screening Chloramphenicol plates (40 μg/mL). Plasmids were extracted and sequenced for confirmation of correct assembly using sequencing primers (Table 1, No. 19 and 20).

2.7. Designing and Engineering an Oxygen-independent reporter library for *D. alaskensis*

2.7.1. Adapting CreiLOV, phiLOV and nanoLUC to MoClo standards

To adapt the coding sequences of the oxygen-independent reporters phiLOV (plasmid was donated by Professor Susan Rosser, University of Edinburgh), and nanoLUC (NanoLUC®, Promega) to MoClo standards, the sequences of interest were amplified using the primers from Table 2.1, No. 33 – 36, with anneal temperatures of 63°C and 65°C respectively. Primers were designed as follows: Forward primer, 9 nucleotides; BsaI recognition site (GGTCTC), 1 nucleotide; Fusion site C (AATG), 2 nucleotides, 15 nucleotides of sequence of interest. Reverse primer, 9 nucleotides; BsaI recognition site (GGTCTC), 1 nucleotide; Fusion site D (ACCT), 2 nucleotides, 15 nucleotides of sequence of interest. PCR amplified DNA of interest was run on a 0.8% agarose gel and extracted. Genes corresponding to the CreiLOV domains were codon optimised for expression in *D. alaskensis* (obtained using bioinformatics tool, JCat [154]) and synthesized by Genewiz (South Plainfield, NJ). CreiLOV domains were flanked by BsaI recognition sites followed by fusion site C nucleotides (NTs) on the 5' end and by fusion site D nucleotides (NTs) on the 3' end. Assembly of new MoClo parts was through a MoClo reaction as follows: Add to a 0.2 mL tube: equimolar 10 – 60 fmol of the DNA amplicons or CreiLOV plasmid and acceptor vector DVA_CD, 10 U of BsaI (NEB), 20 U of Quick T4 DNA Ligase (NEB), 1x T4 DNA Ligase Buffer (NEB), and sterile deionized water to a total volume of 20 μL. Reactions were performed using the following parameters: 16 cycles (37°C for 1.5 min, 16°C for 3 min), followed by 50°C for 5 min and 80°C for 10 min and were then held at 4°C until they were used in transformations. The resulting reaction was inserted into *E. coli* NEB 5-alpha competent cells and plated onto blue/white screening plates with Ampicillin (50 μg/mL). Multiple colonies that showed a white phenotype were picked and grown overnight for plasmid purification. Correct

assembly of DVA_CreiLOV, DVA_phiLOV, and DVA_LUC was confirmed through sequencing using sequence primers (Table 2.1, No. 17 and 18).

2.7.2. Site-directed mutagenesis of BbsI recognition site (DVA_LUC)

The BbsI recognition site found on DVA_LUC plasmid needed to be removed to be compliant with MoClo standards. Through site-directed mutagenesis, the BbsI recognition site was deleted from DVA_LUC. Primers for the deletion of the BbsI recognition site were designed (Table 2.1, No. 37 and 38). The QuikChange Lighting (Agilent) Site-Directed Mutagenesis kit manufacturer's protocol was followed to mutate BbsI recognition site. Mutant plasmids were inserted into chemically competent *E. coli* NEB 5-alpha cells.

2.7.3. Diagnostic Digest Reaction with BsaI

To confirm if parts were adapted to MoClo a BsaI diagnostic digest reaction (NEB protocol) was performed followed by electrophoresis on a 0.8% agarose gel.

2.7.4. Diagnostic Digest Reaction with BbsI

To confirm the deletion of the BbsI recognition site, a diagnostic digestion reaction with BbsI (NEB protocol) was performed, followed by electrophoresis on a 0.8% agarose gel.

2.7.5. Assembly of Transcriptional Units (TUs) for CreiLOV and phiLOV

TUs were assembled by a MoClo assembly reaction. Different TUs were assembled for CreiLOV, *E. coli* CreiLOV and phiLOV. Each TU contains the following parts from the CIDAR MoClo Parts Kit; J23100_AB, J23106_AB, J23116_AB, B0034m_BC, B0015_DE, Kan promoter and acceptor plasmid ΔpMOMoClo. For phiLOV and *E. coli* CreiLOV only one promoter was used (J23100_AB). Assembled TUs were inserted into *E. coli* 5- alpha competent cells and plated onto blue/white screening plates supplemented with 50 µg/mL spectinomycin. White colonies were restreaked onto fresh blue/white screening plates supplemented with spectinomycin (50 µg/mL). Plasmids were isolated and sequenced for confirmation of correct assembly using sequencing primers (Table 2.1, No. 19 and 20).

2.7.6. Fluorescence assay of *E. coli* expressing CreiLOV and phiLOV

Overnight *E. coli* cultures of each TU were grown under aerobic conditions. OD_{600} readings from *E. coli* expressing the TUs were measured using CO8000 Cell Density Meter (WPA, Cambridge, UK). In a Falcon® 96-well Black/Clear Flat Bottom (Corning, NY, USA) cultures were diluted with LB/Spectinomycin to an OD_{600} of 0.15 in a total volume of 200 µL. Plasmid (pMO9075) in *E. coli* cultures was used as a negative control, and LB/Spectinomycin as the blank. Biological triplicates and technical triplicates were used per sample. Plates were incubated for 4 hours at 37°C. Readings were done with a Tecan M200 PRO, where the absorbance was measured at 600 nm (A_{600nm}) and fluorescence for CreiLOV and phiLOV (Ex. 450 nm, Em. 495 nm).

2.7.7. Fluorescence assay of *D. alaskensis* expressing CreiLOV

All TUs were inserted into *D. alaskensis* and cultured under anaerobic conditions. Cultures were grown to early stationary phase (OD_{600}; 0.6 -0.8) under anaerobic conditions. OD_{600} readings from *D. alaskensis* expressing the TUs were measured using a CO8000 Cell Density Meter (WPA, Cambridge, UK). In a Falcon® 96-well Black/Clear Flat Bottom (Corning, NY, USA), cultures were diluted with PGMC/Spectinomycin to an OD_{600} of 0.15 to a total volume of 200 µL. Cells containing the plasmid pMO9075 was used as a negative control, and PGMC/Spectinomycin as blank. Biological triplicates and technical triplicates per sample and controls were used. Plates were incubated anaerobically for 72 hours at 30°C. Readings were done with a Tecan M200 PRO, where the absorbance was measured at 600 nm (A_{600nm}) and fluorescence (CreiLOV, Ex. 450 nm, Em. 495 nm).

2.7.8. Genome mining, cloning and sequence design for increased oxygen-independent reporter library

Biotangents (Edinburgh, UK), conducted the gene mining research and the assembly of the oxygen-independent fluorescent reporter library. Potential oxygen-independent fluorescent reporters were identified through a literature search focused on oxygen-independent GFP, BFP and FbFP proteins and their variants. A total of 12 different oxygen-independent fluorescent reporters were found suitable for testing in *D. alaskensis*. The oligonucleotides and synthetic DNA fragments (gBlock linear dsDNA from Integrated DNA Technologies) used for cloning are described in Table

2.5. Genes corresponding to the oxygen-independent reporters were synthesized as gBlocks, each containing an RBS, designed *in silico* using RBS Calculator [110] (to maximize initiation of translation) and an *E. coli* His terminator. To construct the oxygen-independent library, the pMO9075 plasmid backbone including the putative Kan promoter were PCR-amplified (Q5 High-Fidelity, NEB) and assembled with the gBlocks by HiFi DNA Assembly® Reaction Protocol (NEB). All plasmids with the exception of pMO11 and pMO12 were assembled by Gibson® assembly of the gBlocks with a PCR-amplified pMO9075 backbone. To assemble pMO11 and pMO12, their corresponding gBlocks and pMO9075 were PCR-amplified (Q5 High-Fidelity, NEB) to Golden Gate standards for subsequent assembly.

2.7.9. Screening for fluorescence excitation and emission

For rapid screening of fluorescence emission, 50 ng of each plasmid DNA was inserted into *E. coli* JM109 competent cells and grown under aerobic conditions. Transformed cells were plated on LB/spectinomycin (100 μg/mL). *E. coli* plates were incubated overnight at 37°C under aerobic conditions. Similarly, *D. alaskensis* plates were incubated at 30°C in an anaerobic hood for 7 days. Both the anaerobic and aerobic set of plates were exposed to black light for rapid screening of fluorescence emission.

To test the oxygen-independent reporter library, 200 ng of each plasmid DNA were inserted into freshly made *D. alaskensis* competent cells following the aforementioned method (Section 2.3.2.). Transformed cells were plated on PGMC/spectinomycin (100 μg/mL). Plates were incubated at 30°C in an anaerobic hood for 7 days. Colonies were selected and grown in anaerobic conditions in PGMC/spectinomycin (100 μg/mL) broth and grown to an OD_{600} ~ 1.0. 50 ng of each plasmid DNA was also inserted into *E. coli* JM109 and plated on LB/spectinomycin (100 μg/mL). Plates were incubated overnight at 37°C, with the exception of pMO5 and pMO6 (30°C), as it is their optimal growth temperature. Colonies were selected and grown in aerobic conditions in LB/spectinomycin (100 μg/mL) broth for 16 hours. *D. alaskensis* and *E. coli* cultures were diluted to an OD_{600} of 0.1 in PGMC and LB respectively with spectinomycin (100 μg/mL) and incubated for 4 hours under anaerobic (*D. alaskensis*) and aerobic (*E. coli*) conditions. On a Falcon® 96-well Black/Clear Flat Bottom (Corning, NY, USA) 200 μL aliquots of each culture

were dispensed. *D. alaskensis* and *E. coli* JM109 transformed with the plasmid pMO9075 were used as a negative control and PGMC or LB with spectinomycin as the blanks. Biological triplicates and per sample and controls were used. An oxygen free environment was maintained by sealing the 96 well plates with parafilm and tape. Plates were placed on a Tecan M200 PRO to measure absorbance OD_{600} and fluorescence at a range of wavelengths (Table 3.1, Chapter 3). To characterise pMO9 and pMO10, an array of wavelengths were used: 350-410 nm for excitation and 420 – 500 nm for emission altering each reading by 20 nm.

2.7.10. Adapting the oxygen-independent reporter library to MoClo

To adapt the coding sequences of the oxygen-independent reporters to MoClo standards, the sequences of interest were amplified using the primers in Table 2.1 (No. 13-16), which were designed as mentioned in section 2.6.1. PCR amplified DNA of interest was run on 0.8% agarose gel and extracted (QIAGEN).

2.7.11. Site-directed mutagenesis of BbsI recognition site (pMO8)

The BbsI recognition site found on the pMO8 plasmid needed to be removed to be compliant with MoClo standards. The BbsI recognition site was deleted from DVA_pMO8 through site-directed mutagenesis. The QuikChange Lighting (Agilent) Site-Directed Mutagenesis kit manufacturer's protocol was followed using primers designed to delete the BbsI recognition site (Table 1, No. 27-28). Mutant plasmids were transformed into chemically competent *E. coli* NEB 5-alpha cells.

2.7.12. Diagnostic Digest with BbsI

To confirm the deletion of the BbsI recognition site a diagnostic digestion reaction with BbsI (NEB protocol) was performed, followed by electrophoresis on a 0.8% agarose gel.

2.7.13. Assembly of TUs for oxygen-independent fluorescent reporter library

TUs for PMO7, PMO8, PMO9 and PMO10 were assembled via a MoClo assembly reaction. Each TU contained the following parts from the CIDAR MoClo Parts Kit; J23100_AB, J23106_AB, J23116_AB, B0034m_BC, B0015_DE, Kan promoter (only PMO7) and acceptor plasmid ΔpMOMoClo. Assembled TUs were inserted into *E. coli* NEB 5-alpha competent cells and plated onto blue/white screening plates.

Plates were supplemented with 50 µg/mL spectinomycin. White colonies were restreaked onto fresh blue/white screening spectinomycin plates. Plasmids were isolated and sequenced for confirmation of correct assembly using sequencing primers (Table 2.1, No. 19 and 20).

2.7.14. Fluorescence Assay of *D. alaskensis* expressing oxygen-independent reporters library

D. alaskensis was electrotransformed with all TUs and cultured under anaerobic conditions. Cultures were grown to early stationary phase (OD_{600}; 0.6 -0.8) under anaerobic conditions. OD_{600} readings from *D. alaskensis* expressing the TUs were measured using CO8000 Cell Density Meter (WPA, Cambridge, UK). In a Falcon® 96-well Black/Clear Flat Bottom (Corning, NY, USA) cultures were diluted with PGMC/spectinomycin to an OD_{600} of 0.15 in a total volume of 200 µL. *D. alaskensis* transformed with the plasmid pMO9075 was used as a negative control, and PGMC/spectinomycin as blank. Biological and technical triplicates per sample and controls were used. Plates were incubated for 72 hours at 30°C in an anaerobic hood fed with 10% CO_2, 10% H_2 in nitrogen. Plates were placed in a Tecan M200 PRO and absorbance was measured at 600 nm and fluorescence for PMO7 & PMO8 at Ex. 525 nm, Em. 600 nm; PMO9 & PMO10, Ex. 410 nm, Em. 500 nm.

2.7.15. Fluorescence Microscopy of *D. alaskensis* expressing CreiLOV and PMO7

TUs for CreiLOV LS and PMO7 MS were inserted into *D. alaskensis* and cultured under anaerobic conditions. Cultures were grown to mid-exponential phase (OD_{600}; 0.4 -0.5) under anaerobic conditions. A modified protocol from Fievet *et al* [155] was followed; modified protocol does not use an agar pad. OD_{600} readings from *D. alaskensis* expressing the TUs were measured using CO8000 Cell Density Meter (WPA, Cambridge, UK). In a microcentrifuge tube, 200 µL of each *D. alaskensis* culture was added and centrifuged (13,000 rpm, 3 minutes). The pellet was resuspended with 100 µL of 10 mM TPM buffer (Table 2.4). Cells were incubated under anaerobic conditions for 20 minutes. On a circular microscope cover slide, 25 µL of the sample was placed, followed by 500 µL of 2% liquid non-nutrient agar. The solution was covered with a circular microscope cover slide. Images were acquired using Nikon Ti2 Live Imaging Microscope (Centre Optical Instrumentation

Laboratory, Edinburgh, UK). For pMO7 LS, the filters used were GFP (Ex 474/26 nm, Em 525/40 nm) and for CreiLOV the filters used were GFP (Ex 474/26 nm, Em 525/40 nm), Cy3 (Ex 554/23 nm, Em 596/83 nm) and CFP (Ex 438/24 nm, Em 482/24 nm).

2.7.16. Assembly of TUs expressing both PMO7 and CreiLOV

Two multi-gene expression TUs were assembled (CR LS pMO7 MS and CR Kan pMO7 MS) for the orthogonal expression of PMO7 and CreiLOV via MoClo assembly. The following TUs were assembled first: CR LS, CR Kan, and EF pMO7 MS. Each TU contained the following parts: CR LS (DVA_CreiLOV, J2103_AB, B0034m_BC, B0015_DE and ΔpMOMoClo) CR Kan (DVA_CreiLOV, DVA_Kan, B0034m_BC, B0015_DE and ΔpMOMoClo) and EF pMO7 MS (DVA_pMO7, J23106_EB, B0034m_BC, B0015_DF and DVK_EF). Assembled TUs were inserted into *E. coli* NEB 5-alpha competent cells and plated onto blue/white screening plates. Plates were supplemented with 50 μg/mL spectinomycin (CR LS and CR Kan) and with 50 μg/mL kanamycin (EB pMO7 MS). White colonies were restreaked onto fresh blue/white screening spectinomycin (50 μg/mL) or Kanamycin plates (50 μg/mL). Plasmids were isolated and sequenced for confirmation of correct assembly using sequencing primers (Table 1, No. 19 and 20). Using the assembled TUs, each multi-gene expression TU was assembled by MoClo assembly with BbsI digestion instead of BsaI. TUs contain the following TU components: CR LS pMO7 MS (TU CR LS and TU EF pMO7 MS) and CR Kan pMO7 MS (TU CR Kan and TU EF pMO7 MS). Assembled TUs were transformed into *E. coli* NEB 5-alpha competent cells and plated onto blue/white screening plates. Plates were supplemented with Chloramphenicol (100 μg/mL). White colonies were restreaked onto fresh blue/white screening Chloramphenicol plates (100 μg/mL). Plasmids were isolated and sequenced for confirmation of correct assembly using sequencing primers (Table 2.1, No. 19 and 20).

2.7.17. Fluorescence assay of *E. coli* expressing PMO7 and CreiLOV orthogonally

All TUs were inserted into *E. coli* and cultured under anaerobic and aerobic conditions respectively. Cultures grown to early stationary phase (OD_{600}; 0.6 -0.8) under aerobic conditions. OD_{600} readings were measured using CO8000 Cell Density

Meter (WPA, Cambridge, UK). In a Falcon® 96-well Black/Clear Flat Bottom (Corning, NY, USA) cultures were diluted with LB/Chloramphenicol (100 μg/mL) to an OD_{600} of 0.2 to a final volume of 200 μL. *E. coli* transformed with the plasmid pMO9075 was used as a negative control, CR LS and EF PMO7 MS TUs were used as controls. LB/chloramphenicol (100 μg/mL) as the blank. Biological and technical triplicates per sample and controls were used. Plates were incubated for 4 hours at 37°C. On a Tecan M200 PRO the absorbance at 600 nm and fluorescence were measured at the following wavelengths: PMO7, Ex. 525 nm, Em. 600 nm; CreiLOV, Ex. 450 nm, Em. 495 nm. Further orthogonality was examined by testing TUs to an emission screening with a fixed excitation (PMO7, Ex. 525 nm; CreiLOV, Ex. 450 nm). Emission screening was conducted by iterating 5 nm, starting at their respective excitation wavelength.

2.8. Designing and Engineering a Synthetic RBS library

2.8.1. Design of a synthetic RBS library using RBS Calculator

To design a synthetic RBS specifically for *D. alaskensis* the chosen sequences were predicted using the bioinformatics tool RBS Calculator [110]. The information provided to the bioinformatics tool was the following protein coding sequences: PMO7, pMO8, pMO9, pMO10 and CreiLOV (Section 2.4., Table. 2.5). The organism *D. alaskensis* G20 was selected and maximised proportional scale was used (maximum translation initiation), to ensure the highest translation initiation rate.

2.8.2. Adapting synthetic RBS library to MoClo

The predicted synthetic RBS sequences were adapted to MoClo standards by adding flanking BsaI recognition sites (GGTCTC) followed by fusion site B (TACT) on the 5'end and fusion site C (TTAC) on the 3' end. The synthetic RBS from the library was synthesised in a single gBlock (Table 2.5) (Integrated DNA Technologies) and used for assembly in a MoClo acceptor vector. The library was adapted using the following protocol: To a 0.2 mL tube add equimolar 10 – 60 fmol of the gBlock and acceptor vector DVA_BC, 10 U of BsaI (NEB), 20 U of Quick T4 DNA Ligase (NEB), 1x T4 DNA Ligase Buffer (NEB), and sterile deionized water to a total volume of 20 μL. Reactions were performed using the following parameters: 16 cycles (37°C for 1.5 min, 16°C for 3 min), followed by 50°C for 5 min and 80°C for

10 min and were then held at 4°C. The resulting reactions were inserted into *E. coli* NEB 5-alpha competent cells and plated onto blue/white screening plates. Plates were supplemented with ampicillin (50 μg/mL). Multiple colonies that showed a white phenotype were picked and grown overnight and subsequently used for plasmid purification. Plasmids were then sequenced to confirm RBS sequence for each plasmid (Table 2.1, No. 17 and 18).

2.8.3. Assembly of TUs using synthetic RBS library

To characterise the synthetic RBS library, TUs were assembled expressing oxygen-independent reporters (PMO7 and CreiLOV), under the control of the same promoter (J23106_AB) and terminator (B0015_DE). The following components were used: J23106_AB, B0015_DE, ΔpMOMoClo, synthetic RBS library (RBS 7, RBS 8, RBS 9, RBS 10 or RBS Cr), and an oxygen-independent reporter (PMO7 or CreiLOV). A total of 10 TUs were assembled through MoClo assembly. The resulting reactions were used in *E. coli* NEB 5-alpha transformatons and plated onto blue/white screening plates. Plates were supplemented with 50 μg/mL spectinomycin. White colonies were restreaked onto fresh blue/white screening spectinomycin plates. Plasmids were isolated and sequenced for confirmation of correct assembly using sequencing primers (Table 2.1, No. 19 and 20).

2.8.4. Fluorescence assay of *D. alaskensis* expressing RBS library

D. alaskensis was transformed with all 10 TUs and cultured under anaerobic conditions. Cultures were grown to early stationary phase (OD_{600}; 0.6 -0.8) under anaerobic conditions. OD_{600} readings from *D. alaskensis* expressing the TUs were measured using CO8000 Cell Density Meter (WPA, Cambridge, UK). In a Falcon® 96-well Black/Clear Flat Bottom (Corning, NY, USA) cultures were diluted with PGMC/Spectinomycin (100 μg/mL) to an OD_{600} of 0.15 in a total volume of 200 μL. *D. alaskensis* transformed with the plasmid pMO9075 was used as a negative control, and PGMC/Spectinomycin (100 μg/mL) as the blank. Biological and technical triplicates per sample were used. Plates were incubated for 72 hours at 30°C in an anaerobic hood fed with 10% CO_2, 10% H_2 in nitrogen. On a Tecan M200 PRO the absorbance at 600 nm and fluorescence of PMO7 at Ex. 525 nm, Em. 600 nm; CreiLOV, Ex. 450 nm, Em. 495 nm were measured.

2.9. Designing and Engineering a Synthetic Promoter library

2.9.1. Designing a minimal and native synthetic promoter library using BProm

To design synthetic promoters specifically for *D. alaskensis* the chosen sequences were predicted using the bioinformatics tool BPROM [98]. A minimal promoter design of of the -10 and -35 hexamer boxes and the *E. coli* consensus spacer region (GGCATGCATAAGGCTCG) [156] was chosen for this study. The following housekeeping genes were used to predict the -10 and -35 hexamer boxes: Chaperone *dnaK* (PR-1), *grpE* (PR-3), *groEL* (PR-4), *secE* (PR-7), *secY* (PR-8), *ntH* (PR-9) and *gyrA* (PR-10). Sequences found 150 bp upstream of the housekeeping genes were used for to generate the -35 and -10 hexamer boxes. For a native promoter design, the design was the same as that of a minimal promoter design, but differed in that the spacer region consisted of the sequence between the -10 and -35 hexamer boxes. The native promoter tested in this study was predicted from the sequence of protein translocase subunit SecE (NPR-7).

2.9.2. Adapting the synthetic promoter library to MoClo

The predicted synthetic promoter sequences were adapted to MoClo standards by adding flanking BsaI recognition sites (GGTCTC) followed by a fusion site A (TACT) on the 5'end and a fusion site B (TTAC) on the 3' end. The PR-1, PR-3, PR-4, PR-7, NPR-7 and PR-9 from the library were synthesised in a single gBlock (Table 2.5) (Integrated DNA Technologies) and used for assembly in a MoClo acceptor vector. The library was assembled with the following protocol: Add to a 0.2 mL tube: equimolar 10 – 60 fmol of the gBlock and acceptor vector DVA_AB, 10 U of BsaI (NEB), 20 U of Quick T4 DNA Ligase (NEB), 1x T4 DNA Ligase Buffer (NEB), and sterile deionized water to a total volume of 20 µL. Reactions were performed using the following parameters: 16 cycles (37°C for 1.5 min, 16°C for 3 min), followed by 50°C for 5 min and 80°C for 10 min and were then held at 4°C until they were transformed. The resulting reaction was inserted into *E. coli* NEB 5-alpha and plated onto blue/white screening plates. Plates were supplemented with Ampicillin (50 µg/mL). Multiple colonies that showed a white phenotype were picked and grown overnight for plasmid purification. Plasmids were then sequenced to confirm the promoter sequence for each plasmid (Table 2.1, No. 17 and 18).

PR-8 and PR-10 were assembled by annealing complementary oligonucleotides (Table 2.1, No. 45-48). Oligonucleotides were synthesised by Sigma-Aldrich. Stock solutions of oligonucleotides were hydrated with TE buffer and diluted to 10 µM. In a 0.2 mL tube 10 µL of each complementary oligonucleotide was added along with 30 µL of water. Oligonucleotides were incubated for 5 minutes in a water bath at 100 ^{o}C after which the water bath was turned off and left to cool until it reached room temperature. Successful annealing was confirmed via a 0.8% agarose gel electrophoresis.

2.9.3. Assembly of TUs with synthetic promoter library

To characterise the synthetic promoter library, TUs were assembled expressing oxygen-independent reporters (PMO7 and CreiLOV), under the control of the same RBS (B0034m_BC) and terminator (B0015_DE). The following components were used: B0034m_BC, B0015_DE, ΔpMOMoClo, synthetic promoter library (PR-1, PR-3, PR-4, PR-7, PR-6, PR-9. NPR-7, Pr-8, PR-9 and PR-10), and an oxygen-independent reporter (PMO7 or CreiLOV). A total of 16 TUs were assembled through MoClo assembly. The resulting vectors were inserted into *E. coli* NEB 5-alpha competent cells and plated onto blue/white screening plates. Plates were supplemented with 50 µg/mL spectinomycin. White colonies were restreaked onto fresh blue/white screening spectinomycin plates. Plasmids were isolated and sequenced for confirmation of correct assembly using sequencing primers (Table 2.1, No. 19 and 20).

2.9.4. Fluorescence assay of *D. alaskensis* expressing promoter library

All 16 TUs were electrotransformed into *D. alaskensis* and cultured under anaerobic conditions. Cultures were grown to early stationary phase (OD_{600}; 0.6 -0.8) under anaerobic conditions. OD_{600} readings from *D. alaskensis* expressing the TUs were measured using CO8000 Cell Density Meter (WPA, Cambridge, UK). In a Falcon® 96-well Black/Clear Flat Bottom (Corning, NY, USA) cultures were diluted with PGMC/spectinomycin (100 µg/mL) to an OD_{600} of 0.15 in a total volume of 200 µL. *D. alaskensis* transformed with the plasmid pMO9075 was used as a negative control, and PGMC/spectinomycin as the blank. Biological triplicates and technical triplicates per sample and controls were used. Plates were incubated for 72 hours at 30°C in an anaerobic hood fed with 10% CO_2, 10% H_2 in nitrogen. On a Tecan M200

PRO the absorbance at 600 nm and fluorescence for PMO7 at Ex. 525 nm, Em. 600 nm; CreiLOV, Ex. 450 nm, Em. 495 nm were measured.

2.10. Tailoring NPs synthesis using MoClo Toolkit

2.10.1. Site-directed mutagenesis of BsaI recognition site

The BsaI recognition site found on the pMO_2137 plasmid needed to be removed to be compliant with MoClo standards. Through site-directed mutagenesis, the BsaI recognition site was deleted from pMO_2137. Primers for the deletion of the BsaI recognition site were designed (Table 2.1, No. 31 and 32), and the QuikChange Lighting (Agilent) Site-Directed Mutagenesis kit manufacturer's protocol was followed. Mutant plasmids were inserted into chemically competent *E. coli* NEB 5-alpha cells.

2.9.2. Diagnostic Digest Reaction with BsaI

To confirm the deletion of the BsaI recognition site a diagnostic digest reaction with BsaI (NEB protocol) was performed, followed by electrophoresis on a 0.8% agarose gel.

2.9.3. Adapting NiFe hydrogenase to MoClo

To adapt the NiFe hydrogenase small subunit coding sequences to MoClo standards, the sequence of interest was amplified using the following primers (Table 2.1, No. 29 and 30). Primers were designed as follows: Forward primer, 9 nucleotides (random); BsaI recognition site (GGTCTC), 1 nucleotide; Fusion site C (AATG), 2 nucleotides, 15 base pairs of sequence of interest. Reverse primer, 9 nucleotides (random); BsaI recognition site (GGTCTC), 1 nucleotide; Fusion site D (ACCT), 2 nucleotides, 15 base pairs of sequence of interest. PCR amplified DNA of interest was gel purified. To adapt the sequence to MoClo standards the following protocol was followed: Add to a 0.2 mL tube: equimolar 10 – 60 fmol of the DNA amplicon and acceptor vector DVA_CD, 10 U of BsaI (NEB), 20 U of Quick T4 DNA Ligase (NEB), 1x T4 DNA Ligase Buffer (NEB), and sterile deionized water to a total volume of 20 µL. Reactions were performed using the following parameters: 16 cycles (37°C for 1.5 min, 16°C for 3 min), followed by 50°C for 5 min and 80°C for 10 min and were then held at 4°C until they were transformed. The resulting reaction was inserted into *E. coli* NEB 5-alpha competent cells and plated onto blue/white screening plates. Plates were supplemented with Ampicillin (50 µg/mL). Multiple colonies that

showed a white phenotype were picked and grown overnight for plasmid purification. Correct assembly of DVA_2137 was confirmed via sequencing using sequence primers (Table 2.1, No. 17 and 18).

2.9.4. Assembly of Combinatorial Transcriptional Units of NiFe hydrogenase

TUs were assembled via MoClo assembly. Different TUs were assembled under the expression of the strongest characterised synthetic promoters and RBS. Each TU contained the following parts: J23106_AB, Kan promoter, PR-3, B0034m_BC, RBS-CR, RBS-9, B0015_DE, DVA_2137 and acceptor plasmid ΔpMOMoClo. Assembled TUs were inserted into *E. coli* NEB 5-alpha competent cells and plated onto blue/white screening plates. Plates were supplemented with 50 µg/mL Spectinomycin. White colonies were restreaked onto fresh blue/white screening Spectinomycin plates. Plasmids were isolated and sequenced for confirmation of correct assembly using sequencing primers (Table 2.1, No. 19 and 20).

2.9.5. Production of Pt NPs

Cultures of *D. alaskensis* pMO9075 and *D. alaskensis* inserted with the combinatorial library were grown anaerobically to an OD_{600} of 1.0. OD readings of all cultures were measured, to make sure all samples had similar cell concentrations. Cells were centrifuged for 10 minutes at 4000 rpm. The pellet was washed with 1 mL of 10 mM MOPS (pH 7.5). These steps were repeated once more. The final pellet was resuspended in 1 mL of 10 mM MOPS (pH 7.5). $Pt(IV)Cl_4$ solution was then added to the resuspended cells to a concentration of 2 mM. The solution was left for 2 hours at 30°C under anaerobic conditions, then centrifuged for 10 minutes at 4000 rpm. The pellet was resuspended in 1 mL of 50% acetone and centrifuged for 15 minutes at 13,000 rpm. The supernatant was removed and the pellet was allowed to dry completely. Pellet was then resuspended in 1 mL dH_2O.

2.9.6. Transmission Electron Microscopy (TEM)

A volume of 10 µL of purified NPs and NP/cell suspensions of each sample were spotted onto a 200 mesh copper grid (Agar Scientific) and allowed to dry. Any excess liquid was removed using filter paper. Samples were analysed using a JOEL JEM 1400-Plus TEM with an accelerating voltage of 80 kV. Images were captured

using a GATAN OneView camera. Image post-processing was carried out using ImageJ software.

2.9.7. Inductively Coupled Plasma Optical Emission Spectrometry (ICP-OES)

Inductively Coupled Plasma Optical Emission Spectrometry ICP-OES was used to ascertain the amount of ions present in the nanoparticle samples. A sample of each suspension was sonicated for 30 minutes in a water bath, centrifuged for 1 hour at 20,000 rpm. The supernatant was then added to 14% aqua regia and heated for 8 hours at 80°C. The resulting suspension was diluted in H_2O to a volume of 3 mL and subjected to ICP-OES analysis on a Perkin Elmer Optima 5300 DV ICP-OES.

2.9.8. 2,6-DMP Colorimetric Assay

All the reactions were carried out in a 96-well plate in a total volume of 300 µL. The colorimetric assay consisted of a final concentration of 1 mM 2,6-DMP (Sigma-Aldrich), and 50 mM N-(2-hydroxy-ethyl) piperazine-N'-(2-ethanesulfonic acid) (HEPES) at pH 7. Different concentrations of Pt nanoparticles and Pt ions were used. The optical density of 2,6-DMP in the presence of Pt nanoparticles and ions was measured over a time lapse of 10 minutes at 469 nm using a Thermo Scientific Multiskan GO (Cat#N10588).

2.9.9. Methylene Blue Colorimetric Assay

All reactions were carried out in a 96-well plate in a total volume of 200 µL. The colorimetric detection assay consisted of final concentrations of 40 µM methylene blue (MB), 10 mM Sodium Borohydride, and 10 mM N-(2-hydroxy-ethyl) piperazine-N'-(2-ethanesulfonic acid) (HEPES) at pH 7. Different concentrations of Pt nanoparticles and Pt ions were used. The optical density of MB in the presence of Pt nanoparticles and ions was measured over time at 665 nm using a Thermo Scientific Multiskan GO.

2.11. Cell Surface Engineering of *D. alaskensis*

2.11.1. PCR amplification of EC20/IgA insert and pMO9075 vector and Assembly

The EC20/IgA fragment and pMO9075 plasmid backbone were amplified from pEC20 (donated by Dr Matthew Edmundson, Horsfall Laboratory, University of

Edinburgh) and pMO9075 respectively by PCR (Primers listed in Table 2.1, No. 39 - 42), with annealing temperatures of 48°C and 67°C. The resulting PCR products were confirmed by electrophoresis on a 0.8% agarose gel, then excised and purified. Insert and backbone purified fragments were assembled by HiFi DNA Assembly® Reaction Protocol (NEB). Assembled plasmids were inserted into chemically competent *E. coli* NEB 5-alpha cells.

2.11.2. Diagnostic Digest Reaction with BamHI and BglI

The engineered plasmid (pMOEC20) generated was confirmed through a BamHI and BglI diagnostic digest reaction (NEB protocol) followed by electrophoresis on a 0.8% agarose gel electrophoresis. The plasmid was then sequenced with primers No. 43 and 44 (Table 2.1) for confirmation.

2.11.3. Copper, Platinum and Palladium Survivability Test of *E. coli* expressing EC20

Overnight cultures of *E. coli* pMO9075 and *E. coli* pMOEC20 were grown (20 hours, 37°C, 200 rpm) in 10 mL LB with 50 µg/mL spectinomycin. In a 96-well CytoOne® Plate 250 µL LB with 50 µg/mL spectinomycin and a range of concentrations of $CuSO_4$ (0 mM, 0.5 mM, 1 mM, 2 mM, 4 mM and 5 mM), $Pt(IV)Cl_4$ (0 mM, 0.5 mM, 1 mM, and 2mM) and Na_2PdCl_4 (0 mM, 1 mM, and 2 mM). Overnight cultures were diluted with LB, to an adjusted OD_{600} of 0.1. On Thermo Scientific Multiskan GO, the absorbance at 600 nm were measured every 30 minutes for 22 hours under controlled conditions of 37°C and 200 rpm.

2.11.4. Copper Resistance in Copper containing agar plates

Overnight cultures of *E. coli* pMO9075 and *E. coli* pMOEC20 were grown (20 hours, 37°C, 200 rpm) in 10 mL LB with 50 µg/mL spectinomycin. Serial dilutions of the overnight cultures (10^{-2}, 10^{-4}, and 10^{-6}) were done. A volume of 10 µL of all dilutions and undiluted cultures were spotted onto LB agar plates containing different concentrations of $CuSO_4$ (0 mM, 0.5 mM, 1 mM, 2 mM, 3 mM, 4 mM, 4.3 mM and 4.5 mM 4.7 mM and 5 mM), and supplementred with 50 µg/mL spectinomycin. Plates were incubated overnight (20 hours) at 37°C.

2.11.5. TEM imaging of *D. alaskensis* with copper

Cultures of *D. alaskensis* transformed with pMO9075 and pMOEC20 were grown anaerobically to an OD_{600} of 1.0. Cells were centrifuged for 10 minutes at 4000 rpm. The pellet was washed with distilled water. These steps were repeated twice more. The final pellet was resuspended in distilled water. $CuSO_4$ solution was then added to the resuspended cells to a concentration of 1 mM. The solution was incubated anaerobically for 1 hour at 30°C. TEM grids were prepared as follows; 10 µL of each sample was spotted onto a 200 mesh copper grid (Agar Scientific) and allowed to dry. Any excess liquid was removed using filter paper. Samples were analysed using a JOEL JEM 1400-Plus TEM with an accelerating voltage of 80 kV. Images were captured using a GATAN OneView camera. Image post-processing was carried out using ImageJ software.

2.11.6. ICP-OES of the removal of copper by *D. alaskensis*

Cultures of *D. alaskensis* transformed with pMO9075 and pMOEC20 were grown anaerobically to an OD_{600} of 1.0. Cultures were centrifuged at 4000 rpm, and washed in 1 mL of PGMC (to avoid copper precipitation) three times. $CuSO_4$ solution was then added to the resuspended cells to a concentration of 1 mM. The cells solution were incubated anaerobically for 2 hours at 30°C and then centrifuged at 4000 rpm. The supernatant was then filter sterilised through a 0.22 µm syringe filter and used for copper content measurement using ICP-OES (Perkin Elmer Optima 5300 DV ICP-OES). A minimum of 3 mL of each sample was transferred to a 15 mL Falcon tube. Samples were sonicated. Distilled water without any $CuSO_4$ was used as a blank. A standard curve was made using three standard solutions of 0.1 mM, 1 mM and 5 mM copper in PGMC.

2.12. Data Analysis

All fluorescence assays, survivability assays and catalytic activity data were analysed by a one-way ANOVA, with a Shapiro-Wilk normality test and a Brown-Forsythe equal variance test. When this analysis was not feasible due to the failure of normality or equal variances tests (even after data transformation) an alternative test was conducted (e.g., *t*-test)

Chapter 3: MoClo Toolkit and Synthetic Biology Tools for *D. alaskensis*

3.1. Introduction

DNA assembly techniques have revolutionised biotechnology research and innovation. However, despite many advances in molecular biology, the assembly of DNA remains cumbersome [68]. Within synthetic biology research and industry, Modular Cloning (MoClo) is considered to be efficient and a versatile DNA assembly technology. MoClo is a golden gate, type IIS restriction endonuclease assembly technology that enables the sequential, combinatorial and scar-free assembly of parts in a one-pot reaction [66-68]. Available toolkits and standards such as MoClo have streamlined the process of DNA assembly, and enabled the assembly of DNA parts, genes and pathways in a fast, cost-effective and high throughput manner. MoClo assembly libraries and toolkits are available for numerous model microorganisms, most importantly for *E. coli* [66, 73-75]. However, no such library or toolkit has been reported for *D. alaskensis* or any other SRB. The design and engineering of MoClo tools for *D. alaskensis* will help accelerate research into heavy metal bioremediation and NP synthesis, allowing the quick design, assembly and testing of genes and pathways, tailored for *D. alaskensis.* This study aims to build two different acceptor vectors, one to express a single TU and another to express two TUs. These acceptor vectors are very important, because they will enable the MoClo assembly reactions to construct TUs that can be inserted into *D. alaskensis*, to streamline the easy to use, rapid design-build-test cycles.

A MoClo toolkit would not be complete without the inclusion of reporter genes. The lack of a reporter specifically designed and engineered for *D. alaskensis* has hindered research and prevented the characterisation of expression control elements and bioparts. Reporter proteins have a wide range of applications within synthetic biology, from promoter and RBS variant analysis, as markers for monitoring gene transfer, for visualising gene expression, to drug discovery [127]. Fluorescent proteins are the most common reporter proteins used to characterise synthetic bioparts. However, fluorescent reporter proteins such as green fluorescent protein (GFP) are inactive in anaerobic bacteria, as they strictly require molecular oxygen for

maturation [157, 158]. Low oxygen environments are encountered frequently in a broad range of biomedical and industrial processes, including bioremediation, fermentation of high value biomolecules, and in biotechnology applications of obligate anaerobes [129]. Currently, GFP is not the best fluorescent reporter used in research, as GFP's relatively large size (~25 kDa) may cause constraints associated with dysfunctional GFP fusion proteins [155].

The need to design and engineer a novel oxygen-independent reporter is imperative to enable researchers and industry stakeholders to study synthetic biology applications in anaerobic environments. Recently, flavin-based fluorescent proteins (FbFPs) such as iLOV (light, oxygen or voltage-sensing) fluorescent protein derived from LOV photoreceptor proteins [130, 131], have become the staple oxygen-independent reporters. FbFPs have many advantages when compared to GFP, as they have shown to be expressed by multiple organisms and emit fluorescence under anaerobic conditions [132-136], while they can also act as thermostable and fast-maturing probes with a broad operational pH range [137]. CreiLOV, an FbFP with blue light LOV domains, found in *Chlamydomonas reinhardtii*, has been demonstrated to be the brightest FbFP reporter to date [137]. CreiLOV has a reported quantum yield ~1.5-fold larger than iLOV [130, 137, 138]. FbFPs are promising candidates to serve as a new class of fluorescent reporters in anaerobic conditions. However, the versatile application of FbFPs as robust reporters is currently hindered by their limited brightness [159]. Fluorescence emission by an FbFPs are weak, and they need to be expressed at high levels. Through novel design and directed mutations of existing FbFPs, their fluorescence levels can be improved. Novel oxygen-independent fluorescent reporters show considerable promise, therefore, this study aims to design and engineer an oxygen-independent reporter library specifically for *D. alaskensis*. The library will consist of reporters that work in more than one microorganism (*D. alaskensis* and *E. coli*), show a versatility to work in aerobic and anaerobic conditions and more importantly, will be able to be applied for the characterisation of expression control elements.

3.2. Assembly of single TU acceptor vector ΔpMOMoClo

The *lacZα* gene, fusion sites and the flanking BsaI and BbsI recognition sites from DVK_AE were cloned into the *D. alaskensis* plasmid pMO9075 with confirmation

obtained *via* a blue/white screening test, insert-specific PCR, and a BsaI diagnostic digest reaction. Following assembly, the plasmid was transferred into chemically competent *E. coli* NEB 5-alpha cells. A total of 71 colonies grew overnight. Of these 71 colonies tested, two (colonies 7 and 33) displayed a blue phenotype (Figure 3.1), indicating that the *lacZα* gene had been inserted into the construct. Plasmids from colonies 7 and 33 were extracted, followed by insert specific PCR. Both colonies 7 and 33 were confirmed to have the correct size band by electrophoresis (Figure 3.1, C). To indicate that the BsaI sites needed for the MoClo reaction were present, a diagnostic digest reaction with BsaI was conducted (Figure 3.1, D). Further confirmation was conducted by sequencing. The sequencing results matched the desired sequence.

To be compliant with the MoClo standards, the BbsI recognition site found on the pMOMoClo backbone needed to be removed, by site-directed mutagenesis. Specific primers for the deletion of the BbsI recognition site were designed to delete AAGA bases from the BbsI recognition site (GAAGAC). To confirm the successful deletion of the BbsI site, a diagnostic digestion reaction with BbsI was conducted on plasmids extracted from eight of the colonies which resulted from the mutagenesis. The diagnostic digest was confirmed by electrophoresis (Figure 3.2). Further confirmation was conducted by sequencing. The sequencing results matched the desired sequence.

The newly adapted plasmid ΔpMOMoClo was tested by performing a MoClo assembly reaction using the following components taken from the CIDAR MoClo Parts Kit: (J23100_AB; constitutive strong promoter, B0032m_BC; medium strength RBS, C0012m_CD; controller protein lacl, and B0015_DE; double terminator). When assembled correctly in the acceptor vector ΔpMOMoClo, these parts create a TU. ΔpMOMoClo contains a *lacZα* gene, which in turn contains the assembly insertion sequence, meaning successful insertion will disrupt transcription of the *lacZ* gene. A blue/white screening test was therefore performed with colonies containing a functional *lacZ* displaying a blue phenotype and those containing the assembled TU within the disrupted gene displaying a white phenotype. Following a transformation of *E. coli* NEB 5-alpha cells with the plasmids, 70 colonies grew overnight (Figure

3.3) with 23 colonies showing a white phenotype and 47 colonies with a blue phenotype.

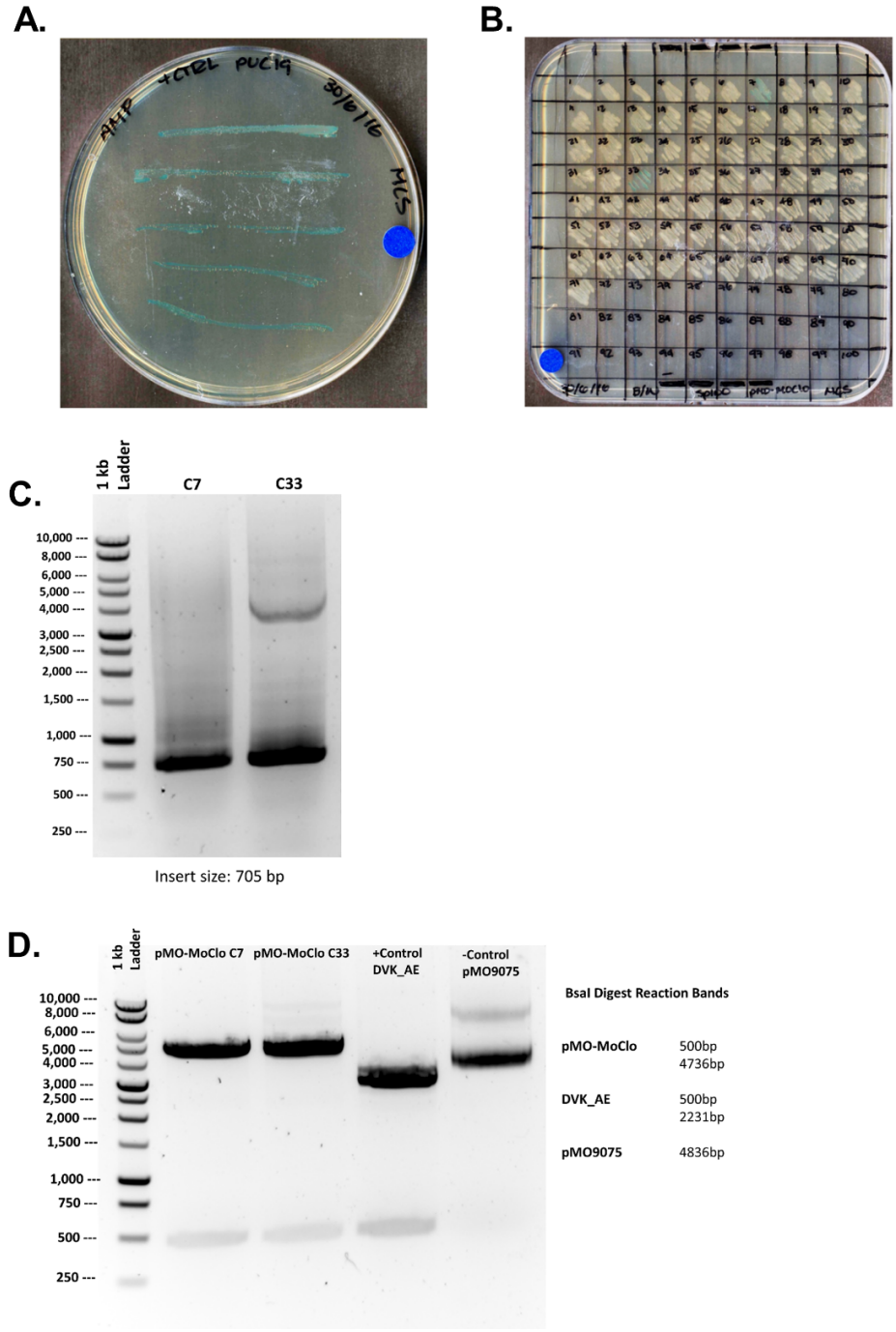

Figure 3.1. Confirmations of the assembly of single TU acceptor vector pMOMoClo. A) Blue/White Screening Results Transformation positive control, *E. coli* (pUC19). B) Re-streaked colonies of Gibson assembly, colonies No. 7 and 33 have a blue phenotype. C) Insert Specific PCR: Agarose Gel electrophoresis. Plasmids purified from colonies C7 and C33 were tested for the presence of full-length insert (702 bp) D) Insert Specific PCR: Agarose Gel Electrophoresis. Diagnostic Digest Reaction with BsaI: Agarose Gel Electrophoresis. Colonies C7 and C33 were tested, both yielding bands at the correct sizes (4736 bp and 500 bp).

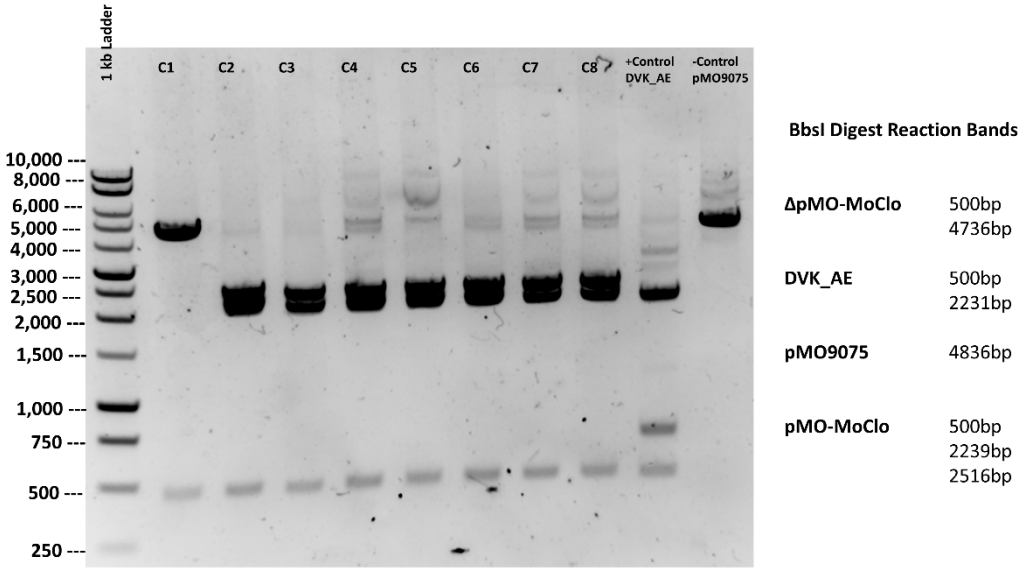

Figure 3.2. Diagnostic Digest Reaction with BbsI: Agarose Gel Electrophoresis. Eight colonies tested (C1 – C8) with two controls. C1 has the correct pattern of bands with only two bands (500 bp and 4736 bp) indicating that this mutant plasmid no longer contains the undesired BbsI recognition site.

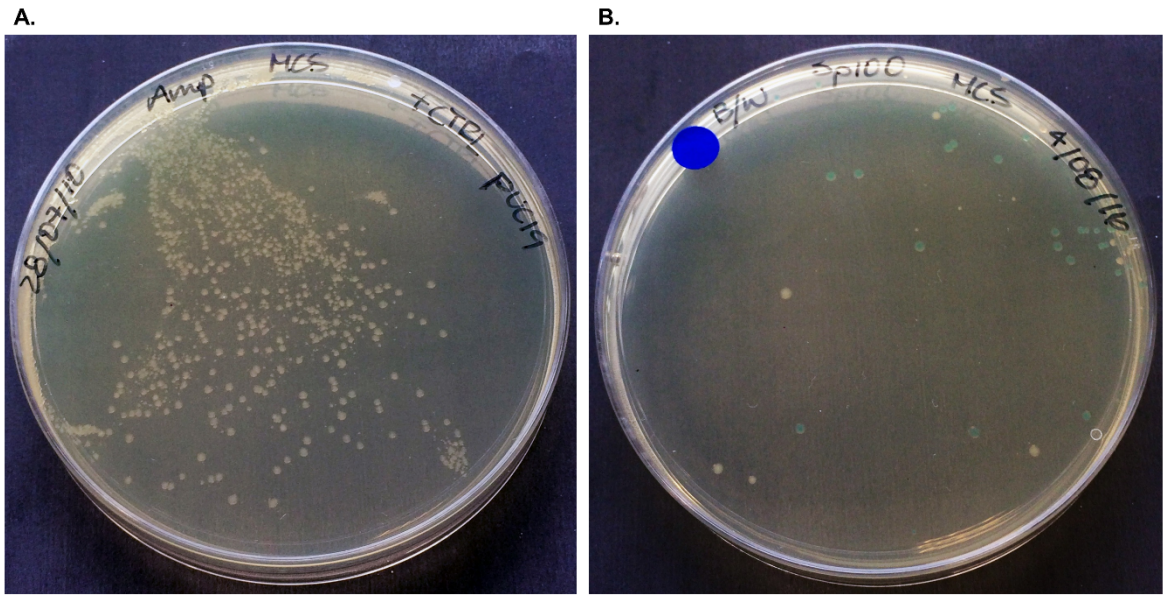

Figure 3.3. Blue White Screening Test. A) Positive control, *E. coli* pUC19. B) MoClo assembly results with plasmid ΔpMoMoClo, 70 colonies in total (23 white colonies and 47 blue colonies).

3.3. Assembly of multi-gene expression acceptor vector ΔpMOMoClo_AF

To assemble ΔpMOMoClo_AF, the Chloramphenicol resistance gene, the *lacZα* gene fusion sites and the flanking BsaI and BbsI recognition sites from DVK_AF were cloned into the *D. alaskensis* plasmid ΔpMO9075, with confirmation obtained *via* a blue/white screening test, and a BbsI and XhoI diagnostic digest reaction. A level 2 acceptor vector is required to have a different selection marker to the level 1 acceptor vector (ΔpMOMoClo, Spectinomycin), therefore ΔpMOMoClo AF was assembled using a Chloramphenicol resistance gene.

To be compliant with the MoClo standards, the BbsI recognition site found on the pMO9075 backbone needed to be removed, which was accomplished through site-directed mutagenesis. Specific primers for the deletion of the BbsI recognition site were designed to delete AAGA bases from the BbsI recognition site (GAAGAC). To confirm the successful deletion of the BbsI site, a diagnostic digestion reaction with BbsI and XhoI was conducted on plasmids extracted from eight of the colonies that resulted from the mutagenesis. The diagnostic digest was confirmed by electrophoresis (Figure 3.4). Final confirmation was done by sequencing the plasmids.

The gBlock (containing the Chloramphenicol resistance gene, *Laczα* gene from acceptor vector DVK_AF and flanked by XbaI and XhoI recognition sites) and ΔpMO9075 were digested with XbaI and XhoI. Correct bands were excised and purified after they were separated on an electrophoresis gel. ΔpMoMoClo AF was assembled by ligating both digested parts. *E. coli* NEB 5-alpha was transformed with the resulting reaction and plated onto blue/white screening plates supplemented with Chloramphenicol. Blue colonies were restreaked onto fresh blue/white screening Chloramphenicol plates (Figure 3.5). Final confirmation was done by sequencing the plasmid, which confirmed the presence of the desired sequence.

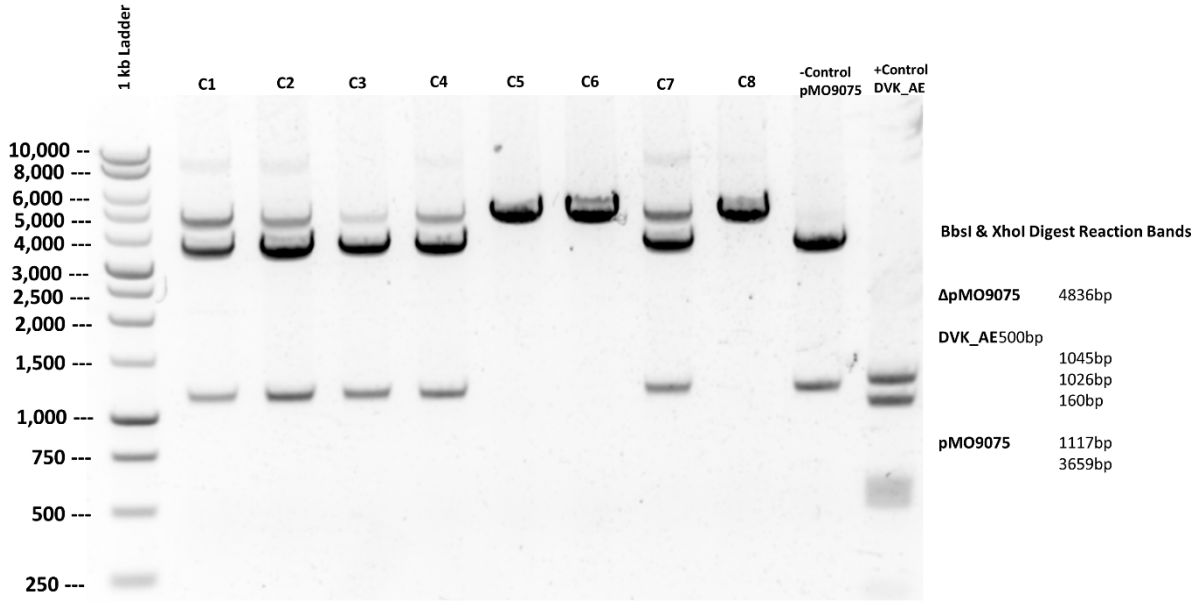

Figure 3.4. Diagnostic Digest Reaction with BbsI and XhoI: Agarose Gel Electrophoresis. Eight colonies tested (C1 – C8) with two controls. C5, C6 and C8 have the correct band with only a single band (~4836 bp) indicating that this mutant plasmid no longer contains the undesired BbsI recognition site. Three bands appear on C1 – C4 and C7 indicating negative results.

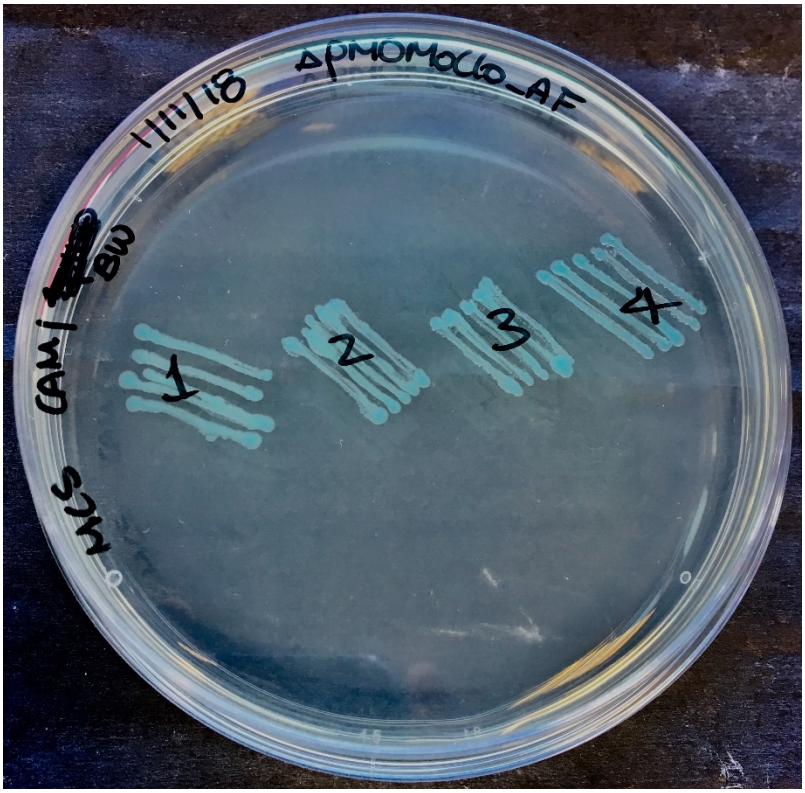

Figure 3.5. Blue/White Screening Results. Re-streaked colonies of ligation reaction.

3.4. Adapting phiLOV, nanoLUC and CreiLOV to MoClo

The CDS of phiLOV, nanoLUC and CreiLOV were successfully adapted to MoClo and each cloned into MoClo donor vector DVA_CD. For phiLOV and nanoLUC, the sequences of interest were amplified with sequence specific primers. These primers were designed to contain flanking BsaI recognition sites, followed by fusion site C (AATG, forward primer) and D (ACCT, reverse primer). Amplified sequences were cloned into DVA_CD through a MoClo assembly reaction. Assembled plasmids (DVA_phiLOV and DVA_LUC) were inserted into chemically competent *E. coli* NEB 5-alpha cells and plated onto blue/white screening plates with ampicillin. For DVA_phiLOV a white colony was chosen to perform an insert-specific PCR, to be confirmed by electrophoresis (Figure 3.6). The colony specific PCR gel showed the correct size band, concluding that DVA_phiLOV was successfully cloned. To further confirm the successful assembly of DVA_phiLOV, a diagnostic digest reaction with BsaI was performed. The diagnostic digest reactions were confirmed by electrophoresis (Figure 3.7). The diagnostic digest gel shows the correct size band, further indicating that DVA_phiLOV was successfully cloned. For DVA_LUC white colonies were purified and plasmid extracted. To confirm a successful assembly, diagnostic digest reaction with BsaI was performed on 7 different plasmids. Digest reactions were run on an electrophoresis gel (Figure 3.8). Gel results indicate that NanoLUC was successfully cloned into DVA_CD. DVA_LUC contained a BbsI recognition site within its CDS sequence, and to comply with MoClo standards, removal of this recognition site was required. This site was removed through site-directed mutagenesis. Specific primers for the deletion of the BbsI recognition site were designed to change GAA to GAG in the restriction site whilst retaining the codon's original coding for glutamine. To confirm the successful deletion of the BbsI recognition site in DVA_LUC a diagnostic digestion reaction with BbsI and BsaI was conducted. The diagnostic digest was confirmed through an electrophoresis gel (Figure 3.9). Both DVA_phiLOV and DVA_LUC were confirmed through sequencing.

Plasmids with the CreiLOV gene (*D. alaskensis* codon optimised) and *E. coli* CreiLOV gene (*E. coli* codon optimised) were synthesized by Genewiz. There was

no need to clone these into the MoClo donor vector DVA_CD because the plasmids were already designed to be compliant with MoClo standards.

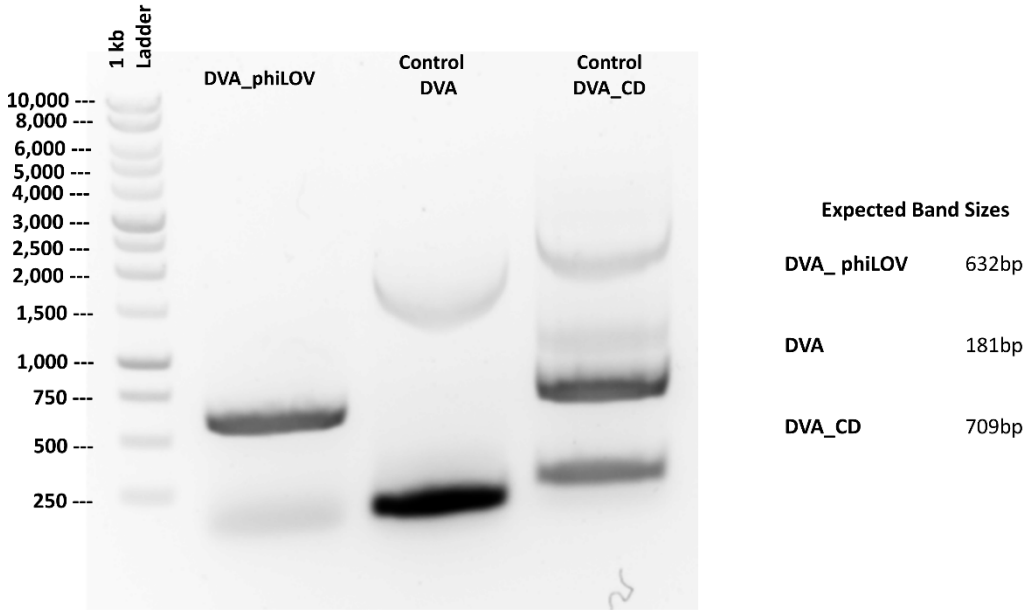

Figure 3.6. Colony Insert Specific PCR: Agarose Gel Electrophoresis. A single colony was tested. DVA_phiLOV showed a single band between the 750 bp and 500 bp marker, which indicated a correct result. Correct size band expected was 632 bp.

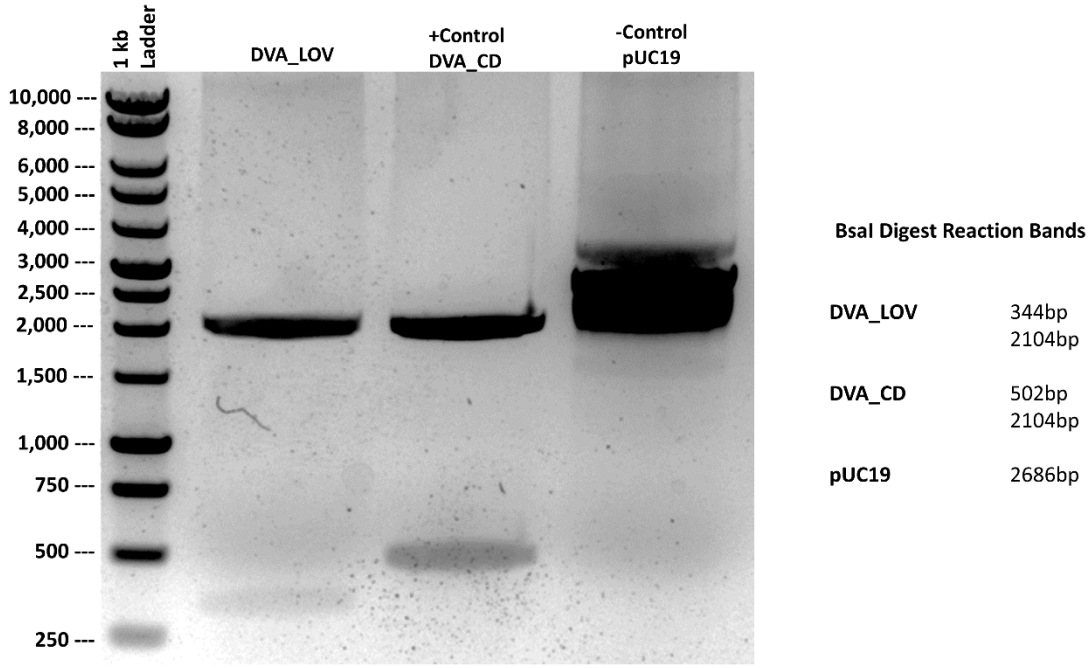

Figure 3.7. Diagnostic Digest Reaction with BsaI: Agarose Gel Electrophoresis. DNA extracted from a single culture was tested. Correct size bands are 344 bp and 2104 bp. Negative control used is pUC19 plasmid.

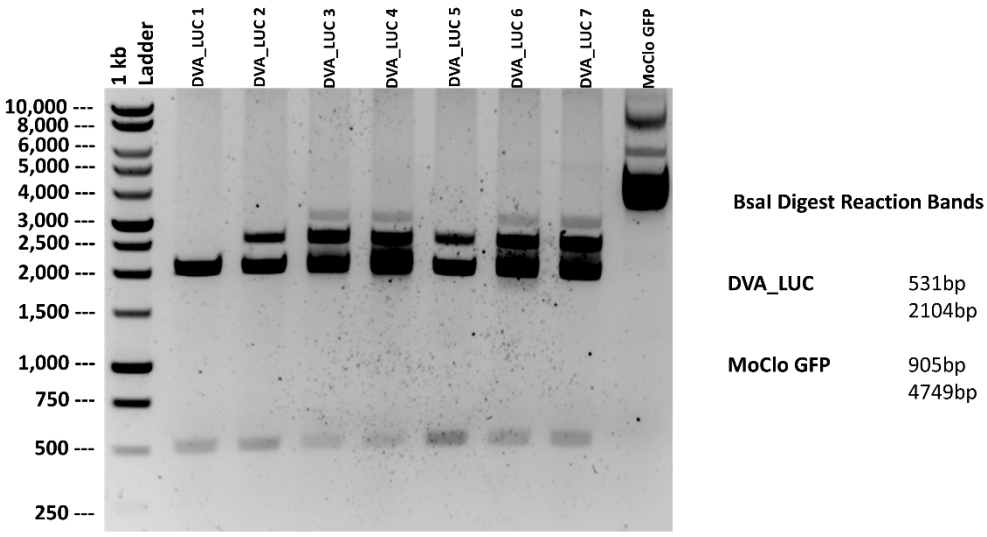

Figure 3.8. Diagnostic Digest Reaction with BsaI: Agarose Gel Electrophoresis. Seven colonies was tested (DVA_LUC1 – DVA_LUC7). Only DVA_LUC1 has the correct results. Only two bands appear on DVA_LUC1 (2000 bp and 500 bp) indicating that this plasmid was correctly assembled. Three bands appear on DVA_LUC2 – DVA_LUC7 indicating negative results.

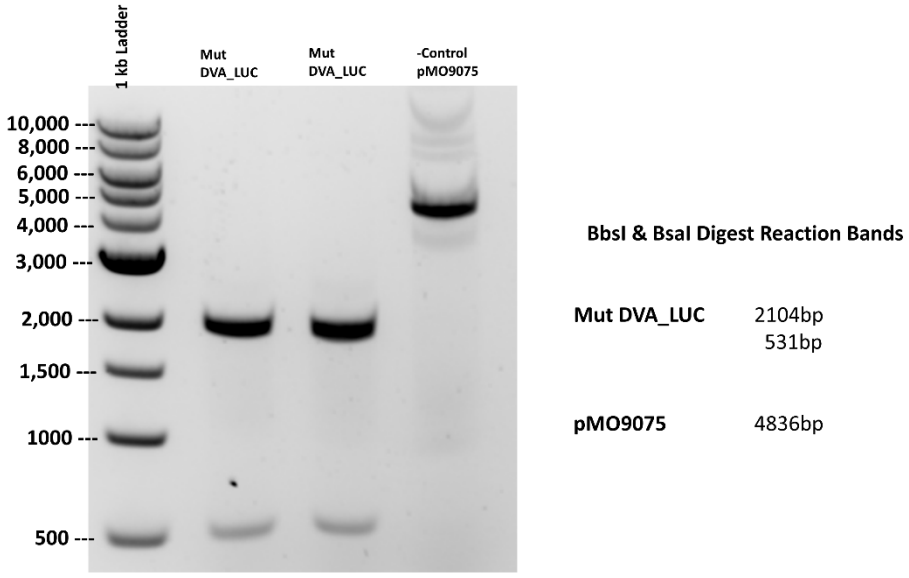

Figure 3.9. Diagnostic Digest Reaction with BbsI and BsaI: Agarose Gel Electrophoresis. Two colonies tested with one negative control (pMO9075). Both have the correct results. Only two bands appear on both plasmids (500 bp and 2000 bp) indicating that this mutant plasmid has a deleted BbsI recognition site.

3.5. Fluorescence assay of *E. coli* expressing CreiLOV and phiLOV

CreiLOV and phiLOV were assembled into different TUs using acceptor vector ΔpMOMoClo, each with the same strong promoter (J2100_AB), strong RBS (B0034m_BC) and terminator (B0015_DE) for each reporter. TUs assembled are as follows: phiLOV, CreiLOV and *E. coli* CreiLOV. TU's were transferred into chemically competent *E. coli* NEB 5-alpha cells and were screened for fluorescence emission upon excitation at 450 nm and emission at 495 nm. Assay graphs are depicted in Figure 3.10. For the 1/100 and 1/5 dilutions all TUs emitted a higher fluorescence in comparison with the negative control (ΔpMOMoClo). For 1/10 dilution, only CreiLOV emitted a higher fluorescence in comparison with the control. Values reported for CreiLOV under all dilutions were statistically significant (one-way ANOVA, P value > 0.05) in comparison with the control.

The statistically significant values obtained for CreiLOV, fluorescence allowed further investigations. TUs expressing CreiLOV were assembled, each with a different *E. coli* promoter strength, the same RBS (B0034m_BC) and the same terminator (B0015_DE), all parts obtained from CIDAR MoClo Parts Kit. TUs assembled are as follows: CreiLOV SS, CreiLOV MS, and CreiLOV LS (SS = strong promoter and RBS; MS = medium promoter and strong RBS; LS = low promoter and strong RBS). TU's were transferred into chemically competent *E. coli* NEB 5-alpha cells and were screened for fluorescence emission upon excitation at 450 nm and emission at 495 nm. Assay graphs are depicted in Figure 3.11. All TUs emitted a higher fluorescence emission in comparison with the negative control (ΔpMoMoClo). Values for cultures diluted in PBS (Figure 3.11A) are not statistically significant (one-way ANOVA, P value < 0.05) in comparison with control. By contrast, all TUs cultures diluted with LB showed values that are statistically significant (one-way ANOVA, P value > 0.05) in comparison with the control (Figure 3.11B).

To visually confirm and to ascertain previous results in a qualitative manner, the fluorescence emission of CreiLOV, on a 96-well plate, several wells were filled with LB supplemented with Spectinomycin. Single colonies from CreiLOV SS, MS and LS were picked and used to inoculate individual wells. pMOMoClo was used a negative control and LB was used as a blank. Biological triplicates were performed.

The plate was incubated overnight at 37°C and shaking at 300 rpm. Image of the 96-well plate under blue light was taken (Figure 3.12). Figure 3.12 depicts all cultures emitting fluorescence under blue light, all to a similar intensity, except those wells with the negative control. Low fluorescence levels were observed by the negative control.

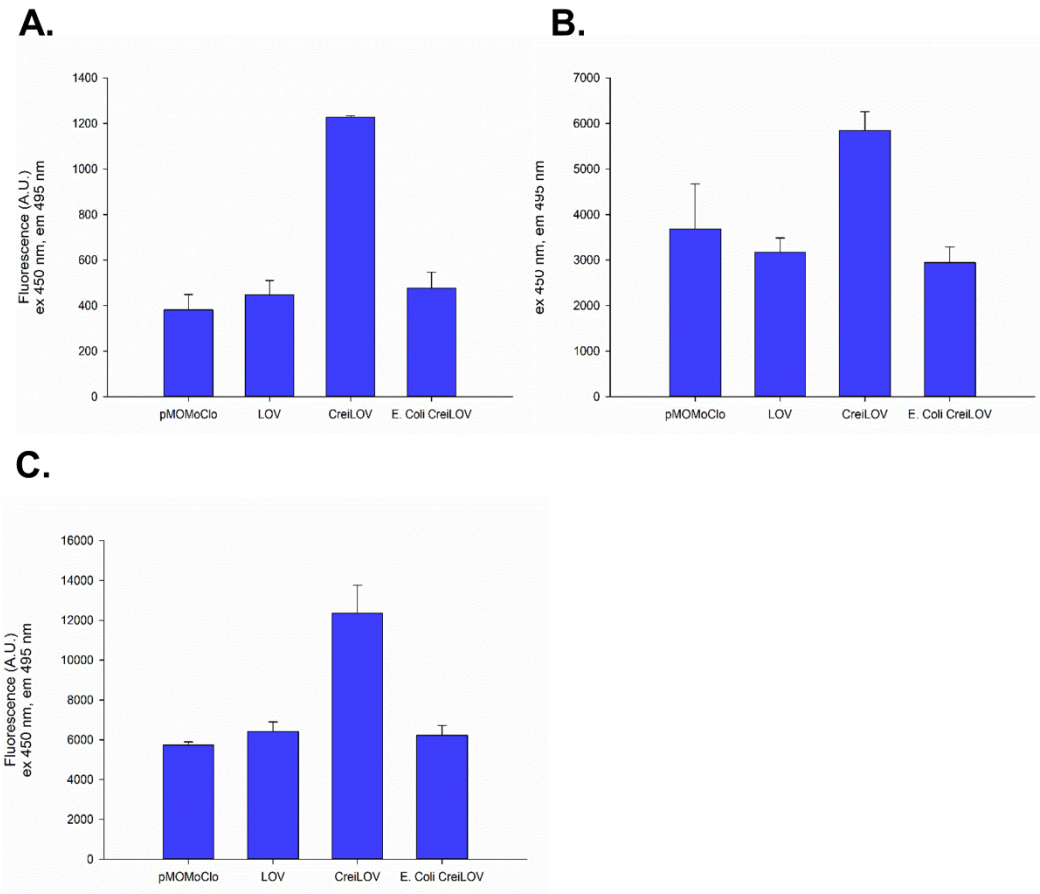

Figure 3.10. Fluorescence assay of *E. coli* expressing phiLOV or CreiLOV under aerobic conditions. Assays were conducted using PBS. All reporters tested are expressed under a strong promoter (J2100_AB), strong RBS (B0034m_BC) and terminator (B0015_DE). A) 1/100 dilution of cultures. B) 1/10 dilution of cultures. C) 1/5 dilution of cultures. Error bars depict the standard deviation of the mean.

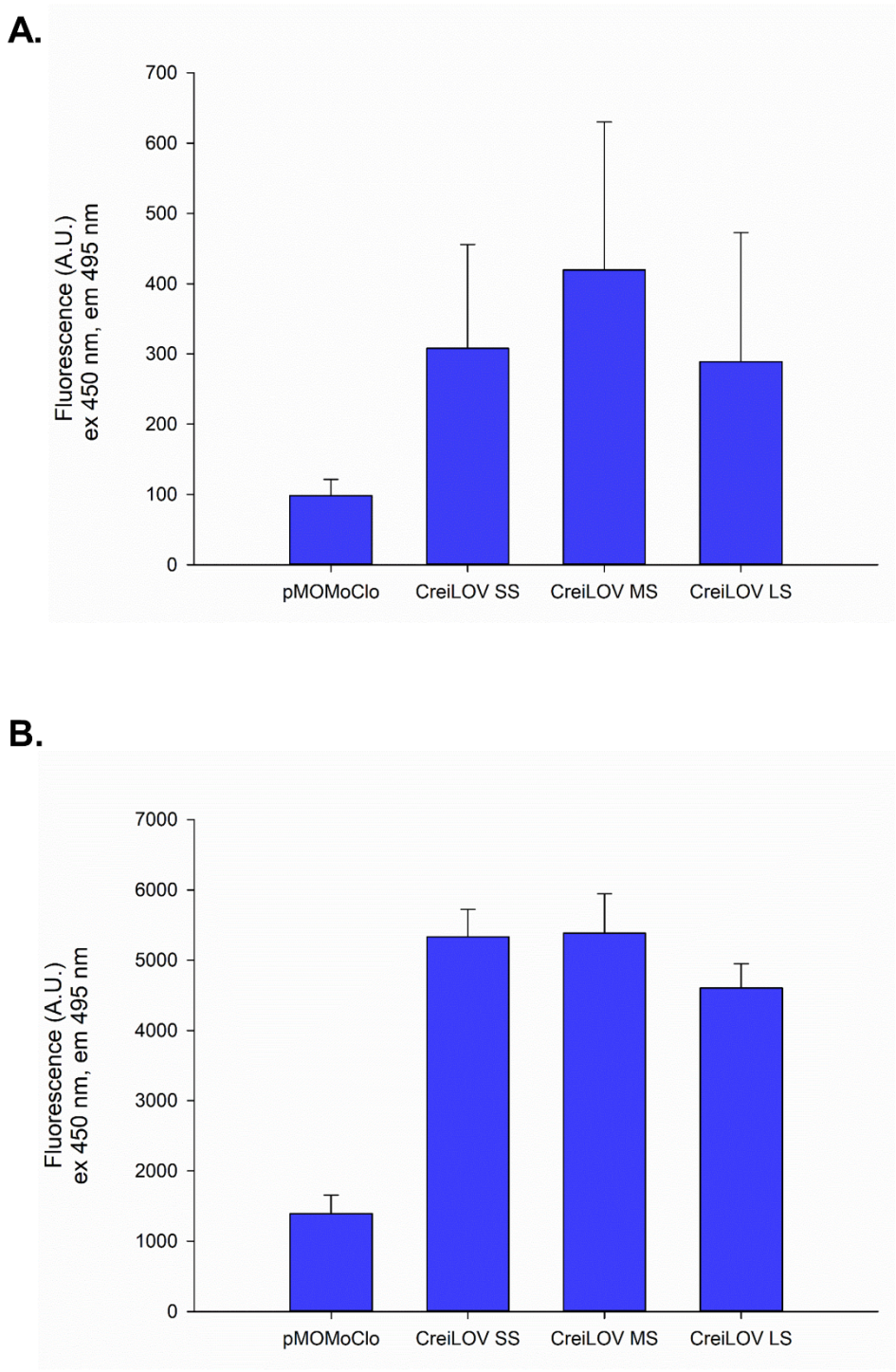

Figure 3.11. Fluorescence assay of *E. coli* expressing CreiLOV under aerobic conditions. TUs assembled for CreiLOV iterating promoter strength (Strong J23100_AB; Medium J23106_AB; Low J23116_AB), same RBS (B0034m_BC) and terminator (B0015_DE). TUs assembled (SS, MS and LS). A) Cultures diluted with PBS. B) Cultures diluted with LB. Error bars depict the standard deviation of the mean.

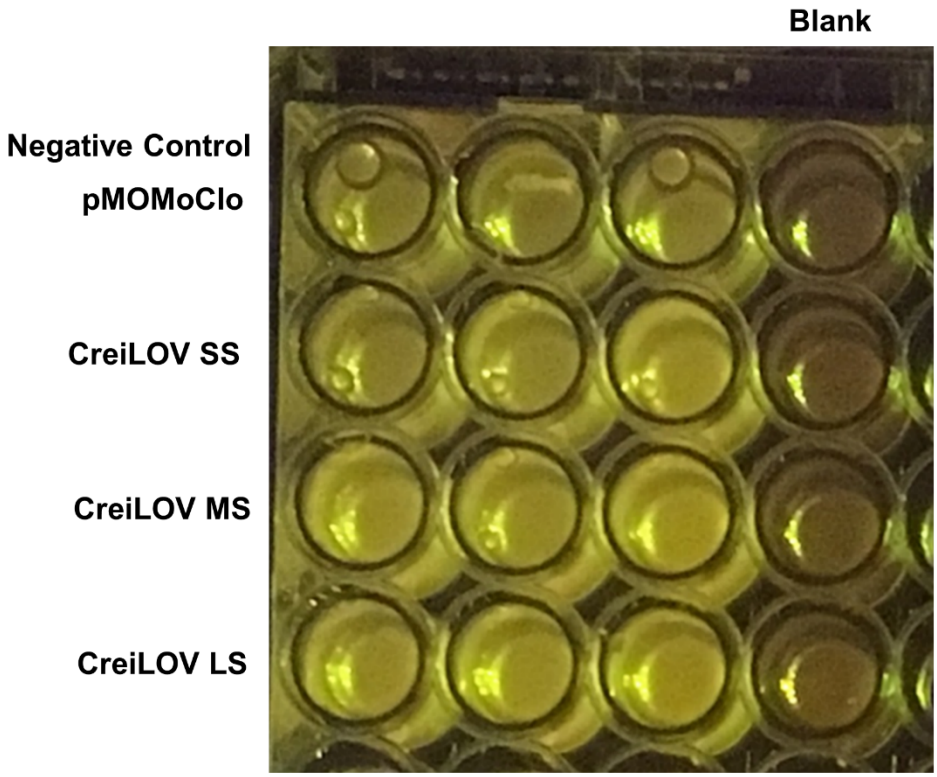

Figure 3.12. Image of *E. coli* expressing CreiLOV under different promoter strengths under blue light. CreiLOV SS, CreiLOV MS, CreiLOV LS and negative control plasmid pMOMoClo. Triple technical repeats for each plasmid.

3.6. Gene mining of the oxygen-independent library

Biotangents (Edinburgh, UK), conducted the gene mining research and the assembly of the oxygen-independent fluorescent reporter library with the exception of CreiLOV.

The oxygen-independent fluorescent reporter library was designed specifically to work under anaerobic conditions by *D. alaskensis*. Following a literature research and sequence homology of oxygen-independent GFP, BFP and FbFPs fluorescent proteins, 12 potential oxygen-independent fluorescent proteins were identified, and to be screened for fluorescence excitation and emission in *E. coli* and *D. alaskensis* under anaerobic and aerobic conditions (Table 3.1). Including within the reporter library were designed enhancements to result in higher fluorescence. For example, GFP-S65A (alanine substituted for serine at position 65) a mutated version of wild-type GFP, has a red-shifted fluorescence excitation spectrum and higher fluorescence intensity than the wild-type [160].

CDS of the oxygen-independent reporter library were codon-optimised for expression in *D. alaskensis,* commercially synthesised as gBlocks and inserted immediately downstream of a putative kanamycin promoter of plasmid pMO9075. Each insert CDS is preceded by a RBS and followed by an *E. coli HisI* terminator (Chapter 2, Table 2.5). Plasmids were assembled through Gibson assembly with the exception of pMO11 and pMO12, which were assembled through Golden Gate. All assemblies were confirmed by sequencing.

Table 3.1. Oxygen-independent reporter library tested in this study.

Reporter Name	Gene & Design	Description	Ex. (nm)	Em. (nm)	Ref.
PMO1	CKM-1 BfgV D8 (BfgV D8)	BFP, from *Vibrio vulnificus*	352	440	*161*
PMO2	CKM-1 BfgV D8 (Truncated BfgV D8)	BFP, from *Vibrio vulnificus*	352	440	*161*
PMO3	CKM-1 BfgV D8 W198N R199K (Truncated BfgV D8 WR198NK)	BFP, from *Vibrio vulnificus*	352	440	*161, 162*
PMO4	LOV (BsLOV)	FbFPs, from *Bacillus subtilis*	449	495	*163*
PMO5	LOV C62A (Truncated BsLOV C62A)	FbFPs, from *Bacillus subtilis*	449	495	*163*
PMO6	LOV (PpLOV)	FbFPs LOV gene, from *Pseudomonas putida*	450	495	*163*
PMO7	GFP from R10-3 mutant (AvGFP R10-3)	GFP mutant, from *Aequorea victoria*	525	600	*164*
PMO8	GFP from R10-3 mutant S66A (AvGFP R10-3 S66A)	GFP mutant, from *Aequorea victoria*	525	600	*164*
PMO9	BFP (mBFP)	BFP, metagenomics	350 – 410	420 - 500	*162*
PMO10	BFP G188S (mBFP G188S)	BFP, metagenomics	350 - 410	420 - 500	*162, 165*
PMO11	LOV C53A (PpLOV C53A)	FbFPs, LOV gene, from *Pseudomonas putida*	450	495	*163*
PMO12	LOV C62A (BsLOV C62A)	FbFPs, LOV gene, from *Bacillus subtilis*	449	495	*163*
CreiLOV	CreiLOV	FbFPs LOV gene, from *Chlamydomonas reinhardii*	450	495	*166*

3.7. Fluorescence screening of the Oxygen-Independent Library

Dr Michael Capeness (Horsfall Laboratory) conducted the fluorescence screening of the oxygen-independent library in *D.alaskensis* under anaerobic conditions and the initial data analysis of such data.

D. alaskensis and *E. coli* JM109 were inserted with the oxygen-independent library (Table 3.1). Cells were grown under anaerobic conditions until they reached the exponential phase. Fluorescence intensity was measured for *E. coli* (Figure 3.13) and *D. alaskensis* (Figure 3.14). All constructs with the exception of PMO1, PMO2, PMO3 and PMO6 were shown to be functional in *E. coli,* giving increased fluorescence intensities of approximately 2-fold and 15-fold above the background level for PMO7 and PMO5 respectively (Figure 3.15). BFP coding sequences from *Vibrio vulnificus* (PMO1, PMO2 and PMO3) did not result in detectable fluorescence by *E. coli* and *D. alaskensis* in comparison to the negative control (pMO9075), therefore no further test were done. All constructs with the exception of PMO4 and PMO9 were shown to be functional in *D. alaskensis*, giving increased fluorescence intensities of up to 2-fold and 3-fold for PMO7 and PMO12 respectively (Figure 3.16). By comparing results between *E. coli* and *D. alaskensis,* a clear difference in reporter expression strength can be observed. LOV based FbFP from *Pseudomonas putida* (PMO6 and PMO11), and BFP from metagenomics (PMO10) in *D. alaskensis* reported a detectable fluorescence emission, in comparison with the negative control (pMO9075). Unlike results obtained for *E. coli,* where PMO6 and PMO10 showed fluorescence at basal levels, PMO10 resulted in a statistically significant (one-way ANOVA, P value < 0.05) fluorescence intensity value. However the BFP identified through metagenomics, (PMO9), yield fluorescence at basal levels in *D. alaskensis*, without the G1885 mutation designed to enhance fluorescence. Mutant GFP R10-3 coding sequences from *Aequorea victoria* (PMO7 and PMO8), and LOV based FbFPs coding sequences from *Bacillus subtilis* (PMO5 and PMO12) when expressed in *D. alaskensis* and *E. coli*, all showed an increase in fluorescence emission in comparison with the negative control. Statistical analyses concluded that the detected values are significant (one-way ANOVA, P value < 0.05) in comparison to those of the negative control. PMO8 differs from PMO7 in that it has an S66A substitution, a substitution that was designed to enhance fluorescence emission in anaerobic

reporters[167]. When expressed in *E. coli* JM109 (Figure 3.13C), PMO8 has a higher fluorescence intensity in comparison with PMO7, with a statistically significant difference between reported values. Such results indicate that the S66A substitution in pMO8 indeed enhanced its reporter utility only in *E.coli*. However, when expressed in *D. alaskensis,* PMO7 has a higher fluorescence intensity than PMO8, and the reported values are statistically significant (one-way ANOVA, P value < 0.05) (Figure 3.14C). The change in fluorescence emission capture between *E. coli* and *D. alaskensis* may be associated with the lack of correct protein folding. Recombinant proteins often fail to reach a native conformation when proteins are heterologously expressed by bacteria [168], which may result in a diminished fluorescence emission. Bottlenecks in transcription and translation, under titration of chaperones and proteases, improper codon usage and inability of disulphide-bond formation are among the main causes of impaired protein folding [169, 170].

For further examination of the BFP metagenome coding sequences (PMO9 and PMO10), each fluorescent reporter was tested within the wavelength range of 350 – 410 nm [162]. This screening was performed to determine the optimum excitation and emission wavelength for these fluorophores; reporters were tested by excitation and emission wavelengths, altering 20 nm for each attempt. The optimum excitation/emission wavelength was found to be 410/500 nm. Detectable fluorescence emission values were measured for *E. coli* (Figure 3.13D) with PMO9 and *D. alaskensis* (Figure 3.14D) with PMO10. Statistical analyses concluded that captured values are not statistically significant (one-way ANOVA, P value > 0.05) in comparison the negative control. Unlike previous studies where the comparison of the expression of oxygen-independent fluorescent reporters between model-organism *E. coli* and other model-organisms reported that values expressed are higher under aerobic conditions, than anaerobic conditions [79]. Fluorescence emissions captured for PMO8 and PMO7 in *D. alaskensis* had intensities of up to 7-fold and 15-fold above the intensities captured for their *E. coli* JM109 counterparts. These results indicate that the heterologous expression of PMO7 and PMO8 were more stable and their synthesis was more favourable when expressed in *D. alaskensis*. Results are not emulated by reporters PMO5 and PMO12, where fluorescence intensities captured for such constructs were more intense in *E. coli* JM109 than in *D. alaskensis*.

Under anaerobic conditions both *E. coli* and *D. alaskensis* emitted autofluorescence. As seen on Figure 3.13A, B and D the autofluorescence reported is higher for *E. coli* (pMO9075) in comparison with values reported for *D. alaskensis* (pMO9075) on Figure 3.14A, B and D. Whereas, the autofluorescence reported on Figure 3.14C for *D. alaskensis* is higher in comparison with values reported for *E. coli* (Figure3.13C). These results indicate that both microorganism autofluorescence different intensities at different wavelengths, which can be associated with their own secretion of flavins into the external media [171].

The versatility of the oxygen-independent reporter library was also tested under aerobic conditions in *E. coli* JM109 cells (Figure 3.15). All oxygen-independent reporters with the exception of PMO1, PMO9 and PMO10 emitted a detectable fluorescence in comparison with the negative control (pMO9075). Unlike with the anaerobic results captured for both strains, PMO2 and PMO3 reported higher fluorescence emission in comparison with the control, however the results were not statistically significant (one-way ANOVA, P value > 0.05). Similarly, to previously obtained results, PMO5 and PMO12 values statistically significant in comparison with to the negative control, suggesting these reporters have the versatility to emit fluorescence under both anaerobic and aerobic conditions. Moreover, PMO5 reported the highest fluorescence emission of the reporter library. PMO6 under aerobic conditions showed values over 15-fold and 9-fold of the values reported for *D. alaskensis and E. coli* respectively. A fluorescent reporter that is able to emit fluorescence under anaerobic and anaerobic environments, has useful properties to study gene expression of obligate anaerobes and facultative anaerobes [135]. Results show that PMO5 is able to emit a fluorescence signal under both aerobic and anaerobic conditions.

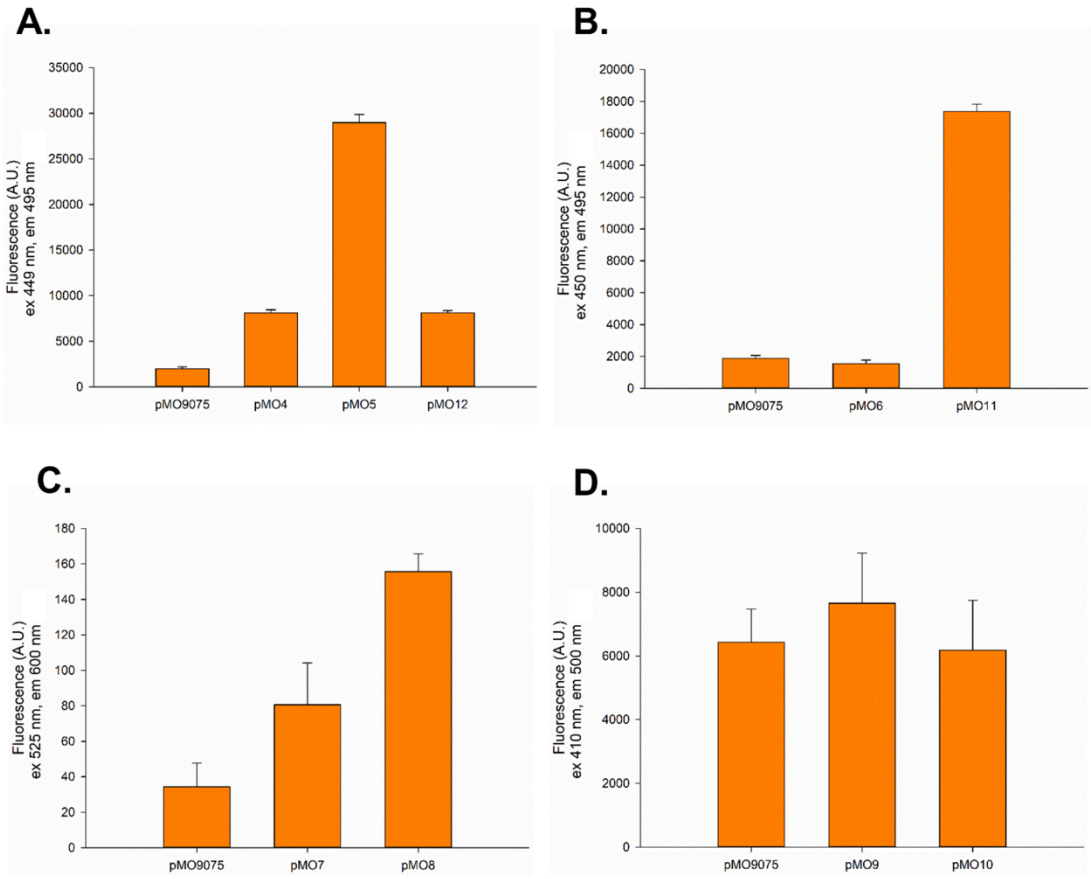

Figure 3.13. Fluorescence assay of *E. coli* expressing oxygen-independent library under anaerobic conditions. All culture cells with inserted plasmids tested were expressed under a constitutive kanamycin promoter and an *E. coli His* terminator. Assays were conducted after 4 hours of incubation under anaerobic conditions for *E. coli* JM109. A) Fluorescence assay expressing PMO4, PMO5 and PMO12. B) Fluorescence assay expressing PMO6 and PMO11. C) Fluorescence assay expressing PMO7 and PMO8. D) Fluorescence assay expressing PMO9, and PMO10. Error bars depict the standard deviation of the mean. Average absorbance values (OD_{600}) are enlisted on the Appendix Chapter, Table A-1.

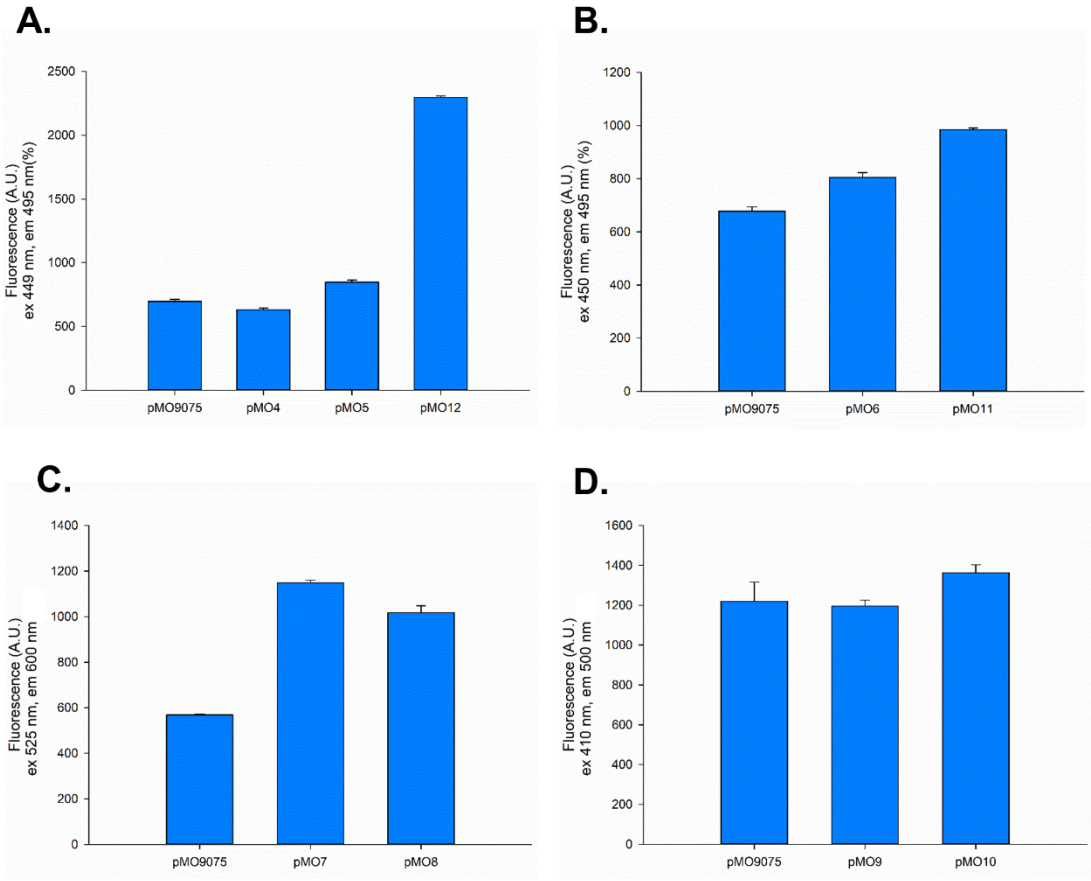

Figure 3.14. Fluorescence assay of *D. alaskensis* expressing oxygen-independent library under anaerobic conditions. All cultured cells with inserted plasmids tested are expressed under a constitutive kanamycin promoter and an *E. coli His* terminator. Assays were conducted after 4 hours of incubation under anaerobic conditions for *D. alaskensis* G20. A) Fluorescence assay expressing PMO4, PMO5 and PMO12. B) Fluorescence assay expressing PMO6 and PMO11. C) Fluorescence assay expressing PMO7 and PMO8. D) Fluorescence assay expressing PMO9, and PMO10. Error bars depict the standard deviation of the mean. Average absorbance values (OD_{600}) are enlisted on the Appendix Chapter, Table A-1.

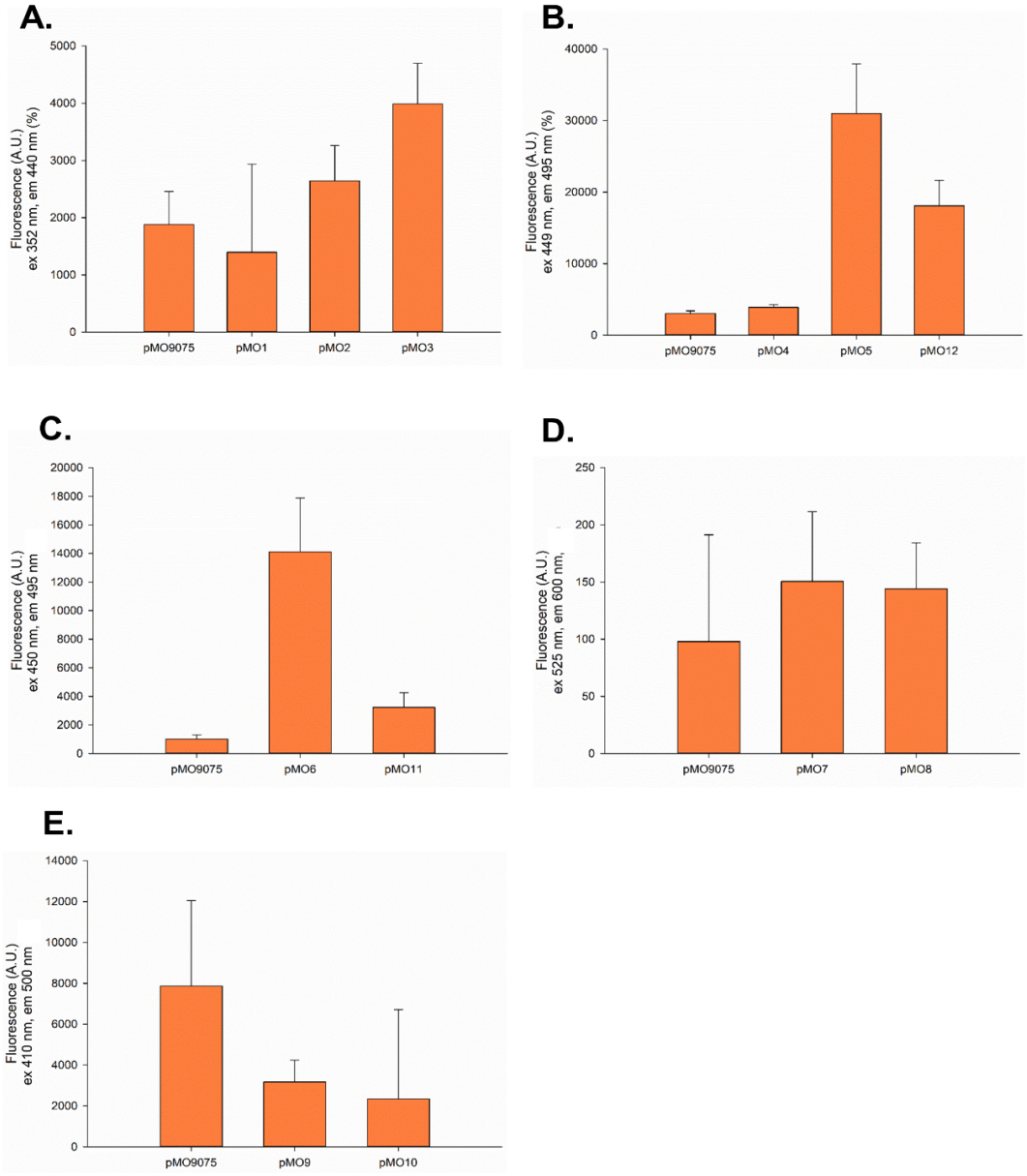

Figure 3.15. Fluorescence assay of *E. coli* expressing oxygen-independent library under aerobic conditions. All cultured cells with inserted plasmids tested were expressed under a constitutive kanamycin promoter and an *E. coli His* terminator. Assays were conducted after 4 hours of incubation under aerobic conditions for *E. coli*. A) Fluorescence assay expressing PMO1, PMO2 and PMO3. B) Fluorescence assay expressing pMO4, pMO5 and pMO12. C) Fluorescence assay expressing PMO6 and PMO11. D) Fluorescence assay expressing PMO7 and PMO8. E) Fluorescence assay expressing PMO9 and PMO10. Error bars depict the standard deviation of the mean. Average absorbance values (OD_{600}) are enlisted on the Appendix Chapter, Table A-1.

3.8. Adapting pMO7 and pMO8 to MoClo

Sequences for PMO7 and PMO8, were adapted to MoClo standards, because they both are simple to quantify, and the excitation and emission wavelength generate a low background activity. PMO12 was not chosen as it might cause a metabolic burden when overexpressed. Moreover, PMO12 may also not be suitable to characterise expression control elements with similar strength, as a high expression may cause a saturation of fluorescence, preventing an accurate characterisation. Using gene-specific primers to amplify sequence of interest, the reporters were cloned into donor vector DVA_CD through MoClo assembly reactions. Following assembly, the plasmids were transferred into chemically competent *E. coli* NEB 5-alpha cells. White colonies were cultured and their plasmids were extracted. Further confirmed through sequencing the plasmids with results showing the presence of the desired sequence. To be compliant with MoClo standards, the BbsI recognition site found on the DVA_pMO8 needed to be removed, which was accomplished through site-directed mutagenesis. Specific primers for the deletion of BbsI recognition site were designed to change GAA to GAG in the restriction site whilst retaining the codon's original coding for glutamine. To confirm the successful deletion of the BbsI recognition site on DVA_pMO8, a diagnostic digestion reaction with BbsI and BsaI was conducted on four colonies and visualised on an electrophoresis gel (Figure 3.16). Further confirmed through sequencing. The sequencing results matched the desired sequence.

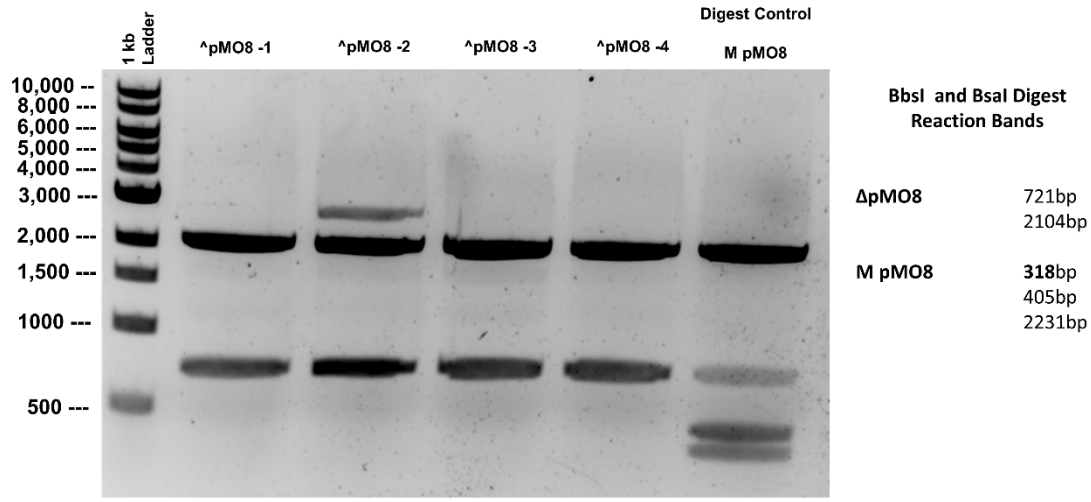

Figure 3.16. Diagnostic Digest Reaction with BbsI and BsaI: Agarose Gel Electrophoresis. Four different colonies were tested (pMO8-1 – pMO8-4). All colonies had conclusive results that the BbsI recognition site was successfully removed. Negative control non-mutated pMO8 shows more than two bands.

3.9. Fluorescence assay of MoClo adapted oxygen-independent library

PMO7 from *Aequorea victoria* and CreiLOV were considered optimal due to its simple quantification, high fluorescence yield in *D. alaskensis*, its low background activity emitted from the negative control (pMO9075), and the fact that it does not cause a significant metabolic burden in *D. alaskensis.* All are necessary factors for accurate characterisation of synthetic expression control elements [79, 127].

The MoClo adapted oxygen-independent reporters were assembled into different TUs, each with a different *E. coli* promoter strength, same RBS and same terminator. TUs assembled into ΔpMOMoClo are as listed on Table 3.2. Afterwards, all constructs were transferred into *D. alaskensis* competent cells and were screened for fluorescence emission upon excitation with the previously determined wavelengths (Figure 3.17). Values were depicted as fluorescence/OD since their growth and cell density had considerably different values among all fluorescent reporters, and fluorescence values were normalized by OD values. All TUs expressing PMO7 and CreiLOV emitted fluorescence at significant levels in comparison with the negative control (pMO9075). Importantly, 3 of the TUs, pMO7 MS, CreiLOV LS, and CreiLOV Kan reported statistically significant (one-way ANOVA, P value < 0.05) fluorescence emission in comparison with the negative control. The values obtained indicate that the use of different *E. coli* promoters does impact on the fluorescent emission captured for *D. alaskensis,* and these values differ among each reporter tested. For PMO7 the promoter strength order is as follows: M (J23106_AB) > L (J23116_AB) > Kan > S (J23100_AB). For CreiLOV the promoter strength order is as follows: Kan > L (J23116_AB) > M (J23106_AB) > S (J23100_AB). Our finding correlates previous research our findings of the order promoter strength changes when expressing different CDS [172]. The expression of heterologous genes impedes a normal cellular growth rate, and regardless of the microorganism, such heterologous expression will cause a metabolic load or metabolic burden. This metabolic load can differ depending on the heterologous gene being expressed [172, 173]. Results suggest that adapting the oxygen-independent reporters to MoClo standards, changes their relative fluorescence emission. All Golden Gate approaches require specific fusion sites to enable the sequential assembly of parts. These fusion sites are unavoidable scars between each expression control element. Scars found between the coding

sequence and the upstream sequence can have a substantial impact on the functional properties of such, by affecting the mRNA structure transcribed [75].

Table 3. 2. PMO7, PMO8, PMO9, PMO10 and CreiLOV TUs assembled and tested in this chapter

TUs	Promoter	RBS	CDS	Terminator
pMO7 SS	J23100_AB	B0034m_BC	PMO7	B0015_DE
pMO7 MS	J23106_AB			
pMO7 LS	J23116_AB			
pMO7 Kan	Kanamycin promoter			
pMO8 SS	J23100_AB		PMO8	
pMO8 MS	J23106_AB			
pMO8 LS	J23116_AB			
pMO8 Kan	Kanamycin promoter			
CreiLOV SS	J23100_AB		CreiLOV	
CreiLOV MS	J23106_AB			
CreiLOV LS	J23116_AB			
CreiLOV Kan	Kanamycin promoter			

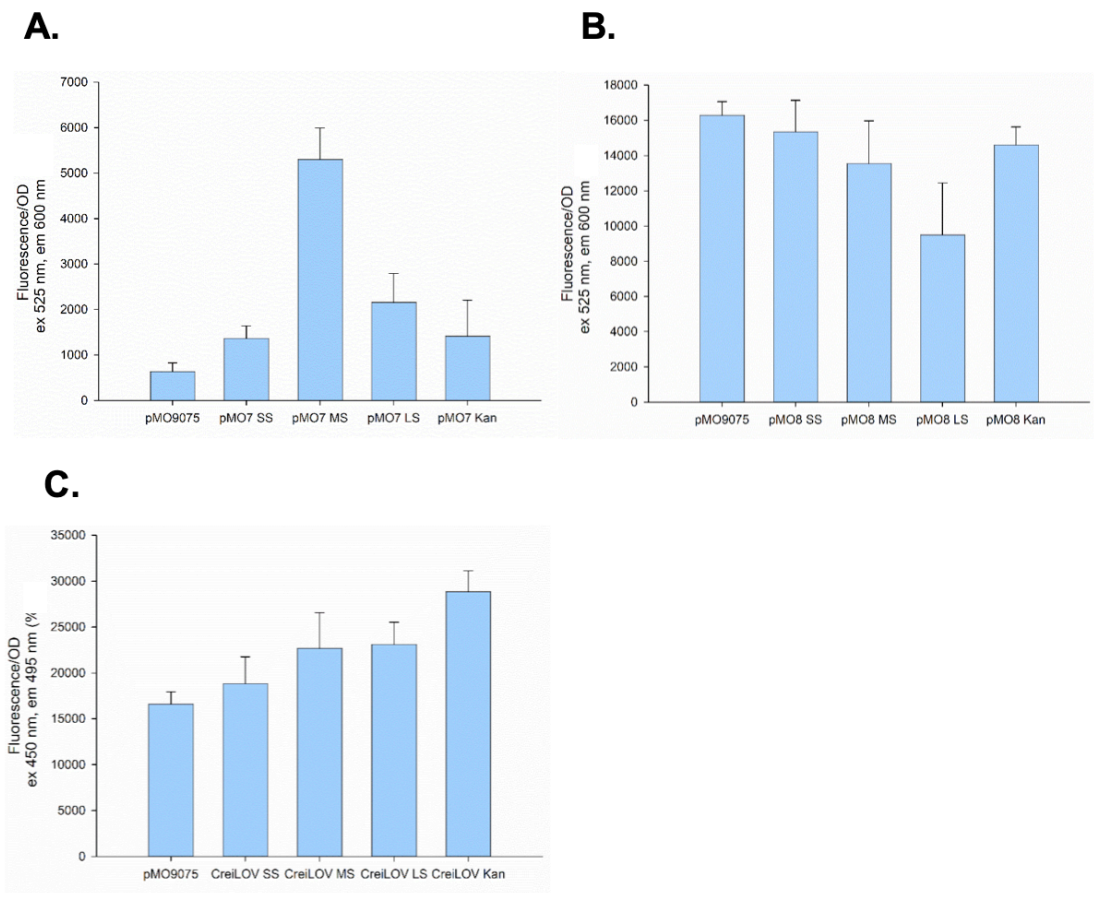

Figure 3.17. Fluorescence assay of TUs expressing anaerobe reporters in *D. alaskensis*. All assay were conducted after 72 hours. Four different TUs expressing the anaerobic reporters with different promoter strengths (strong, medium, low and Kan) and same RBS strength were tested in comparison with the negative control pMO9075. A) Fluorescence Assay of PMO7 reporter. B) Fluorescence Assay of PMO8 reporter. C) Fluorescence Assay of CreiLOV reporter on *D. alaskensis*. Error bars depict the standard deviation of the mean. Average absorbance values (OD_{600}) are enlisted on the Appendix Chapter, Table A-1.

3.10. Fluorescence Microscopy of *D. alaskensis* expressing pMO7 and CreiLOV

From the TUs expressing pMO7 and CreiLOV previously assembled and characterised, those that reported the highest fluorescence emission values were chosen to be tested to be viewed under a fluorescence microscope. The TUs pMO7 MS and CreiLOV LS were inserted into competent *D. alaskensis* cells and incubated under anaerobic conditions until they reached the exponential phase. A modified protocol version of Fievet et al [155] was followed to attempt to visualise *D. alaskensis* cells under a fluorescence microscope. The sole modification to the protocol was that instead of placing washed cells onto an agar pad, cells were mixed with lukewarm agar to prevent cell motility. A single sample was tested for each TU, and *D. alaskensis* (pMO9075) was used as the negative control. Images were taken using a Nikon Ti2 Live Imaging Microscope (Centre Optical Instrumentation Laboratory, Edinburgh, UK). For pMO7 a GFP filter was used (Figure 3.18). For CreiLOV, GFP Cy3 and CFP filters were used, to test the entire range of excitation and emission wavelengths that could cause CreiLOV to emit fluorescence (Figures 3.19 and 3.20). Results were inconclusive due to excessive background noise and therefore no significant fluorescence emission was captured for either pMO7 or CreiLOV samples. *D. alaskensis* cells were not fluorescent under any of the filters used. The software used to analyse the images, increases the fluorescence of the background. The bright circular figures that appear in Figure 3.20 were agar bubbles due to air trapped when lukewarm agar was poured over the samples. From these attempts to visualise *D. alaskensis* under a fluorescence microscope it can be concluded that the protocol is not optimal and that the correct fluorescence filters need to be used to analyse the fluorophores used in this study. Since both fluorophores tested are novel, no filters were commercially available. Future fluorescence microscopy studies with such fluorophores should only be attempted when the correct filter or technology are available.

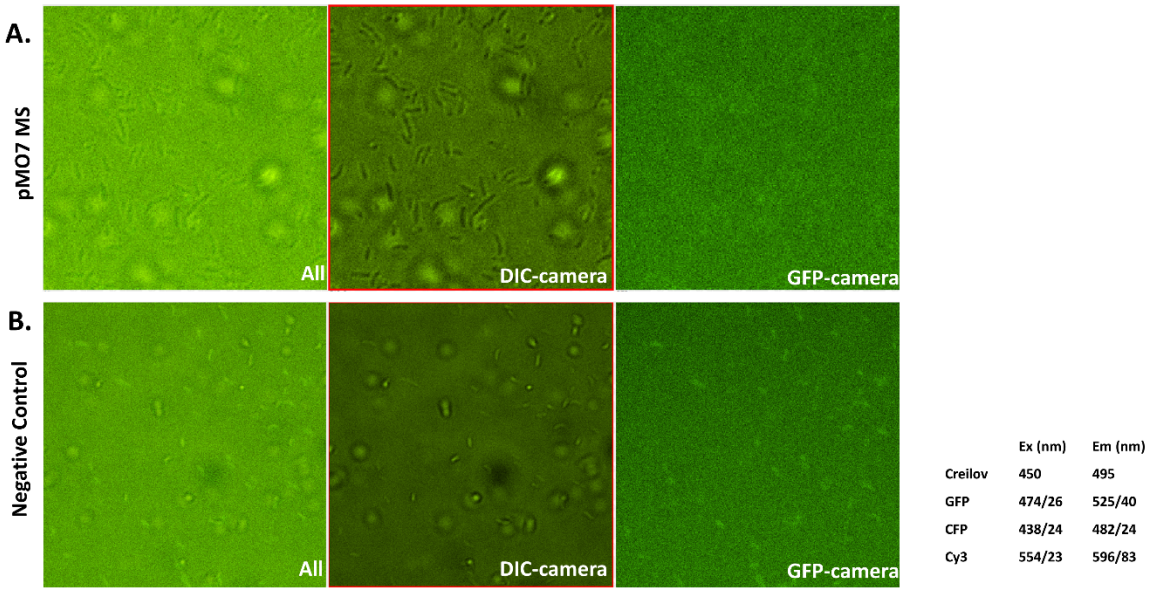

Figure 3.18. Fluorescence Microscopy of *D. alaskensis* expressing pMO7. A) Fluorescence microscopy of *D. alaskensis* (pMO7 MS), DIC-camera image, GFP-camera image and combined render of images. B) Fluorescence microscopy of *D. alaskensis* pMO9075 (negative control), DIC-camera image, GFP-camera image and combined render of images.

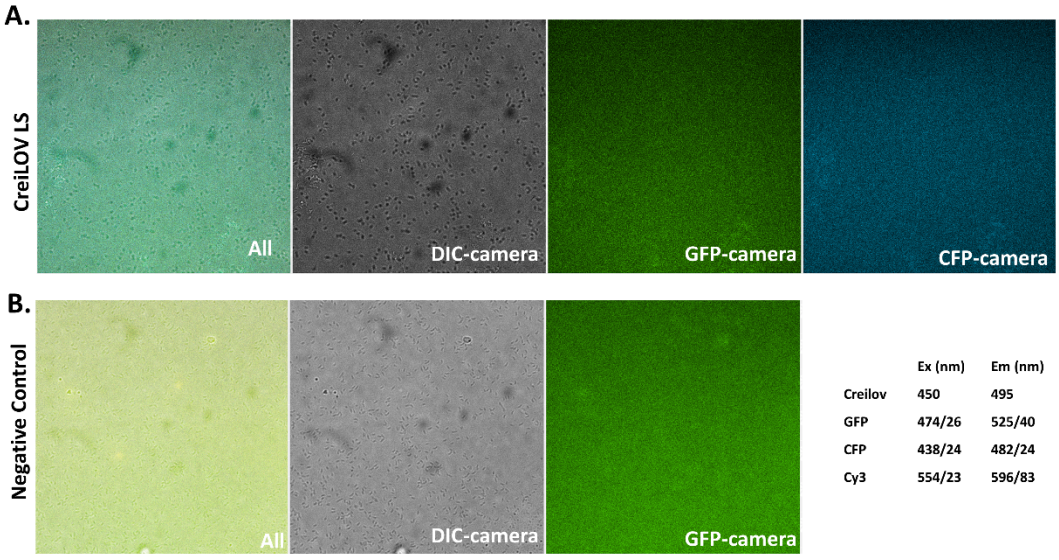

Figure 3.19. Fluorescence Microscopy of *D. alaskensis* expressing CreiLOV. A) Fluorescence microscopy of *D. alaskensis* (CreiLOV LS), DIC-camera image, GFP-camera image, CFP-camera image and combined render of images. B) Fluorescence microscopy of *D. alaskensis* pMO9075 (negative control), DIC-camera image, GFP-camera image and combined render of images.

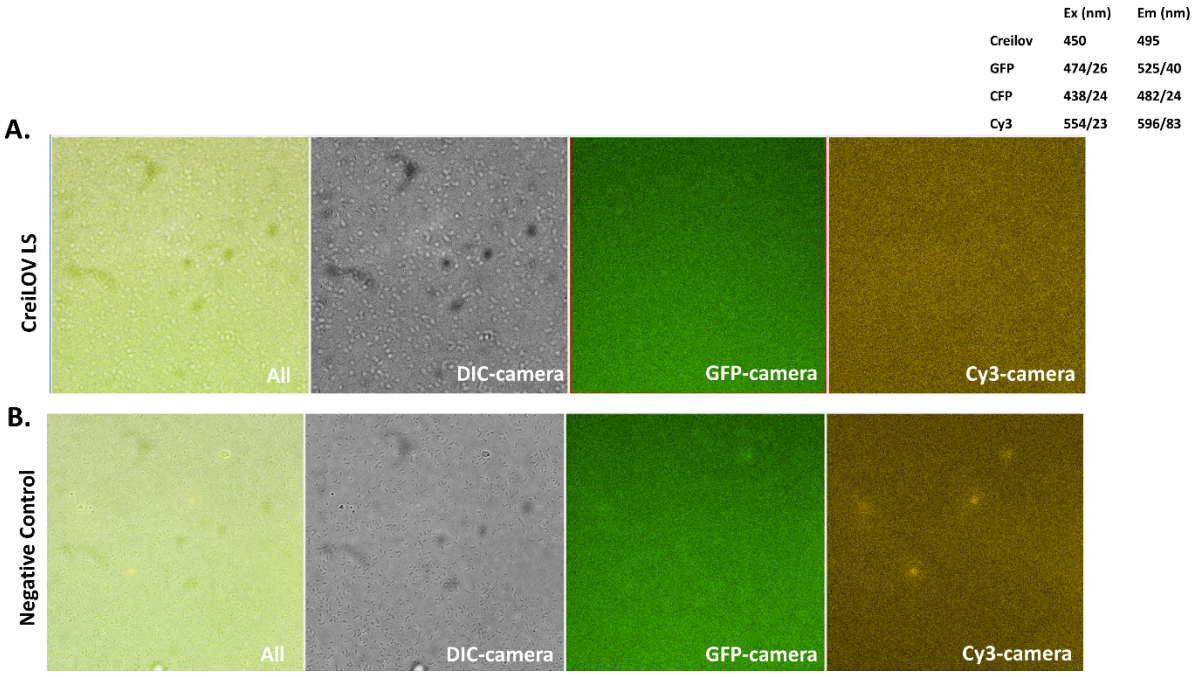

Figure 3.20. Fluorescence Microscopy of *D. alaskensis* expressing CreiLOV. A) Fluorescence microscopy of *D. alaskensis* (CreiLOV LS), DIC-camera image, GFP-camera image, Cy3-camera image and combined render of images. B) Fluorescence microscopy of *D. alaskensis* pMO9075 (negative control), DIC-camera image, GFP-camera image, Cy3-camera image and combined render of images.

3.11. Orthogonal expression of oxygen-independent reporters CreiLOV and pMO7

Using ΔpMoMoClo AF as an acceptor vector, two multi-gene expression TUs were assembled, CR LS pMO7 MS and CR Kan pMO7 MS, expressing CreiLOV and pMO7 orthogonally. Assembled TUs were transferred into electrocompetent *D. alaskensis* cells and into competent *E. coli* NEB 5-alpha cells. Tests with *D. alaskensis* were unsuccessful as no cells grew after the transformation, possibly because the chloramphenicol resistance gene was not expressed in *D. alaskensis,* which was needed for selection. Attempts to test CR Kan pMO7 MS in *E. coli* were unsuccessful as colonies did not grow in liquid media, unlike the previous TU, CR LS pMO7 MS fluorescence assay tests in *E. coli* using the aforementioned methods . This TU was screened for orthogonal fluorescence emission of both reporters, CreiLOV and pMO7. Values obtained for cultures incubated under anaerobic environments are shown in Figure 3.21, and under aerobic conditions in Figure 3.22. Similar to previously obtained results, high values were obtained for CreiLOV in both conditions (aerobic and anaerobic). Under both conditions, the values obtained for CreiLOV are statistically significant (one-way ANOVA, P value > 0.05) in comparison with the negative control (pMO9075). Values obtained for the expression of CreiLOV were higher than those obtained previously in Figure 3.11. What may have caused these results is that the plate reader is capturing both fluorophores's emission. PMO7 is a GFP mutant from *A. victoria* that forms a red chromophore and is active with an excitation and emission of 525 nm and 600 nm respectively, under anaerobic conditions. PMO7 was stable in the presence and absence of oxygen, thus it emitted fluorescence under both conditions. PMO7 also had a green spectra emission in the presence of oxygen [164], which may have caused the capture of uncharacteristically high values. Since CreiLOV has an excitation and emission spectra (Ex 450 nm, Em 495 nm) within GFP's spectra (Ex 485 nm, Em 535 nm), it may explain the values captured. When assays are not conducted in anaerobic conditions, gas exchange occurs and the presence of oxygen may activate both reporters (CreiLOV and PMO7) to conformations active in aerobic conditions. Previous research on GFP reddening has concluded that some GFP variants, similar PMO7 (GFP mutant from *A. victoria*) shift their fluorescence emission. These GFP

variants under hypoxic environments its GFP fluorescence shifts to a red fluorescence, but then it shifts back to green fluorescence after reoxygenation of the cells [167, 174].

Ultimately, the successful orthogonal expression of both reporters under aerobic and anaerobic environments was not achieved. These tests prove that the expression of more than one protein in *E. coli* can be achieved using this multi-gene acceptor vector (ΔpMoMoClo AF). Attempts to express both reporters in *D. alaskensis* were unsuccessful. The lack of growth of the cells inserted with TUs was indicative that multi-gene acceptor vector ΔpMoMoClo AF was not suitable to work in *D. alaskensis.*

To ascertain that PMO7 and CreiLOV are not orthogonal, a fluorescence assay with TUs expressing only CreiLOV and pMO7 (TUs that were assembled into CR LS pMO7 MS), the empty plasmid (pMO9075) and CR LS pMO7 MS were tested (Figure 3.23). In addition, an emission scan assay with a fixed excitation at 450 nm was conducted for all of the above (Figure 3.24). Both graphs (Figure 3.23 and Figure 3.25) conclude that CreiLOV and PMO7 expressed by CR LS pMO7 MS are not expressed orthogonally, because excitation and emission spectra between both reporters coincide and fluorescence is emitted on both accords. TU expressing solely CreiLOV has a fluorescence emission smaller that CR LS pMO7 MS, which correlates with fact that PMO7 is also expressed and therefore has a higher fluorescence. Also from Figure 3.23B, it can be concluded that reporter CreiLOV emits a fluorescence of similar intensity to that of pMO7 when excited at 525 nm. With such results in mind, an emission scan assay with a fixed excitation at 525 nm was conducted for all of the previously tested plasmids (Figure 3.25). These results show further conclusive results that PMO7 and CreiLOV are not orthogonal.

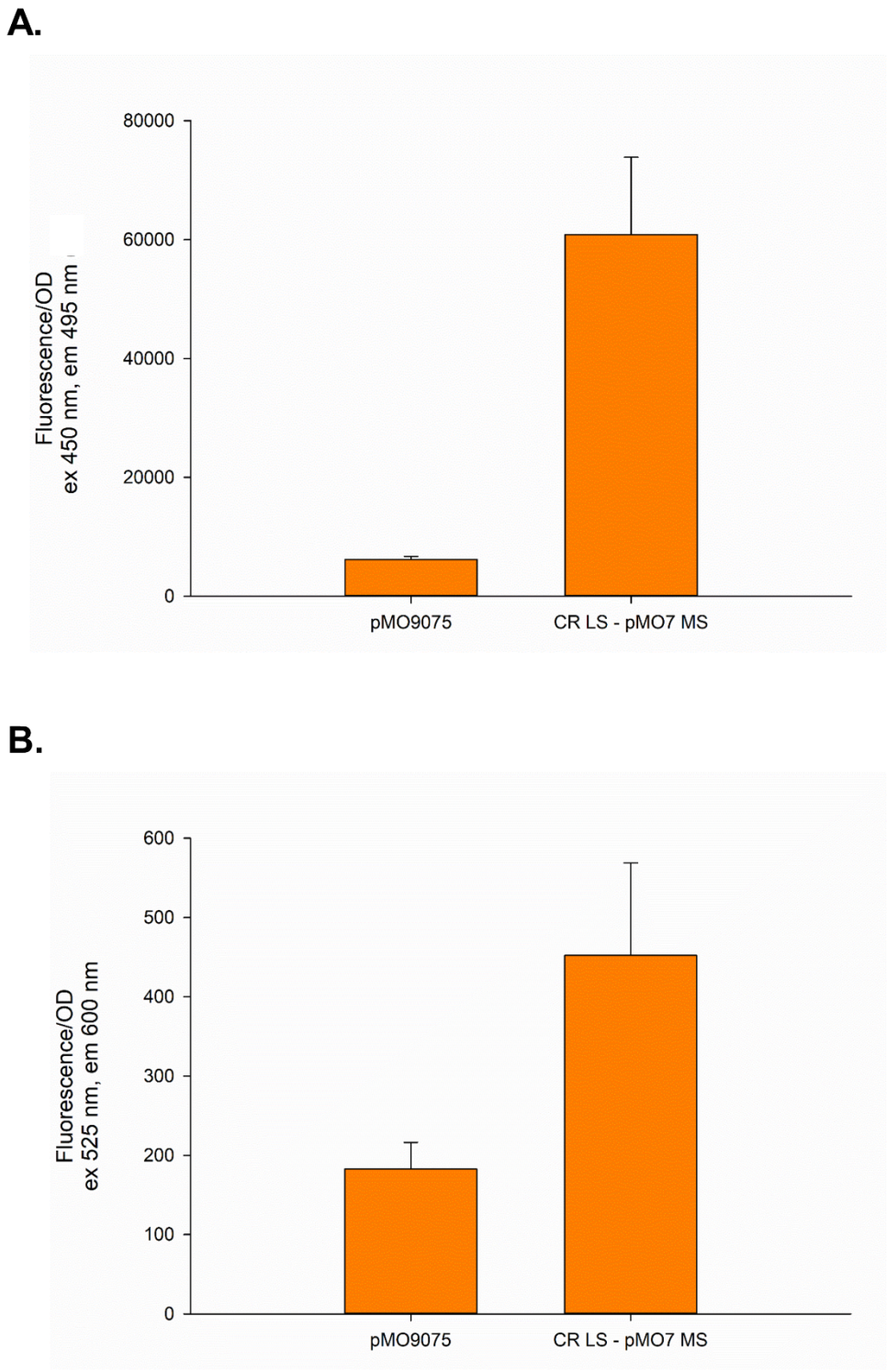

Figure 3.21. Fluorescence assay of *E. coli* expressing multi-gene expression TU under anaerobic conditions. A) Fluorescence assay of reporter CreiLOV. B) Fluorescence assay of reporter PMO7. Error bars depict the standard deviation of the mean.

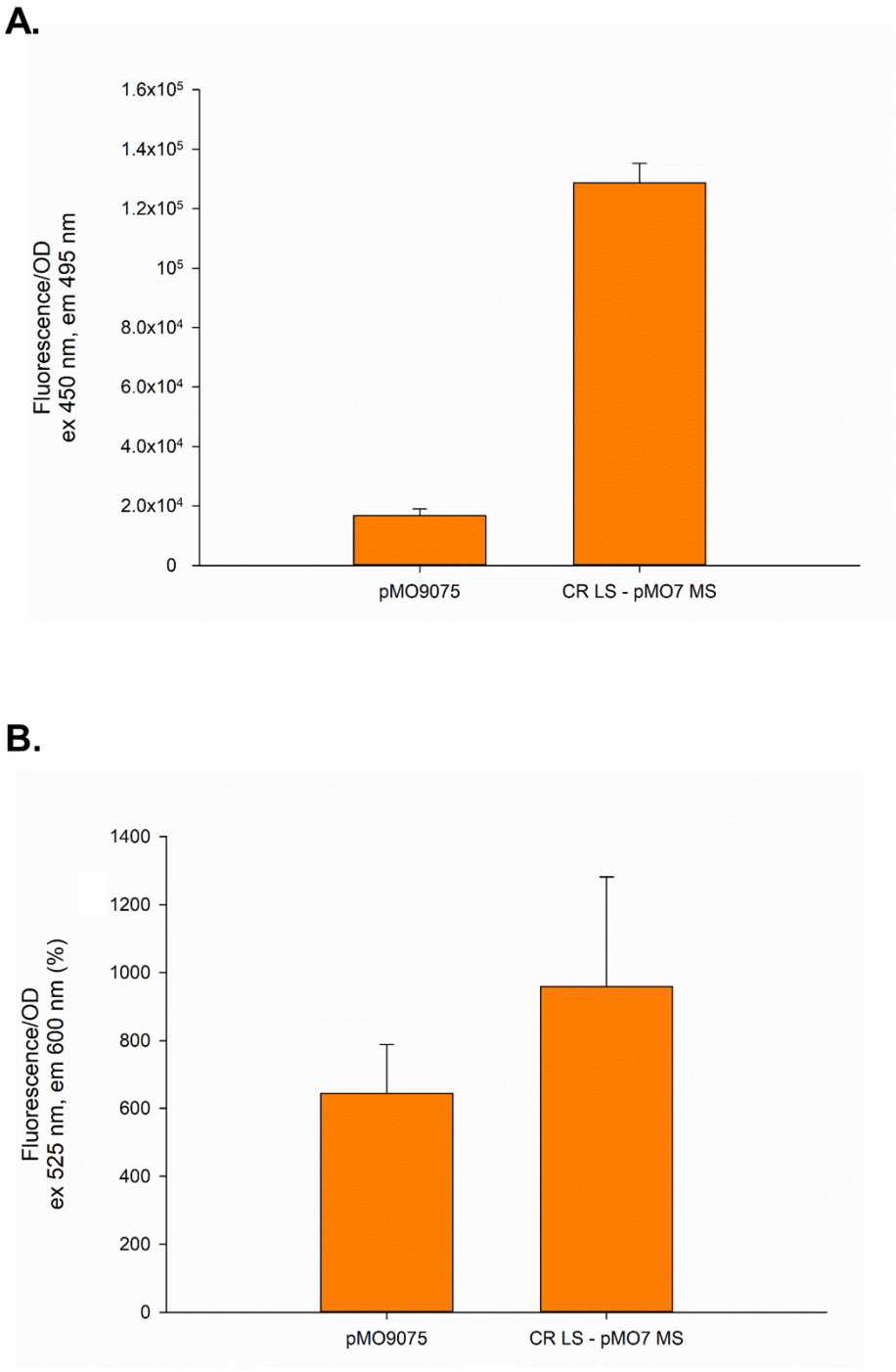

Figure 3.22. Fluorescence assay of *E. coli* expressing multi-gene expression TU under aerobic conditions. A) Fluorescence assay of CreiLOV reporter. B) Fluorescence assay of PMO7 reporter. Error bars depict the standard deviation of the mean.

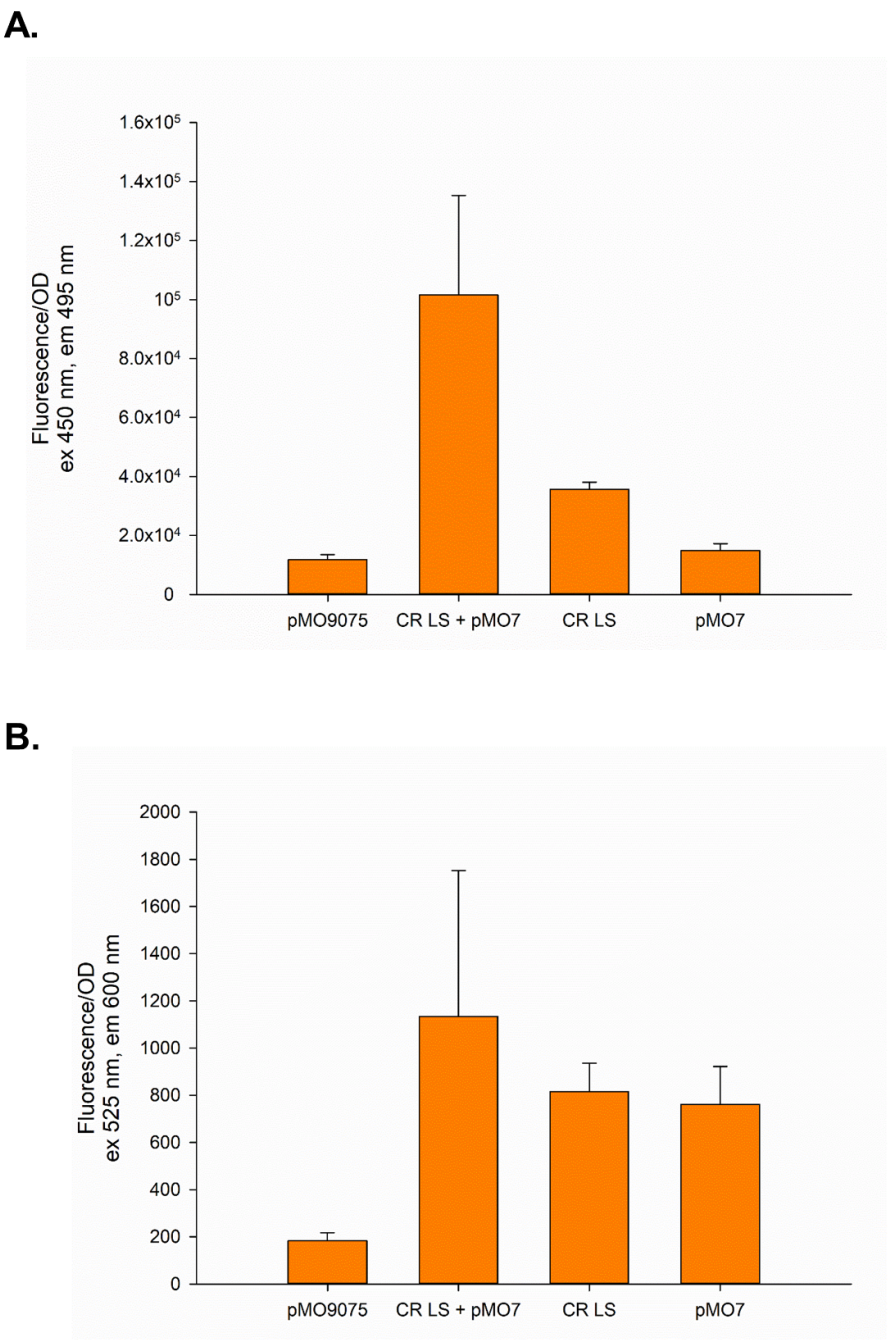

Figure 3.23. Fluorescence assay of *E. coli* expressing multi-gene expression TU under anaerobic conditions. A) Fluorescence assay at 450/495 corresponding to CreiLOV reporter and potential aerobic pMO7. B) Fluorescence assay at 525/600 corresponding to pMO7 reporter. Error bars depict the standard deviation of the mean.

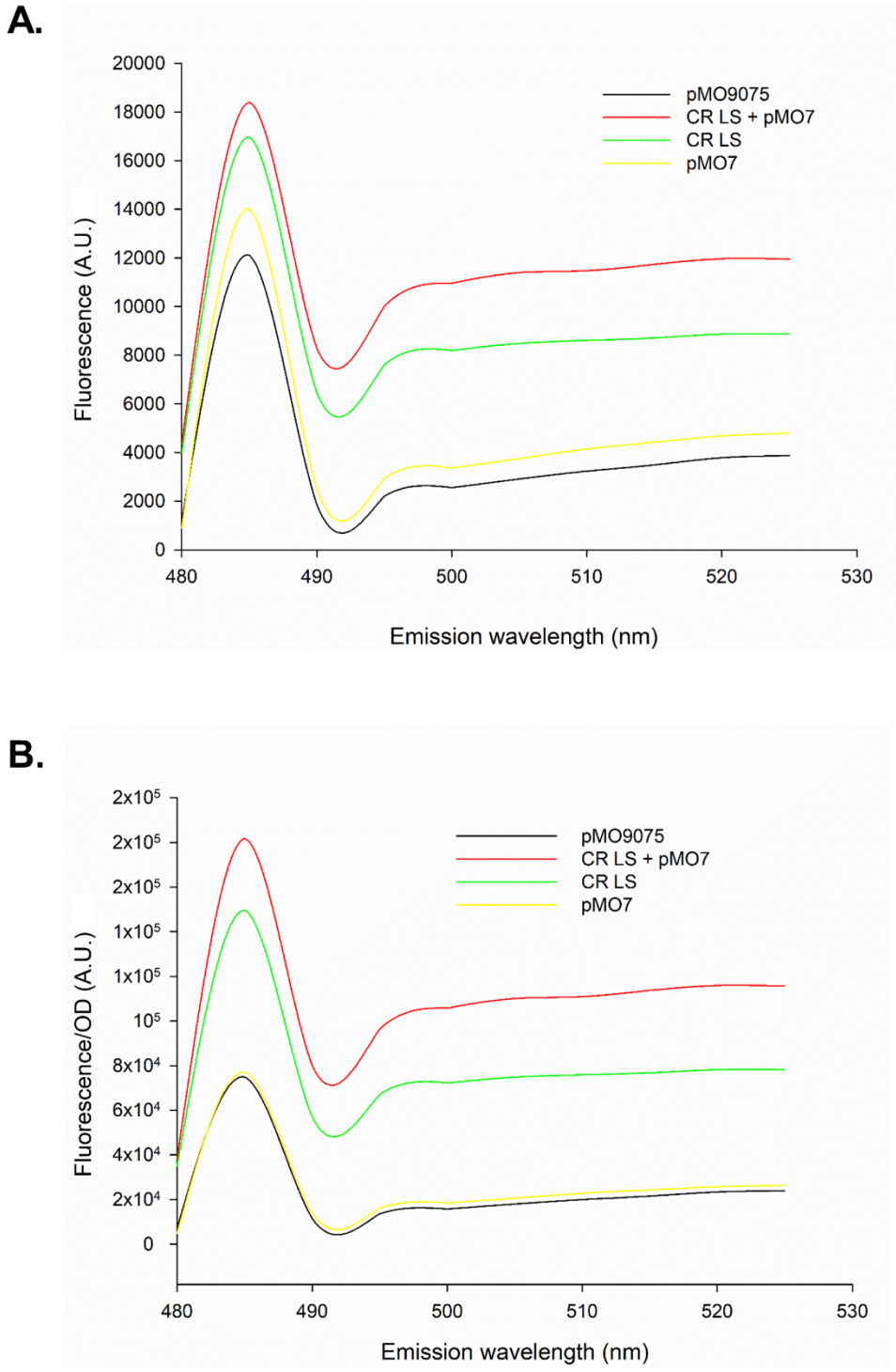

Figure 3.24. Fluorescence emission scan with fixed 450 nm excitation of *E. coli* expressing multi-gene expression TU under anaerobic conditions. A) CreiLOV emission scan fluorescence values. B) CreiLOV emission scan fluorescence/OD values.

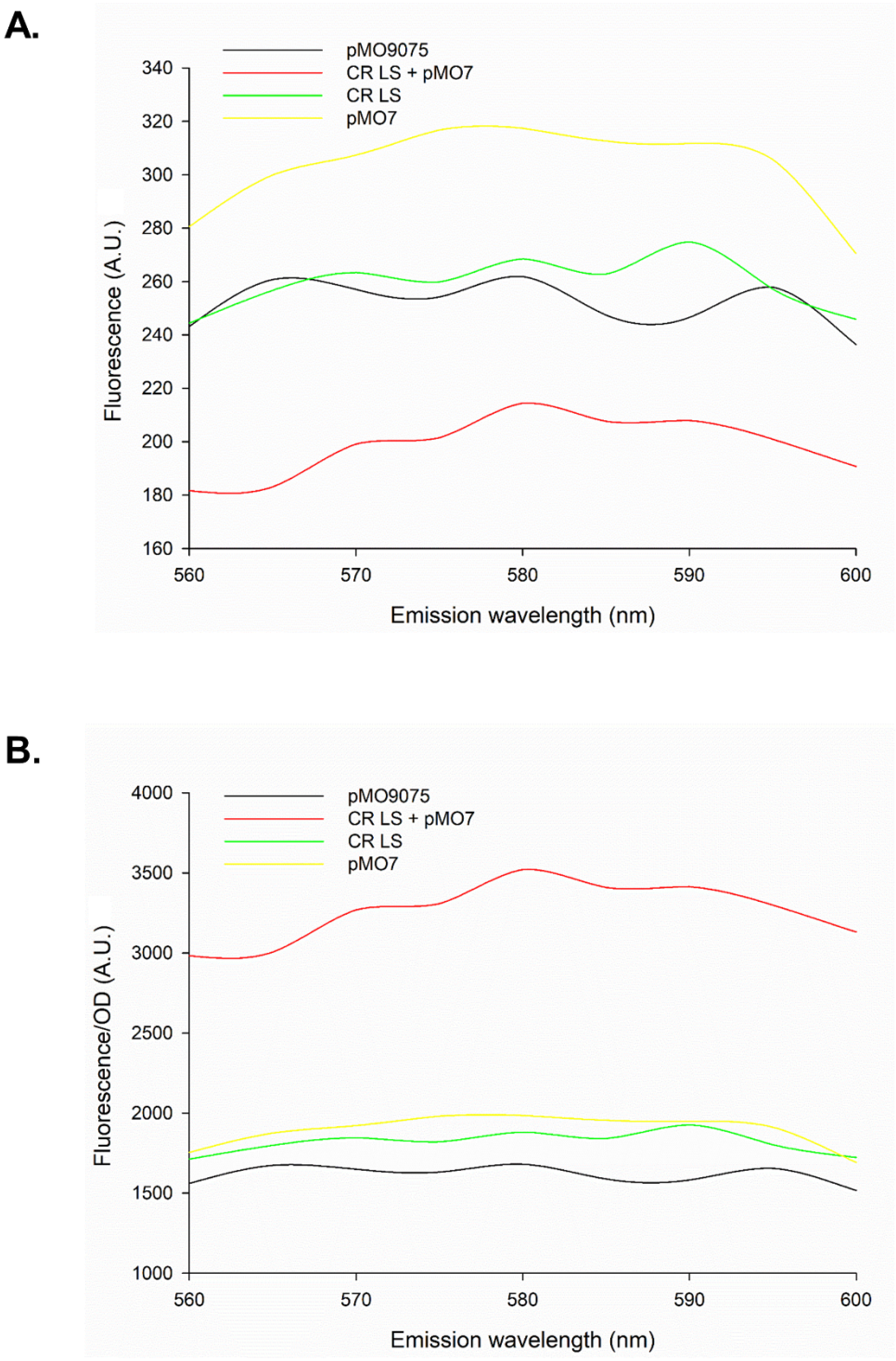

Figure 3.25. Fluorescence emission scan with fixed 525 nm excitation of *E. coli* expressing multi-gene expression TU under anaerobic conditions. A) PMO7 emission scan fluorescence values. B) PMO7 emission scan fluorescence/OD values.

3.12. Discussion

D. alaskensis is a non-model organism and no synthetic biology tools have been specifically engineered for it. As described in the introduction, *D. alaskensis* is also a microorganism with great potential in bioremediation and biocorrosion, but the further understanding and applications of this bacterium can only be realised with the development of such synthetic biology tools. Many synthetic biology tools are available for researchers using model organisms such as *E. coli* and by exploiting and adapting these to *D. alaskensis* we can more easily engineer it to our specifications.

Since most molecular biology manipulations are done in *E. coli*, due to the plasmid, pMO9075 having an *E. coli* origin of replication (pUC origin of replication), it was decided to adapt already existing *E. coli* synthetic biological tools to *D. alaskensis.* Synthetic biological tools e.g. Golden Gate tools such as MoClo are available for *E. coli*; CIDAR MoClo [66], EcoFLEX [73], Mobius Assembly [74] and newly created Start-Stop Assembly [75]. The CIDAR MoClo library bioparts were derived from the BioBricks™, Registry of Standards Biological Parts and were specifically selected to be functional and reliable in synthetic biology designs. For these reasons and the availability of only CIDAR MoClo and EcoFLEX toolkits at the time of conception, tools designed and engineered for *D. alaskensis* were made with the CIDAR MoClo specifications.

The MoClo acceptor plasmid, ΔpMOMoClo is the essential plasmid for the use of any MoClo biopart to assemble TUs correctly. This tool has enabled the easy to use, rapid design-build-test iteration cycles in *D. alaskensis.* With this tool, the rapid and cost-effective DNA assembly of synthetic bioparts could form the foundation of the design-build-test paradigm. Genes responsible for the synthesis of heavy metal nanoparticles in *D. alaskensis* and other relevant genes can be rapidly assembled and tested.

The final construct of ΔpMOMoClo was confirmed through insert-specific PCR, BsaI diagnostic digest, and further confirmation by sequencing. Ultimately, the feasibility and the proper use of ΔpMOMoClo as the acceptor vector in a MoClo assembly reaction with CIDAR MoClo bioparts was proven successful through a

blue/white screening test and further DNA sequencing. The multi-gene expression acceptor vector pMOMoClo_F was also successfully assembled in this study.

The lack of reporter proteins specifically designed and engineered for *D. alaskensis* has hindered the research and prevented the characterisation of expression control elements and bioparts. This study provides a well-characterised library of oxygen-independent fluorescent reporters. Previously researched reporters (CreiLOV, nanoLUC and phiLOV) were tested and only CreiLOV was found suitable for synthetic biology applications in *D. alaskensis*. From the results obtained, phiLOV was not an optimal reporter in comparison with CreiLOV, because CreiLOV showed a higher fluorescence emission. NanoLUC an enzymatic reaction that relies on a substrate to emit luminescence. For synthetic biology purposes, like those of characterising expression control elements, like promoters and RBS, the fluorescence quantification has a direct relation to the actual transcription and translation rate of heterologous proteins expressed. Whereas a luminescence quantification has an indirect relation, because it is reliant on an enzymatic reaction and the need of a substrate [127]. Both CreiLOV and phiLOV work under the same wavelength spectrum, since both fluorophores are from the same family of LOV based FbFPs [166], but CreiLOV has been reported to be the brightest of the FbFPs [130, 138, 166].

The versatility of fluorescent reporters is important. Properties that enable a fluorescent reporter to emit a fluorescent signal in aerobic environments and that is not affected by the lack of oxygen, makes this reporter a useful tool to study gene expression of obligate anaerobes [135]. Reporters were tested in *E. coli* under aerobic conditions; significant different results were obtained from those reported under anaerobic conditions. It is known that most fluorescent reporters such as GFP require oxygen and are inactive under anaerobic conditions [157, 158]. The reporters showed higher fluorescence emission values when expressed under aerobic conditions than anaerobic conditions. An oxidation step may be required for proper maturation of the chromophore as it helps with the overall correct folding of the structure of FbFPs and GFP-like chromophores, as well as to prevent the formation of inclusion bodies [175].

The characterisation of oxygen-independent fluorescent reporters has been achieved using various organisms. Under anaerobic conditions, phiLOV was characterised for

its use in *Clostridium difficile* [176], FbFPs from *P. putida* (PpFbFP) [137], *B. subtilis* (EcFbFP) [137], *C. reinhardtii* (CreiLOV) [166] and *Vaucheria frigida* (VafLOV) [166] have been characterised in *E. coli*. Our research, found numerous possible oxygen-independent reporters to characterise promoters, unlike another research where CreiLOV and phiLOV were not suitable for use in *Clostridium acetobutylicum* [79]. Not only did our study concluded that CreiLOV was characterised to be suitable for synthetic biology applications in *D. alaskensis*, it was proven that five different oxygen-independent reporters are adequate (CreiLOV, PMO7, PMO8, PMO5, and PMO12). Whereas in the aforementioned research, both CreiLOV and phiLOV were found unsuitable reporters for synthetic biological applications in *C. acetobutylicum*.

The use of well-characterised parts is an important aspect in synthetic biology. Synthetic biology relies on the assumption that the properties from such components in a certain context will be maintained the same in a different context [156]. The characterised *E. coli* promoters (J23100_AB, J23106_AB, and J23116_AB from CIDAR MoClo Parts Kit) and Kan promoter, their expression strengths in *D. alaskensis* do not match the expression strengths in *E. coli* [66]. Since promoters were designed specifically for each organism and are key for bacterial transcription, the values obtained indicate that indeed promoters designed for *E. coli* have a different strength order when expressed in *D. alaskensis*. The expression rate of heterologous proteins differs among organisms [177]. Transcription factors differ between *E. coli* (Gamma proteobacterium) and *D. alaskensis* (Delta proteobacterium). Due to their unique evolutionary pathways each class of proteobacteria developed transcription factors with different DNA recognition motifs [177], resulting in a different expression strength of heterologous proteins between organisms. This study has conclusive results that the order of strengths of the promoters change when expressing different CDS. When different CDS are expressed under the same promoter, their order of strength changes. Such results are due to the different metabolic load depending on the heterologous gene being expressed [172, 173].

The simultaneous expression of both CreiLOV and PMO7 in *E. coli* was achieved in this study, albeit their expression was not orthogonal, since they cannot be quantified independently. Values obtained for CreiLOV were different from those previously obtained, where values were considerably higher when PMO7 is also expressed.

These results could be associated with the PMO7 fluorescence emission within GFP-like spectra, like those of CreiLOV FbFPs wavelenghts. These results can be explained because the expression of more than one heterologous protein will cause a higher metabolic burden than when expressing just one. Moreover, the formation of inclusion bodies, and error prone protein folding of such proteins [169, 170], could explain the difference between the values obtained.

Although the use of novel cloning methods such as MoClo can help streamline and speed up the DNA assembly of bioparts and genes, it may affect the overall expression rate of heterologous proteins. The assembly of genes via MoClo is easy, fast and cost effective in comparison with traditional DNA assembly methods, but the use of fusion sites between each expression control element may affect protein expression. Since these fusion sites (tetramer sequences) are transcribed to mRNA and then translated into proteins, their position may affect the mRNA transcribed and therefore have an effect on the expression rate of heterologous proteins [75]. Ultimately, if you are looking for a DNA assembly method that is fast and reliable, and uses previously characterised expression control elements, MoClo is a very reliable DNA assembly method. For metabolic engineering, you require a predictable value or outcome. If using MoClo to test a metabolic pathway, it is imperative to characterise all the MoClo adapted expression control elements, to be able to predict an outcome, or to tailor a metabolic pathway to a desired outcome.

To conclude, the oxygen-independent reporters that are adequate for synthetic biology applications and for its use as quantitative reporters to characterise expression control elements are PMO7 and CreiLOV. Both oxygen-independent reporters were chosen to be adequate because, both are simple to quantify, and the excitation and emission wavelength generate a low background activity. Moreover, the fact that both emit fluorescence at different wavelengths, and are different genes, will provide comparative results when characterising expression control elements with each oxygen-independent reporter.

Chapter 4: Synthetic Libraries of Expression Control Elements for *D. alaskensis*

4.1. Introduction

A functional prokaryotic gene requires the following expression control elements: a promoter, an RBS, a protein coding sequence (CDS) and a terminator. For a gene to be functional, it requires each individual part to be assembled in order. In synthetic biology, each of these expression control elements can be studied in isolation and characterised individually under defined conditions. Allowing the rational modification of native pathways and the construction of synthetic and heterologous pathways, leading to genetic devices that give a predictable response [39].

A promoter can be defined as any DNA sequence that can independently facilitate the binding of transcription factors and enable transcription initiation [85]. The consensus *E. coli* σ^{70} core promoter structure consists of a -35-hexamer and a -10-hexamer motifs, and are separated by a spacer region with a consensus length of 17 bp [156]. This core promoter region is considered a minimal promoter [84-86], as these are the minimal elements necessary to enable transcription initiation [85]. The synthetic promoters tested in this study were designed with a rational minimal design or minimal promoter. Moreover, the use of an *E. coli* 17 bp consensus sequence as the spacer region for a rational minimal design was used because a promoter with this design would be considered a synthetic promoter, whereas using the actual spacer region found in between the predicted -35 hexamer and -10 hexamer motifs, would be considered a native promoter. The prediction of both motifs was made using the bioinformatics tool BProm [98], which predicts the conserved core promoter elements regulated by σ^{70} factors. Conserved sequences are predicted by BProm's algorithm that can discern between promoter and non-promoter sequences by using a collection of known *E. coli* promoter sequences [98]. The rational design of constitutive minimal promoters was conducted by using housekeeping genes' sequences to generate both motifs. Sequences were inputted into BProm to predict the core promoter motifs, and were separated by a consensus *E. coli* spacer region sequence (GGCATGCATAAGGCTCG) [156].

The RBS is an ubiquitous genetic part that is located upstream of a protein CDS, usually beginning at least 35 nucleotides before the start codon of a protein CDS [110]. The RBS is essential for the controlled expression of a heterologous protein as it regulates the translation initiation, which is a key rate-limiting step, because it controls how many ribosomes begin translation and how many of them finish it [110]. In synthetic biology, being able to predict the function of parts is an important part of the design process, so the use of bioinformatics tools such as RBS Calculator [110] are useful when designing a synthetic RBS sequence. The RBS Calculator can be provided with a protein sequence and will generate a synthetic RBS sequence that will yield a user-desired translation initiation rate (TIR). The RBS calculator combines a biophysical model with stochastic optimization, to create a quantitative relationship between the nucleotides (A, G, C and U) and a potential TIR for a given protein CDS [110]. It iterates all combination of sequences and predicts the best synthetic RBS sequence for the chosen TIR.

This chapter will focus on the design and engineering of synthetic RBS and promoter libraries, specifically tailored for *D. alaskensis*. The synthetic RBS and promoter libraries consists of five and eight different characterised expression control elements respectively. Both synthetic libraries were characterised in *D. alaskensis* using two different oxygen-independent reporters, PMO7 and CreiLOV.

4.2. Design of a synthetic RBS library using RBS calculator

The bioinformatics tool RBS Calculator [110] was used in this study to design synthetic RBSs to allow control of the initiation of protein expression in *D. alaskensis*. The CDS sequences of CreiLOV, PMO7, PMO8, PMO9, and PMO10 were entered into the programme with a maximized proportional scale (maximum translation initiation) and organism of choice (*Desulfovibrio alaskensis* G20). The synthetic RBS sequences generated for all protein CDS are shown in Table 4.1.

Table 4. 1. Synthetic RBS sequences used in this study.

Protein CDS	Predicted RBS Sequence provided by RBS Calculator
CreiLOV	TCAATTTTTAAAAAATCACAAGGAAGGAGGTATTAT
PMO7	ATCCACACAAGTCGAACAATATAAGGAAGGAGGTAAACG
PMO8	CTGGTTATCCGCGAGGAAATTAAAGGCATAGGTTTTTTT
PMO9	AACTGAGTTAGAGCTAAGAGGAACTATTTT
PMO10	TACTGCTCGACAATAAAAACTAATAACTGGAGGAGGTTT AAC

4.3. Adapting RBS library to MoClo

The synthetic RBS sequences generated by RBS Calculator were adapted to MoClo standards through the addition of the required restriction sites and adapter sequences (Table 4.2). The resulting sequences were synthesised as a single gBlock (RBS Library, Chapter 2, Table 2.5) and cloned into the donor vector DVA_BC through a single MoClo assembly reaction. See Figure 4.1 for an illustration of the gBlock bioparts library assembly protocol. This assembly method uses a blue/white screen to allow for the easy identification of colonies containing the desired insert, in this case those being white colonies. Plasmids from multiple colonies were sequenced, with results showing all of the desired RBSs were covered by the library, with several variants appearing multiple times. Multiple results can be achieved in a single MoClo reaction, given that the gBlock contains multiple parts, and all are complaint with MoClo standards (contain flanking BsaI recognition sites, and fusion sites B and C), a single reaction can result in the successful assembly of the entire library. This method is cost and time effective, because the synthetic library assembly can be completed in a single reaction, unlike traditional cloning methods which requires PCR amplification, restriction digest and ligations steps with DNA clean-ups performed after each step.

Table 4. 2. Library of RBS sequences generated by RBS calculator and adapted to MoClo. RED: Restriction Sites; UNDERLINED: Adapted Sequence; BLUE: Fusion Site B; GREEN: Fusion Site C.

MoClo adapted RBS	MoClo adapted RBS Sequence
PMO7 RBS	ACTAGGGGTCTCATACTATATCCACACAAGTCGAACAA TATAAGGAAGGAGGTAAACGATAATGAGAGACCATAT CC
CreiLOV RBS	ACTAGGGGTCTCATACTATTCAATTTTTAAAAAATCAC AAGGAAGGAGGTATTATATAATGAGAGACCATATCC
PMO10 RBS	ACTAGGGGTCTCATACTATTACTGCTCGACAATAAAAA CTAATAACTGGAGGAGGTTTAACATAATGAGAGACCAT ATCC
PMO8 RBS	ACTAGGGGTCTCATACTATCTGGTTATCCGCGAGGAAA TTAAAGGCATAGGTTTTTTTATAATGAGAGACCATATC C
PMO9 RBS	ACTAGGGGTCTCATACTATAACTGAGTTAGAGCTAAGA GGAACTATTTTATAATGAGAGACCATATCC

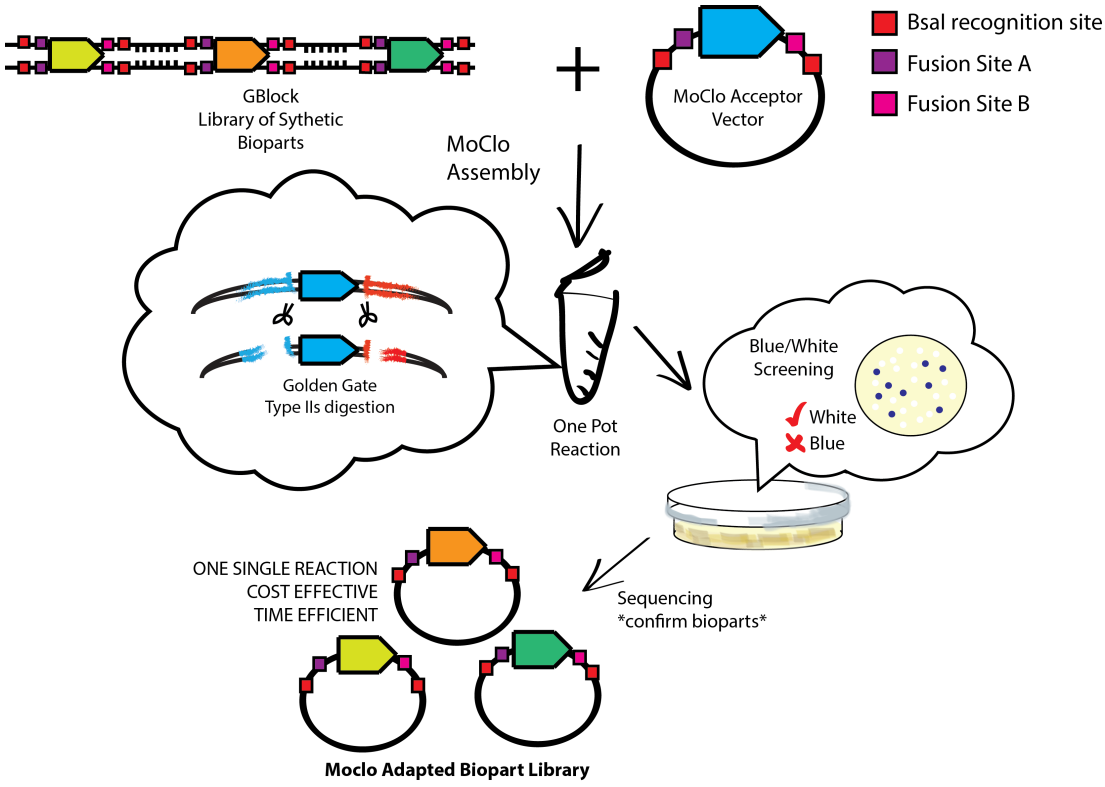

Figure 4. 1. gBlock bioparts' library assembly protocol. MoClo adapted bioparts are commercially synthesised as a gBlock (may use more than 1 gBlock to assemble library). The bioparts library is assembled in a single MoClo reaction using the gBlock and the corresponding donor vector. Resulting assembled plasmids are inserted into competent cells and incubated overnight on blue/white screening plates. White colonies are selected, cultured overnight, plasmid extracted and confirmed through sequencing.

4.4. Fluorescence assay of synthetic RBS library expressing PMO7 and CreiLOV

The synthetic RBS library containing all five RBSs was assembled into different TUs expressing either PMO7 or CreiLOV, each with the same promoter (J23106_AB) and terminator (B0015_DE) obtained from the CIDAR MoClo Parts kit. The promoter J23106_AB was chosen because it has the highest order of strength (Chapter 3). TUs assembled are listed on Table 4.3. Afterwards, all TUs were inserted into *D. alaskensis* competent cells and were screened for fluorescence at the appropriate wavelengths (PMO7 ex 525 nm, em 600 nm; CreiLOV ex 450 nm, em 495 nm) (Figure 4.2). Whilst all TUs had fluorescence values higher than that of the negative control (pMO9075) it was only statistically significant (one-way ANOVA, P value > 0.05) for one TU expressing PMO7 (RBS-CR) (Figure 4.2A) and for three expressing CreiLOV (RBS-8, RBS-9 and RBS-10) (Figure 4.2B). From the values obtained, it does indicate that the same RBS sequences with different protein CDS sequences affect the protein expression levels. This results correlate with research that concluded that the TIR can potentially decrease by approximately 500-fold when reusing the same RBS sequence with different protein CDSs [108]. Here, the expression strength order of the synthetic RBSs changed when expressing a different protein CDS; for PMO7 the order of strength was RBS-CR > RBS-10 > RBS-9 > RBS-7 > RBS-8, while for CreiLOV it was RBS-9 > RBS-10 > RBS-8 > RBS-7 > RBS-CR. The synthetic RBS sequences obtained with the RBS calculator are generated based on a specific protein CDS, meaning that it would be expected that RBS-7 and RBS-CR should give the highest expression when expressing PMO7 and CreiLOV respectively. However, both are towards the lower end of their strength orders, indicating that the RBS Calculator algorithm used to generate the RBS sequences must be used with caution as a simple change of organism to generate sequences using the RBS Calculator may skew the predicted results and not be as accurate as those predicted with *E. coli*. As the RBS Calculator was built using *E. coli* as the biophysical model, meaning it may not be accurate when using it for other organisms.

Table 4. 3. TUs assembled using synthetic RBS library

TUs	Promoter	RBS	CDS	Terminator
RBS-7	J23106_AB	7	PMO7	B0015_DE
RBS-8		8		
RBS-9		9		
RBS-10		10		
RBS-CR		CR		
RBS-7		7	CreiLOV	
RBS-8		8		
RBS-9		9		
RBS-10		10		
RBS-CR		CR		

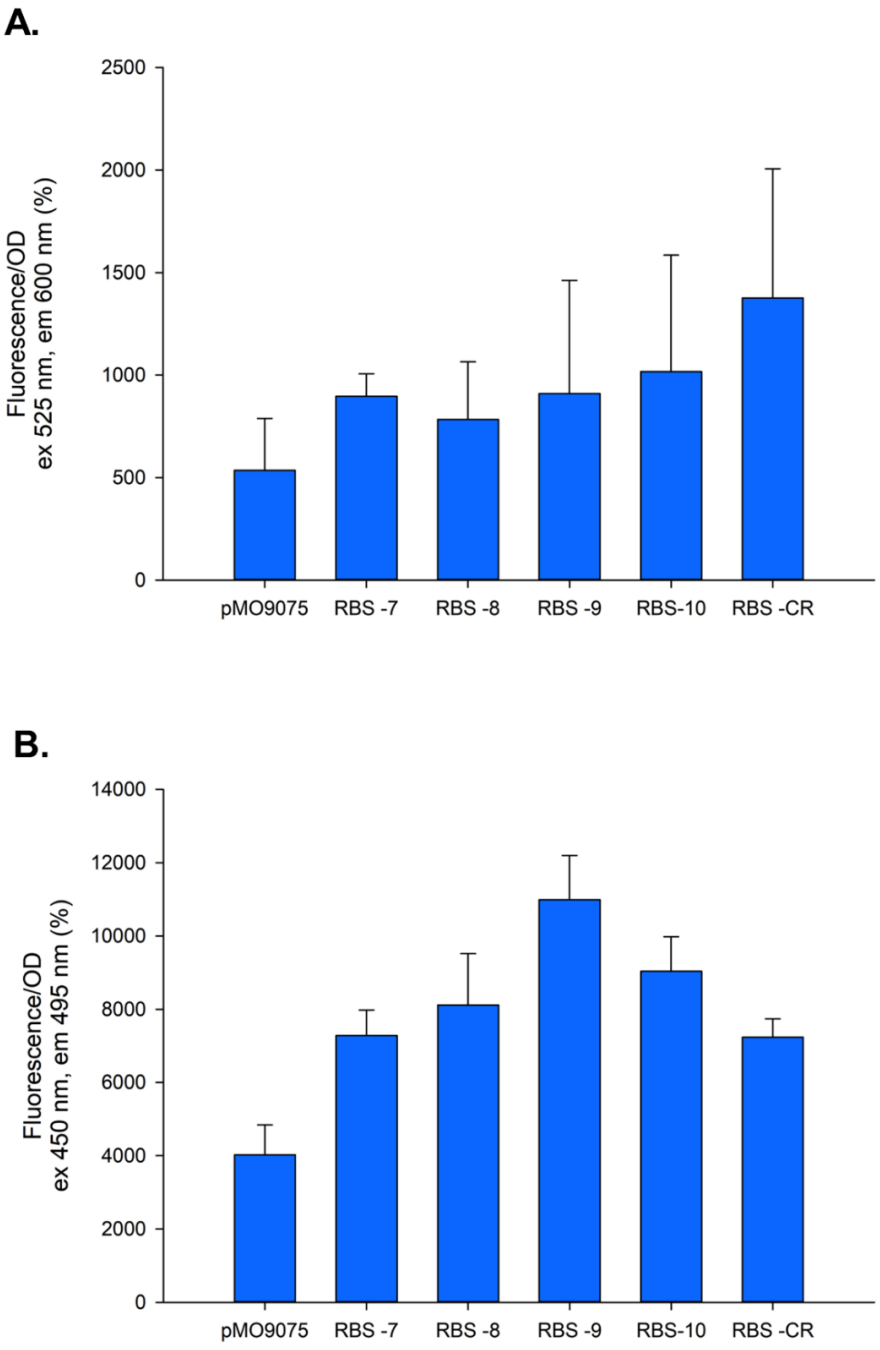

Figure 4. 2. Fluorescence Assay of synthetic RBS library expressing oxygen-independent reporters. A) Fluorescence assay of *D. alaskensis* expressing PMO7. B) Fluorescence assay of *D. alaskensis* expressing CreiLOV. Five different TUs expressing PMO7 and CreiLOV with the same promoter and different RBS (RBS- 7, RBS- 8, RBS- 9, RBS- 10 and RBS-CR) were tested in comparison to the negative control pMO9075. Experiments were performed in technical and biological triplicates. Error bars depict the standard deviation of the mean. Average absorbance values (OD_{600}) are enlisted on the Appendix Chapter, Table A-2.

4.5. Design of synthetic promoter library using Bprom

The bioinformatics tool Bprom [98] can predict significant features of bacterial promoter regions based on conserved promoter sequences. To design minimal promoters the -10 and -35 motifs were predicted, by inputting sequences of 7 different housekeeping genes up to 150 bp upstream of their CDS sequence (obtained from KEGG [178]). Housekeeping genes were used because they maintain a constant expression and are used to generate constitutive promoters [179]. The design of the synthetic promoters used in this study utilised the predicted -10 and -35 motifs separated by the *E. coli* consensus spacer region (GGCATGCATAAGGCTCG) [156]. The housekeeping genes, *dnaK*, *grpE*, *groEL*, *secE*, *secY*, *ntH* and *gyrA* were used in this study to predict the core promoter elements (Table 4.4). The sequences for the synthetic minimal promoters and native promoter (NPR-7) used in this study are listed on Table 4.5.

Table 4. 4. Predicted synthetic - 35 and -10 motif sequences used in this study.

PR#	Housekeeping Gene	Predicted -35 Sequence	Predicted -10 Sequence
1	*dnaK*	TTGCCC	TCTTAATTT
3	*grpE*	TTGACT	TACTACATT
4	*groEL*	TGGTCA	GGCTATCAT
7	*secE*	TTCACC	AGGTAGTCT
8	*secY*	TTCAAA	CGTTACGAA
9	*ntH*	TTCCTG	ATGTACAGT
10	*gyrA*	TTCAGA	GGTTACCAT

Table 4. 5. List of sequences of the synthetic minimal and native promoters design used in this study. RED: -35 Sequence; BLUE: -10 Sequence. **Note: the only native promoter design is NPR-7

PR#	Promoter Design
1	TTGCCC GGCATGCATAAGGCTCG TCTTAATTT
3	TTGACT GGCATGCATAAGGCTCG TACTACATT
4	TGGTCA GGCATGCATAAGGCTCG GGCTATCAT
7	TTCACC GGCATGCATAAGGCTCG AGGTAGTCT
8	TTCAAA GGCATGCATAAGGCTCG CGTTACGAA
9	TTCCTG GGCATGCATAAGGCTCG ATGTACAGT
10	TTCAGA GGCATGCATAAGGCTCG GGTTACCAT
NPR-7	TTCACC GCGAGACCAAGT AGGTAGTCT

4.6. Adapting the promoter library to MoClo

The designed synthetic promoter sequences were successfully adapted to MoClo standards and cloned into the MoClo donor vector DVA_AB by synthesising the MoClo adapted promoter sequences (Table 4.6) into gBlocks (MIN PROM LIBRARY, Chapter 2, Table 2.5), with the exception of PR-8 and PR-10 which were assembled by oligonucleotide annealment. See Figure 4.1 for an illustration of the gBlock bioparts library assembly protocol. In the first instance, an attempt was made to assemble by oligonucleotide annealment. However since only PR-8 and PR-10 were successful. A new method was devised using gBlocks with the library already adapted to MoClo. Most of the library was cloned into donor vector DVA_AB through a MoClo assembly reaction. In two reactions, the entire library was successfully adapted to MoClo. On the first attempt, not all synthetic promoters were successfully adapted to MoClo, as several colonies sequences' chromatograms aligned with the same synthetic promoter. A new gBlock was designed (PROM Library 2, Chapter 2, Table 2.5), omitting the promoter sequences that were successfully assembled on the first attempt. The assembly of the remaining synthetic promoters was achieved with this gBlock. Although full library coverage required two assembly reactions, it was still an easy, cost and time effective method to assemble these synthetic libraries in comparison with traditional cloning methods.

Table 4. 6. Designed synthetic promoter sequences adapted to MoClo. RED: Restriction Sites; UNDERLINED: Adapted Sequence; BLUE: Fusion Site A; GREEN: Fusion Site B.

PR#	MoClo adapted Promoter Sequence
1	ACTAGGGGTCTCAGGAGATTTGCCC GGCATGCATAAGGCTCG TCTTAATTTATTACTAGAGACCATATCC
3	ACTAGGGGTCTCAGGAGATTTGACT GGCATGCATAAGGCTCG TACTACATTATTACTAGAGACCATATCC
4	ACTAGGGGTCTCAGGAGATTGGTCA GGCATGCATAAGGCTCG GGCTATCATATTACTAGAGACCATATCC
7	ACTAGGGGTCTCAGGAGATTTCACC GGCATGCATAAGGCTCG AGGTAGTCTATTACTAGAGACCATATCC
8	ACTAGGGGTCTCAGGAGATTTCAAA GGCATGCATAAGGCTCG CGTTACGAAATTACTAGAGACCATATCC
9	ACTAGGGGTCTCAGGAGATTTCCTG GGCATGCATAAGGCTCG ATGTACAGTATTACTAGAGACCATATCC
10	ACTAGGGGTCTCAGGAGATTTCAGA GGCATGCATAAGGCTCG GGTTACCATATTACTAGAGACCATATCC
NPR-7	ACTAGGGGTCTCAGGAGATTTCACC GCGAGACCAAGT AGGTAGTCTATTACTAGAGACCATATCC

4.7. Fluorescence assay of the synthetic promoter library expressing PMO7 and CreiLOV

The synthetic promoter library was assembled into different TUs expressing either PMO7 or CreiLOV, each with the same RBS (B0034m_BC) and terminator (B0015_DE) obtained from CIDAR MoClo Parts kit. RBS B0034m_BC was chosen because throughout this research it was used to characterise promoters (Chapter 3). TUs assembled are listed on Table 4.7. All TUs were inserted into *D. alaskensis* competent cells and transformed cells were then screened for fluorescence at the appropriate wavelengths (PMO7 ex 525 nm, em 600 nm; CreiLOV ex 450 nm, em 495 nm) (Figure 4.3). For PMO7, all TUs with the exception of PR-8 and PR-10 emitted a higher fluorescence in comparison to negative control (pMO9075). PR-8 and PR-10 were not assembled to express CreiLOV for this reason. For TUs expressing PMO7 all TUs with the exception of PR-8 and PR-10 reported values that are statistically significant, whereas all of the values reported for TUs expressing CreiLOV are not statistically significant (Figure 4.3B). Although most TUs report a higher value in comparison to control, by comparing all values for PMO7 TUs (Figure 4.3A) and CreiLOV TUs (Figure 4.3B), values are not statistically significant among when comparing each TU. Indicating there is no clear strength order of the synthetic promoters. Focusing only on the values captured, for PMO7 the promoter strength order is as follows: PR-4 > PR-3 > PR-1 > PR-7 > NPR-7. For CreiLOV the promoter strength order is as follows: PR-9 > NPR-7 > PR-7 > PR-4 > PR-3 > PR-1. From the values obtained, it does indicate that the same promoter sequences with different protein CDS affect fluorescence emission. Previous research correlates this finding, where promoter strength differs between the heterologous proteins being expressed [172]. BProm predicts the conserved sequence motifs using an algorithm that discriminates between promoter sequences and non-promoter sequences, based on a set of known promoters from the *E. coli* genome [98, 180], and can be problematic when designing promoters for a different microorganism. The low levels of fluorescence observed across the library of promoters may be due to the BProm algorithm being based on *E. coli* promoters and its σ^{70} factors, meaning it may not be suitable for predicting promoters in *D. alaskensis*.

Figure 4. 7. TUs assembled using synthetic promoter library

TUs	Promoter (PR#)	RBS	CDS	Terminator
PR-1	1	B0034m_BC	PMO7	B0015_DE
PR-3	3			
PR-4	4			
PR-7	7			
NPR-7	NPR-7			
PR-8	8			
PR-9	9			
PR-10	10			
PR-1	1		CreiLOV	
PR-3	3			
PR-4	4			
PR-7	7			
NPR-7	NPR-7			
PR-9	9			

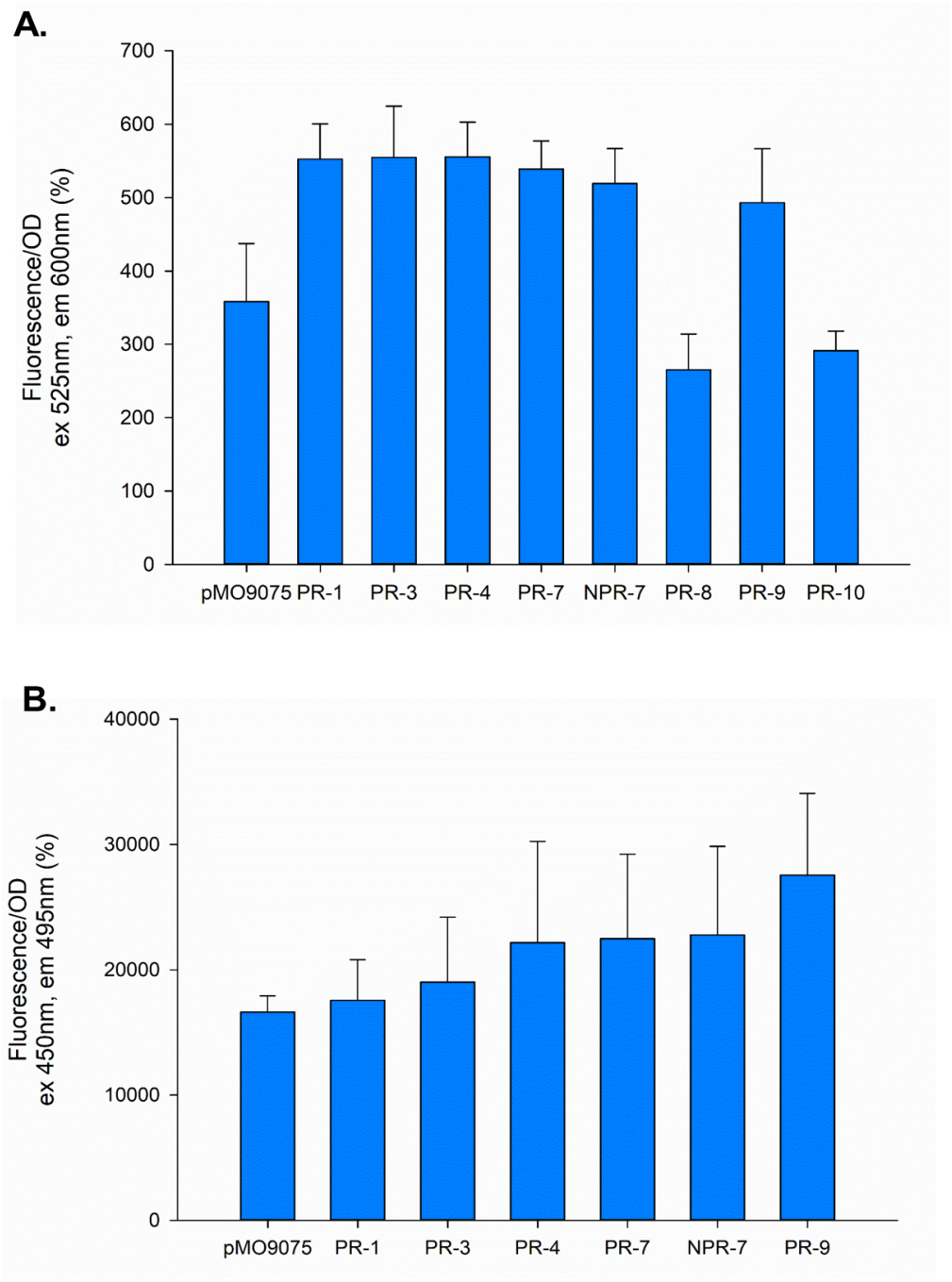

Figure 4. 3. Fluorescence Assay of synthetic promoter library expressing oxygen-independent reporters. A) Fluorescence assay of *D. alaskensis* expressing PMO7. B) Fluorescence assay of *D. alaskensis* expressing CreiLOV. Each TU used the same RBS. The negative control was pMO9075. Experiments were performed in technical and biological triplicate. Error bars depict the standard deviation of the mean. Average absorbance values (OD_{600}) are enlisted on the Appendix Chapter, Table A-2.

4.8. Discussion

Expression control elements such as promoters and RBS are important targets for engineering as they allow for the rational modification of native pathways and the construction of synthetic and heterologous pathways. They need to be fully characterised so that their effects on native metabolic pathways and the expression of heterologous pathways are predictable, and therefore can be fine-tuned. This is especially important when using a non-model organism such as *D. alaskensis.* Metabolic engineering has not extensively been tried on *D. alaskensis* and where previous work on protein expression has relied upon natural, already existing promoter and RBS sequences, this study achieved its aim to design, engineer and characterise synthetic expression control elements for *D. alaskensis*.

The synthetic RBS library was designed using the bioinformatics tool RBS Calculator, but the reliance on such a tool has its limitations; as it was designed for use with *E. coli*. Its predictions might not be accurate for all other organisms, but the algorithm was expected to have should have a close relationship with similar Gram-negative bacteria, such as *D. alaskensis.* However, not only was the tool designed specifically for *E. coli* and all the environmental and growth factors related to this organism. For example, the RBS calculator considered interactions at 37°C, whereas throughout this research *D. alaskensis* was grown at a temperature of 30°C. Such temperature changes, are likely to have a significant effect on the RNA folding and its TIR [115]. Previous research has ascertained that using the RBS Calculator and their predicted transcription initiation rates are not accurate in an wet lab experimental setting, where the *in silico* customised TIR values and experimental data are considerably different [116]. Herein, our data suggest that the RBS calculator was useful for designing RBS parts in *D. alaskensis;* however, the fine control of the RBS strength was not possible with this prediction program [181]. Characterised synthetic RBS libraries have been designed and tested in *E. coli* [108, 110], though not many synthetic RBS libraries have been designed using bioinformatics tools for other organisms, with the exception of the RBS library designed for *Synechococcus* sp. strain PCC 7002 [116]. Other RBS libraries have been designed without the use of bioinformatics tools, by locating a consensus RBS sequence of 15 bp upstream of the CDS of *Flavobacterium hibernum*, and characterised using a fluorescent reporter [182].

However, a synthetic RBS library specifically designed for an SRB or an anaerobic bacterium such as *D. alaskensis*, to our knowledge has never been reported.

The synthetic RBS library was characterised with two different protein CDSs, PMO7 and CreiLOV. The fluorescence assay results obtained show a clear difference strength in order between the protein CDS, which is in keeping with previous research stating that RBS sequences change its TIR depending on the protein CDS expressed [108]. A clear order of strength among all elements of the RBS library, provide a great opportunity for future fine-tuned expression of heterologous pathways in *D. alaskensis.*

The synthetic promoter library was designed using the bioinformatics tool BProm, which is a promoter sequence predictor that relies on predefined σ^{70} motifs from *E. coli.* BProm uses the homology of known promoters, specifically of those of *E. coli*, to predict potential promoter sequence motifs, that in occasions may not be accurate [106]. Again, there is no guarantee that the algorithm will have the same prediction performance with other organisms, such as *D. alaskensis,* and this tool is reported to to produce many false positives or show poor sensitivity when using long sequences of whole genomes [106, 183]. An alternative experimental method has been demonstrated, in the identification of *Helicobacter pylori* promoters by primer extension with sequence-specific FAM-labelled primers [184]. It is possible to confirm the actual transcription start point (promoter region) that the *in silico* analysis predicted. Published research ascertained *in silico* findings through primer extension analysis of RNA samples from *Francisella tularensis* [107]. This research also concluded that of all the transcription start points experimentally determined were located within a range of 1 to 5 nucleotides of the promoter region predicted *in silico* [107], which establishes the veracity of this approach. The *in silico* promoter region prediction has a small margin of error, but a margin error that is likely to be greater in a bacteria like *D. alaskensis.*

The synthetic promoter library tested in this study was generated using housekeeping genes. Differences in promoter consensus found upstream of some housekeeping genes in Gram-negative bacteria compared to those found in *E. coli* [179], suggest

differences in their respective sigma factors, that will affect the predicted promoter sequence and its overall performance.

The synthetic promoter library was also characterised with two different protein CDS, PMO7 and CreiLOV. Fluorescence assay results obtained do not have a clear strength order and no TU expressing CreiLOV had a statistically significant fluorescence emission in comparison with control. TUs with promoters PR-8 and PR-10 did not emit any fluorescence emission with PMO7. PR-1, PR-3, PR-4, PR-7, NPR-7 and PR-9 when expressing PMO7 all reported values that are statistically significant. The fact that all these promoters, were not statistically significant when expressing CreiLOV, indicates that the protein CDS significantly affects the promoter strength. Additionally, the use of bioinformatics tools for the promoter prediction may be problematic, because the specific interactions between proteins and DNA sequences are very complex [106]. All expression control elements involved are highly degenerate, so recognition of characteristic sequences within promoter elements is difficult [106]. However, a strength order among all elements of the library provide a great opportunity for the future metabolic engineering applications with *D. alaskensis*. Unlike our data, previous published work, obtained a defined order of synthetic promoters for *Clostridium acetobutylicum* [79], *Synechococcus* sp. strain PCC 7002 [116], *E. coli* [118, 156, 185-187], and *F. tularensis* [107]. However, a synthetic promoter library specifically designed for an SRB or an anaerobic bacterium such as *D. alaskesnsis*, to our knowledge has never been reported.

To conclude, the expression control elements specifically designed for *D. alaskensis* and those characterised on Chapter 3, which are adequate for metabolic engineering purposes, and further tested on Chapter 6 are as follow: promoters: J23106_AB, Kanamycin promoter and PR-3; RBS: B0032m_BC, RBS-CR and RBS-9. These expression control elements were chosen because they all reported high fluorescence over OD_{600} values.

Our results also conclude that using bioinformatics tools and algorithms that were designed using *E. coli* as a model organism, are not as accurate to predict expression control elements for *D. alaskensis*. However, the prediction of the expression control elements used in this study only relied only on one bioinformatics tool for each

(promoter and RBS). The predictions could've been different using other bioinformatics' algorithms. For future reference, it is advised to use multiple bioinformatics' algorithms to predict expression control elements. By entering the same sequence, predict the expression control elements using multiple algorithms, then enlist and compare them to generate a consensus sequence. This consensus sequence can then be adapted to MoClo standards and rapidly characterised.

Synthetic biology aspires to bring predictable outcomes to biology, and one of the tools for this is the engineering of expression control elements. Moreover, the genetic tools presented here, enable the rapid construction of a finely controlled genetic circuit within *D. alaskensis*. The tools have the potential to accelerate the field of synthetic biology within SRB and anaerobe microorganisms. While this study achieved the design and engineering of expression control elements, further research needs to be done to account for the lack of a clear strength order in the synthetic promoter library, this problem can potentially be solved by further characterising all expression control elements through RT-PCR

Chapter 5: Cell Surface Engineering of *D. alaskensis*

5.1. Introduction

Metals play an integral role in the life processes of microorganisms; for example some metals such as copper and nickel are essential micronutrients for various redox processes [4], and magnesium and zinc stabilise enzymes and DNA through electrostatic forces [4]. However, some metals are nonessential and are potentially toxic to microorganisms at certain concentrations. Consequently, microorganisms evolved the ability to discern and uptake the essential metals, and utilise it as one mechanism to resist higher concentrations of toxic metals. Mechanisms of metal resistance in microorganisms are as follows: the metal exclusion by permeability barrier, active transport of metals away from cell/organism, intracellular sequestration (protein binding), extracellular sequestration, enzymatic detoxification, reduction in metal sensitivity [4] and the ability to convert heavy metals into less toxic nanoparticle form [5].

Cell surface engineering can be used to harness applications such as the bioremediation and bioaccumulation of heavy metals. Bacteria can be used to display heterologous proteins on their outer membranes by fusing a trans-membrane protein as an anchoring motif to the desired protein to be displayed [143]. It is hypothesised that the use of this technique can enhance *D. alaskensis'* ability to thrive in environments with high concentrations of heavy metals by tethering metal-binding proteins to its outer membrane.

The use of cell surface engineering for displaying naturally occurring, cysteine-rich metal-binding peptides such as methallothioneins and phytochelatins tethered to the microorganisms' outer membrane has been performed in various bacteria [143-145], but it has never been reported for *D. alaskensis*. Recombinant *E. coli* strains co-expressing phytochelatin synthase, an enzyme responsible for synthesizing phytochelatins from glutathione, and methallothionenin was able to synthesize different metal NPs [6]. Synthetic chelatins such as EC20, are polypeptide chelators rich in metal binding amino acids, and have been used in cell surface engineering research, such as for the synthesis of metal NPs [11]. The synthetic phytochelatin EC20 has previously been used to enhance the bioaccumulation of heavy metals in

microorganisms [148]. More recently, recombinant *E. coli* strains expressing phytochelatin synthase, phytochelatins and metallothionein, were able to synthesize EuSe NPs, which exhibited high fluorescence, magnetic and anticancer properties [149]. These achievements in *E. coli* set a precedent for attempts to express synthetic chelatins such as EC20 in *D. alaskensis.* The expression of EC20 has been reported for other Gram-negative bacteria microorganisms such as *Moraxella sp* [145], *E. coli* [6, 188] *Pseudomonas putida* [150] and *Ralstonia eutropha* [151]. These findings are indicative of the possibility of achieving the expression of metal-binding proteins to the outer membrane of *D. alaskensis.*

EC20's metal-binding properties offer an increased affinity, metal-binding capacity and/or specificity and selectivity for a target metal ion [152]. A way to insert EC20 in the outer membrane is to add a signal peptide sequence to the EC20 gene, along with the sequence for the autotransporter β-domain of the *Neisseria gonorrhoeae* immunoglobulin A (IgA) protease precursor, which is a transmembrane domain [188].

Expression of EC20 in *D. alaskensis* has not been reported, but it was thought that it may enhance its metal resistance and even its NP synthesis capabilities. In this study the expression of EC20 in *E. coli* and *D. alaskensis* was tested to evaluate if such expression enhances their resistance to Pt, Pd and Cu. Pt and Pd were chosen because *D. alaskensis* has the innate ability survive in an environment highly enriched with Pt and Pd, and can also synthesize platinum group metal NPs [5]. Cu was chosen because EC20 has a high affinity for Cu [189], and to identify if *D. alaskensis* has the ability to synthesize Cu NPs with or without the expression of EC20.

5.2. Assembly of pMOEC20

The EC20/IgA fusion gene was inserted into the *D. alaskensis* plasmid (pMO9075) by Gibson assembly, and confirmed by diagnostic digest with BamHI and BglI conducted on DNA extracted from four different colonies. Such diagnostic digest reactions were conducted to confirm the successful insertion of EC20/IgA insert, which has an additional BamHI and BglI recognition site to those already present on the pMO9075 backbone (BamHI x1, BglI x2). The diagnostic digest was confirmed through electrophoresis (Figure 5.1). A successful digestion should have two bands

for BamHI digestion (band sizes: 366 bp and 5,979 bp) and three bands for the BglI digestion (Band sizes: 1,259 bp, 1,808 bp and 3,278 bp). Colony number 1 had the correct sized bands on both digestion reactions. To confirm the correct assembly, the plasmid from colony 1 was sent for sequencing. The sequencing results matched the desired EC20/IgA plasmid sequence.

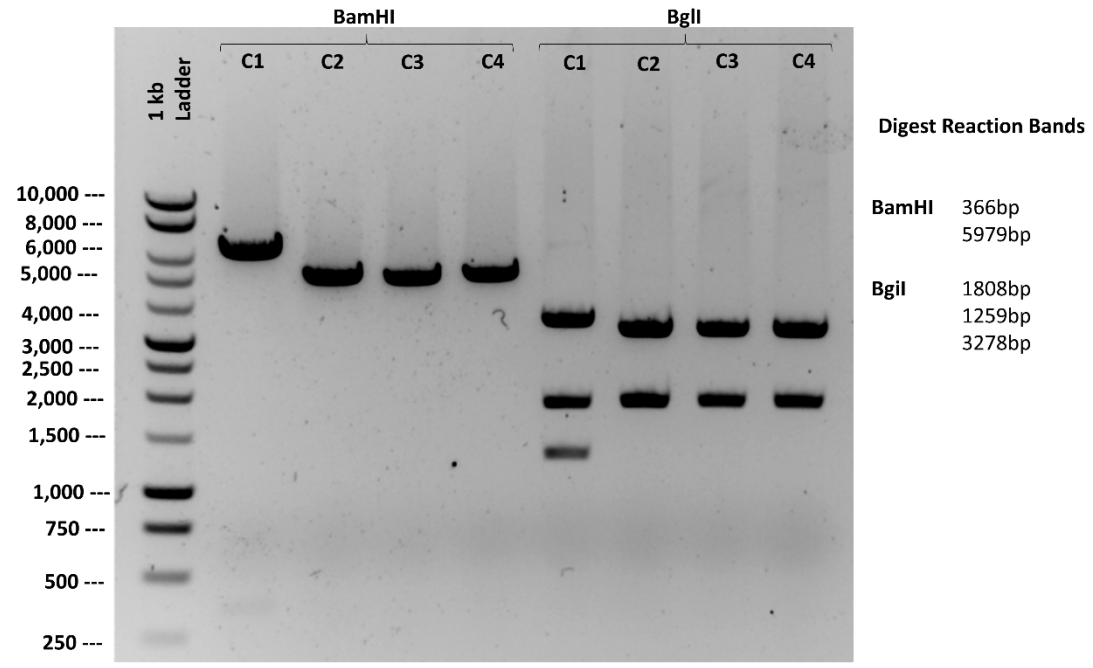

Figure 5. 1. Diagnostic Digest Reaction with BamHI and BglI: Agarose Gel Electrophoresis. Four colonies were tested (C1, C2, C3 and C4). **C1 has the correct size bands.**

5.3. Survivability test of *E. coli* expression EC20/IgA to Pt

To test if the heterologous expression of EC20 on the outer membrane of a microorganism will influence its tolerance to platinum concentrations, cultures of *E. coli* pMO9075 and pMOEC20 were grown in a 96-well plate in the presence of different concentrations of platinum. OD_{600} values were captured every hour to assess how platinum may affect the growth of the bacteria with and without the expression of EC20. Growth was compared for each strain at 0 mM, 0.5 mM, 1 mM and 2 mM Pt (Figure 5.2). Growth curves with no Pt have the characteristic sigmoidal shaped curve. When Pt is present, the sigmoidal shape of the curve is lost, as the growth rate during the exponential phase is reduced. No apparent growth at 2 mM Pt in *E. coli* pMO9075 was observed. At the higher Pt concentrations (1 and 2 mM) the overall OD_{600} values are higher for pMOEC20, than those of the control strain (pMO9075). Values for *E. coli* pMOEC20 with 1 and 2 mM are of approximately 0.05 and 0.04 respectively, unlike values observed for *E. coli* pMO9075 (0.025 and 0.023 respectively). At 1 mM 2 mM Pt *E. coli* pMOEC20 appears to grow under such conditions, but never reached a distinguishable exponential phase of growth. Contrary, at 0.5 mM Pt both *E. coli* with different plasmids behaved very similarly, two different exponential phases occurred (2-5 hours and 20 -25 hours), and between exponential phases the graph depicts a stationary phase (5-15 hours). At 0.5 mM Pt, *E. coli* pMO9075 appeared to reach a higher OD_{600} in comparison with pMOECC20. However, no statistical difference was found while comparing the OD_{600} values of pMO9075 and pMOEC20, which can be associated with the standard deviation values, suggesting results are error prone or variable.

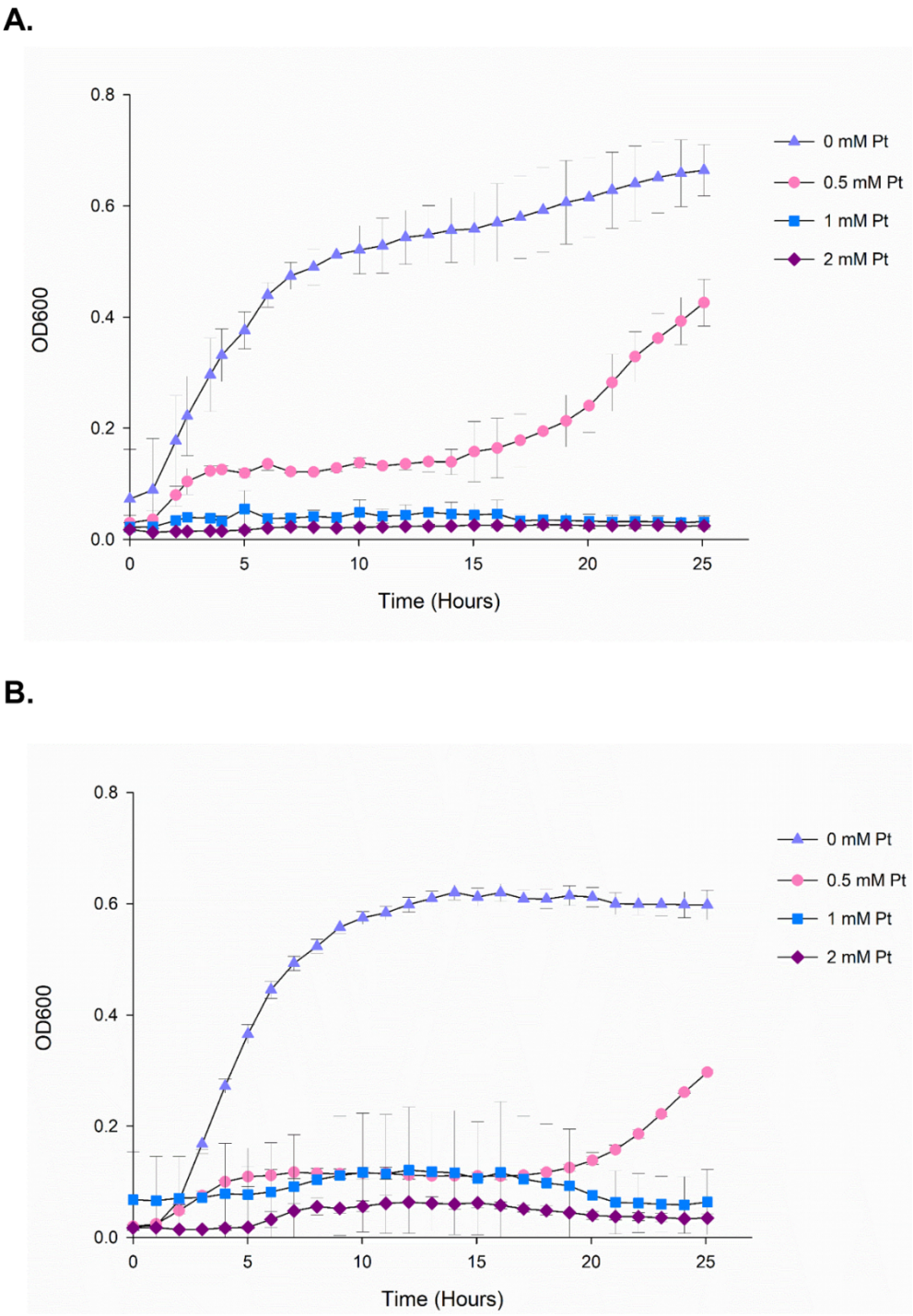

Figure 5. 2. Survivability test with different concentrations of Pt. A) Growth curves of control *E. coli* pMO9075. B) Growth curves of *E. coli* pMOEC20. LB was supplemented with 0 mM, 0.5 mM, 1 mM, and 2 mM Pt. Error bars depict the standard deviation of the mean.

5.4. Survivability test of *E. coli* expression EC20/IgA to Pd

Similarly to the previously discussed Pt tests, the growth of cells was also compared at different Pd concentrations. Growth curves of *E. coli* pMO9075 and *E. coli* pMOEC20 at different Pd concentration are depicted on the following figures: 0 mM, 0.5 mM, 1 mM and 2 mM Pd (Figure 5.3). The growth curves without Pd have the characteristic sigmoidal shape curve. At higher concentrations (1 and 2 mM), the sigmoidal shape of the curve is lost during the timeframe of the experiment, where the growth rate during the exponential phase is reduced compared to no Pd; no apparent growth at 2 mM Pd in *E. coli* pMOEC20. At higher Pd concentrations (1 and 2 mM) the overall OD_{600} values are higher for pMO9075, than those of the strain expressing EC20 (pMOEC20). At the stationary phase (25 hours), the values at those concentrations for pMOEC20 are of approximately 0.04 and 0.02 respectively. Whereas for pMO9075 OD_{600} values are 0.05 and 0.1 respectively. When in the presence of 1 mM or 2 mM Pd, *E. coli* pMO9075 grew. Conversely, at 0.5 mM Pd, both *E. coli* (pMO9075 and pMOEC20) behaved very similarly, but there is no apparent exponential phase. *E. coli* pMO9075 reached a higher OD_{600} in comparison with pMOECC20, and no statistical difference was found while comparing OD_{600} values of pMO9075 and pMOEC20, which can be associated with the standard deviation values, suggesting results are error prone or variable.

A.

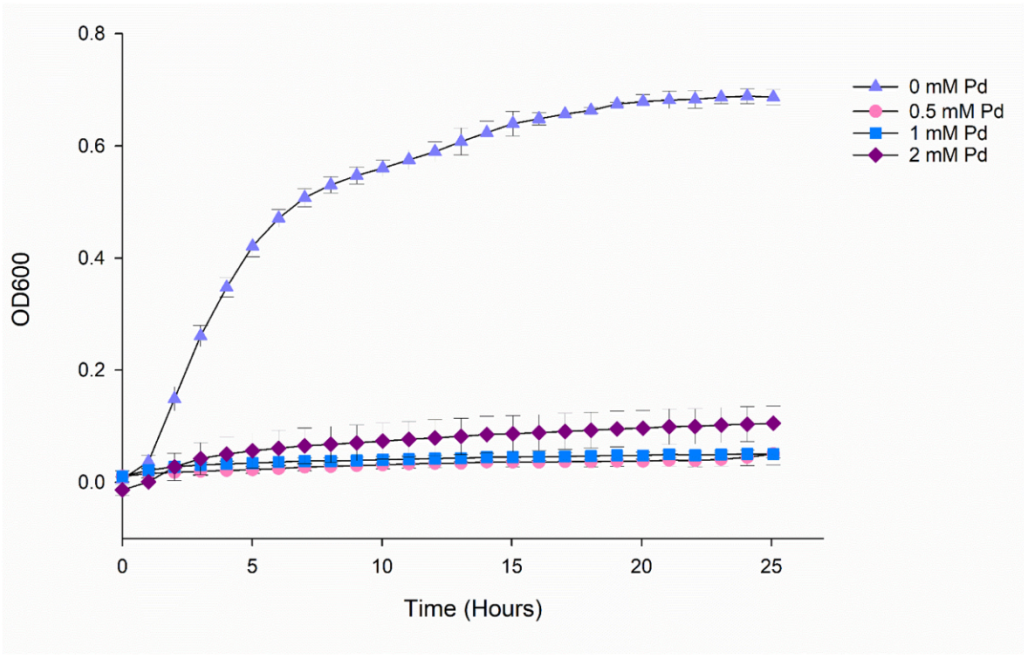

B.

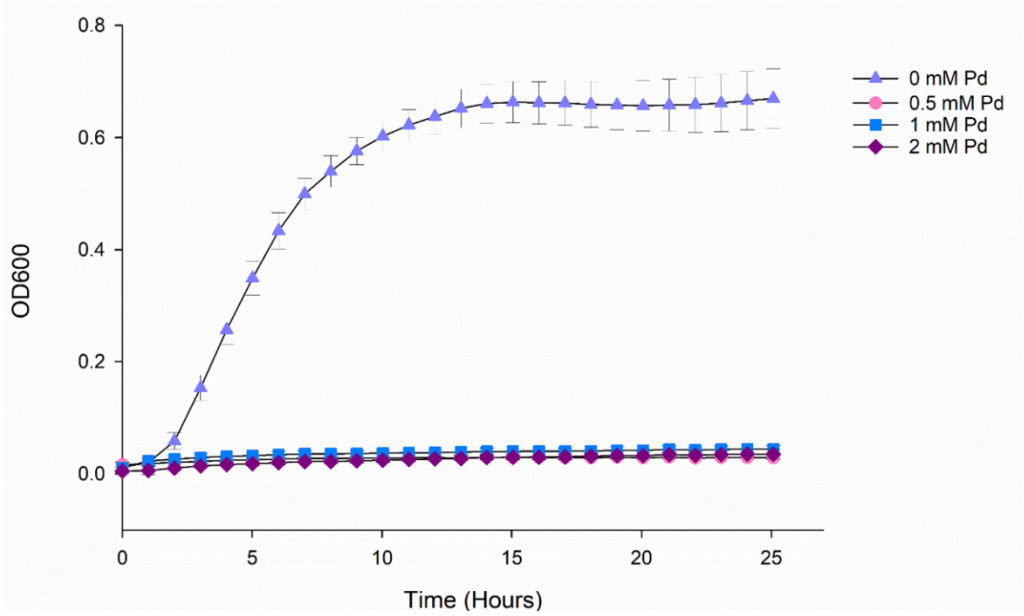

Figure 5. 3. Survivability test with different concentrations of Pd. A) Growth curves of control *E. coli* pMO9075. B) Growth curves of *E. coli* pMOEC20. LB was supplemented with 0 mM, 0.5 mM, 1 mM, and 2 mM Pd. Error bars depict the standard deviation of the mean.

5.5. Survivability test of *E. coli* expression EC20/IgA to Cu

Similarly to the previously described experiments conducted with Pt and Pd, the growth of cells was compared at different Cu concentrations. Overnight cultures of *E. coli* JM109 containing pMOEC20 were spotted onto agar plates, which had varying concentrations of copper added. These plates were then incubated overnight. Figure 5.10 compares the growth of *E. coli* pMO9075 and *E. coli* pMOEC20. *E. coli* pMO9075 grew relatively well in the presence of copper, but ceased to grow at 4.7 mM. This strain also displayed a reduced colony density at 4 mM. The relative resistance to copper of such strain could be associated with the fact that *E. coli* has some tolerance to copper [190, 191]. Since pMOEC20 has bacterial growth up to 5 mM, the results show that the heterologous expression of EC20 conferred a higher bacterial resistance to copper. However, pMOEC20 growth on the 5 mM plate showed a reduced or stunted growth in diluted samples, most likely due to the reduced cell density in diluted samples. Cell density may affect the culture's resistance to higher concentrations of copper, something that has been observed with resistance to antibiotics, where studies have reported a higher resistance to antibiotics at higher cell density [192, 193]. This can be explained by an accumulation of cells on the border of the colony, at higher cell densities, that hinder the entrance of harmful compounds and thus present a defence mechanism.

E. coli variants containing pMO9075 and pMOEC20 were also cultured in liquid media in the presence of different concentrations of copper and their OD_{600} measured for 23 hours to assess the metals impact on growth. (Figure 5.11). The resultant curves with low concentrations of copper (0 mM, 0.5 mM, 1 mM, 2 mM and 3 mM) have the characteristic sigmoidal shape. At higher concentrations (4 mM and 5 mM), the sigmoidal shape of the curve is lost, meaning the growth rate during the exponential phases is reduced in comparison with other copper concentration tested, and no growth of *E. coli* pMO9075 was observed at 5 mM copper. At the higher copper concentrations (3, 4 and 5 mM) the overall cell density was higher for pMOEC20 than it was for the control strain (pMO9075) showing that *E. coli* containing pMOEC20 has a higher tolerance to copper in comparison to *E. coli* pMO9075.

Analyses were performed to determine the statistical significance between the strains. To evaluate whether the expression of EC20 had impact on the growth of bacteria in the presence of varying concentrations of copper, growth rates of the log phase (from 2 hours to 6 hours) were calculated (Table 5.1). The growth rate of the control *E. coli* pMO9075 was not affected at 0.5 mM and 1 mM copper. At the concentration of 2 mM copper *E. coli* pMO9075 growth rate is affected, conversely the growth rate of *E. coli* pMOEC20 is affected at 3 mM copper. When comparing growth rates between the two strains, it was apparent that pMOEC20 grew faster. Therefore, the results indicate that the heterologous expression of EC20 on the outer membrane confer to bacteria, specifically *E. coli*, a survivability advantage over the control (pMO9075), allowing it to grow in media containing up to 4 mM copper.

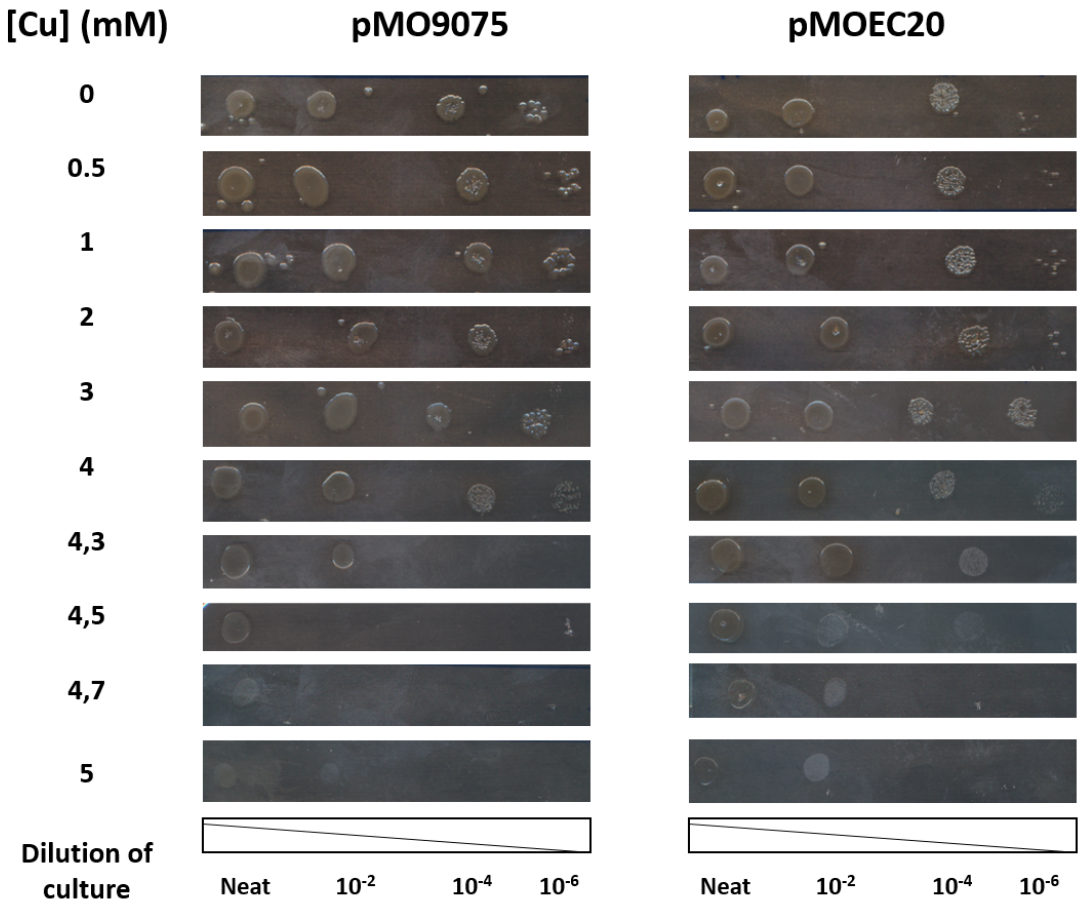

Figure 5.4. Copper survivability test in *E. coli.* Comparison of *E. coli* pMO9075 and pMOEC20. Cultures were spotted at different cell dilutions on agar plates supplemented with varying concentrations of Cu and incubated for 20 hours, at 37°C.

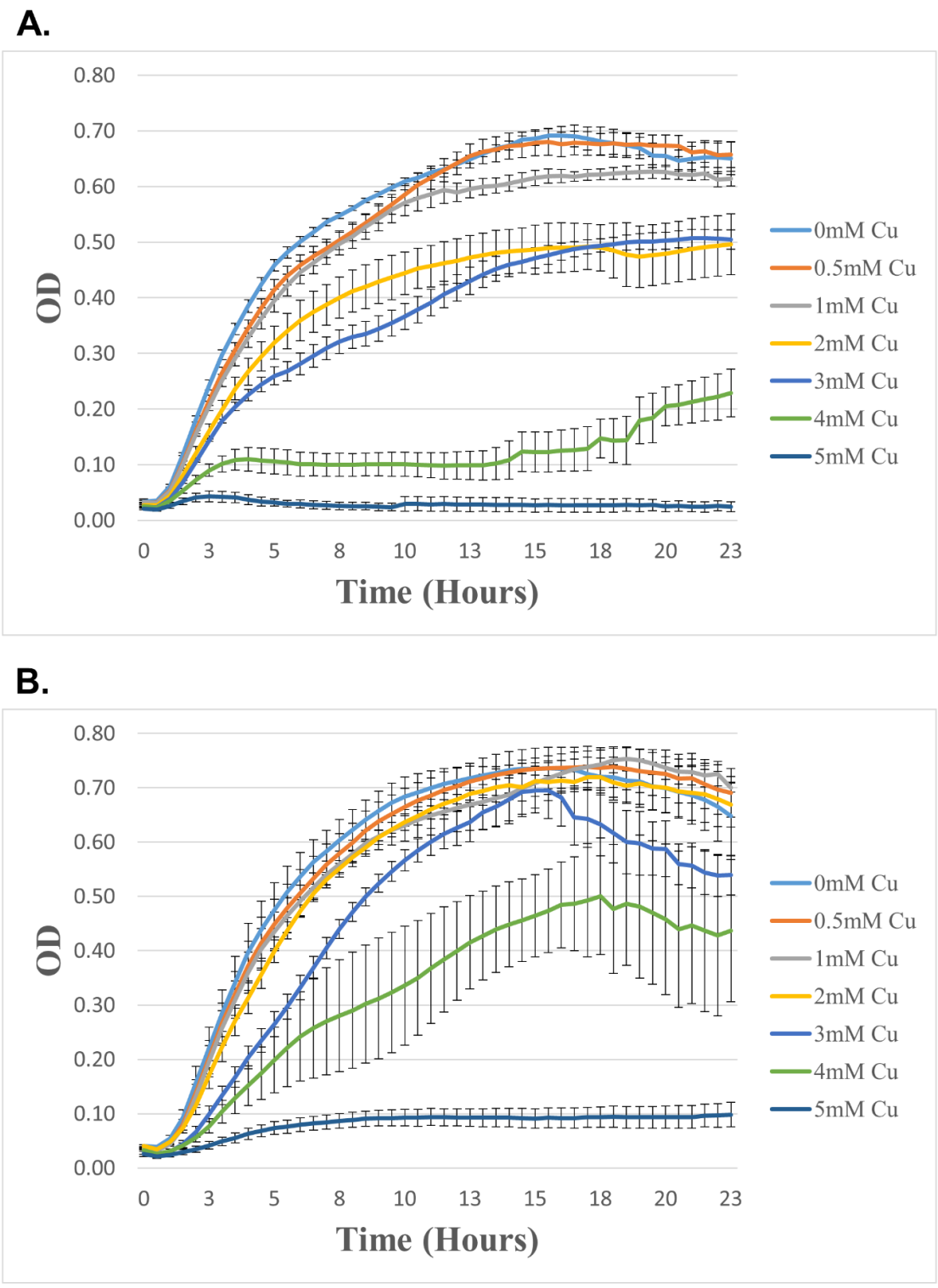

Figure 5.5. Survivability test with different concentrations of Cu. A) Growth curves of control *E. coli* pMO9075. B) Growth curves of *E. coli* pMOEC20. LB was supplemented with 0 mM, 0.5 mM, 1 mM, 2 mM, 3 mM, 4 mM and 5 mM. Cu**.** Error bars depict the standard deviation of the mean.

Table 5. 1. Growth rates of pMOEC20 and pMO9075 during the exponential growth phase at different concentrations of copper. Time points used to calculate growth rate: 3 hours and 15 hours.

	Specific Growth Rate (OD_{600}/min)			Max OD_{600}	
[Cu] (mM)	**pMOEC20**	**pMO9075**	**%Rate increase**	**pMOEC20**	**pMO9075**
0	0.001575	0.001327	19	0.691	0.691
0.5	0.001524	0.001233	24	0.735	0.678
1	0.00149	0.001204	24	0.753	0.626
2	0.001481	0.000988	50	0.719	0.504
3	0.001103	0.000727	52	0.695	0.506
4	0.000773	0.000116	566	0.500	0.228
5	0.000188	-4.8×10^{-5}	292	0.098	0.024

5.6. Transmission electron microscopy of *D. alaskensis* G20

D. alaskensis has the ability to synthesize nickel and platinum group metal NPs [5] and also has the ability to precipitate gold [194]. It was hypothesised that *D. alaskensis* could able to synthesize Cu NPs, so TEM images of *D. alaskensis* G20 in 1 mM Cu were taken (Figure 5.6). As phytochelatins bind strongly to Cu ions, and have a greater affinity for Cu than other heavy metals [189], we also analysed *D. alaskensis* pMOEC20. NPs were observed on the distilled water and copper control (Figure 5.12A). Images taken with the TEM gave inconclusive results, where *D. alaskensis* does not to produce Cu NPs, and the expression of EC20 does not enhance their production. The lack of Cu NP is likely to be because EC20 has a high affinity to copper ions, thus preventing them to enter the cell to be reduced into NPs. Another reason could be that *D. alaskensis* does not have a copper reduction mechanism. The morphology of *D. alaskensis* pMOEC20 cells in image 5.6D in the absence of copper were more irregular in comparison with cells grown in the presence of Cu (Figure 5.12E). This is most likely due to the overexpression of EC20. Since EC20 is tethered to the outer membrane, its overexpression and transportation onto the outer membrane may cause cell morphology changes.

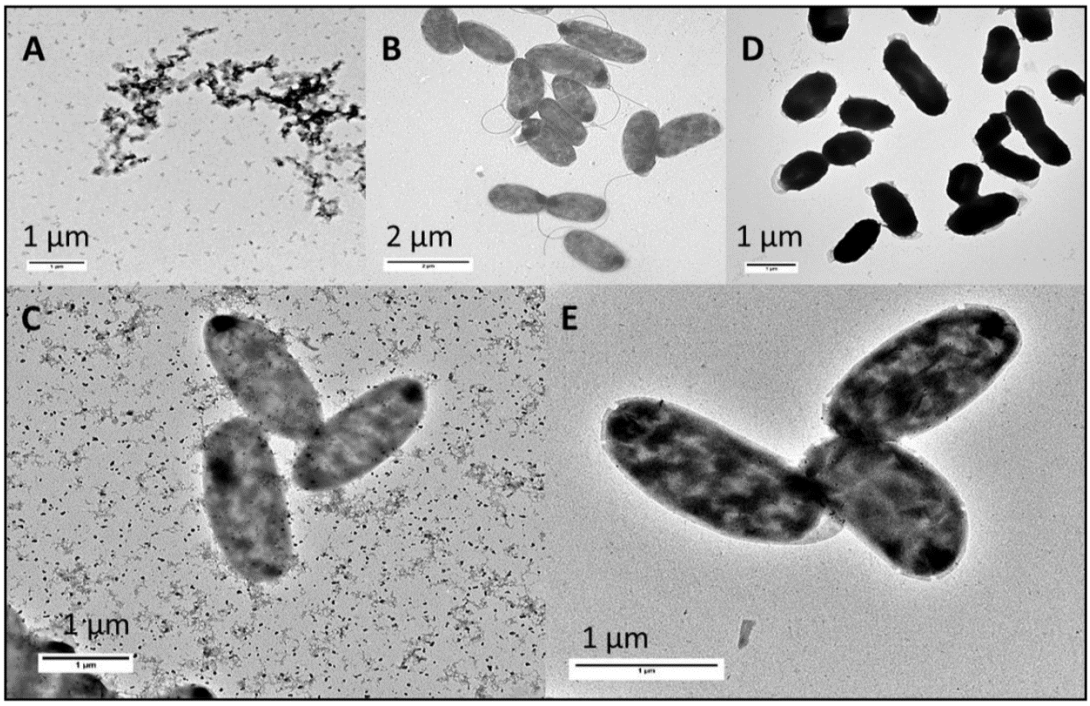

Figure 5. 6. TEM images of *D. alaskensis* G20 pMO9075 and pMOEC20. A) Control of distilled water and 1 mM Cu. B) *D. alaskensi*s pMO9075 with distilled water. C) *D. alaskensi*s pMO9075 with 1 mM Cu. D) *D. alaskensi*s pMOEC20 with distilled water. E) *D. alaskensi*s pMOEC20 with 1 mM Cu.

5.7. Inductively coupled plasma- optical emission spectrometry analysis of removal of Cu by *D. alaskensis*

In order to evaluate the amount of copper that *D. alaskensis* is able to remove from a solution of 1 mM Cu, ICP-OES analysis was carried out. Both strains of *D. alaskensis* (pMO9075 and pMOEC20) were able to remove all the copper from the solution (Figure 5.7). Results obtained show that the expression of the heterologous protein EC20 does not affect the ability of *D. alaskensis* to remove copper. This may be because *D. alaskensis* is accumulating copper ions inside the cell.

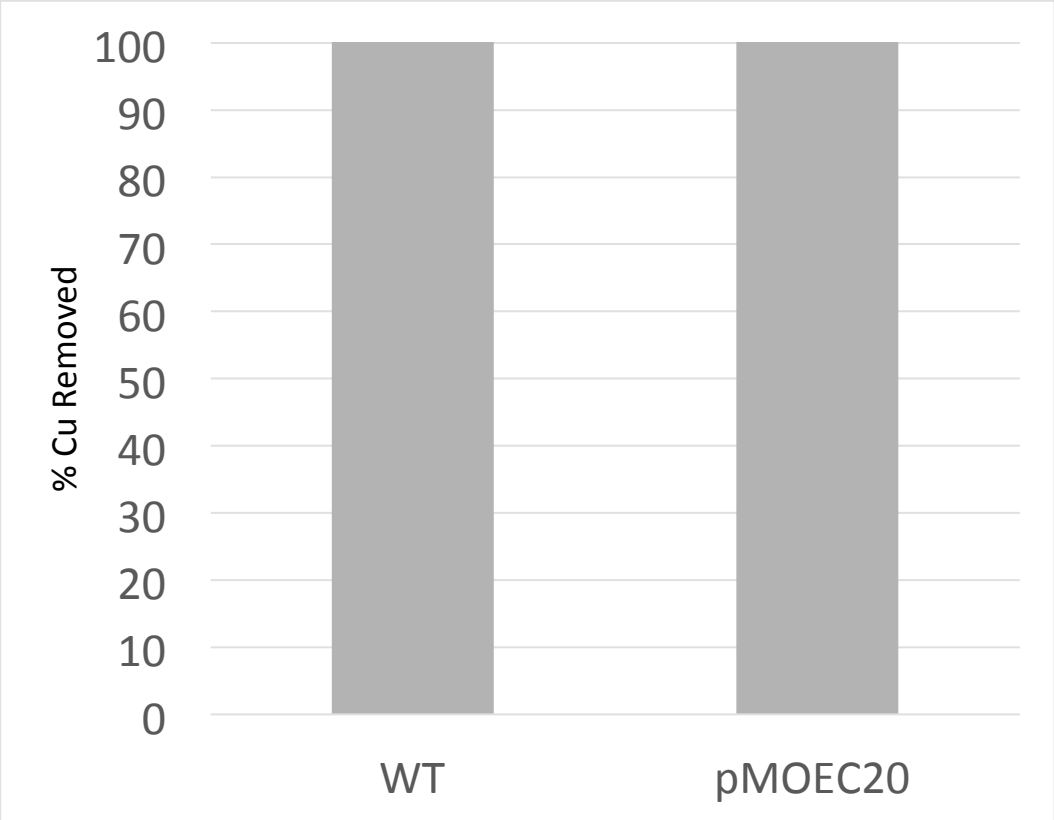

Figure 5. 7. ICP-OES Analysis. Percentage of copper removed by *D. alaskensis,* incubated with 1 mM Cu. WT: wild type *D. alaskensis* G20; pMOEC20: *D. alaskensis* expressing phytochelatin EC20.

5.8. Discussion

Successful insertion of the EC20/IgA into pMO9075 and its confirmation through diagnostic digest reactions and sequencing validates the cloning of insert EC20/IgA, to assemble pMOEC20.

Overall, the results obtained in *E. coli* indicate that the expression of EC20 does confer a certain heavy metal survivability advantage over the control. However, since EC20 has a higher affinity for Cu [189] than for Pt or Pd, it had a greater effect on *E. coli*'s tolerance to Cu concentrations higher than 2 mM in comparison to Pt and Pd, where *E. coli* did not survive concentrations higher than 2 mM . The expression of EC20 does not directly confer a higher resistance to Pd or Pt. Results observed for Pd and Pt are not significant since the error bars on Figure 5.2 and Figure 5.3 are considerable. Contrary to the Pt growth curve graphs, Pd growth curves show how the control (pMO9075) has a higher growth rate during the exponential phase in comparison to pMOEC20. In addition, results indicate that *E. coli* has a resistance mechanism to Cu and not to Pt or Pd. Control *E. coli* survived Cu concentrations of 3 mM and *E. coli* pMOEC20 up to 4 mM. Whereas wild type and *E. coli* pMOEC20, did not survive concentrations higher than 0.5 mM of Pt and Pd, growth was stunted and never reached exponential phase. EC20 conferred a higher increase in resistance to Pt than it did to the other metals, because when expressed it enabled *E. coli* to increase its resistance from 0.5 mM to 2 mM Pt. Whereas, EC20 only conferred an additional 1 mM of Cu resistance, from 3 mM to 4 m. EC20 did not confer additional resistance to Pd.

EC20 has previously been expressed in bacteria to chelate a number of heavy metals, including cadmium [145], mercury [145, 195], zinc, lead, copper, nickel, and molybdenum [196] and arsenic [188]. No research has been published to suggest that the expression of EC20 on the outer membrane of a bacterium will be able to chelate Pt and Pd. However, EC20 is able to chelate Cu ions when expressed by *Cupriavidus metallidurans*. Although *C. metallidurans* is a different microorganism to *D. alaskensis,* it was hypothesised that the expression of EC20 on the outer membrane of *D. alaskensis* will make it more tolerant to Cu.

A previous study concluded that *D. alaskensis* is susceptible to low concentrations of Cu (16 μM) [197]. The survivability to Cu, Pt and Pd growth curves previously done in this study for *E. coli* were attempted with *D. alaskensis,* but as the reading was done aerobically, *D. alaskensis* did not grow properly, and the values obtained were inconclusive, since data obtained is not reliable to a normal bacterial growth. Experiments were performed in a microplate reader that regulates temperature, but the area is oxygenated, and therefore not in anaerobic conditions. When *D. alaskensis* cultures were added to the media with Cu, Pd, and Pt, the metals precipitated. The precipitation of the metals prevented ions being available for the microorganism to uptake. To try to prevent the precipitation of the metals in the media and to avoid inaccurate readings, experiments were repeated with an added shaking step before the OD_{600} readings. This shaking step was added to prevent the effects of the metal precipitation on the OD_{600} readings. The formation of precipitated metal sediments, make it difficult to monitor cell growth because it obscures the OD_{600} readings. Results were still inconclusive, for all set-ups where *D. alaskensis* was not growing at optimal conditions, and the shaking of the plate made no significant change on the values recorded. Optimisation of the protocol is required, but it will be very complicated to emulate the experiments and results obtained with *E. coli* in *D. alaskensis* because the of *D. alaskensis* anaerobic requirements. A solution to this problem would be to take samples every 12 hours and take OD_{600} readings inside the anaerobic chamber, therefore the experiment conducted will be strictly in anaerobic conditions. Alternative methods to assess the effects of Pt, Pd and other heavy metals have on *D. alaskensis* can be used. The agar well diffusion and the tube dilution methods have previously been used to assess metal toxicity [198].

The agar well diffusion method relies on the addition of a metal salt solution in a central well (1 cm in diameter and 4mm in depth) to a nutrient agar plate. Plates can be incubated at 37°C for 24 hours to allow the metal salt solution to diffuse into the agar, which will cause a concentration gradient of the metal [198]. Under anaerobic conditions, *D. alaskensis* can be inoculated in radial streaks and in duplicate, to then be incubated at 30°C for 72 hours or more. After incubation, the area of growth inhibition (in mm) can be measured. The percentage of the bacterial tolerance can be

calculated in terms of the ratio: length of the growth in mm versus length of the total inoculated streak.

The tube dilution method relies on the addition of the desired metal salt concentration to the liquid nutrient media (final volume of 10 mL) and then sterilised at 110°C for 15 minutes. Under anaerobic conditions, previously cultured *D. alaskensis* is inoculated onto the tube and incubated at 30°C for 72 hours or more [198]. Using controls as follows: positive control, metal-deficient medium with *D. alaskensis*; negative control, that consists metal-supplemented medium without *D. alaskensis*.

The production of Pd and Pt nanoparticles by *D. alaskensis* is carried out in the presence of MOPS (3-(N-morpholino)propanesulfonic acid) buffer, pH 7.0. A similar protocol was used when investigating Cu NP production, but it resulted in the precipitation of copper prior to the addition of cells. Therefore, distilled water was substituted for MOPS. The results concluded that *D. alaskensis* is not able to synthesize NPs. This result was unexpected as *D. alaskensis* has been shown to be resistant to a wide range of metals and is able to synthesize a wide range of NPs from those metals. While it was hypothesised that *D. alaskensis* contains a pathway for the synthesis of Cu NPs it is also likely that the substitution of distilled water for MOPS means that a constant pH is not maintained, which could have a major influence on NP synthesis and the resulting morphologies of any NP produced [199].

ICP-OES studies confirmed that the expression of EC20 by *D. alaskensis* does not affect the Cu removal from the media, since no difference between pMOEC20 and the control strain (pMO9075) was observed in these studies' results. Furthermore, the lack of Cu NPs synthesis by *D. alaskensis* observed in the TEM image supports that EC20 acts just as a 'holding area' for metals. Meaning EC20 binds metals and prevents their uptake by the cell, ultimately reducing their toxic effect, but it does not play a role in metal removal or NP synthesis [188].

CuNPs have been associated as antibacterial agents [200] , and in some cases capable of inhibiting SRBs such as *Desulfovibrio marinisediminis* [201]. This last study screened for different biogenic CuONPs antibacterial activity on *D. manirinisediminis*. The fact that CuONPS inhibits growth of an SRB, may indicate why *D. alaskensis* G20

was unable to synthesise CuNPs, but only accumulate/remove Cu ions from the solution. Moreover, no scientific research has been published to state that a *Desulfovibrio* sp is capable of synthesising CuNPs.

Chapter 6: Tailoring NPs synthesis using MoClo Toolkit

6.1. Introduction

This chapter will focus on the on a proof of concept application of all the previous efforts depicted on this thesis. The synthetic biology tools that were developed specifically for *D. alaskensis,* including the newly characterised synthetic promoters, and RBSs enabled the facile and cost-effective assembly of a combinatorial library of TUs, with the aim to the tailor nanoparticle' size. It will also highlight the importance of the use synthetic biology tools, and how their applications help streamline the design, build, and test cycle of the biogenic nanoparticles synthesis research.

Nanoparticles are currently being synthesised through chemical and physical methods on an industrial scale. However, traditional methods for the synthesis of NPs are not sustainable. Chemical and physical NP synthesis methods require high temperatures, and/or pressures resulting in high energy consumption and the generation of large amounts of waste [11]. In recent years, research has shifted to harness biology to synthesise NPs. A biological approach has many advantages over chemical and physical methods. Reactions are catalysed in aqueous solutions at standard temperature and pressure (cost-effective and low energy syntheses) [11]. It does not require solvents or harmful chemicals, making the NP biosynthesis a more sustainable method. Furthermore, NP synthesis by microbes does not require the use of a pure starting material; therefore, it can be used for the biosynthesis of NPs and for the bioremediation of contaminated water, land and waste [29, 31].

The biogenic synthesis of metal NPs has drawbacks and problems that need to be addressed, in order for them to be comparable with monodispersed NPs synthesised chemically or physically. Amongst them, is that biogenic metal NPs may be produced with a broad morphology and size range [11], which could be problematic, because the catalytic activity of NPs is size dependant [202]. The ability to synthesis NPs with a monodispersed size is imperative. Biogenic NPs require a homogeneous size in order to be successfully commercialised. In an effort to address this problem, synthetic biology, nanobiotechnology and genetic engineering are being harnessed to

improve and, most importantly, tailor NPs synthesis. Metal NPs' size can be tailored using microbial nanocompartments called encapsulins. The defined size and shape of the encapsulins allows the size-constrained synthesis in their interior, resulting in a homogeneous and monodisperse population of NPs [203]. A research study showed the synthesis of monodispersed biogenic magnetite (Fe_3O_4) NPs, using Dps proteins (DNA binding proteins, bear a strong similarity to ferritins) from starved *Listeria innocua* cells [204]. An alternative method for the synthesis of a monodispersed magnetite was reported using bacterial organelles called magnetosomes, such as the magnetosome protein Mms6, a small protein embedded on the interior of the magnetosome membrane associated with the synthesis of magnetite [205]. Mms6 is produced by magnetotactic bacterium *Magnetospirilum magneticum* AMB-1 [205]. These examples highlight that research has successfully tailored biogenic NPs' size by using nanostructures to constrain the NP size within a defined structure.

Desulfovibrio sp mechanism for platinum group metals (more importantly Pt and Pd) reduction is hypothesised to occur due to the bacteria incorporating the metals into their electron transfer pathways [5]. The reduction of Pt and Pd occurs in the periplasm, where hydrogenases such as NiFe hydrogenase are able to reduce Pt and Pd ions to NPs. The overexpression of key periplasmic proteins and enzymes, which play a part in the NP synthesis mechanism, may help elucidate how to tailor biogenic metal NPs' size, without the use of nanocompartments. NiFe hydrogenase, is an enzyme present in *D. alaskensis* that plays an important role in the hydrogen metabolism of SRB [206], and a key role in the dissimilatory metal reduction by SRB [13, 207]. The involvement of a NiFe hydrogenase in Pd(II) reduction in *Desulfovibrio* sp, was proved by comparing hydrogenase-negative mutant strains to hydrogenase-positive strains [208]. The NiFe hydrogenase appeared to serve as a nucleation site for NP formation and also assisted in NP growth by supplying electrons for metal reduction [208]. The overexpression of the NiFe hydrogenase may provide additional electrons for the reduction of heavy metals in *D. alaskensis*, therefore making it better at reducing metal ions to NPs. NiFe hydrogenase from *Desulfovibrio* spp are comprised of a small and large subunit, which are encoded in a single operon [209, 210]. The small subunit of a NiFe hydrogenase contains a signal peptide consistent with their periplasmic localisation [209]. The use of a genetically engineered *D. alaskensis* to

overexpress the NiFe hydrogenase small subunit, resulted in the formation of larger Pt NPs in *D. alaskensis* [211]. This proof-of-principle research showed the feasibility of genetically engineered *D. alaskensis* to alter NP sizes.

Using the MoClo tools designed and engineered in this study, the *D. alaskensis* NiFe hydrogenase small subunit gene (KEGG, Dde_2137) was adapted to MoClo standards. A combinatorial library of TUs, expressing the NiFe hydrogenase small subunit under the control of the synthetic promoters and RBS previously characterised in this study, were assembled using MoClo. The design, build, test, analyse cycle was put into practice with the application of the MoClo synthetic biology tools now available for *D. alaskensis*. The aim of the study was to test if a controlled variation of expression of the NiFe hydrogenase small subunit, would affect the overall size of Pt NPs. Results demonstrate the importance of the NiFe hydrogenase in the mechanism of Pt reduction to NPs, and the fine tuning of NiFe hydrogenase expression can be harnessed to tailor NP size to a desired monodisperse size range.

6.2. Adapting NiFe hydrogenase to MoClo

The NiFe hydrogenase small subunit gene was cloned into the DVA_CD donor vector with confirmation obtained *via* a diagnostic digest reaction and sequencing. To be compliant with MoClo standards, the BsaI recognition site found in the NiFe hydrogenase gene needed to be mutated, which was accomplished through site-directed mutagenesis. Primers for the deletion of the BsaI recognition site were designed to change GGT to GGC in the restriction site whilst retaining the codon's original coding for glycine. To confirm the successful deletion of the BsaI site, a diagnostic digestion reaction with BsaI and EcoRI was conducted on plasmids extracted from six of the colonies obtained from the mutagenesis reaction. The diagnostic digestion was run on an electrophoresis gel (Figure 6.1). Colonies 1 - 3 and 6 showed a correct digestion pattern, concluding that the BsaI recognition site was mutated. Final confirmation was done by sequencing. The sequencing results matched the desired sequence.

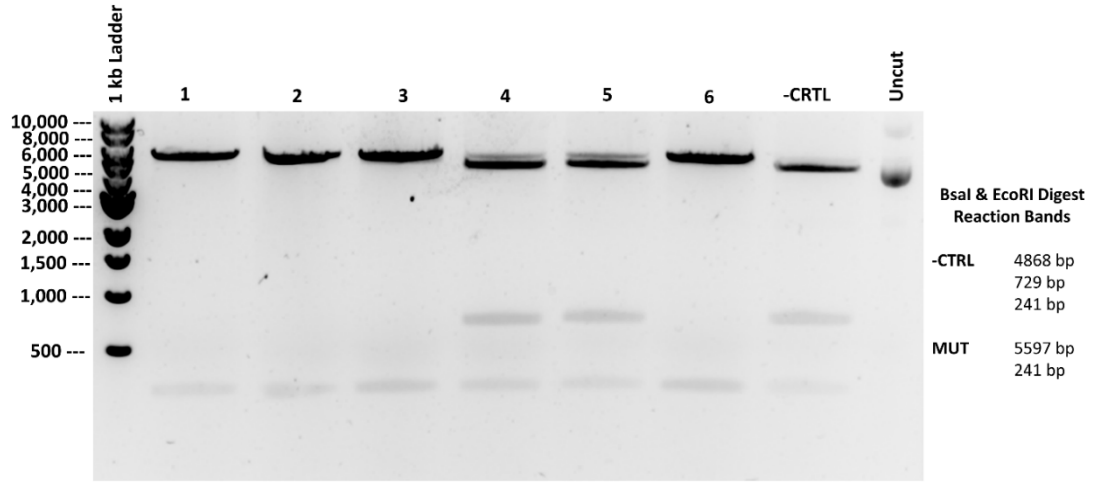

Figure 6. 1. Diagnostic Digestion Reaction with BsaI and EcoRI: Agarose Gel Electrophoresis. DNA extracted from six colonies were tested. Four lanes yielded bands at the correct size (5597 bp and 241 bp). Negative control is the non-mutated plasmid. Mutated plasmids show two bands, non-mutated plasmids show three bands.

6.3. Assembly of combinatorial TUs of NiFe hydrogenase

The NiFe hydrogenase combinatorial TU library was assembled to express NiFe hydrogenase small subunit under controlled expression, using previously characterised promoters and RBS. Each TU was assembled with the same terminator (B0015_DE), DVA_2137 (NiFe hydrogenase CDS), iterating promoters: Kan, PR-3 and J2106_AB, and RBS: RBS-CR, RBS-9 and B0032m_BC. All these parts are necessary to assemble a TU with the acceptor vector ΔpMOMoClo. A total of 9 different TUs were assembled: 2137_M S, 2137_M CR 2137_M 9, 2137_Kan S, 2137_ Kan CR, 2137_ Kan 9, 2137_3 S, 2137_ 3 CR, and 2137_3 9. A detailed description of the TUs assembled and tested in this study are listed on Table 6.1. Since ΔpMOMoClo contains a *lacZ-α* gene, as part of the MoClo method, a blue/white screening test was performed. The successfully assembled plasmids were transformed into chemically competent *E. coli* NEB 5-alpha cells, DNA extracted, purified, and confirmed by DNA sequencing.

Table 6. 1. TUs assembled and tested in this study. All promoters and RBS were previously characterised in this study.

TUs	Promoter	RBS	CDS	Terminator
M-S	J23106_AB	B0032m_BC	DVA_2137	B0015_DE
M-CR		RBS -CR		
M-9		RBS -9		
Kan-S	Kanamycin promoter	B0032m_BC		
Kan-CR		RBS -CR		
Kan-9		RBS -9		
3-S	PR-3	B0032m_BC		
3-CR		RBS -CR		
3-9		RBS -9		

6.4. Transmission electron microscopy of combinatorial library

The NiFe hydrogenase combinatorial library was transformed into *D. alaskensis* competent cells and cultured until they reached an OD_{600} of 1.0. To observe how a controlled variation of expression rates of the NiFe hydrogenase small subunit affect the Pt NP synthesis, TEM images were taken of *D. alaskensis* inserted with the combinatorial library and pMO9075 in presence of 2 mM Pt (Figure 6.2). NP sizes were measured using ImageJ software. The frequency of the NPs size was calculated in percentages, and illustrated as histograms on Figure 6.3. The negative control, pMO9075, showed Pt NPs dispersed across most size ranges, but 50% of NPs have a size between 201 – 300 nm. The combinatorial NiFe hydrogenase library, displayed a varied size range for Pt NPs, varying from 15 nm to 823 nm. Contrary to the control, most plasmids tested had a larger percentage of NPs within a smaller size range. Plasmids, 2137_3 CR (Figure 6.3 B), 2137_M 9 (Figure 6.3F) and 2137_M S (Figure 6.3G), respectively have a 29%, 27% and 29% frequency of NPs within the 101 – 200 nm size range. Plasmids, 2137_3 9 (Figure 6.3C), 2137_3 S (Figure 6.3D), 2137_M CR (Figure 6.3E) and 2137_Kan S (Figure 6.3J), respectively have a 45%, 35%, 45% and 23% frequency of NPs within the 0 – 100 nm size range. The only plasmid with a relative similarity to negative control was 2137_Kan CR (Figure 6.3H), which has a low 29% of NPs with a size range between 201 - 300 nm, but has a higher frequency of smaller and bigger NPs than the negative control. Plasmid 2137_Kan 9 (Figure 6.3I), has a 36% NP size frequency of 301-400 nm, and synthesising considerably bigger NPs than the negative control.

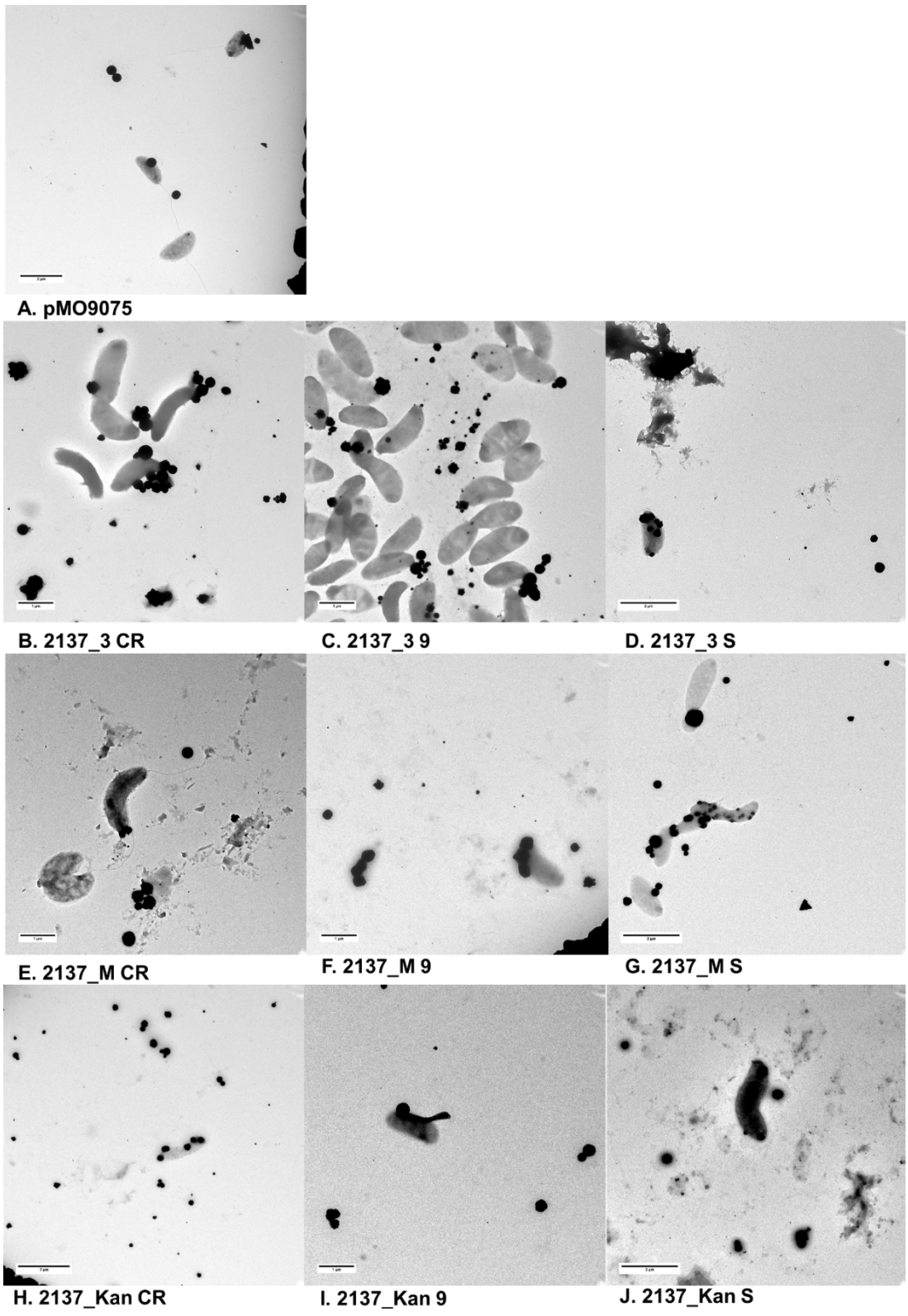

Figure 6. 2. TEM Images of Pt NPs and *D. alaskensis.* Representative electron micrographs Pt NPs produced by the NiFe hydrogenase combinatorial library. Scale bar = 3 μm (H); 2 μm (A, D, G and J); 1 μm (B, C, E, F and I).

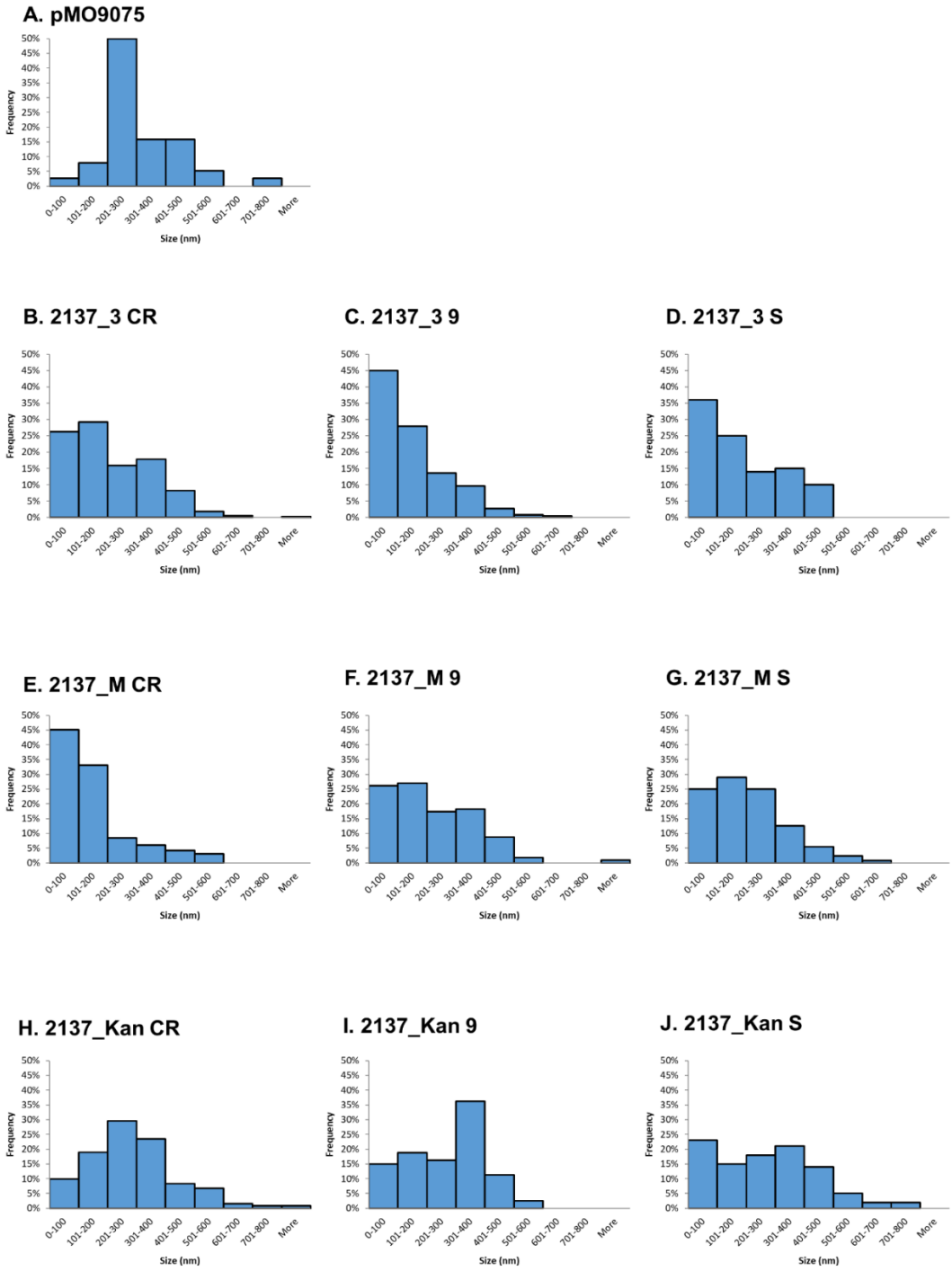

Figure 6. 3. Pt NP Size Frequency Histograms Synthesised by *D. alaskensis.* A) pMO9075 (negative control), N = 38. B) 2137_3 CR, N = 377. C) 2137_3 9, N = 258. D) 2137_3 S, N = 100. E) 2137_M CR, N = 166. F) 2137_M 9, N = 115. G) 2137_M S, N = 128. H) 2137_Kan CR, N = 132. I) 2137_Kan 9, N = 80. J) 2137_Kan S, N = 100. The NiFe hydrogenase combinatorial library had a larger percentage of NPs within a smaller size range in comparison with negative control (A).

6.5. Inductively coupled plasma- optical emission spectrometry of combinatorial library

In order to ascertain the total ionic concentrations of Pt NPs and Pt ions respectively, ICP-OES analysis was carried out for all samples obtained from the NiFe hydrogenase combinatorial library. All strains were able to produce considerable amounts of Pt NPs (Figure 6.4), some concentrations remained in ionic form (Figure 6.5). Some strains from the NiFe combinatorial library synthesised higher concentrations of Pt NPs in comparison with the control (pMO9075 = 152.87 mg/L). The strain with the highest Pt NP synthesis was M-S (256.59 mg/L), and the lowest concentration synthesised was Kan-9 (159.16 mg/L), which had a value close to the control. Statistical analyses of all samples concluded that the values obtained were not statistically significant, which is indicative that the values obtained do not necessarily reflect the strains' ability to synthesise Pt NPs. Some Pt ions are not reduced into nanoparticle form, and therefore remain as Pt ions in small concentrations. All strains including the control (pMO9075 = 6.17 mg/L) showed considerably small ionic concentrations of Pt. The strain reporting the highest ionic concentration was Kan-CR (14.47 mg/L; SD 13.7), construct under the expression control of a Kanamycin promoter and a RBS-CR, and the lowest ionic concentration was 3-CR (2.09 mg/L; SD 0.104), construct expressing under the expression control of PR-3 promoter and a RBS-CR.

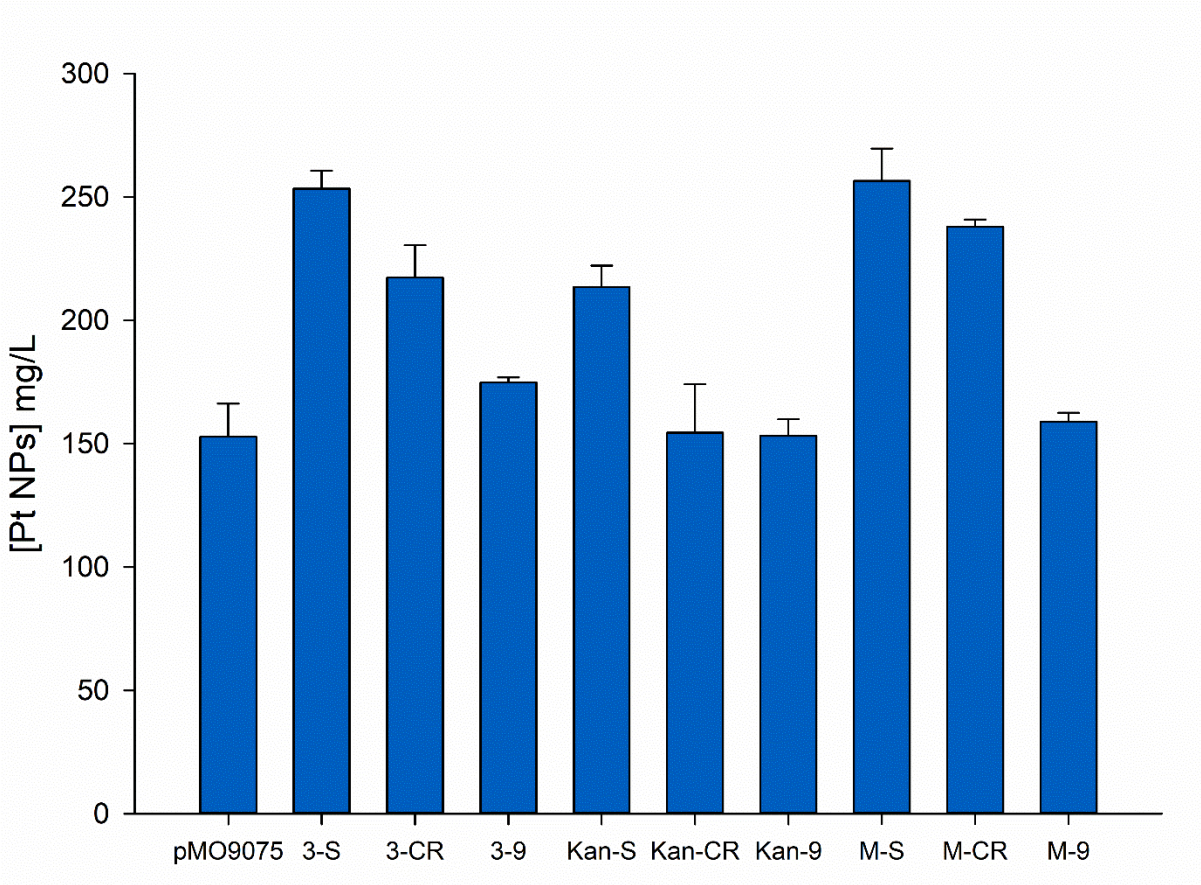

Figure 6. 4. Total concentration of Pt NPs from NiFe hydrogenase combinatorial library. Average total values in mg/L are as follow: pMO9075 = 152.87; 3-S = 253.38; 3- CR = 217.46; 3-9 = 174.86; Kan-S 213.56; Kan-CR; 154.50; Kan-9 = 153.16; M-S = 256.59; M-CR = 237.92; M-9 = 159.02. Error bars depict the standard deviation of the mean.

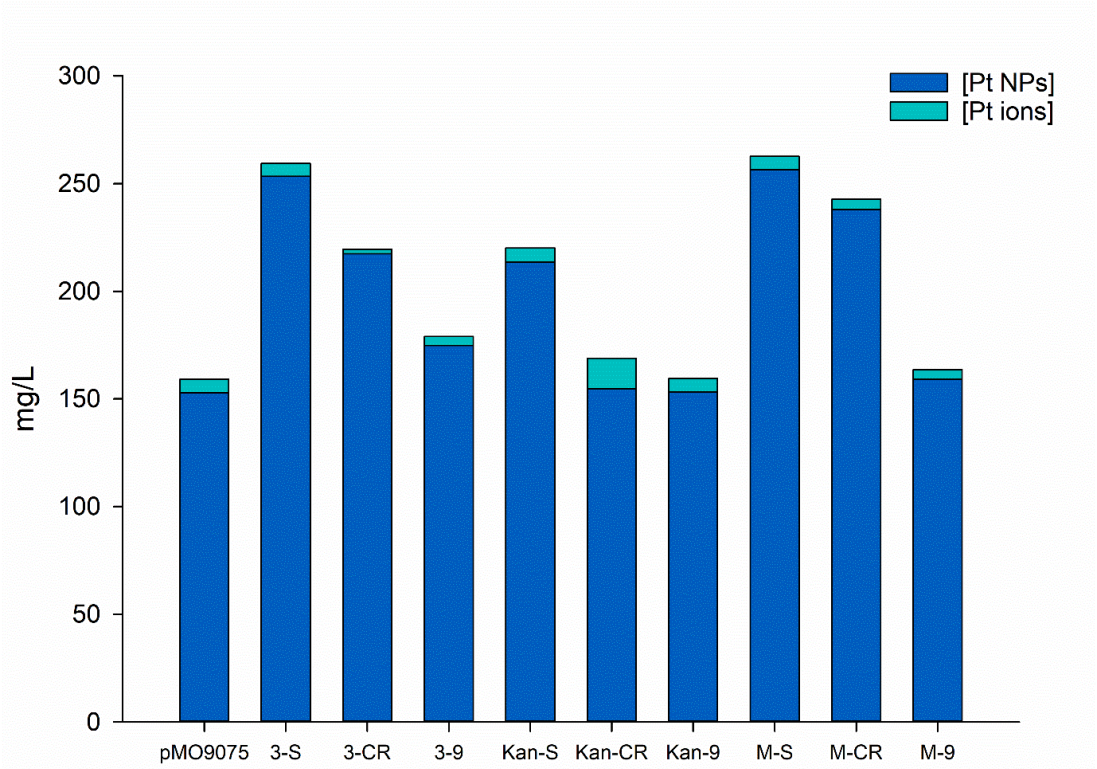

Figure 6. 5. Overall total concentration of Pt detected with ICP-OES. Pt ions are not reduced completely to Pt NPs, PT ions concentrations remain. This graph depicts and compares the total concentrations of Pt NPs in comparison with those that remained as Pt ions.

6.6. Colorimetric assays of the NiFe hydrogenase combinatorial library

To investigate the catalytic activity of NPs synthesised by the NiFe hydrogenase combinatorial library, the NPs' redox activity was quantified using methylene blue (MB) and sodium borohydride ($NaBH_4$). When NPs are introduced to a MB-BH_4 solution, they act as a reducing agent [212]. Reducing the dye from its oxidised state to its reduced state results in a colour change from blue (oxidised state) to colourless (reduced state). This colour change can be used to quantify the reduction rate by measuring the optical density of methylene blue in the solution at 665 nm. In an attempt to accurately measure the combinatorial library's NP catalytic activity, assays were set up with different Pt NP concentrations. A clock reaction is happening for most assays, because the OD values are oscillating throughout time. Meaning in the presence of BH_4 and Pt NPs, MB is rapidly reduced to leucomethylene blue (LMB) and then oxidised back to MB within seconds or minutes. The clock reaction of methylene blue, is due to the fact that LMB is prone to oxidation by oxygen in the air after a gentle shake [213]. Many factors may affect the speed of the oscillating clock reaction of MB-BH_4 in presence of Pt NPs. Factors such as: nanoparticle size, nanoparticle metal type, shaking time, MB concentration and nanoparticle concentration [213, 214]. The MB-BH_4 colorimetric assay results are as follows: 6 ppm Pt (Figure 6.6), 5 ppm Pt (Figure 6.7), 4 ppm Pt (Figure 6.8), 2 ppm Pt (Figure 6.9) and 0.2 ppm Pt (Figure 6.10). All graphs depict a nanoparticle-catalysed clock reaction. Most factors were controlled when attempting to quantify the catalytic activity of biosynthesised NPs, but it was not possible have a homogeneous NPs size, since the NiFe hydrogenase combinatorial library synthesised Pt NPs with a varied size dispersion. A size dispersion that is considerably varied among NPs synthesised by the entire combinatorial library. By closely analysing the graphs, the higher the Pt concentration the less oscillation occurred, during which most reached an asymptotic value (value close to zero) for a prolonged time. NPs synthesised by plasmids expressing the NiFe hydrogenase under Kan-9 (Kan promoter and RBS-9) and Kan – CR (Kan promoter and RBS-CR) had a faster catalytic activity in comparison with controls and other NPs synthesised by the library.

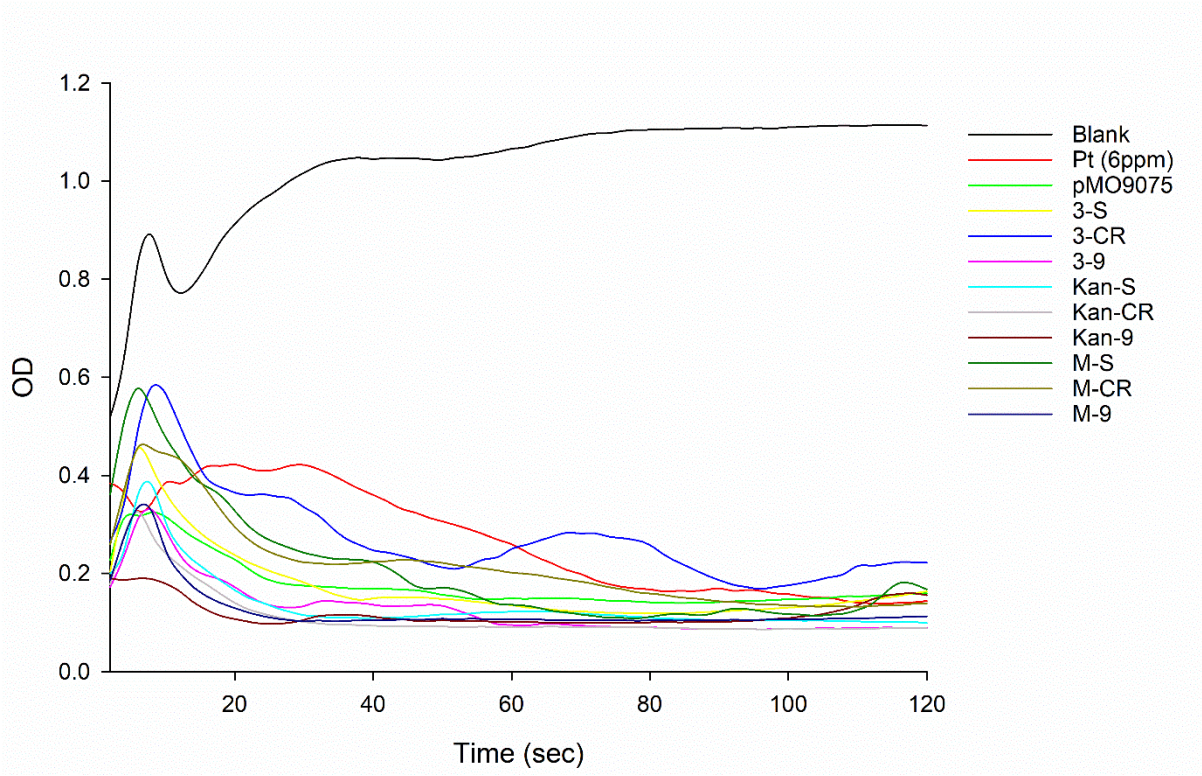

Figure 6. 6. MB colorimetric assay at 665 nm of NiFe combinatorial library with 6 ppm Pt.

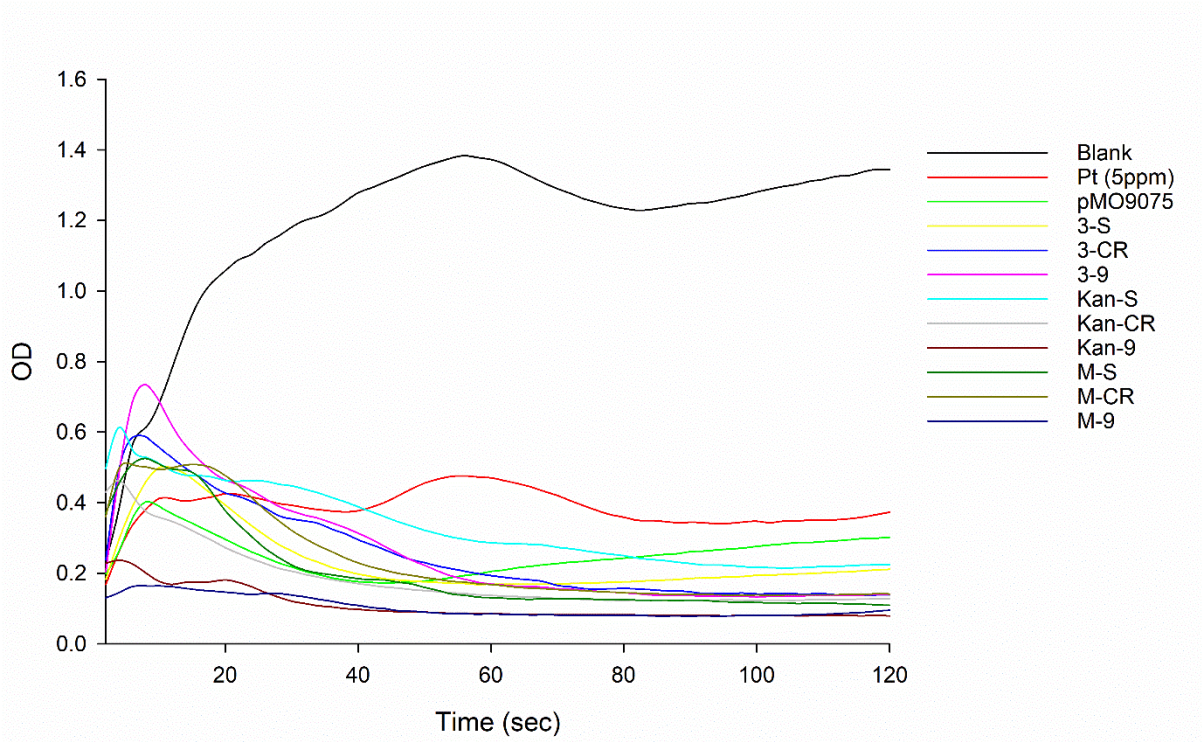

Figure 6. 7. MB colorimetric assay at 665 nm of NiFe combinatorial library with 5 ppm Pt.

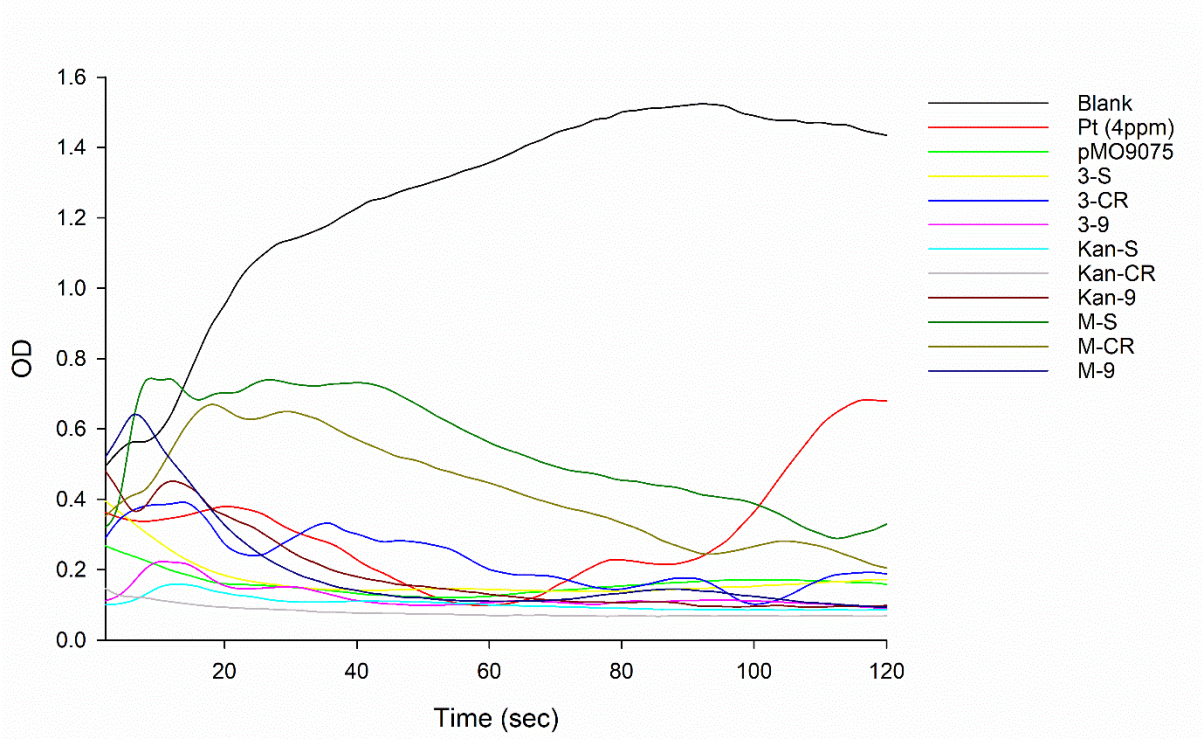

Figure 6. 8. MB colorimetric assay at 665 nm of NiFe combinatorial library with 4 ppm Pt.

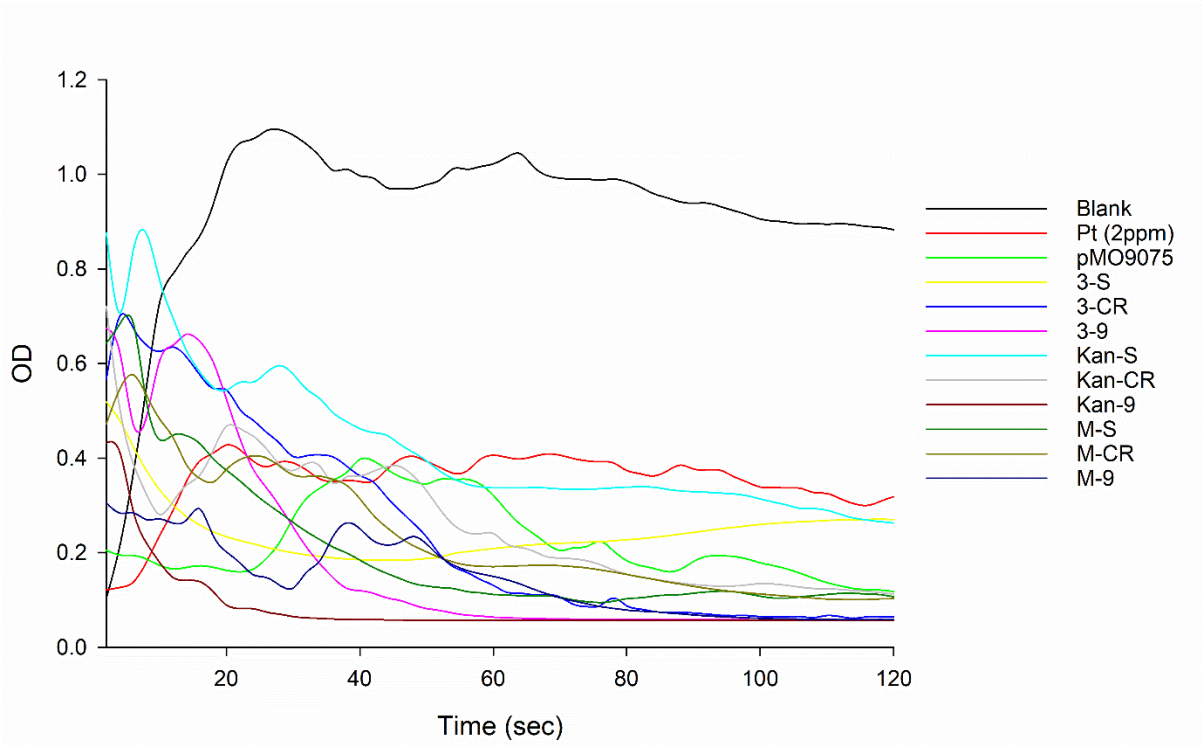

Figure 6. 9. MB colorimetric assay at 665 nm of NiFe combinatorial library with 2 ppm Pt.

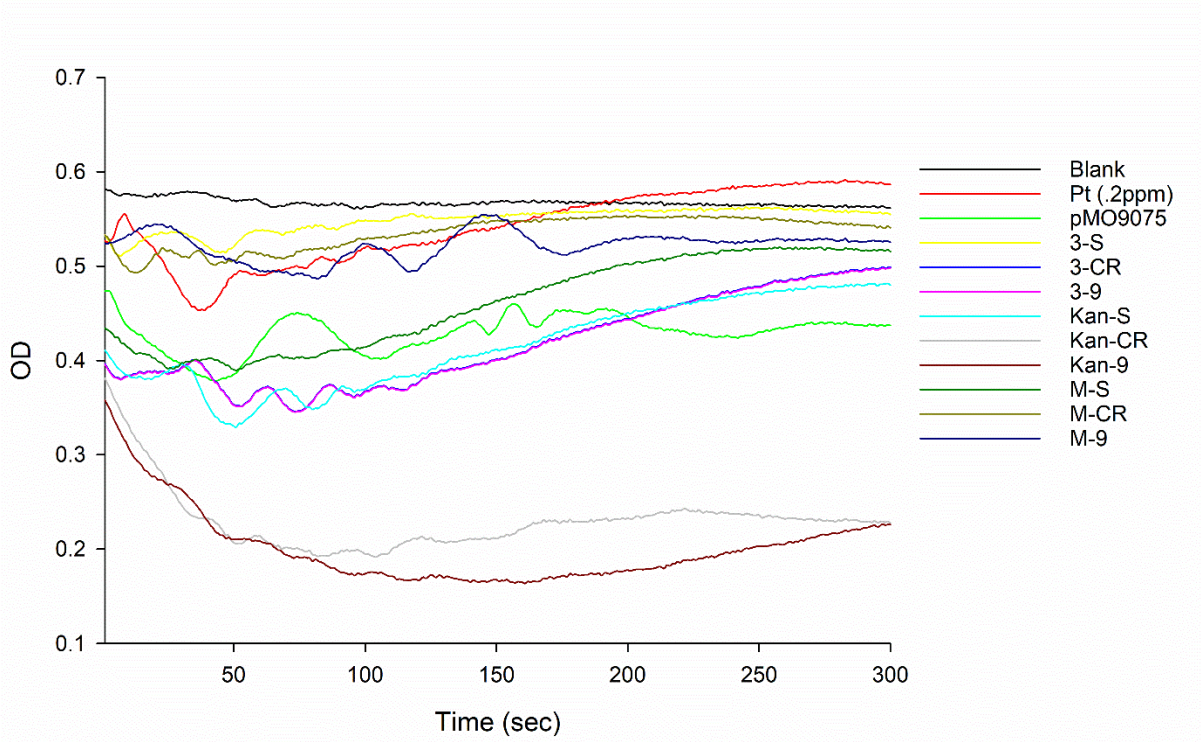

Figure 6. 10. MB colorimetric assay at 665 nm of NiFe combinatorial library with 0.2 ppm Pt.

To further investigate the catalytic activity of NPs synthesised by the combinatorial library, the NPs' oxidative activity was quantified using 2,6-dimethoxyphenol (DMP). When nanoparticles are introduced to a solution containing 2,6-DMP, they act as an oxidising agent [215]. Due to their catalytic activity, biogenic Pt NPs can be assessed using this colorimetric assay. Unlike the MB-BH_4 colorimetric assay, a clock reaction would not occur with the 2,6-DMP assay. The NiFe hydrogenase combinatorial library synthesised Pt NPs showed different oxidase activities (Figure 6.11) at pH 7, with an increased relative oxidative activity at higher concentrations of Pt NPs. The oxidative activity order of all samples tested with 0.5 mM Pt concentration is as follows: Kan-CR > 3-9 > pMO9075 > M-CR > Kan-S > 3-S > M-9 > Kan- 9 > M-S > 3-CR. The oxidative activity order of all samples tested with 0.3 mM Pt concentration is as follows pMO9075 > Kan-CR > Kan-S > M-CR > 3-9 > 3-S > M-9 > M-S > Kan-9 > 3 – CR. Values obtained are not statistically significant, with the exception of Kan-CR vs 3-CR with 0.5 mM Pt and pMO9075/Kan-CR vs 3-CR with 0.3 mM Pt. To ascertain that the Pt ion concentrations of all samples were not affecting their oxidative activity, the respective Pt ions concentrations (0.1, 0.25, 0.3 and 0.5 mM) were tested. The low measurements recorded for all Pt ion concentrations, indicated that Pt ions are not very reactive in oxidative reactions at neutral pH. By analysing the values captured at 0.25 mM, 0.3 mM, and 0.5 mM Pt, their catalytic activity changed considerably between 0.25 mM to 0.3 mM, despite the small concentration change. The change was more apparent for Kan-S samples, as a change from 0.25 mM to 0.3 mM Pt, increased its catalytic activity 30-fold. Their oxidative catalytic activity did not have a considerable change from 0.3 mM to 0.5 mM, as values were not statistically significant among each other. Such results are likely to be associated with the aggregation or agglomeration of NPs, which may mitigate their catalytic activity.

In theory, the TUs with a smaller NP size distribution should have a higher oxidative activity. TUs synthesising the smallest Pt NPs were 3-9 and M-CR, both produced 45% of their Pt NPs with a size distribution of 0-100 nm. However, 3-9 had the second highest oxidative activity and M-CR placed in the middle of the order. Whereas the one reporting the highest oxidative activity TU Kan-CR, has a more

dispersed PT NPs size frequency (30% of Pt NPs with a size range of 201 -300 nm). The TU with the lowest oxidative activity was 3-CR, which has a dispersed Pt NP size distribution (30% of Pt NPs with a size range of 101- 200 nm), a higher percentage of smaller Pt NPs in comparison with the TU with the highest oxidative activity, Kan-CR. These results indicate the importance of the promoter, the only difference between 3-CR and Kan-CR is the promoter used. The controlled expression of NiFe hydrogenase small subunit by the Kanamycin promoter produced Pt NPs, which showed higher oxidative values in comparison with those produced by TUs controlling NiFe hydrogenase expression with promoters PR-3 and M (J2106_AB).

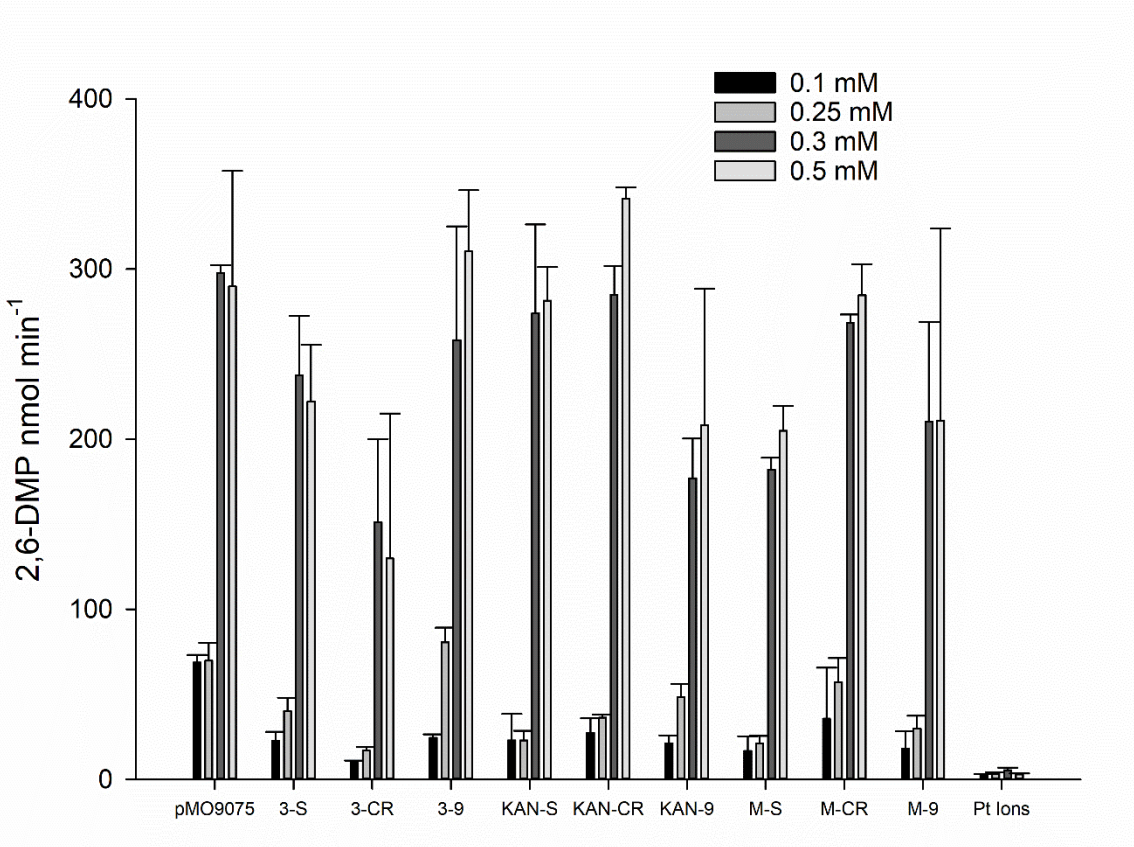

Figure 6. 11. 2,6- DMP colorimetric assay at 469 nm of NiFe hydrogenase combinatorial library at different Pt concentrations. Error bars depict the standard deviation of the mean.

6.7. Discussion

The expression of the NiFe hydrogenase small subunit under the control of different expression control elements in *D. alaskensis* was successfully achieved in this study. The assembly of the combinatorial library was easily accomplished in a facile, cost and time-effective way, which surpasses the effectiveness of what can be done by using traditional DNA assembly methods. Traditional DNA assembly methods are cumbersome and often time consuming, but with the use of newly designed and engineered MoClo tools developed for *D. alaskensis*, the time required to generate a combinatorial library was considerably reduced and streamlined. From conception to completion, this project took less than 6 months, an achievement that couldn't have been accomplished without the use of synthetic biology tools. This specific approach for the combinatorial synthesis of NPs, to our knowledge has never been reported, however NiFe hydrogenase libraries (lacking one or more of the NiFe hydrogenases) of recombinant *E. coli* have been assembled using traditional cloning methods [8]. Libraries assembled to control the expression of NiFe hydrogenase, to our knowledge has never been reported, particularly because our study is using characterised expression control elements specifically designed for *D. alaskensis*. Studies have been published, where NiFe hydrogenase deficient strains of *Desulfovibrio fructosivorans* showed a different Pd NP synthesis to wild-type [208]. Another research study successfully changed the expression of outer membrane cytochrome (MtrC), and soluble redox shuttled (flavins) to radically change the Pd NP phenotype in *Shewanella oneidensis* [216].

All plasmids assembled when transferred to *D. alaskensis* were able to synthesise Pt NPs, with a significant NP size range in comparison with the control (pMO9075), notably synthesising a higher percentage of smaller NPs. Such results also indicate that NiFe hydrogenase plays a key role on the Pt NP synthesis, and that depending on the expression control elements used, the size of Pt NPs changes. Our results support published research, which reported that engineered *E. coli* lacking one or more of the NiFe hydrogenases exhibit altered phenotypes of Pd NPs and Pd depositions within the cells [8]. Our results also support the aforementioned study with NiFe hydrogenase lacking mutant strains of *D. fructosivorans*, that also reported a variety of Pd NPs phenotypes and how the absence of NiFe hydrogenase affect the Pd NPs to cluster in

the periplasm [208]. Our study of the combinatorial library of NiFe hydrogenase goes further to conclude that the different expressions rates of NiFe hydrogenase, affect the Pt NPs size, to the findings of published research with NiFe hydrogenase lacking strains [208].

The expression of the NiFe hydrogenase small subunit did not hinder *D. alaskensis'* ability to successfully reduce Pt ions to Pt NPs, but it also did not enhance its ability to synthesise NPs. ICP-OES results indicate that regardless of the plasmid inserted into *D. alaskensis,* the remaining Pt ion concentrations after NP synthesis are considerably lower than the Pt NP concentrations. Values obtained from testing the library were not statistically significant compared to each other, meaning that all plasmids equally reduced ions to similar amounts of Pt NPs.

The biogenic Pt NPs synthesised by the NiFe hydrogenase combinatorial library were able to catalyse both reduction and oxidisation reactions with model substrates. Although their catalytic activities were not comparable, the Pt NPs tested proved to have better oxidative catalytic activities, than reducing catalytic activities. The MB-BH_4 colorimetric assays did not yield conclusive results; hence, it was not possible to assign an order depending on their calculated catalytic activities. Only Kan-9, Kan-CR and 3-S showed a normal curve. Unlike our results, a research study proved that biogenic Au NPs and Ag NPs synthesised by *Breynia rhamnoides* are able to reduce 4-NP (4-nitrophenol) to 4-AP (aminophenol) in the presence of a BH_4 substrate [217]. 4-NP-BH_4 is also a colorimetric assay, similar to the MB-BH_4 colorimetric assay. However, this reaction is slower and is not a clock reaction, so conclusive catalytic rates were calculated.

All Pt NPs synthesised by the NiFe hydrogenase combinatorial library exhibited an oxidative activity. The activity of Pt NPs was not significant across all samples tested, with the exception of Kan-CR (0.5 and 0.3 mM Pt) and pMO9075 (0.3 mM Pt) with 3-CR. When closely comparing results from the 2,6-DMP assays, catalytic activities reported with 0.3 and 0.5 mM Pt are not statistically significant to each other. The small catalytic activity changes between 0.3 mM and 0.5 mM Pt can be explained by the aggregation/agglomeration of NPs. Aggregation and/or agglomeration of NPs caused a reduction in the active surface area, thus mitigating

their catalytic activity [211]. Research shows that the further you increase the concentration of Pt NPs the more they will agglomerate and have different catalytic activities than isolated Pt NPs [218]. The characterisation of Pt NPs with the 2,6-DMP assay was undertaken at a neutral pH of 7, because it was previously shown not to be as reactive at a lower pH, although Pt ions were shown to be highly reactive [211]. Our research obtained similar results to those previously reported, where all biogenic Pt NPs showed an oxidative activity of approximately 300 2,6-DMP nmol min^{-1} [211]. Unlike such research study, where only wild type *D. alaskensis* strains were used to synthesise Pt NPs, our study reported oxidative activities of Pt NPs synthesised by a NiFe hydrogenase combinatorial library.

Pt NPs synthesised by plasmid Kan-CR showed the highest oxidation catalytic activity, and yielded a discernible curve with the MB-BH_4 colorimetric assay. However the recorded values were not comparable among all the samples, hence it was not possible to confirm whether Pt NPs synthesised by Kan-CR had the highest reducing activity among the samples tested. Published studies on non-biogenic Pt NPs concluded that its oxidative catalytic properties are shape and size dependant [219]. This study also emphasised the importance of testing NPs activities of monodispersed NPs, because the different size and shapes of NP will be variable within samples tested and will affect its oxidative catalytic activity.

Alternative methods to understand and characterise heavy metal NPs are available. A study achieved to characterise single NP's size and catalytic activity employing a method called, scanning electrochemical cell microscopy (SECCM) [220]. SECCM, is a method that combines the electrochemical and physical characterisation at the single NP level, where the NP's catalytic activity is studied on a TEM grid [220]. The downside to this method is that it characterises a single NP, whereas the synthesis of biogenic NPs has an inherent variance in NP size and shape. Another method to characterise biogenic NP is by surface plasmon resonance (SPR). SPR is a powerful label-free method used to study the binding between two macromolecules, where one of the two is immobilised on a sensor chip surface and the other is interacting by lowing over it [220]. This method was proven to be useful to characterise Pt NP's catalytic activity [221] and its regarded as a rapid and accurate method to characterise NPs with variance in NP size and shape [222].

To conclude, the NiFe hydrogenase combinatorial library synthesised Pt NPs with a wide NP size dispersion in comparison with the control (pMO9075). To be comparable with chemical synthesised NPs, biogenic NPs require a monodisperse size distribution. TUs, 3-9 and M-CR show the highest percentage (45%) of NPs within the 0 – 100 nm size range, a percentage that is considerably higher than the control (less than 5%). These results indicate that 3-9 and M-CR strains are at better suited at synthesising monodisperse NPs. Furthermore, the 2,6-DMP colorimetric assay also concluded that 3-9 has one of the best oxidative catalytic activity from the combinatorial library. Overall, 3-9 is the strain best suited for the synthesis of monodisperse Pt NPs and still has a high oxidative catalytic activity in comparison with control. Further characterisations studies need to be done to fully ascertain the NP's catalytic activity. Using SPR in addition to the colorimetric methods, may elucidate

Chapter 7: Overall Discussion and Future Plans

In this thesis, the lack of synthetic biology tools available for the non-model organism *D. alaskensis* is addressed. The main contribution of this work is the *D. alaskensis* MoClo Toolkit (See Figure 7.1), which consist of 19 bioparts. The toolkit contains an oxygen-independent reporter library (PMO7, CreiLOV, nanoLUC and phiLOV), a synthetic promoter library (PR-1, PR-3, PR-4, PR-7, NPR-7, PR-8, PR-9 and PR-10), a synthetic RBS library (RBS-7, RBS-8, RBS-9, RBS-10, RBS-CR) and two acceptor vectors (pMOMoClo, and pMOMoClo_AF). The *D. alaskensis* MoClo Toolkit primarily enables the assembly of single-gene TUs, which can be inserted and tested in *D. alaskensis* and *E. coli*. Furthermore, with the array of bioparts available in this toolkit, allows the assembly of single-gene combinatorial libraries. In addition, if new bioparts are required, these can be easily synthesise as a gBlock and adapted to MoClo following the protocol used on Chapter 4, Figure 4.1. An already available sequence of interest (within a plasmid) can be MoClo adapted by following the protocol used on Chapter 2, Section 2.7.1.

MoClo is a modular multi-part DNA assembly method, whose framework of specified steps, rules and design constrains including predefined fusion sites allow a highly efficient multipart assembly of individual constructs or combinatorial constructs. However, these benefits come with certain drawbacks like the fixed 'scar' sequences found in between parts in the assembled construct, the required used of suitable assembly donor and acceptor vectors, and to prepare the sequence of interest to the appropriate MoClo format. Whereas in comparison to modular DNA assembly methods, non-modular DNA assembly methods rely on sequence overlaps to direct assembly, and have a greater need for custom oligonucleotide primers (at least one pair per junction between part) and sequence verification (assembly is done via PCR, which is error-prone) and are less suitable for combinatorial assembly due to lower efficiency (low yield of clones are obtained following transformation so smaller libraries are generated) and a greater potential to bias particularly due to repetitive sequences [75].

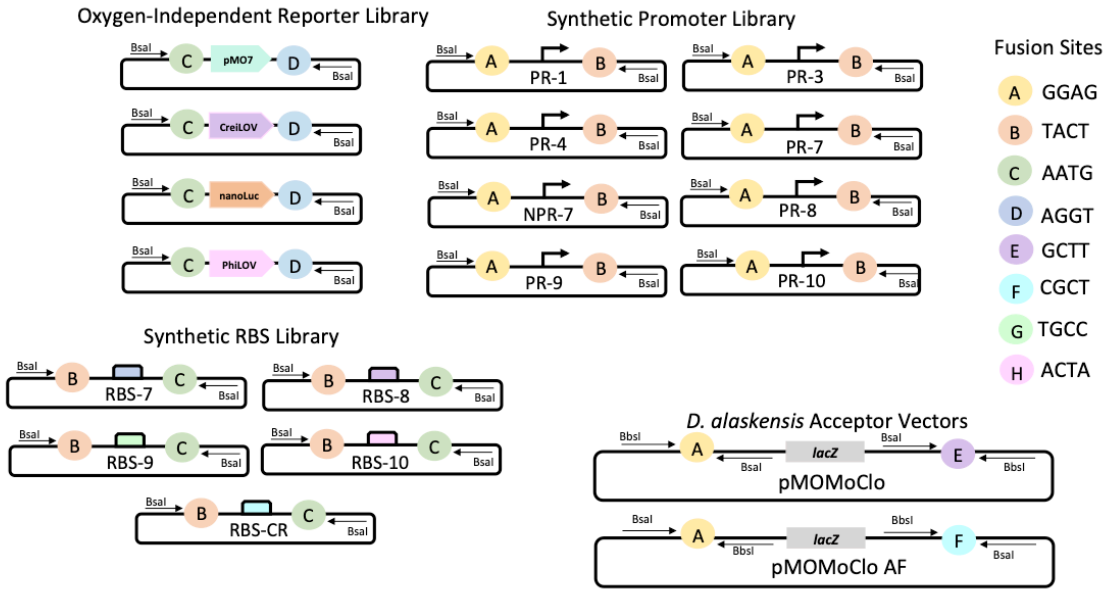

Figure 7. 1. *D. alaskensis* MoClo Toolkit. The toolkit consists two *D. alaskensis* acceptor vectors (single and multi-gene acceptor vectors), an oxygen-independent reporter library, a synthetic promoter library and a synthetic RBS library. The oxygen-independent reporter library consists of: PMO7, CreiLOV (both characterised in *E. coli* and *D. alaskensis*), nanoLUC and phiLOV (both only characterised in *E. coli*). The synthetic promoter library consists of: 8 different constitutive promoters characterised in *D. alaskensis*. The synthetic RBS library consists of: 5 different RBS characterised in *D. alaskensis*.

The ultimate aim of this thesis was to accelerate the research of heavy metal bioremediation and NP synthesis. The use of the *D. alakensis* MoClo toolkit as a method to assemble a NiFe hydrogenase combinatorial library was proven to be an easy, time and cost effective method, since the project took less than 6 months from conception to completion. This proof of concept project set the precedent for future similar projects, where multiple combinatorial libraries of NP synthesis genes can be assembled.

Genes of interest were identified through proteomic analysis of *D. alaskensis* in response to platinum and palladium [20]. This study highlighted proteins involved in both the reductive pathways and the wider stress-response systems of *D. alaskensis* to platinum and palladium [20]. This same study found 7 proteins that were specific to either platinum or palladium (Protein ID: Pt, Dde_2642; Dde_2137; Dde_2138; Dde_0168; Dde_1279; Dde_1545; Dde_1214. Pd, Dde_0444; Dde_2315; Dde_3028; Dde_1618; Dde_ 2641; Dde_2200; Dde_1699) [20]. Great opportunity lies on the overexpression or deletion of these specific proteins, since a potential NP size and morphology change could occur when the above proteins' expression rate or lack thereof changes in comparison to the wildtype. From the aforementioned proteins, it is advised to first test those with the highest reported protein abundance in presence of Pt, and Pd: (Protein ID: Pt, Dde_2642; Dde_0168. Pd, Dde_0444; Dde_2315.) [20].

Following the synthetic biology's cycle (design, build and test), insurmountable data and knowledge can be generated by utilising the *D. alaskensis* MoClo toolkit. In collaboration with research facilities specialised in the assembly of large plasmid libraries, that use highly automated platforms, like the Edinburgh Genome Foundry (EGF). Automated laboratories and facilities use acoustic droplet ejection (ADE) coupled with DNA assembly methods like Golden Gate Type IIs (MoClo). Acoustic droplet ejection is a liquid handling technology that uses acoustic sound waves to rapidly move low-volumes (nL – pL) without any physical contact [223]. Liquid handling technologies like ADE, increase operational speeds, reduce the working volumes (particularly of enzymes and reagents, making it cost-effective), reduce the need for a generally error-prone human handling, and ultimately contribute to substantial workflow cost savings [223].

For this future project, plasmids containing the proteins of interest will be assembled under the control of different expression control elements. The combinatorial library sequentially can be transformed into *D.* alaskensis. Using *D. alaskensis* cultures inserted with the plasmids, biogenic NPs are synthesised and then characterised using TEM and colorimetric assays. The characterisation of biogenic NPs synthesised by *D. alaskensis* inserted with all the plasmids of a combinatorial library has a downside. As concluded on Chapter 7, the use of colorimetric assays to characterise biogenic NPs is not entirely accurate, since they are not monodisperse in size and values are not statistically significant among the samples tested. To characterise biogenic NPs synthesised using large combinatorial libraries it is imperative to use more accurate and rapid screening methods. These methods can help narrow the number of plasmids (in a large combinatorial library) to be further analysed (particularly for TEM imaging). The advised protocol for this project is illustrated on Figure 7.2.

With the *D. alaskensis* MoClo toolkit, any future user can easily design and rapidly characterise new synthetic promoter, RBS and terminator libraries, that can be utilised in future for biogenic NP synthesis research. In this thesis, synthetic promoters with a rational minimal design were characterised and used for NP synthesis. In the future it is advised to design promoter libraries with other designs (native design, and different promoter architecture). Moreover, the design of positively and negatively regulated promoters can be achieved and tested, in an attempt to tightly regulate *D. alaskensis* NP synthesis.

Additionally, this thesis provides a characterised oxygen-independent reporter library specifically engineered for *D. alaskensis*. Since there is a need of oxygen-independent reporters, to enable researchers and industry stakeholders to study synthetic biology applications in anaerobic environments, the Horsfall Lab is further testing the oxygen-independent reporter library with other research and industrially relevant anaerobic microorganisms.

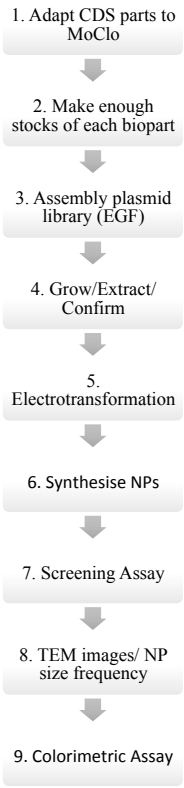

Figure 7. 2. Proposed protocol for rapid assembly and testing of combinatorial libraries. (1.) CDS of interest are adapted to MoClo standards following previously mentioned protocols (Chapter 2). (2.) Equimolar stocks of all necessary bioparts are made. (3.) Using automated laboratory facilities, and their nanoliquid dispensers assemble libraries, using the equimolar bioparts' stocks and following the MoClo assembly protocol (Chapter 2, Section 2.2.9). (4.) White colonies are selected, cultured, plasmid extracted and confirmed by sequencing. (5.) One plasmid of each CDS (all with the same expression control elements) is electrotransformed into *D. alaskensis*, following the aforementioned protocol (Chapter 2, Section 2.4.2). (6.) Biogenic NPs are synthesised following the previously mentioned protocol (Chapter 2, Section 2.9.5). (7.) Rapid and accurate screening of the catalytic activity of the biogenic NPs is done with the following methods: scanning electrochemical cell microscopy [220] and surface plasmon resonance [221]. Results are analysed and compared to select an ideal CDS. Repeat step 5 and 6 with the rest of the plasmids from expressing the selected CDS. (8.) NP size frequency is calculated using TEM images (Chapter 2, Section 2.9.6) (9.) Conduct a colorimetric assay to analyse the biogenic NPs catalytic activity.

Appendix – Additional Data

Table A-1. Chapter 3 Relevant Absorbance Values (Average OD_{600})

Figure 3.13. Average Absorbance Values

	Values		Values		Values		Values
pMO9075	0.710	pMO9075	0.710	pMO9075	0.710	pMO9075	0.710
pMO4	0.693	pMO6	0.544	pMO7	0.516	pMO9	0.564
pMO5	0.557	pMO11	0.530	pMO8	0.552	pMO10	0.633
pMO12	0.628						

Figure 3.14. Average Absorbance Values

	Abs		Abs		Abs		Abs
pMO9075	0.288	pMO9075	0.288	pMO9075	0.288	pMO9075	0.288
pMO4	0.199	pMO6	0.318	pMO7	0.317	pMO9	0.383
pMO5	0.276	pMO11	0.389	pMO8	0.335	pMO10	0.313
pMO12	0.342						

Figure 3.15. Average Absorbance Values

	Abs		Abs		Abs
pMO9075	0.161	pMO9075	0.161	pMO9075	0.161
pMO4	0.165	pMO6	0.077	pMO1	0.139
pMO5	0.077	pMO11	0.070	pMO2	0.125
pMO12	0.097			pMO3	0.133

	Abs		Abs
pMO9075	0.161	pMO9075	0.161
pMO7	0.022	pMO9	0.171
pMO8	0.019	pMO10	0.043

Figure 3.17. Average Absorbance Values

	Abs		Abs		Abs
pMO9075	0.180	pMO9075	0.106	pMO9075	0.204
pMO7 SS	0.184	CreiLOV SS	0.108	pMO8 SS	0.199
pMO7 MS	0.172	CreiLOV MS	0.102	pMO8 MS	0.214
pMO7 LS	0.178	CreiLOV LS	0.106	pMO8 LS	0.207
pMO7 Kan	0.170	CreiLOV Kan	0.265	pMO8 Kan	0.211

Table A-2. Chapter 4 Relevant Absorbance Values (Average OD_{600})

Figure 4.2. Average Absorbance Values

A.	Abs	B.	Abs
pMO9075	0.285	pMO9075	0.268
RBS-7	0.247	RBS-7	0.227
RBS-8	0.230	RBS-8	0.236
RBS-9	0.264	RBS-9	0.193
RBS-10	0.235	RBS-10	0.249
RBS-CR	0.279	RBS-CR	0.214

Figure 4.3. Average Absorbance Values

A.	Abs	B.	Abs
pMO9075	0.345	pMO9075	0.154
PR-1	0.316	PR-1	0.192
PR-3	0.301	PR-3	0.165
PR-4	0.290	PR-4	0.150
PR-7	0.297	PR-7	0.143
NPR-7	0.314	NPR-7	0.150
PR-8	0.346	PR-9	0.121
PR-9	0.357		
PR-10	0.278		

References

[1] Faramarzi, M. A., and Sadighi, A. (2013) Insights into biogenic and chemical production of inorganic nanomaterials and nanostructures, *Adv Colloid Interface Sci 189-190*, 1-20.

[2] Schrofel, A., Kratosova, G., Safarik, I., Safarikova, M., Raska, I., and Shor, L. M. (2014) Applications of biosynthesized metallic nanoparticles - a review, *Acta Biomater 10*, 4023-4042.

[3] Singh, S. N., and Tripathi, R. D. (2012) *Environmental Bioremediation Technologies*, Springer.

[4] Bruins, M. R., Kapil, S., and Oehme, F. W. (2000) Microbial resistance to metals in the environment, *Ecotoxicol Environ Saf 45*, 198-207.

[5] Capeness, M. J., Edmundson, M. C., and Horsfall, L. E. (2015) Nickel and platinum group metal nanoparticle production by Desulfovibrio alaskensis G20, *N Biotechnol 32*, 727-731.

[6] Park, T. J., Lee, S. Y., Heo, N. S., and Seo, T. S. (2010) In vivo synthesis of diverse metal nanoparticles by recombinant Escherichia coli, *Angew Chem Int Ed Engl 49*, 7019-7024.

[7] Pantidos, N., and Horsfall, L. E. (2014) Biological Synthesis of Metallic Nanoparticles by Bacteria, Fungi and Plants, *Journal of Nanomedicine & Nanotechnology 05*.

[8] Deplanche, K., Caldelari, I., Mikheenko, I. P., Sargent, F., and Macaskie, L. E. (2010) Involvement of hydrogenases in the formation of highly catalytic Pd(0) nanoparticles by bioreduction of Pd(II) using Escherichia coli mutant strains, *Microbiology 156*, 2630-2640.

[9] Cai, J., Kimura, S., Wada, M., and Kuga, S. (2009) Nanoporous Cellulose as Metal Nanoparticles Support, *Biomacromolecules 10*, 87-94.

[10] Das, V. L., Thomas, R., Varghese, R. T., Soniya, E. V., Mathew, J., and Radhakrishnan, E. K. (2014) Extracellular synthesis of silver nanoparticles by the Bacillus strain CS 11 isolated from industrialized area, *3 Biotech 4*, 121-126.

[11] Cueva, M. E., and Horsfall, L. E. (2017) The contribution of microbially produced nanoparticles to sustainable development goals, *Microb Biotechnol 10*, 1212-1215.

[12] Hulkoti, N. I., and Taranath, T. C. (2014) Biosynthesis of nanoparticles using microbes- a review, *Colloids Surf B Biointerfaces 121*, 474-483.

[13] Lovley, D. R., Widman, P. K., Woodward, J. C., and Phillips, E. J. P. (1993) Reduction of Uranium by Cytochrome C3 of Desulfovibrio vulgaris, *Appl Environ Microbiol 59*, 3572-3576.

[14] Lloyd, J. R., Ridley, J., Khizniak, T., Lyalikova, N. N., and Macaskie1, L. E. (1999) Reduction of Technetium by Desulfovibrio desulfuricans: Biocatalyst Characterization and Use in a Flowthrough Bioreactor, *Appl Environ Microbiol 65*, 2691–2696.

[15] Lloyd, J. R., Yong, P., and Macaskie, L. E. (1998) Enzymatic Recovery of Elemental Palladium by Using Sulfate-Reducing Bacteria, *Appl Environ Microbiol 64*, 4607–4609.

[16] Chardin, B., Dolla, A., Chaspoul, F., Fardeau, M. L., Gallice, P., and Bruschi, M. (2002) Bioremediation of chromate: thermodynamic analysis of the

effects of Cr(VI) on sulfate-reducing bacteria, *Appl Microbiol Biotechnol 60*, 352-360.

[17] Payne, R. B., Gentry, D. M., Rapp-Giles, B. J., Casalot, L., and Wall, J. D. (2002) Uranium Reduction by Desulfovibrio desulfuricans Strain G20 and a Cytochrome c3 Mutant, *Applied and Environmental Microbiology 68*, 3129-3132.

[18] Hauser, L. J., Land, M. L., Brown, S. D., Larimer, F., Keller, K. L., Rapp-Giles, B. J., Price, M. N., Lin, M., Bruce, D. C., Detter, J. C., Tapia, R., Han, C. S., Goodwin, L. A., Cheng, J. F., Pitluck, S., Copeland, A., Lucas, S., Nolan, M., Lapidus, A. L., Palumbo, A. V., and Wall, J. D. (2011) Complete genome sequence and updated annotation of Desulfovibrio alaskensis G20, *J Bacteriol 193*, 4268-4269.

[19] Weimer, P. J., Kavelaar, M. J. V., Michel, C. B., and NG, T. K. (1988) Effect of Phosphate on the Corrosion of Carbon Steel and on the Composition of Corrosion Products in Two-Stage Continuous Cultures of Desulfovibrio desulfuricans, *Applied and Environmental Microbiology 54*, 386-396.

[20] Capeness, M. J., Imrie, L., Muhlbauer, L. F., Le Bihan, T., and Horsfall, L. E. (2019) Shotgun proteomic analysis of nanoparticle-synthesizing Desulfovibrio alaskensis in response to platinum and palladium, *Microbiology*.

[21] Yong, P., Mikheenko, I. P., Deplanche, K., Redwood, M. D., and Macaskie, L. E. (2010) Biorefining of precious metals from wastes: an answer to manufacturing of cheap nanocatalysts for fuel cells and power generation via an integrated biorefinery?, *Biotechnol Lett 32*, 1821-1828.

[22] Mabbett, A. N., Sanyahumbi, D., Yong, P., and Macaskie, L. E. (2006) Biorecovered Precious Metals from Industrial Wastes: Single-Step Conversion of a Mixed Metal Liquid Waste to a Bioinorganic Catalyst with Environmental Application, *Environmental Science and Technology 40*, 1015-1021.

[23] Elias, D. A., Suflita, J. M., McInerney, M. J., and Krumholz, L. R. (2004) Periplasmic Cytochrome c3 of Desulfovibrio vulgaris Is Directly Involved in H2-Mediated Metal but Not Sulfate Reduction, *Applied and Environmental Microbiology 70*, 413-420.

[24] Rapp-Giles, B. J., Casalot, L., English, R. S., Joseph A. Ringbauer, J., Dolla, A., and Wall, J. D. (2000) Cytochrome c3 Mutants of Desulfovibrio desulfuricans, *Appl Environ Microbiol 66*, 671–677.

[25] Bunge, M., Sobjerg, L. S., Rotaru, A. E., Gauthier, D., Lindhardt, A. T., Hause, G., Finster, K., Kingshott, P., Skrydstrup, T., and Meyer, R. L. (2010) Formation of palladium(0) nanoparticles at microbial surfaces, *Biotechnol Bioeng 107*, 206-215.

[26] Gopal, J., Hasan, N., Manikandan, M., and Wu, H. F. (2013) Bacterial toxicity/compatibility of platinum nanospheres, nanocuboids and nanoflowers, *Sci Rep 3*, 1260.

[27] Rosenberg, B., Renshaw, E., Vancamp, L., Hartwick, J., and Drobnik, J. (1967) Platinum-Induiced Filamentous Growth in Escherichia coli, *Journal of Bacteriology 93*, 716-721.

[28] Glaister, B. J., and Mudd, G. M. (2010) The environmental costs of platinum–PGM mining and sustainability: Is the glass half-full or half-empty?, *Minerals Engineering 23*, 438-450.
[29] Macaskie, L. E., Mikheenko, I. P., Yong, P., Deplanche, K., Murray, A. J., Paterson-Beedle, M., Coker, V. S., Pearce, C. I., Cutting, R., Pattrick, R. A. D., Vaughan, D., van der Laan, G., and Lloyd, J. R. (2010) Today's wastes, tomorrow's materials for environmental protection, *Hydrometallurgy 104*, 483-487.
[30] Ilhan, S., Nourbakhsh, M. N., Kiliçarslan, S., and Ozdag, H. (2004) Removal of chromİum, lead and copper ions from industrial waste waters by staphylococcus saprophyticus, *Turkish Electronic Journal of Biotechnology 2*, 50-57.
[31] Pollmann, K., Raff, J., Merroun, M., Fahmy, K., and Selenska-Pobell, S. (2006) Metal binding by bacteria from uranium mining waste piles and its technological applications, *Biotechnol Adv 24*, 58-68.
[32] Wall, J. D., Rapp-Giles, B. J., and Rousset, M. (1993) CharacterizationofaSmallPlasmidfromDesulfovibrio desulfuricans and Its Use for Shuttle Vector Construction, *Journal of Bacteriology 175*, 4121-4128.
[33] Groh, J. L., Luo, Q., Ballard, J. D., and Krumholz, L. R. (2005) A method adapting microarray technology for signature-tagged mutagenesis of Desulfovibrio desulfuricans G20 and Shewanella oneidensis MR-1 in anaerobic sediment survival experiments, *Appl Environ Microbiol 71*, 7064-7074.
[34] Pereira, P. M., He, Q., Valente, F. M., Xavier, A. V., Zhou, J., Pereira, I. A., and Louro, R. O. (2008) Energy metabolism in Desulfovibrio vulgaris Hildenborough: insights from transcriptome analysis, *Antonie Van Leeuwenhoek 93*, 347-362.
[35] Gupta, R. D. (2000) The phylogeny of proteobacteria: relationships to other eubacterial phyla and eukaryotes, *FEMS Microbiology Reviews 24*, 361-402.
[36] Edmundson, M. C., Capeness, M., and Horsfall, L. (2014) Exploring the potential of metallic nanoparticles within synthetic biology, *N Biotechnol 31*, 572-578.
[37] Keasling, J. (2006) The Promise of Synthetic Biology, In *Frontiers of Engineering: Reports on Leading-Edge Engineering from the 2005 Symposium* (Engineering, N. A. o., Ed.), National Academies Press.
[38] Baldwin, G., Bayer, T., Dickinson, R., Ellis, T., Freemont, P. S., Kitney, R. I., Polizzi, K., and Stan, G.-B. (2015) *Synthetic Biology — A Primer*, Imperial College Press.
[39] Ellis, T., Adie, T., and Baldwin, G. S. (2011) DNA assembly for synthetic biology: from parts to pathways and beyond, *Integr Biol (Camb) 3*, 109-118.
[40] Zhang, W., and Nielsen, D. R. (2014) Synthetic biology applications in industrial microbiology, *Front Microbiol 5*, 451.
[41] Adkins, J., Pugh, S., McKenna, R., and Nielsen, D. R. (2012) Engineering microbial chemical factories to produce renewable "biomonomers", *Front Microbiol 3*, 313.
[42] Lamsen, E. N., and Atsumi, S. (2012) Recent progress in synthetic biology for microbial production of C3-C10 alcohols, *Front Microbiol 3*, 196.

[43] Lee, S. J., Lee, S. J., and Lee, D. W. (2013) Design and development of synthetic microbial platform cells for bioenergy, *Front Microbiol 4*, 92.
[44] Weber, W., and Fussenegger, M. (2011) Emerging biomedical applications of synthetic biology, *Nature Reviews Genetics 13*, 21-35.
[45] Tumpey, T. M., Basler, C. F., Aguilar, P. V., Zeng, H., Solorzano, A., Swayne, D. E., Cox, N. J., Katz, J. M., Taubenberger, J. K., Palese, P., and Garcıa-Sastre, A. (2005) Characterization of the Reconstructed 1918 Spanish Influenza Pandemic Virus, *Science 310*, 77-80.
[46] Yang, J., and Reth, M. (2010) Oligomeric organization of the B-cell antigen receptor on resting cells, *Nature 467*, 465-469.
[47] Wise de Valdez, M. R., Nimmo, D., Betz, J., Gong, H. F., James, A. A., Alphey, L., and Black, W. C. t. (2011) Genetic elimination of dengue vector mosquitoes, *Proc Natl Acad Sci U S A 108*, 4772-4775.
[48] Weber, W., and Fussenegger, M. (2009) The impact of synthetic biology on drug discovery, *Drug Discov Today 14*, 956-963.
[49] Weber, W., Schoenmakers, R., Keller, B., Gitzinger, M., Grau, T., Baba, M. D.-E., Sander, P., and Fussenegger, M. (2008) A synthetic mammalian gene circuit reveals antituberculosis compounds, *PNAS 105*, 9994–9998.
[50] Ro, D. K., Paradise, E. M., Ouellet, M., Fisher, K. J., Newman, K. L., Ndungu, J. M., Ho, K. A., Eachus, R. A., Ham, T. S., Kirby, J., Chang, M. C., Withers, S. T., Shiba, Y., Sarpong, R., and Keasling, J. D. (2006) Production of the antimalarial drug precursor artemisinic acid in engineered yeast, *Nature 440*, 940-943.
[51] Ajikumar, P. K., Xiao, W. H., Tyo, K. E., Wang, Y., Simeon, F., Leonard, E., Mucha, O., Phon, T. H., Pfeifer, B., and Stephanopoulos, G. (2010) Isoprenoid pathway optimization for Taxol precursor overproduction in Escherichia coli, *Science 330*, 70-74.
[52] Kämpf, M. M., Christen, E. H., Ehrbar, M., Baba, M. D.-E., Hamri, G. C.-E., Fussenegger, M., and Weber, W. (2010) A Gene Therapy Technology-Based Biomaterial for the Trigger-Inducible Release of Biopharmaceuticals in Mice, *Advanced Functional Materials 20*, 2534-2538.
[53] Forbes, N. S. (2010) Engineering the perfect (bacterial) cancer therapy, *Nat Rev Cancer 10*, 785-794.
[54] Bereza-Malcolm, L. T., Mann, G., and Franks, A. E. (2015) Environmental sensing of heavy metals through whole cell microbial biosensors: a synthetic biology approach, *ACS Synth Biol 4*, 535-546.
[55] Aleksic, J., de Mora, K., Millar, A., Davidson, B., Kozma-Bognar, L., Ma, H., French, C., Bizzari, F., Elfick, A., Wilson, J., Cai, Y., Seshasayee, S. L., Nicholson, J., and Ivakhno, S. (2007) Development of a novel biosensor for the detection of arsenic in drinking water, *IET Synthetic Biology 1*, 87-90.
[56] Wan, X., Volpetti, F., Petrova, E., French, C., Maerkl, S. J., and Wang, B. (2019) Cascaded amplifying circuits enable ultrasensitive cellular sensors for toxic metals, *Nat Chem Biol*.
[57] Diep, P., Mahadevan, R., and Yakunin, A. F. (2018) Heavy Metal Removal by Bioaccumulation Using Genetically Engineered Microorganisms, *Front Bioeng Biotechnol 6*, 157.

[58] Dvorak, P., Nikel, P. I., Damborsky, J., and de Lorenzo, V. (2017) Bioremediation 3.0: Engineering pollutant-removing bacteria in the times of systemic biology, *Biotechnol Adv 35*, 845-866.
[59] Gilbert, E. S., Walker, A. W., and Keasling, J. D. (2003) A constructed microbial consortium for biodegradation of the organophosphorus insecticide parathion, *Appl Microbiol Biotechnol 61*, 77-81.
[60] Purnick, P. E., and Weiss, R. (2009) The second wave of synthetic biology: from modules to systems, *Nat Rev Mol Cell Biol 10*, 410-422.
[61] Anderson, J. C., Dueber, J. E., Leguia, M., Wu, G. C., Goler, J. A., Arkin, A. P., and Keasling, J. D. (2010) BglBricks: A flexible standard for biological part assembly, *Journal of Biological Engineering 4*.
[62] Horton, R. M., Hunt, H. D., Ho, S. N., Pullen, J. K., and Pease, L. R. (1989) Engineering hybrid genes without the use of restriction enzymes: gene splicing by overlap extension, *Gene 77*, 61-68.
[63] Quan, J., and Tian, J. (2009) Circular Polymerase Extension Cloning of Complex Gene Libraries and Pathways, *PLoS One 4*.
[64] Way, J. C., Collins, J. J., Keasling, J. D., and Silver, P. A. (2014) Integrating biological redesign: where synthetic biology came from and where it needs to go, *Cell 157*, 151-161.
[65] Gibson, D. G., Young, L., Chuang, R. Y., Venter, J. C., Hutchison, C. A., 3rd, and Smith, H. O. (2009) Enzymatic assembly of DNA molecules up to several hundred kilobases, *Nat Methods 6*, 343-345.
[66] Iverson, S. V., Haddock, T. L., Beal, J., and Densmore, D. M. (2016) CIDAR MoClo: Improved MoClo Assembly Standard and New E. coli Part Library Enable Rapid Combinatorial Design for Synthetic and Traditional Biology, *ACS Synth Biol 5*, 99-103.
[67] Patron, N. J. (2016) Blueprints for green biotech: development and application of standards for plant synthetic biology, *Biochem Soc Trans 44*, 702-708.
[68] Casini, A., Storch, M., Baldwin, G. S., and Ellis, T. (2015) Bricks and blueprints: methods and standards for DNA assembly, *Nat Rev Mol Cell Biol 16*, 568-576.
[69] Trubitsyna, M., Michlewski, G., Cai, Y., Elfick, A., and French, C. E. (2014) PaperClip: rapid multi-part DNA assembly from existing libraries, *Nucleic Acids Res 42*, e154.
[70] Breitling, R., and Takano, E. (2015) Synthetic biology advances for pharmaceutical production, *Curr Opin Biotechnol 35*, 46-51.
[71] Lee, M. E., DeLoache, W. C., Cervantes, B., and Dueber, J. E. (2015) A Highly Characterized Yeast Toolkit for Modular, Multipart Assembly, *ACS Synth Biol 4*, 975-986.
[72] Larroude, M., Park, Y. K., Soudier, P., Kubiak, M., Nicaud, J. M., and Rossignol, T. (2019) A modular Golden Gate toolkit for Yarrowia lipolytica synthetic biology, *Microb Biotechnol*.
[73] Moore, S. J., Lai, H. E., Kelwick, R. J., Chee, S. M., Bell, D. J., Polizzi, K. M., and Freemont, P. S. (2016) EcoFlex: A Multifunctional MoClo Kit for E. coli Synthetic Biology, *ACS Synth Biol 5*, 1059-1069.
[74] Andreou, A. I., and Nakayama, N. (2018) Mobius Assembly: A versatile Golden-Gate framework towards universal DNA assembly, *PLoS One 13*, e0189892.

[75] Taylor, G. M., Mordaka, Paweł M., and Heap, J. T. (2018) Start-Stop Assembly: a functionally scarless DNA assembly system optimized for metabolic engineering, *Nucleic Acids Research*.
[76] Engler, C., Youles, M., Gruetzner, R., Ehnert, T. M., Werner, S., Jones, J. D., Patron, N. J., and Marillonnet, S. (2014) A golden gate modular cloning toolbox for plants, *ACS Synth Biol 3*, 839-843.
[77] Martella, A., Matjusaitis, M., Auxillos, J., Pollard, S. M., and Cai, Y. (2017) EMMA: An Extensible Mammalian Modular Assembly Toolkit for the Rapid Design and Production of Diverse Expression Vectors, *ACS Synth Biol 6*, 1380-1392.
[78] Crozet, P., Navarro, F. J., Willmund, F., Mehrshahi, P., Bakowski, K., Lauersen, K. J., Perez-Perez, M. E., Auroy, P., Gorchs Rovira, A., Sauret-Gueto, S., Niemeyer, J., Spaniol, B., Theis, J., Trosch, R., Westrich, L. D., Vavitsas, K., Baier, T., Hubner, W., de Carpentier, F., Cassarini, M., Danon, A., Henri, J., Marchand, C. H., de Mia, M., Sarkissian, K., Baulcombe, D. C., Peltier, G., Crespo, J. L., Kruse, O., Jensen, P. E., Schroda, M., Smith, A. G., and Lemaire, S. D. (2018) Birth of a Photosynthetic Chassis: A MoClo Toolkit Enabling Synthetic Biology in the Microalga Chlamydomonas reinhardtii, *ACS Synth Biol*.
[79] Mordaka, P. M., and Heap, J. T. (2018) Stringency of Synthetic Promoter Sequences in Clostridium Revealed and Circumvented by Tuning Promoter Library Mutation Rates, *ACS Synth Biol 7*, 672-681.
[80] Marchisio, M. A. (2018) *Introduction to Synthetic Biology: About Modeling, Computation, and Circuit Design*, Springer.
[81] Feklistov, A., Sharon, B. D., Darst, S. A., and Gross, C. A. (2014) Bacterial sigma factors: a historical, structural, and genomic perspective, *Annu Rev Microbiol 68*, 357-376.
[82] Kazakov, A. E., Rajeev, L., Chen, A., Luning, E. G., Dubchak, I., Mukhopadhyay, A., and Novichkov, P. S. (2015) sigma54-dependent regulome in Desulfovibrio vulgaris Hildenborough, *BMC Genomics 16*, 919.
[83] Buck, M., Gallegos, M. T., Strudholme, D. J., Guo, Y., and Gralla, J. D. (2000) The Bacterial Enhancer-Dependent ?54 (?N) Transcription Factor, *JOURNAL OF BACTERIOLOGY 182*, 4129-4136.
[84] Gilman, J., and Love, J. (2016) Synthetic promoter design for new microbial chassis, *Biochem Soc Trans 44*, 731-737.
[85] Blazeck, J., and Alper, H. S. (2013) Promoter engineering: Recent advances in controlling transcription at the most fundamental level, *Biotechnol J 8*, 46-58.
[86] Smale, S. T., and Kadonaga, J. T. (2003) The RNA polymerase II core promoter, *Annu Rev Biochem 72*, 449-479.
[87] Murakami, K. S., and Darst, S. A. (2003) Bacterial RNA polymerases: the wholo story, *Current Opinion in Structural Biology 13*, 31-39.
[88] Saecker, R. M., Record, M. T., Jr., and Dehaseth, P. L. (2011) Mechanism of bacterial transcription initiation: RNA polymerase - promoter binding, isomerization to initiation-competent open complexes, and initiation of RNA synthesis, *J Mol Biol 412*, 754-771.
[89] Hook-Barnard, I. G., and Hinton, D. M. (2009) The promoter spacer influences transcription initiation via sigma70 region 1.1 of Escherichia coli RNA polymerase, *Proc Natl Acad Sci U S A 106*, 737-742.

[90] Shultzaberger, R. K., Chen, Z., Lewis, K. A., and Schneider, T. D. (2007) Anatomy of Escherichia coli sigma70 promoters, *Nucleic Acids Res 35*, 771-788.
[91] Campagne, S., Marsh, M. E., Capitani, G., Vorholt, J. A., and Allain, F. H. (2014) Structural basis for -10 promoter element melting by environmentally induced sigma factors, *Nat Struct Mol Biol 21*, 269-276.
[92] Mulligan, M. E., Brosius, J., and McClure, W. R. (1985) Characterization in Vitro of the Effect of Spacer Lengoth on the Activity of Escherichia Coli RNA Polymerase at the TAC promoter, *The Journal of Biological Chemistry 260*, 3529-3538.
[93] Singh, S. S., Typas, A., Hengge, R., and Grainger, D. C. (2011) Escherichia coli sigma70 senses sequence and conformation of the promoter spacer region, *Nucleic Acids Res 39*, 5109-5118.
[94] Alper, H., Fischer, C., Nevoigt, E., and Stephanopoulos, G. (2005) Tuning genetic control through promoter engineering, *PNAS 102*, 12678–12683.
[95] Jensen, P. R., and Hammer, K. (1998) The Sequence of Spacers between the Consensus Sequences Modulates the Strength of Prokaryotic Promoters, *Appl Environ Microbiol 64*, 82–87.
[96] Boer, H. A. D., Comstock, L. J., and Vasser, M. (1983) The tac promoter: A functional hybrid derived from the trp and lac promoters, *PNAS 80*, 21-25.
[97] Haldimann, A., Daniels, L. L., and Wanner, B. L. (1998) Use of New Methods for Construction of Tightly Regulated Arabinose and Rhamnose Promoter Fusions in Studies of the Escherichia coli Phosphate Regulon, *Journal of Bacteriology 180*, 1277–1286.
[98] Solovyev, V., and Salamov, A. (2011) Automatic Annotation of Microbial Genomes and Metagenomic Sequences, In *Metagenomics and its Applications in Agriculture, Biomedicine and Environmental Studies* (Li, R. W., Ed.), pp 61-78, Nova Science Publishers.
[99] de Avila, E. S. S., Echeverrigaray, S., and Gerhardt, G. J. (2011) BacPP: bacterial promoter prediction--a tool for accurate sigma-factor specific assignment in enterobacteria, *J Theor Biol 287*, 92-99.
[100] Reese, M. G. (2001) Application of a time-delay neural network to promoter annotation in the Drosophila melanogaster genome, *Computer and Chemistry 26*, 51–56.
[101] Klucar, L., Stano, M., and Hajduk, M. (2010) phiSITE: database of gene regulation in bacteriophages, *Nucleic Acids Res 38*, D366-370.
[102] Jong, A. d., Pietersma, H., Cordes, M., Kuipers, O. P., and Kok, J. PePPER: a webserver for prediction of prokaryote promoter elements and regulons, *BMC Genomics 13*.
[103] Mao, X., Ma, Q., Zhou, C., Chen, X., Zhang, H., Yang, J., Mao, F., Lai, W., and Xu, Y. (2014) DOOR 2.0: presenting operons and their functions through dynamic and integrated views, *Nucleic Acids Res 42*, D654-659.
[104] Munch, R., Hiller, K., Grote, A., Scheer, M., Klein, J., Schobert, M., and Jahn, D. (2005) Virtual Footprint and PRODORIC: an integrative framework for regulon prediction in prokaryotes, *Bioinformatics 21*, 4187-4189.
[105] Umarov, R. K., and Solovyev, V. V. (2017) Recognition of prokaryotic and eukaryotic promoters using convolutional deep learning neural networks, *PLoS One 12*, e0171410.

[106] Burden, S., Lin, Y. X., and Zhang, R. (2005) Improving promoter prediction for the NNPP2.2 algorithm: a case study using Escherichia coli DNA sequences, *Bioinformatics 21*, 601-607.
[107] Zaide, G., Grosfeld, H., Ehrlich, S., Zvi, A., Cohen, O., and Shafferman, A. (2011) Identification and characterization of novel and potent transcription promoters of Francisella tularensis, *Appl Environ Microbiol 77*, 1608-1618.
[108] Salis, H. M., Mirsky, E. A., and Voigt, C. A. (2009) Automated design of synthetic ribosome binding sites to control protein expression, *Nat Biotechnol 27*, 946-950.
[109] Oesterle, S., Gerngross, D., Schmitt, S., Roberts, T. M., and Panke, S. (2017) Efficient engineering of chromosomal ribosome binding site libraries in mismatch repair proficient Escherichia coli, *Sci Rep 7*, 12327.
[110] Salis, H. M. (2011) The ribosome binding site calculator, *Methods Enzymol 498*, 19-42.
[111] Bonde, M. T., Kosuri, S., Genee, H. J., Sarup-Lytzen, K., Church, G. M., Sommer, M. O., and Wang, H. H. (2015) Direct mutagenesis of thousands of genomic targets using microarray-derived oligonucleotides, *ACS Synth Biol 4*, 17-22.
[112] Bonde, M. T., Pedersen, M., Klausen, M. S., Jensen, S. I., Wulff, T., Harrison, S., Nielsen, A. T., Herrgard, M. J., and Sommer, M. O. (2016) Predictable tuning of protein expression in bacteria, *Nat Methods 13*, 233-236.
[113] Jeschek, M., Gerngross, D., and Panke, S. (2016) Rationally reduced libraries for combinatorial pathway optimization minimizing experimental effort, *Nat Commun 7*, 11163.
[114] Na, D., and Lee, D. (2010) RBSDesigner: software for designing synthetic ribosome binding sites that yields a desired level of protein expression, *Bioinformatics 26*, 2633-2634.
[115] Reeve, B., Hargest, T., Gilbert, C., and Ellis, T. (2014) Predicting translation initiation rates for designing synthetic biology, *Front Bioeng Biotechnol 2*, 1.
[116] Markley, A. L., Begemann, M. B., Clarke, R. E., Gordon, G. C., and Pfleger, B. F. (2015) Synthetic biology toolbox for controlling gene expression in the cyanobacterium Synechococcus sp. strain PCC 7002, *ACS Synth Biol 4*, 595-603.
[117] Kelly, J. R., Rubin, A. J., Davis, J. H., Ajo-Franklin, C. M., Cumbers, J., Czar, M. J., de Mora, K., Glieberman, A. L., Monie, D. D., and Endy, D. (2009) Measuring the activity of BioBrick promoters using an in vivo reference standard, *J Biol Eng 3*, 4.
[118] Yang, S., Liu, Q., Zhang, Y., Du, G., Chen, J., and Kang, Z. (2018) Construction and Characterization of Broad-Spectrum Promoters for Synthetic Biology, *ACS Synth Biol 7*, 287-291.
[119] Markakis, K., De Las Heras, A., and Elfick, A. (2017) Analytical approach for the calculation of promoter activities based on fluorescent protein expression data, *Engineering Biology 1*, 77-85.
[120] Hwang, H. J., Lee, S. Y., and Lee, P. C. (2018) Engineering and application of synthetic nar promoter for fine-tuning the expression of metabolic pathway genes in Escherichia coli, *Biotechnol Biofuels 11*, 103.

[121] Platteeuw, C., Simons, G., and Vos, W. M. D. (1994) Use of the Escherichia coli 13-Glucuronidase (gusA) Gene as a Reporter Gene for Analyzing Promoters in Lactic Acid Bacteria, *Appl Environ Microbiol 60*, 587-593.
[122] Feustel, L., Nakotte, S., and Durre, P. (2004) Characterization and Development of Two Reporter Gene Systems for Clostridium acetobutylicum, *Applied and Environmental Microbiology 70*, 798-803.
[123] Edwards, A. N., Pascual, R. A., Childress, K. O., Nawrocki, K. L., Woods, E. C., and McBride, S. M. (2015) An alkaline phosphatase reporter for use in Clostridium difficile, *Anaerobe 32*, 98-104.
[124] Lee, J., Jang, Y. S., Papoutsakis, E. T., and Lee, S. Y. (2016) Stable and enhanced gene expression in Clostridium acetobutylicum using synthetic untranslated regions with a stem-loop, *J Biotechnol 230*, 40-43.
[125] Wood, K. V. (1995) Selection of an optimal reporter gene for cell-based high throughput screening assays., *Curr Opin Biotechnol 6*, 50-58.
[126] Suto, C. M., and Ignar, D. M. (1997) Selection of an Optimal Reporter Gene for Cell-Based High Throughput Screening Assays, *Journal of Biomedical Screening 2*, 7-9.
[127] Naylor, L. H. (1999) Reporter gene technology: the future looks bright, *Biochem Pharmacol 58*, 749-757.
[128] Bronstein, I., Fortin, J., Stanley, P. E., Stewart, G. S. A. B., and Kricka, L. J. (1994) Chemiluminescent and Bioluminescent Reporter Gene Assays, *Analytical Biochemistry 219*, 169-181.
[129] Borkowski, O., Ceroni, F., Stan, G. B., and Ellis, T. (2016) Overloaded and stressed: whole-cell considerations for bacterial synthetic biology, *Curr Opin Microbiol 33*, 123-130.
[130] Buckley, A. M., Petersen, J., Roe, A. J., Douce, G. R., and Christie, J. M. (2015) LOV-based reporters for fluorescence imaging, *Curr Opin Chem Biol 27*, 39-45.
[131] Drepper, T., Eggert, T., Circolone, F., Heck, A., Krauss, U., Guterl, J. K., Wendorff, M., Losi, A., Gartner, W., and Jaeger, K. E. (2007) Reporter proteins for in vivo fluorescence without oxygen, *Nat Biotechnol 25*, 443-445.
[132] Choi, C. H., DeGuzman, J. V., Lamont, R. J., and Yilmaz, O. (2011) Genetic transformation of an obligate anaerobe, P. gingivalis for FMN-green fluorescent protein expression in studying host-microbe interaction, *PLoS One 6*, e18499.
[133] Drepper, T., Huber, R., Heck, A., Circolone, F., Hillmer, A. K., Buchs, J., and Jaeger, K. E. (2010) Flavin mononucleotide-based fluorescent reporter proteins outperform green fluorescent protein-like proteins as quantitative in vivo real-time reporters, *Appl Environ Microbiol 76*, 5990-5994.
[134] Tielker, D., Eichhof, I., Jaeger, K. E., and Ernst, J. F. (2009) Flavin mononucleotide-based fluorescent protein as an oxygen-independent reporter in Candida albicans and Saccharomyces cerevisiae, *Eukaryot Cell 8*, 913-915.
[135] Lobo, L. A., Smith, C. J., and Rocha, E. R. (2011) Flavin mononucleotide (FMN)-based fluorescent protein (FbFP) as reporter for gene expression in the anaerobe Bacteroides fragilis, *FEMS Microbiol Lett 317*, 67-74.

[136] Walter, J., Hausmann, S., Drepper, T., Puls, M., Eggert, T., and Dihne, M. (2012) Flavin mononucleotide-based fluorescent proteins function in mammalian cells without oxygen requirement, *PLoS One 7*, e43921.
[137] Mukherjee, A., Walker, J., Weyant, K. B., and Schroeder, C. M. (2013) Characterization of flavin-based fluorescent proteins: an emerging class of fluorescent reporters, *PLoS One 8*, e64753.
[138] Arinkin, V., Granzin, J., Rollen, K., Krauss, U., Jaeger, K. E., Willbold, D., and Batra-Safferling, R. (2017) Structure of a LOV protein in apo-state and implications for construction of LOV-based optical tools, *Sci Rep 7*, 42971.
[139] Kuroda, K., and Ueda, M. (2011) Molecular design of the microbial cell surface toward the recovery of metal ions, *Curr Opin Biotechnol 22*, 427-433.
[140] Nriagu, J. O., and Pacyna, J. M. (1988) Quantitative assessment of worldwide contamination of air, water and soils by trace metals, *Nature 333*, 134-139.
[141] Kapoor, A., and Viraraghavan, T. (1995) Fungal Biosorption - An Alternative Treatment Option For Heavy Metal Bearing Wastewaters: A Review, *Bioresource Technology 53*, 195-206.
[142] Lovley, D. R., and Coates, J. D. (1997) Bioremediation of metal contamination, *Curr Opin Biotechnol 8*, 285-289.
[143] Lee, S. Y., Choi, J. H., and Xu, Z. (2003) Microbial cell-surface display, *Trends in Biotechnology 21*, 45-52.
[144] Samuelson, P., Gunneriusson, E., Nygren, P.-A., and Sta˚hl, S. (2002) Display of Proteins on Bacteria, *Journal of Biotechnology 96*, 129-154.
[145] Bae, W., Mulchandani, A., and Chen, W. (2002) Cell surface display of synthetic phytochelatins using ice nucleation protein for enhanced heavy metal bioaccumulation, *Journal of Inorganic Biochemistry 88*, 223–227.
[146] Jose, J., and Meyer, T. F. (2007) The autodisplay story, from discovery to biotechnical and biomedical applications, *Microbiol Mol Biol Rev 71*, 600-619.
[147] Schuurmann, J., Quehl, P., Festel, G., and Jose, J. (2014) Bacterial whole-cell biocatalysts by surface display of enzymes: toward industrial application, *Appl Microbiol Biotechnol 98*, 8031-8046.
[148] Saleem, M., Brim, H., Hussain, S., Arshad, M., Leigh, M. B., and Zia ul, H. (2008) Perspectives on microbial cell surface display in bioremediation, *Biotechnol Adv 26*, 151-161.
[149] Kim, E. B., Seo, J. M., Kim, G. W., Lee, S. Y., and Park, T. J. (2016) In vivo synthesis of europium selenide nanoparticles and related cytotoxicity evaluation of human cells, *Enzyme Microb Technol 95*, 201-208.
[150] Valls, M., Atrian, S., Lorenzo, V. d., and Fernández, L. A. (2000) Engineering a mouse metallothionein on the cell surface of Ralstonia eutropha CH34 for immobilization of heavy metals in soil, *Nature Biotechnology 18*, 661-665.
[151] Tsai, D.-Y., Tsai, Y.-J., Yen, C.-H., Ouyang, C.-Y., and Yeh, Y.-C. (2015) Bacterial surface display of metal binding peptides as whole-cell biocatalysts for 4-nitroaniline reduction, *RSC Advances 5*, 87998-88001.
[152] Mejáre, M., and Bülow, L. (2001) Metal-binding proteins and peptides in bioremediation and phytoremediation of heavy metals, *Trends in Biotechnology 19*, 67-73.

[153] Li, X., and Krumholz, L. R. (2007) Regulation of arsenate resistance in Desulfovibrio desulfuricans G20 by an arsRBCC operon and an arsC gene, *J Bacteriol 189*, 3705-3711.
[154] Grote, A., Hiller, K., Scheer, M., Munch, R., Nortemann, B., Hempel, D. C., and Jahn, D. (2005) JCat: a novel tool to adapt codon usage of a target gene to its potential expression host, *Nucleic Acids Res 33*, W526-531.
[155] Fievet, A., Ducret, A., Mignot, T., Valette, O., Robert, L., Pardoux, R., Dolla, A. R., and Aubert, C. (2015) Single-Cell Analysis of Growth and Cell Division of the Anaerobe Desulfovibrio vulgaris Hildenborough, *Front Microbiol 6*, 1378.
[156] Davis, J. H., Rubin, A. J., and Sauer, R. T. (2011) Design, construction and characterization of a set of insulated bacterial promoters, *Nucleic Acids Res 39*, 1131-1141.
[157] Remington, S. J. (2006) Fluorescent proteins: maturation, photochemistry and photophysics, *Curr Opin Struct Biol 16*, 714-721.
[158] Ruhdal, P., and Hammer, K. (1997) The Sequence of Spacers between the Consensus Sequences Modulates the Strength of Prokaryotic Promoters, *Applied and Environmental Microbiology 64*, 82–87.
[159] Mukherjee, A., Weyant, K. B., Walker, J., and Schroeder, C. M. (2012) Directed evolution of bright mutants of an oxygen-independent flavin-binding fluorescent protein from Pseudomonas putida, *JOurnal of Biological Engineering 6*.
[160] Inouye, S., Umesono, K., and Tsuji, F. I. (1999) Special Properties of Green Fluorescent Protein-S54A, In Mutant and Variants of GFP, In *Methods in Enzymology*, pp 444-449, Academic Press.
[161] Kao, T. H., Chen, Y., Pai, C. H., Chang, M. C., and Wang, A. H. (2011) Structure of a NADPH-dependent blue fluorescent protein revealed the unique role of Gly176 on the fluorescence enhancement, *J Struct Biol 174*, 485-493.
[162] Hwang, C. S., Choi, E. S., Han, S. S., and Kim, G. J. (2012) Screening of a highly soluble and oxygen-independent blue fluorescent protein from metagenome, *Biochem Biophys Res Commun 419*, 676-681.
[163] Bioscience, J. (2012) Evoglow Basic Kit, Product Information.
[164] Mishin, A. D., Subach, F. V., Yampolsky, I. V., King, W., Lukyanov, K. A., and Verkhusha, V. V. (2008) The First Mutant of the *Aequorea Victoria* Green Fluorescent Protein That Forms a Red Chromophore, *Biochemistry 47*, 4666-4673.
[165] Chang, C. C., Chuang, Y. C., Chen, Y. C., and Chang, M. C. (2004) Bright fluorescence of a novel protein from Vibrio vulnificus depends on NADPH and the expression of this protein is regulated by a LysR-type regulatory gene, *Biochem Biophys Res Commun 319*, 207-213.
[166] Mukherjee, A., Weyant, K. B., Agrawal, U., Walker, J., Cann, I. K., and Schroeder, C. M. (2015) Engineering and characterization of new LOV-based fluorescent proteins from Chlamydomonas reinhardtii and Vaucheria frigida, *ACS Synth Biol 4*, 371-377.
[167] Takahashi, E., Takano, T., Nomura, Y., Okano, S., Nakajima, O., and Sato, M. (2006) In vivo oxygen imaging using green fluorescent protein, *Am J Physiol Cell Physiol 291*, C781-787.

[168] Baneyx, F., and Mujacic, M. (2004) Recombinant protein folding and misfolding in Escherichia coli, *Nat Biotechnol 22*, 1399-1408.
[169] Sorensen, H. P., and Mortensen, K. K. (2005) Advanced genetic strategies for recombinant protein expression in Escherichia coli, *J Biotechnol 115*, 113-128.
[170] Sorensen, H. P., and Mortensen, K. K. (2005) Soluble expression of recombinant proteins in the cytoplasm of Escherichia coli, *Microb Cell Fact 4*, 1.
[171] Mihalcescu, I., Van-Melle Gateau, M., Chelli, B., Pinel, C., and Ravanat, J. L. (2015) Green autofluorescence, a double edged monitoring tool for bacterial growth and activity in micro-plates, *Phys Biol 12*, 066016.
[172] Bienick, M. S., Young, K. W., Klesmith, J. R., Detwiler, E. E., Tomek, K. J., and Whitehead, T. A. (2014) The interrelationship between promoter strength, gene expression, and growth rate, *PLoS One 9*, e109105.
[173] Glick, B. R. (1995) Metabolic Load and Heterologous Gene Expression, *Biotechnology Advances 13*, 247-261.
[174] Acharya, A., Bogdanov, A. M., Grigorenko, B. L., Bravaya, K. B., Nemukhin, A. V., Lukyanov, K. A., and Krylov, A. I. (2017) Photoinduced Chemistry in Fluorescent Proteins: Curse or Blessing?, *Chem Rev 117*, 758-795.
[175] Reid, B. G., and Flynn, G. C. (1997) Chromophore Formation in Green Fluorescent Protein, *Biochemistry 36*, 6786-6791.
[176] Buckley, A. M., Jukes, C., Candlish, D., Irvine, J. J., Spencer, J., Fagan, R. P., Roe, A. J., Christie, J. M., Fairweather, N. F., and Douce, G. R. (2016) Lighting Up Clostridium Difficile: Reporting Gene Expression Using Fluorescent Lov Domains, *Sci Rep 6*, 23463.
[177] Leyn, S. A., Suvorova, I. A., Kazakov, A. E., Ravcheev, D. A., Stepanova, V. V., Novichkov, P. S., and Rodionov, D. A. (2016) Comparative genomics and evolution of transcriptional regulons in Proteobacteria, *Microb Genom 2*, e000061.
[178] Kanehisa, M., Sato, Y., Furumichi, M., Morishima, K., and Tanabe, M. (2019) New approach for understanding genome variations in KEGG, *Nucleic Acids Res 47*, D590-D595.
[179] Typas, A., and Hengge, R. (2006) Role of the spacer between the -35 and -10 regions in sigmas promoter selectivity in Escherichia coli, *Mol Microbiol 59*, 1037-1051.
[180] Gordon, L., Chervonenkis, A. Y., Gammerman, A. J., Shahmuradov, I. A., and Solovyev, V. V. (2003) Sequence alignment kernel for recognition of promoter regions, *Bioinformatics 19*, 1964-1971.
[181] Li, G. W., Burkhardt, D., Gross, C., and Weissman, J. S. (2014) Quantifying absolute protein synthesis rates reveals principles underlying allocation of cellular resources, *Cell 157*, 624-635.
[182] Chen, S., Bagdasarian, M., Kaufman, M. G., and Walker, E. D. (2007) Characterization of strong promoters from an environmental Flavobacterium hibernum strain by using a green fluorescent protein-based reporter system, *Appl Environ Microbiol 73*, 1089-1100.
[183] Shahmuradov, I. A., Mohamad Razali, R., Bougouffa, S., Radovanovic, A., and Bajic, V. B. (2017) bTSSfinder: a novel tool for the prediction of promoters in cyanobacteria and Escherichia coli, *Bioinformatics 33*, 334-340.

[184] Lloyd, A. L., Marshall, B. J., and Mee, B. J. (2005) Identifying cloned Helicobacter pylori promoters by primer extension using a FAM-labelled primer and GeneScan analysis, *J Microbiol Methods 60*, 291-298.
[185] Singh, S. S., Typas, A., Hengge, R., and Grainger, D. C. (2011) Escherichia coli sigma(7)(0) senses sequence and conformation of the promoter spacer region, *Nucleic Acids Res 39*, 5109-5118.
[186] Rudge, T. J., Brown, J. R., Federici, F., Dalchau, N., Phillips, A., Ajioka, J. W., and Haseloff, J. (2016) Characterization of Intrinsic Properties of Promoters, *ACS Synth Biol 5*, 89-98.
[187] Segall-Shapiro, T. H., Sontag, E. D., and Voigt, C. A. (2018) Engineered promoters enable constant gene expression at any copy number in bacteria, *Nat Biotechnol 36*, 352-358.
[188] Edmundson, M. C., and Horsfall, L. (2015) Construction of a Modular Arsenic-Resistance Operon in E. coli and the Production of Arsenic Nanoparticles, *Front Bioeng Biotechnol 3*, 160.
[189] Lyubenova, L., and Schröder, P. (2010) Uptake and Effect of Heavy Metals on the Plant Detoxification Cascade in the Presence and Absence of Organic Pollutants, In *Soil Heavy Metals* (Sherameti, I., and Varma, A., Eds.), Springer.
[190] Espirito Santo, C., Taudte, N., Nies, D. H., and Grass, G. (2008) Contribution of copper ion resistance to survival of Escherichia coli on metallic copper surfaces, *Appl Environ Microbiol 74*, 977-986.
[191] Rensing, C., and Grass, G. (2003) Escherichia colimechanisms of copper homeostasis in a changing environment, *FEMS Microbiology Reviews 27*, 197-213.
[192] Udekwu, K. I., Parrish, N., Ankomah, P., Baquero, F., and Levin, B. R. (2009) Functional relationship between bacterial cell density and the efficacy of antibiotics, *J Antimicrob Chemother 63*, 745-757.
[193] Butler, M. T., Wang, Q., and Harshey, R. M. (2010) Cell density and mobility protect swarming bacteria against antibiotics, *Proc Natl Acad Sci U S A 107*, 3776-3781.
[194] Deplanche, K., and Macaskie, L. E. (2008) Biorecovery of gold by Escherichia coli and Desulfovibrio desulfuricans, *Biotechnol Bioeng 99*, 1055-1064.
[195] Bae, W., Mehra, R. K., Mulchandani, A., and Chen, W. (2001) Genetic engineering of Escherichia coli for enhanced uptake and bioaccumulation of mercury, *Appl Environ Microbiol 67*, 5335-5338.
[196] Biondo, R., da Silva, F. A., Vicente, E. J., Souza Sarkis, J. E., and Schenberg, A. C. (2012) Synthetic phytochelatin surface display in Cupriavidus metallidurans CH34 for enhanced metals bioremediation, *Environ Sci Technol 46*, 8325-8332.
[197] Sani, R. K., Peyton, B. M., and Brown, L. T. (2001) Copper-Induced Inhibition of Growth of Desulfovibrio desulfuricans G20: Assessment of Its Toxicity and Correlation with Those of Zinc and Lead, *Applied and Environmental Microbiology 67*, 4765-4772.
[198] Hassen, A., Saidi, N., Cherif, M., and Boudabous, A. (1998) Resistance of Environmental Bacteria to Heavy Metals, *Bioresource Technology 64*, 7-15.

[199] Mott, D., Galkowski, J., Wang, L., Luo, J., and Zhong, C.-J. (2007) Synthesis of Size-Controlled and Shaped Copper Nanoparticles, *Langmuir 23*, 5740-5745.
[200] Pantidos, N., Edmundson, M. C., and Horsfall, L. (2018) Room temperature bioproduction, isolation and anti-microbial properties of stable elemental copper nanoparticles, *N Biotechnol 40*, 275-281.
[201] Alasvand Zarasvand, K., and Rai, V. R. (2016) Inhibition of a sulfate reducing bacterium, Desulfovibrio marinisediminis GSR3, by biosynthesized copper oxide nanoparticles, *3 Biotech 6*, 84.
[202] Suchomel, P., Kvitek, L., Prucek, R., Panacek, A., Halder, A., Vajda, S., and Zboril, R. (2018) Simple size-controlled synthesis of Au nanoparticles and their size-dependent catalytic activity, *Sci Rep 8*, 4589.
[203] Giessen, T. W., and Silver, P. A. (2016) Converting a Natural Protein Compartment into a Nanofactory for the Size-Constrained Synthesis of Antimicrobial Silver Nanoparticles, *ACS Synth Biol 5*, 1497-1504.
[204] Ceci, P., Chiancone, E., Kasyutich, O., Bellapadrona, G., Castelli, L., Fittipaldi, M., Gatteschi, D., Innocenti, C., and Sangregorio, C. (2010) Synthesis of iron oxide nanoparticles in Listeria innocua Dps (DNA-binding protein from starved cells): a study with the wild-type protein and a catalytic centre mutant, *Chemistry 16*, 709-717.
[205] Staniland, S. S., and Rawlings, A. E. (2016) Crystallizing the function of the magnetosome membrane mineralization protein Mms6, *Biochem Soc Trans 44*, 883-890.
[206] Voordouw, G., Niviere, V., Ferris, F. G., Fedorak, P. M., and Westlake, D. W. S. (1990) Distribution of Hydrogenase Genes in Desulfovibrio spp. and Their Use in Identification of Species from the Oil Field Environment, *Applied and Environmental Microbiology 56*, 3748-3754.
[207] Lovley, D. R., Roden, E. E., Phillips, E. J. P., and Woodward, J. C. (1993) Enzymatic iron and uranium reduction by sulfate-reducing bacteria, *Marine Geology 113*, 41-53.
[208] Mikheenko, I. P., Rousset, M., Dementin, S., and Macaskie, L. E. (2008) Bioaccumulation of palladium by Desulfovibrio fructosivorans wild-type and hydrogenase-deficient strains, *Appl Environ Microbiol 74*, 6144-6146.
[209] Li, C., Peck, H. D., LeGall, J., and Przybyla, A. E. (1987) Cloning, characterization, and sequencing of the genes encoding the large and small subunits of the periplasmic [NiFe]hydrogenase of Desulfovibrio gigas, *DNA 6*, 539-551.
[210] Rousset, M., Dermoun, Z., Hatchikian, C. E., and Belaich, J.-P. (1990) Cloning and sequencing of the locus encoding the large and small subunit genes of the periplasmic [NiFe]hydrogenase from Desulfovibrio fructosovorans, *Gene 94*, 95-101.
[211] Capeness, M. J., Echavarri-Bravo, V., and Horsfall, L. E. (2019) Production of Biogenic Nanoparticles for the Reduction of 4-Nitrophenol and Oxidative Laccase-Like Reactions, *Frontiers in Microbiology 10*.
[212] Corredor, C., Borysiak, M. D., Wolfer, J., Westerhoff, P., and Posner, J. D. (2015) Colorimetric detection of catalytic reactivity of nanoparticles in complex matrices, *Environ Sci Technol 49*, 3611-3618.

[213] Pal, T., and Ray, C. (2014) Nanoparticle Mediated Clock Reaction: a Redox Phenomenon, In *Metal Nanoparticles for Catalysis: Advances and Applications* (Tao, F., Ed.), pp 203-218, Royal Society of Chemistry.
[214] Pande, S., Jana, S., Basu, S., Sinha, A. K., Datta, A., and Pal, T. (2008) Nanoparticle-Catalyzed Clock Reaction, *The Journal of Physical Chemistry C 112*, 3619-3626.
[215] Revathi, R., Rameshkumar, A., and Sivasudha, T. (2016) Interaction of Mesotetrakis (2,6,dimethoxyphenol) Porphyrin with AuTiO2 Nanoparticles: A Spectroscopic Approach, *Journal of Nanoscience and Nanotechnology 16*, 6209-6215.
[216] Dundas, C. M., Graham, A. J., Romanovicz, D. K., and Keitz, B. K. (2018) Extracellular Electron Transfer by Shewanella oneidensis Controls Palladium Nanoparticle Phenotype, *ACS Synth Biol*.
[217] Gangula, A., Podila, R., M, R., Karanam, L., Janardhana, C., and Rao, A. M. (2011) Catalytic reduction of 4-nitrophenol using biogenic gold and silver nanoparticles derived from Breynia rhamnoides, *Langmuir 27*, 15268-15274.
[218] Maillard, F., Schreier, S., Hanzlik, M., Savinova, E. R., Weinkauf, S., and Stimming, U. (2005) Influence of particle agglomeration on the catalytic activity of carbon-supported Pt nanoparticles in CO monolayer oxidation, *Phys. Chem. Chem. Phys. 7*, 385-393.
[219] Mostafa, S., Behafarid, F., Croy, J. R., Ono, L. K., Li, L., Yang, J. C., Frenkel, A. I., and Cuenya, B. R. (2010) Shape-Dependent Catalytic Properties of Pt Nanoparticle, *Journal of the American Chemical Society 132*, 15714–15719.
[220] Kleijn, S. E., Lai, S. C., Miller, T. S., Yanson, A. I., Koper, M. T., and Unwin, P. R. (2012) Landing and catalytic characterization of individual nanoparticles on electrode surfaces, *J Am Chem Soc 134*, 18558-18561.
[221] Yang, H., He, L. Q., Hu, Y. W., Lu, X., Li, G. R., Liu, B., Ren, B., Tong, Y., and Fang, P. P. (2015) Quantitative Detection of Photothermal and Photoelectrocatalytic Effects Induced by SPR from Au and Pt Nanoparticles, *Angew Chem Int Ed Engl 54*, 11462-11466.
[222] Canovi, M., Lucchetti, J., Stravalaci, M., Re, F., Moscatelli, D., Bigini, P., Salmona, M., and Gobbi, M. (2012) Applications of surface plasmon resonance (SPR) for the characterization of nanoparticles developed for biomedical purposes, *Sensors (Basel) 12*, 16420-16432.
[223] Kanigowska, P., Shen, Y., Zheng, Y., Rosser, S., and Cai, Y. (2016) Smart DNA Fabrication Using Sound Waves: Applying Acoustic Dispensing Technologies to Synthetic Biology, *J Lab Autom 21*, 49-56.